PARAMETRIC SPATIAL MODAL ANALYSIS OF BEAMS

by

Charles Mark Archibald

Dissertation submitted to the Faculty of the

Virginia Polytechnic Institute and State University

in partial fulfillment of the requirements

for the degree of

## DOCTOR OF PHILOSOPHY

in

Mechanical Engineering

APPROVED:

Dr. A. L. Wicks, Chairman

Dr. L. D. Mitchell

Dr. R. L. West

Dr. F. J. Pierce
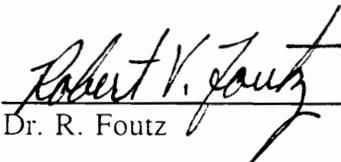
Dr. R. Foutz
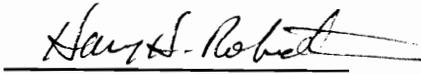
Dr. H. H. Robertshaw

ABSTRACT

PARAMETRIC SPATIAL MODAL ANALYSIS OF BEAMS

by

CHARLES MARK ARCHIBALD

Dr. A. L. Wicks, Committee Chairman

Mechanical Engineering

(ABSTRACT)

Modal analysis is the experimental characterization of the dynamical behavior of a structure. Recent advances in laser velocimetery have made available to the experimentalist a rich, new source of vibration data. Data can now be obtained from many different spatial locations on a structure. A method is presented to use this new data for the analysis of beams. Two approaches are investigated: minimum residual methods and boundary condition methods. The minimum residual approaches include autoregressive methods and non-linear least squares techniques. Significant contributions to sample rate considerations for parametric sinusoidal estimation resulted from this research. The minimum residual methods provide a good correlation between the measured data and the

fitted model. However, they do not yield a true modal decomposition of the spatial data. The boundary condition approach provides a complete modal model that is based on the spatial data and is completely compatible with classical beam theory. All theoretical constraints are included in the procedure. Monte Carlo investigations describe the statistical characteristics of the methods. Experiments using beams validate the methods presented. Advantages and limitations of each approach are discussed.

ACKNOWLEDGMENT

I would like to thank my major advisor, Dr. Al Wicks, for his help and support during the course of my graduate study at Virginia Tech. He introduced me to modal analysis while I was working on my master's degree, and has continued to provide support and encouragement through my doctoral studies. For my knowledge and interest in modal analysis and signal processing, I am deeply indebted to him.

Dr. Bob West has been a great asset. His insight and probing questions have greatly helped me in my research. This dissertation is a much finer document because of his suggestions.

I would also like to thank the remaining members of my committee, Dr. Larry Mitchell, Dr. Felix Pierce, and Dr. Robert Foutz. Each has provided assistance, advice, and good counsel.

A special thanks also goes to Dr. Harry Robertshaw, who stepped in to help at the last minute.

TABLE OF CONTENTS

xiii

LIST OF FIGURES

.

LIST OF TABLES

CHAPTER 1: INTRODUCTION

Analysis of the vibration characteristics of structures is an extremely important aspect of modern engineering practice. Incomplete dynamic analysis can lead to excessive noise and premature failure of structural components. In the increasingly competitive world of technology, such failures can not be tolerated.

Modal analysis is the experimental study of the dynamical behavior of structures. Many structures are of such complexity that analytical analyses must be verified by experiments. Thus the experimental approach is very important. Often modal analysis is conducted in a laboratory under controlled conditions. These conditions include the support for the structure during the test and the type of excitation used to initiate the vibrations. It is not unusual for structural components to be isolated, that is, tested separately from other components, during such a test.

The experimentalist must arm him or her self with an array of analysis tools. These tools include not only the requisite hardware required to initiate and measure the structural vibrations, but also the data processing algorithms and software needed to obtain useful information from the large quantities of raw data. The better equipped the analyst, the better he or she is able to develop a meaningful model of the dynamic behavior of the structure. In an attempt to provide a wider range of modal analysis tools, researchers work

to develop new hardware and associated algorithms and software for modal analysis. It is not unusual for a new instrumentation system (hardware) to be developed first, which spawns active research into data processing methods that fully exploit the potential of the new system. Often such new methods must be initially developed and proven for relatively simple structures. Subsequently, they may be applied to more complex structures. The research documented in this dissertation is of this nature.

Traditionally, modal analysis has been conducted using transducers that must be physically attached to a structure. Force transducers measure inputs to the structure and accelerometers are used to measure the response. The measured data is time based -- that is, a single data record consists of many measurements taken at one location on the structure over some period of time. This approach is widely used and is effective for many structures. However, it does have drawbacks. For light structures, physically attaching an accelerometer can alter the dynamic response of the structure. This is particularly noticeable at high frequencies or if the accelerometer is heavy. Also, the response data is only available at those locations at which the accelerometers are located. If response data is desired at many locations the analysis can become very difficult and time consuming.

A recent development in dynamic instrumentation eliminates these drawbacks. Dynamic response data can be measured optically using a scanning laser vibrometer. Any point on

2

a structure can be scanned with a laser, provided that a clear line-of-sight exists between the laser and the structure. The amplitude of the velocity response of the vibration is measured at each location. This eliminates the need for accelerometers for response measurement. It also provides for high spatial density vibration data, that is, measurements at very many spatial locations on the structure. The data is based on location, and not on time. Thus, the very nature of the data is different from the more traditional time-based measurements. This difference requires new data processing algorithms to fully exploit the capabilities of the laser system. This is an area of active research. Spatial modal analysis is the term applied to the implementation of these new analysis methods based on spatially distributed data.

A wide diversity exists in the types of structures for which the scanning laser vibrometer may be used. It is not feasible to develop a single method for analysis of spatial data for all these different type of structures. Thus, it is important to find effective algorithms for common simple structures. A beam is one such structure. A beam is a one-dimensional structural element that vibrates in flexure. Of course, no real structures are truly one-dimensional. However, there are three good reasons for studying beams: (1) The dynamical behavior of many structures is very similar to that of an ideal beam, (2) More complex structures may be modelled as system of ideal beams, (3) Classical solutions for the dynamical behavior of beams exist. All of these reasons contribute to the fact that beams should provide a good test bed for spatial modal analysis algorithms.

3

This dissertation documents research directed toward developing a spatial modal analysis method applicable to vibrating beams. In particular, it is desired to develop methods that will produce a parametric spatial modal model. A parametric model is one that describes the vibration in terms of a small number of modal parameters. If these parameters are extracted directly from the data, as opposed to a transformation of the measured data, the analysis method is said to be parametric.

The objective of this research is thus:

· To develop parametric spatial modal analysis algorithms that can characterize the dynamical behavior of beams.

This objective is realized in the Boundary Condition Beam Analysis method described in Chapter 6. This method is based on estimating the boundary conditions of the beam. A spatial modal model is then derived. Other approaches are also investigated. The applicability of autoregressive methods to generate spatial modal models is an interesting option. Another approach uses non-linear least squares to generate a modal model. These last two methods are essentially curve-fitting methods. They are very useful for smoothing data, but they are not as effective for generating a complete modal model.

This dissertation describes the background, development, and evaluation of each of these approaches. The respective advantages and limitations are documented. Chapter 2 provides the background required to understand the context and importance of this research. A review of the appropriate literature is included. The relationship between the time-domain methods currently in use and the spatial-domain methods is described.

Chapter 3 describes the effect of sample rate on parametric sinusoidal estimation. This is important for autoregressive analysis of beams. It also has significance for any application in which autoregressive sinusoidal estimation is used. In this context, the research reflected in this chapter is a significant contribution in the field of signal processing.

Theories of beam vibration are presented in Chapter 4. This provides the basis for understanding the different spatial modal methods. These methods are based on classical, or Euler-Bernoulli theory, which is described in detail. Timoshenko beam theory is also discussed as a means of determining the applicability of classical theory.

Chapter 5 is concerned with the minimum residual spatial modal analysis methods. These approaches fit a deterministic function to the measured data. Since measured data always contains noise, an exact fit, in which the model passes through every data point, includes effect of noise. This is not desirable. A fit is considered good if the residual error -- the

difference between the model and the measured data -- is minimized. Two such approaches are presented, one based on an autoregressive analysis and the other based on a multi-dimensional Newton's method. These models are shown to effectively fit spatial data provided resonance excitation is used. They are most appropriate when data smoothing is desired. These methods do not always yield accurate modal parameters, however.

Chapter 6 is devoted to the Boundary Condition Beam Analysis. This method is a true spatial modal analysis. The modes of vibration are decomposed from the data. This is accomplished by estimating the boundary conditions for the beam and applying classical beam theory. The method generates meaningful models and has much potential for future applications.

Chapters 7 and 8 are devoted to evaluation and analysis of the three spatial modal analysis methods. Chapter 7 describes studies regarding the errors inherent with the three methods. The minimum residual models are shown to be biased in many cases. Chapter 8 presents experiments utilizing real beams. The validity of each of the methods is investigated and described.

Chapter 9 summarizes the research and presents conclusions and recommendations for future study. The principal contributions and conclusions of this research can be summarized as:

- The Boundary Condition Beam Analysis method is an effective spatial modal analysis technique for beams.

- Minimum residual spatial modal methods are useful for smoothing spatial data.

- Minimum residual spatial modal methods exhibit a bias error when the excitation frequency varies from one of the natural frequencies of the beam.

- An optimum number of samples per period exists for parametric sinusoidal estimation methods. This is always the case for spatial beam data.

NOMENCLATURE

α, λ	Chapter 1 - Exponential constants
α, β	Chapter 4 - Timoshenko exponents
β	Spatial frequency
Δ	Time interval or sample period
K	Matrix condition number
Λ	Frequency matrix
ν	BCBA experimental modal weighting factor
ρ	Mass density
σ^2	Variance
σ_i	Singular value
τ	Delay lag
φ_i	i^{th} mode shape
Φ_i	i^{th} normalized mode shape
ω	Excitation frequency
Ω	Discrete frequency
ω_n	Natural frequency
A	Chapter 1 - Constant
A	Area

a_i	Autoregressive coefficient
b_i	Moving Average coefficient
BCBA	Boundary Condition Beam Analysis
c	OTLS column dimension
C_i	Modal coefficient
$\acute{C}_i$	Shear modal coefficient
D	Matrix delay factor
D	Matrix delay index
E	Modulus of elasticity
E[ ]	Expected value
I	Identity matrix
I	Area moment of inertia
j	Imaginary number
J	Jacobian matrix
J	Mass moment of inertia
k	Stiffness
K_i	Rotational Stiffness
L	Beam length
LSSD	Least Squares Spatial Domain
m	Mass; Mode index
M	Mode shape matrix

9

M_i	Modal weighting factor for i^{th} mode
N	Number of data points
n_k	Random measurement noise
p	Autoregressive model order
P,Q	Chapter 5 - Parameter Sets
R	Correlation matrix
R_{xx}	Autocorrelation function
SNR	Signal-to-Noise Ratio
SPSR	Sinusoidal-Period to Sample points Ratio
V_k	Deterministic component of signal
V	Velocity
V´	Derivative of Velocity with respect to spatial coordinate
w(x,t)	Complete solution to beam differential equation
W,E	Noise matrix
Y	Data matrix
y_k	Measured signal
z	Complex variable
C	Set of all complex numbers
‖A‖	Norm of matrix **A**

Matrices will be designated by bold capital letters (**R**, **Y**, **V**).

Vectors will be designated by bold small case letters (**n**, **y**, **v**).

If ambiguity exits, brackets [] will indicate matrices and braces

{} will indicate vectors.

CHAPTER 2: BACKGROUND AND OVERVIEW

INTRODUCTION

The concept of parametric spatial modal analysis -- processing high-density spatial vibration data to obtain parameterized modal models -- is feasible only because of the prior contributions of many distinguished engineers and scientists. The foundation is built solidly on the work of such great men as Euler and Timoshenko, who developed classical and advanced theories for vibration of beams. The signal processing algorithms would be impossible without the work of such men as G. Udny Yule and more recently V. F. Pisarenko and Gene Golub, among many others. This century has seen the blossoming of methods for processing time-series data as computers have come of age. These parametric time-series analysis methods provide the background for spatial analysis. Recent advances in instrumentation technology, such as scanning laser vibrometers, provide a new and rich source of vibration data.

This chapter provides a background from which parametric spatial modal analysis can be understood. It provides not only the technical prerequisites for understanding the following chapters, but also an element of historical perspective -- the origins, or genealogy, of this research. Early time-series analysis strategies are presented, along with

12

modal analysis applications. Some of the computational problems typically encountered, such as assumptions regarding measurement noise and sample rate considerations, are discussed. A review of beam vibration theory is included, along with a brief discussion of laser vibrometery. This 'genealogy' of the research is summarized in Fig. 1.

Parametric spatial modal analysis is possible only by the union of three diverse technologies -- time-series analysis, dynamics, and laser vibrometery. These branches are delineated in the figure. Each branch will be discussed. It is hoped that this chapter will be sufficient to provide the background in which the following chapters can be understood.
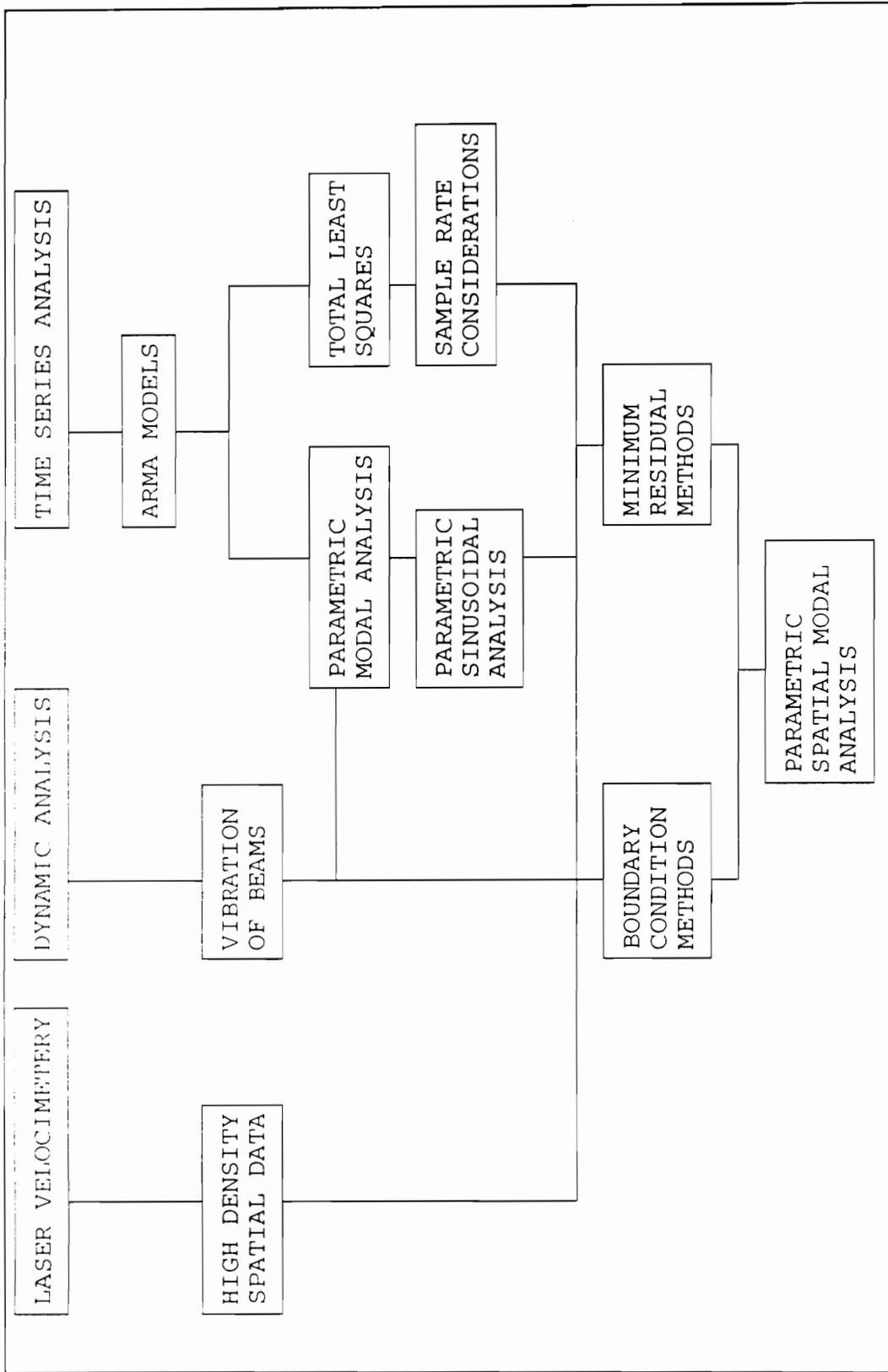
Figure 1 Parametric spatial modal analysis of beams -- research flow chart.

14

TIME SERIES ANALYSIS

ARMA MODELS

Autoregressive-Moving Average (ARMA) models have been used for modeling many different types of time series. These are very general models, in that virtually any random, stationary process can be described with an ARMA model. Essentially, the time series is considered to be a process with a white noise input. The input can be considered as a series of random shocks to the system. The output at any time can be determined from a set of both preceding inputs and outputs. ARMA models are very useful for forecasting future trends in a series. Given the measured time series y_k and the unmeasured random shocks n_k, an ARMA model can be described mathematically by

$$\sum_{i=0}^{p} a_i y_{k-i} = \sum_{i=0}^{q} b_i n_{k-i} \qquad (2.1)$$

where the a_i's and the b_i's are the autoregressive and moving-average coefficients, respectively. The discrete time index is k. The order of the ARMA process is (p,q), where p is the autoregressive model order, and q is the moving-average model order. Thus, Eq. 2.1 describes an ARMA(p,q) process.

15

Often, a process does not require a full ARMA model. Two special case models are the autoregressive (AR) model and the moving average (MA) model. If $p = 0$, then a moving-average model results. The stochastic process y_k can be described exclusively in terms of a finite set of past random shocks. A moving average model has the form

$$y_k = \sum_{i=0}^{q} b_i n_{k-i} \qquad (2.2)$$

If $q = 0$, then the model is termed autoregressive. The time series y_k can be accurately represented with a finite set of past values and a single random shock. The autoregressive form is

$$y_k = \sum_{i=1}^{p} a_i y_{k-i} + n_k \qquad (2.3)$$

A dual relationship exists between AR and MA processes. An AR process can be described, as in Eq. 2.3, with a finite number of parameters, i.e., the finite set of autoregressive coefficients $\{a_0, a_1, a_2, ... a_p\}$. It has been shown that this process can also be described by MA model of infinite order, i.e., an AR process can be described by Eq. 2.2

16

with $q = \infty$ (Box and Jenkens, 1976). Likewise, a MA process can be described by a finite difference equation, as in Eq. 2.2, or by an infinite order AR process (Eq. 2.3 with $p = \infty$). This is known as duality between autoregressive and moving average processes.

An early pioneer of autoregressive modeling was G. Udny Yule. In 1927, Yule developed an autoregressive model to determine periodicities in Wolfer's sunspot data (Yule, 1927)[1]. He was motivated by the realization that the autoregressive parameters could reveal the frequencies of disturbed periodic series. Yule imagined a fundamentally deterministic process that was driven by random shocks. His classic example is an oscillating pendulum. A group of mischievous boys randomly pelt the pendulum with peas. The resulting motion of the pendulum would be dependent not only on the dynamic characteristics of the pendulum, but also on the random shocks caused by the peas. The result of this philosophy was the development of the autoregressive model.

George E. P. Box and Gwilym M. Jenkens published what is now the classic text on ARMA modeling, Time Series Analysis, Forecasting and Control (Box & Jenkens, 1976). They provide an in-depth analysis of AR, MA, and ARMA models, with various applications. Three broad categories of problems are treated: forecasting time series, evaluation of transfer functions, and design of control systems. ARMA models are treated thoroughly, including integrated models (ARIMA) and seasonal models. These models and

---

[1] References are given at the back of the dissertation.

methods are excellent tools for many problems. However, they are very general models in that no problem-specific assumptions are made about the data. In many situations, for example where forecasting is required, these models function quite well. However, dynamic and modal analysis problems are sufficiently well-defined that more sophisticated, 'tailor made', algorithms should be employed. A number of specialized algorithms have been developed for this purpose.

Many of these specialized methods still rely on ARMA models. The expanding field of exploratory geophysics in the 1960's brought several notable geologists into the time-series analysis arena. The problem at hand was estimation of the spectrum of seismic data. John Burg presented the Maximum Entropy Method (MEM) in 1967 (Burg, 1967) He postulated that the spectrum estimator that best fit the measured data was the most random, or the spectrum with maximum entropy consistent with the data. The method involved computing the spectrum from a finite number of autocorrelation lags. The autocorrelation function was shown to fit an autoregressive relationship. Thus Burgs maximum entropy process is an autoregressive process.

Parzen developed another approach to dynamic ARMA modeling in 1968 (Parzen, 1968). Along with the work of Burg, this marked the beginnings of custom-tailoring ARMA models to dynamic data. A great many investigators then turned to the problem about this time. Two excellent survey papers were published in 1981 and 1982 include overviews

of ARMA modeling as applied to spectral estimation. Robinson presents a historical perspective (Robinson, 1982), while Kay and Marple present the current (as of 1981) perspective of spectral estimation (Kay & Marple, 1981).

PARAMETRIC MODAL ANALYSIS

The algorithms developed by Burg and Parzen initiated customization of ARMA models for spectrum analysis. At that time modal analysis was just becoming a practical experimental tool. Experimental Modal Analysis (EMA) consists of developing a dynamic model of a structure based on measured vibrational responses. The primary signal processing methods involve Fourier transforms. These frequency-domain approaches are attractive because of the computational ease of the Fast Fourier Transform (FFT) (Cooley & Tukey, 1965). However, the work of Burg and Parzen motivated a number of investigators to pursue time-domain approaches. These methods offer statistical advantages over frequency-domain methods. They are also known as parametric methods. A parametric model of a system is one that describes the system with a finite number of parameters.

19

Modal analysis typically involves the analysis of multiple signals that are comprised, for the most part, of damped sinusoids. Most, but not all, parametric modal analysis methods resemble ARMA models. This is because of a special AR relationship that exists for sinusoidal signals. This relationship is described below. The specifics of many of these methods bears little resemblance to the methods of Box and Jenkens, save for the autoregressive equation. Thus these are sometimes referred to as ARMA-like models.

The application of ARMA models to modal analysis springs from the fact that a system of damped sinusoids can be modeled as a "self-exciting" autoregressive process. For example, the discrete sinusoidal signal

$$v_k = \sum_{i=1}^{m} A_i e^{\alpha_i k} \sin(\omega_i k + \phi_i) \tag{2.4}$$

can also be represented by the AR relation

$$v_k = \sum_{i=1}^{p} a_i v_{k-i} \tag{2.5}$$

Notice that, unlike the AR relation in Eq. 2.3, no random input term is present. A sinusoidal signal requires only initial conditions to satisfy the autoregression. This is why it is termed "self-exciting". It can also be shown that the AR relationship of Eq. 2.5 holds

20

for the more general case of all complex exponential. Thus, Eq. 2.5 can model any discrete complex exponential function of the form

$$v_k = \sum_{i=1}^{p} C_i e^{\lambda_i k} \qquad C, \lambda \in \mathbb{C} \qquad (2.6)$$

Where $\mathbb{C}$ is the set of all complex numbers (C and λ are, in general, complex).

The family of complex exponential functions in Eq. 2.6 includes exponential, damped, and undamped harmonic functions. If λ is purely imaginary, the resulting signal is harmonic. If λ is purely real, the signal is exponential. If λ is complex, then a damped sinusoid results. The resulting time series v_k is real if all complex terms occur in conjugate pairs. If all real exponential terms occur in signed pairs, then hyperbolic functions result. All of these forms exhibit the AR nature of Eq. 2.5. This relationship can be stated in a theorem.

Theorem 1: Let v_k be the discrete, complex exponential series

$$v_k = \sum_{i=1}^{p} C_i e^{\lambda_i k} \qquad C, \lambda \in \mathbb{C} \qquad (2.7)$$

21

obtained by sampling a continuous complex exponential signal. Then the series v_k satisfies the autoregressive relationship

$$\sum_{i=0}^{p} a_i v_{k-i} = 0 \qquad (2.8)$$

where the autoregressive coefficients $\{a_0, a_1 \dots a_p\}$ are the coefficients of the polynomial $A(z)$ defined by

$$A(z) = \prod_{i=1}^{p} (z - e^{\lambda_i \Delta}) \qquad (2.9)$$

In Eq. 2.9, Δ is the sample interval.

A detailed proof of this theorem is found in appendix A2.1.

The AR nature of complex exponential has led to a large amount of research in parametric modal analysis. ARMA models provide a compact, parameterized means to describe the data. This has lured many investigators to develop methods for fitting ARMA or ARMA-like models to modal data. These methods are generally termed time-domain methods to differentiate them from Fourier transform based approaches (frequency domain).

22

Many of these methods can trace their roots back to Prony's method. Baron De Prony in 1795 developed a method to fit gas expansion data to a linear sum of exponential functions (Prony, 1795). His original method involved fitting p real exponential functions exactly to p data points. This bears little resemblance to the modal analysis algorithms of today. However, his work has had a significant impact. What has come to be called Prony's method involves condensing the non-linear least squares problem of fitting data to a set of complex exponential into two linear least squares problems and one polynomial rooting problem. The first step consists of estimating the AR coefficients of Eq. 2.8. The system characteristic Eq. is then rooted to obtain the poles of Eq. 2.9. The poles contain the exponents, which provide the complex frequencies and damping ratios. With the exponents known, the complex coefficients of Eq. 2.7 can be found using any ordinary least squares procedure. The amplitudes and phases can then be found from these coefficients.

Hildebrand described two implementations of Prony's method in 1956 (Hildebrand, 1956). This basic approach has been used in a number of different algorithms. One method that can trace its roots back to Prony is the Complex Exponential method (Brown, et al, 1979). The Polyreference method (Vold, 1982) is an extension of the Complex Exponential method to include multiple response locations. It is thus a multiple time series analysis. Other methods that use a similar approach include Oversize Eigenmatrix Method and the Oversize Total Least Squares method. These methods differ in the particular approach

23

taken to solve the least squares problem. They are similar in that two linear least squares procedures and a polynomial rooting procedure are included. The Oversize Total Least Squares method will be described in detail under Total Least Squares Methods.

The Data Dependent Systems method, developed by Sudhakar Pandit in 1983, uses a more classic ARMA modeling method to obtain modal parameters (Pandit, 1984, 1986). The free response data is analyzed with an ARMA$(n,n-1)$ model. The AR coefficients describe the deterministic component of the signal, and the MA coefficients describe the stochastic content. The data is successively fitted with larger models (n increases) until no significant change in the model is noted. This is considered to be the parsimonious model.

The Autoregressive Least Squares or simply Least Squares method has not been widely implemented, as it has been shown to lead to biased results. This method fits the AR model using traditional least squares methods. If additive measurement noise is present, the parameter estimates will be biased. Considerable overspecification of the AR model order is required in order to improve the estimates. However, this overspecification results in spurious poles that must be differentiated from the true poles, an often non-trivial task.

The Correlation Fit method, developed by Cooper and Wright in 1985, is a means of avoiding the bias error inherent in the AR approach (Cooper & Wright, 1985). The

method uses a least squares fit of the autocorrelation function values. Only lags greater than zero are used. The zeroth autocorrelation lag of a sinusoid in additive noise contains the variance of the random content. Eliminating this lag effectively eliminates the bias error. The correlation fit method has been shown to yield consistent, accurate parameter estimates.

Several investigators have developed time-domain modal analysis techniques that do not utilize the autoregressive nature of sinusoids. The Ibrahim Time Domain (ITD) method (Ibrahim & Mikulcik, 1977) is one such approach. The method uses free response data. Because the responses at any time t are correlated with the responses at a time $t+\Delta t$, response matrices temporally separated by Δt can be combined to form a transformation matrix. The eigenvalues of this matrix contain the natural frequencies and damping ratios. The eigenvectors contain the initial conditions. The Eigensystem Realization Algorithm (ERA) (Juang & Pappa, 1984) is a similar approach. The primary difference between these two methods is the solution strategy. The ERA uses singular value decomposition.

One additional method worth noting is Smith Least Squares (W. R. Smith, 1981). This method uses an iterative approach to directly estimate modal parameters from the measured data. It is based on a multidimensional Newton-Raphson least squares method developed for damped sinusoids. The method is also capable of simultaneous analysis of multiple time records. Kevin E. Smith analyzed the method, and found it to provide

25

accurate parameter estimates (Kevin E. Smith, 1984). The method requires initial parameter estimates, which can be obtained from a Fourier transform of the data.

The brief descriptions presented here provide an idea of the state of the art in parametric dynamic modeling. These are some of the principal time-domain methods used in modal analysis. Various permutations and modifications can be found for all of these methods.

A number of survey papers compare the various parametric methods used for modal analysis. See, for example, Cooper & Wright, Füllekrug, Cunod & Sage, or Astrom & Eykhoff (Cooper & Wright, 1985; Füllekrug, 1989; Cunod & Sage, 1968; Astrom & Eykhoff, 1971). In general, the different methods differ in noise assumptions and solution strategy. Most of the parametric time-domain methods are fundamentally similar, however.

PARAMETRIC SINUSOIDAL ESTIMATION

Engineers and scientists from many disciplines are faced with the problem of estimating sinusoidal parameters from noisy data. From exploratory geology to communications, sinusoidal data is common, and thus sinusoidal estimation is an important problem. Modal

analysis is primarily concerned with estimating damped sinusoids. Thus, in a sense, parametric sinusoidal estimation is a special case of parametric modal analysis. Most of the methods described above can, in fact, estimate sinusoids. However, for pure, undamped sinusoids, the system poles lie on the unit circle. This presents problems for some of the former algorithms. Methods designed explicitly to estimate pure (undamped) sinusoids in noise have been developed. One of the most important is Pisarenko Harmonic Decomposition (PHD). Also, many of the ARMA-like methods described above can be modified to constrain the poles to the unit circle.

An important assumption that must always be made in parametric analysis is the nature of noise. Different methods treat noise differently. Applying Yule's autoregressive assumption implies that the sinusoidal signal is actually modified by random shocks. In most cases where sinusoidal estimation is the goal, this is not a realistic assumption. A better assumption is that the underlying signal is deterministic, a sinusoid for example, and the noise is added to that signal by measurement errors, etc.

If additive noise is in fact the case, attempts to fit the data with an AR model will lead to biased frequency estimates. Pisarenko Harmonic Decomposition is based on the assumption of additive noise. It thus provides unbiased estimates of the sinusoidal parameters.

27

It can be shown that a complex exponential function in the presence of additive noise is a special case of an ARMA model. If the measured data is designated y_k, the deterministic sinusoidal component v_k, and the stochastic component n_k, the assumption of additive noise can be represented by

$$y_k = v_k + n_k \tag{2.10}$$

If the deterministic component v_k consists of a linear sum of exponential

$$v_k = \sum_{i=1}^{p} C_i e^{\lambda_i k} \qquad C, \lambda \in \mathbb{C} \tag{2.11}$$

then, from Theorem 1 it can be expressed as the homogenous autoregressive function

$$\sum_{i=0}^{p} a_i v_{k-i} = 0 \tag{2.12}$$

28

Solving Eq. 2.10 for v_k, substituting into Eq. 2.12 and rearranging reveals that a sinusoid in additive noise can be represented by a special case ARMA model:

$$\sum_{i=0}^{p} a_i y_{k-i} = \sum_{i=0}^{p} a_i n_{k-i} \qquad (2.13)$$

Thus, the assumption of additive noise leads to an ARMA model in which the autoregressive coefficients and moving average coefficients are identical. This is why a simple AR model is inadequate. It also leads to the possibility of special sinusoidal estimation methods.

In 1973 V. Pisarenko developed a method for sinusoidal estimation now known as Pisarenko Harmonic Decomposition (PHD) (Pisarenko, 1973). It is a computationally efficient, unbiased method for estimating sinusoidal parameters. It is significant in that it assumes additive noise. A description of the theory involved is presented.

The PHD method assumes that the noise series n_k is a normally distributed, zero mean random process, that is,

$$n_k \sim N(0, \sigma^2)$$

29

It is further assumed that the deterministic component is a sinusoidal function, i.e.

$$v_k = \sum_{i=1}^{m} A_i \sin(\omega_i k + \Phi_i)$$

The ARMA relation of Eq. 2.13 can be written in matrix form as

$$y^T a = n^T a$$

where

$$y^T = [y_k \ y_{k-1} \ y_{k-2} \ \cdots \ y_{k-p}]$$
$$n^T = [n_k \ n_{k-1} \ n_{k-2} \ \cdots \ n_{k-p}]$$
$$a^T = [a_0 \ a_1 \ a_2 \ \cdots \ a_p]$$

and p is equal to twice the number of real sinusoidal components $(p=2m)$. Premultiplying by y and taking the expectation gives

$$E[yy^T]a = E[yn^T]a$$

The expected value of yy^T is the covariance matrix, C_{yy}. From Eq. 2.10,

30

$$E[yn^T] = E[vn^T] + E[nn^T]$$

$$= 0 + \sigma^2 I$$

Since n_k and v_k are uncorrelated. Thus

$$C_{yy}a = \sigma^2 Ia$$

or

$$[C_{yy}\text{-}\sigma^2 I]a = 0$$

Thus, Pisarenko Harmonic Decomposition involves an eigenanalysis of the covariance matrix. The minimum eigenvalue is proportional to the variance of the random content, and the corresponding eigenvector contains the AR coefficients. The roots of a polynomial containing these coefficients are the poles of the system. The covariance matrix C_{yy} is a symmetric Topelitz matrix of dimension $p+1$. The eigenvectors of a symmetric matrix are also symmetric, that is, $a_i = a_{p-i}$. This in turn forces the poles onto the unit circle. Thus PHD results in estimates of only undamped sinusoids.

Pisarenko Harmonic Decomposition is important because of the manner in which noise is treated. It is a definitive break with the AR model used in many other methods. Additional sinusoidal estimation methods have been used by numerous investigators,

31

however. Prony's method has been applied to sinusoidal estimation. See Hildebrand (1956) or Patton (1988) for two different approaches using Prony's method. Kay (1988) presents a number of different eigenanalysis methods for sinusoidal estimation, including Pisarenko Harmonic Decomposition. The MUSIC algorithm (Schmidt 1981, Marple 1987) has been widely used as well. It is also a method based on estimating the poles from a noise subspace. In addition, some of the parametric modal analysis methods can also be used for sinusoidal estimation.

TOTAL LEAST SQUARES

Pisarenko Harmonic Decomposition is an approach to sinusoidal estimation that assumes additive noise. This results in unbiased frequency estimates. Autoregressive least squares is biased for additive noise processes because it assumes that past values of the series are known exactly. The difference between the two approaches is analogous to the difference between ordinary least squares and total least squares. Both least squares approaches solve an overdetermined system of equations for a 'best fit' of unknowns. Given the $(m \times n)$ data matrix A and the $(m \times 1)$ observation vector b, a vector x is found that approximately solves the problem $Ax=b$.

Ordinary least squares methods assume all errors are confined to the observation vector and the data matrix is exact, i.e. no errors. Clearly, in many applications, and of particular interest in parametric analysis where additive noise is assumed, this is an incorrect assumption. The Total Least Squares (TLS) method is one way to include data matrix errors in the least squares analysis. Gene Golub and Charles Van Loan have studied the TLS problem extensively, and developed a TLS solution (Golub & Van Loan, 1980).

Ordinary least squares and total least squares can be contrasted as follows. The ordinary least squares can be described as solving

$$Ax = \{b+r\}$$

by finding the minimum $\|r\|_2$ subject to $\{b+r\} \in$ range A. The vector r contains the errors associated with b. It is implicitly assumed that the matrix A is known exactly. In many cases, such as polynomial regression, this is a valid assumption. However, if A is constructed with measured data, as is the case with all of the methods presented here, then it is expected to contain measurement errors, or noise. The total least squares formulation addresses this problem. Total Least Squares can be described as solving

$$[A+E]x = \{b+r\}$$

33

by finding the minimum $\|E/r\|_F$ subject to $\{b+r\} \in$ range $[A+E]$. The random content of both the data matrix and the observation vector is included. A unique minimizing x may or may not exist for a particular problem. Golub and Van Loan present an algorithm to solve TLS problems using singular value decomposition. The minimum-norm vector x_{LS} is computed when the solution is not unique.

The total least squares approach is appropriate for parametric sinusoidal estimation when additive noise is assumed. Pisarenko Harmonic Decomposition can be loosely classified as a total least squares method, even though the algorithmic implementation is quite different from that usually encountered in TLS formulations. Two TLS methods used for parametric modal analysis closely follow Golub and Van Loan's algorithm. These methods are the Oversized Eigenmatrix Method (OEM) (Yang, 1985) and the Oversized Total Least Squares (OTLS) method (Archibald, 1990). Both the OEM and the OTLS use singular value decomposition to solve the total least squares problem. Each also uses an oversized data matrix, that is, the number of columns in the data matrix can be larger than the model order of the system. This allows analysis even when the system model order in not known a-priori. It also results in excess poles. The difference in the two methods is the manner in which the true poles are segregated from the spurious poles. Oversize Total Least Squares is described in detail below. The differences between OEM and OTLS are noted.

The OTLS method involves decomposition of a circulant data matrix such that a basis set of vectors spanning the noise space is obtained. This space, S_N, contains all solutions to the TLS problem. A method is developed to choose a vector in S_N such that all spurious, or noise poles are zero. System parameters are then obtained directly from that vector. The assumptions regarding the data are identical with those used in PHD except that the deterministic component is not restricted to sinusoids. These assumptions can be summarized as

$$v_k = \sum_{i=1}^{p} C_i e^{\lambda_i k} \qquad C, \lambda \in \mathbb{C}$$

$$y_k = x_k + n_k$$

$$n_k \sim N(0, \sigma^2)$$

From Theorem 1 it is known that y_k satisfies a pth order difference equation. If N measured data points, $y_0 \cdots y_N$, are available, the following matrix system of equations can be constructed:

$$Ya = [X+W]a = 0$$

35

Here Y is a circulant matrix of dimension (m,n) consisting of the measured (i.e., noise corrupted) data. This matrix has the form:

$$\begin{bmatrix} y_{n-1} & y_{n-2} & \cdots & y_0 \\ y_n & y_{n-1} & \cdots & y_1 \\ \vdots & & & \\ y_N & y_{N-1} & \cdots & y_{N-n+1} \end{bmatrix}$$

The objective is to minimize, in some sense, the noise matrix W, subject to the constraint that $[X+W]$ is singular. Stewart (1973) has shown that, given the singular value decomposition (SVD) of Y as

$$U^T Y V = \Sigma = diag\{\sigma_1 \ \sigma_2 \ \cdots \ \sigma_n\}$$

with $\quad \sigma_1 >= \cdots >= \sigma_p >= \sigma_{p+1} = \cdots = \sigma_n$

and $\ U, V$ orthogonal,

then $\quad \sigma_n = minimum \ \|W\|_F$

$\quad\quad rank \ X < n.$

36

Here $\|W\|_F$ is the Frobenius norm of W, given by

$$\|A\|_F = \Sigma\Sigma \ b_{ij}^2.$$

Furthermore, the minimum is given by

$$W^{\cdot} = -Yvv^T$$

where v is any vector is the subspace S_N, defined by

$$S_N = span\{v_{p+1} \ v_{p+2} \cdots v_n\}.$$

Here v_i represents the ith column of V the right singular vectors of Y. The implication is that the minimization problem can be solved in a reasonable sense by use of the SVD.

It is clear that if n-p > 1, the TLS solution is not unique. Indeed, a solution can be written for any vector in S_N. The first p columns of V define the signal subspace, S_s. These vectors each satisfy the system difference equation. The columns in S_N are random vectors orthogonal to S_s. Thus, the roots of a polynomial with coefficients taken as elements of any column of S_N contain, as a subset, the poles of the deterministic component. The

37

OEM method exploits this characteristic by choosing the poles common to several columns of S_N as the true poles. Since the remaining poles of each vector are random, and thus do not correspond between the vectors, they are discarded.

The OTLS method employs a linear transformation to find a vector v_t in S_N such that the last n-$(p+1)$ elements are identically zero. Since the roots of any vector in S_N contain the poles of the system under investigation, the roots of the first $p+1$ non-zero elements of v_t are the desired poles. No extraneous poles appear, since the remaining zeros in v_t produce no poles. Since the last n-p right singular vectors of Y span S_N, the desired vector v_t can be found as a linear combination of these vectors. This can be done by forming a system of equations from the last n-p rows and columns of the matrix V. Form the system

$$Z_m C = z_v$$

where

$$z_v = [\ v_{p+2,n}\ v_{p+3,n}\ \cdots\ v_{n,n}\ ]^T$$
$$C = [\ c_1\ c_2\ \cdots\ c_{n-(p+2)}\ ]^T$$

38

$$Z_m = \begin{bmatrix} v_{p+2,p+1} & v_{p+2,p+2} & \cdots & v_{p+2,n-1} \\ v_{p+3,p+1} & v_{p+3,p+2} & \cdots & v_{p+3,n-1} \\ \vdots & & & \\ v_{n,p+1} & v_{n,p+2} & \cdots & v_{n,n-1} \end{bmatrix}$$

Once the coefficient vector C is obtained, the vector v_t can be easily computed. Augment C with 1 in the last row such that

$$C' = [\ c_1\ c_2\ \cdots\ c_{n-(p+2)}\ 1\ ]^T$$

Then the last n-p columns of V, multiplied by C', yield the desired vector v_t.

$$[\ v_{p+1} \qquad v_{p+2} \quad \cdots \qquad v_n\ ]\ C' = v_t$$

$$v_t = [\ a_1\ a_2\ \cdots\ a_p\ 0\ 0\ \cdots\ 0\ ]^T = [\ a^T\ 0^T\ ]^T$$

The vector a contains the coefficients of the system difference equation. The roots of this equation are the system poles. Once the poles have been determined, the residues, A_i i = $1 \cdots p$, can be computed by an ordinary linear least-squares procedure such as described by Patton.

SAMPLE RATE CONSIDERATIONS FOR SINUSOIDAL ESTIMATION

All of the ARMA and ARMA-like methods for parametric sinusoidal estimation rely on solving a system of difference equations. The quality of the parameter estimates for any of these methods is dependent on the ratio of the sample period to the signal period. It has been shown that an optimum sample rate exists for estimation of a single sinusoid in additive noise, and that optimum is 4 samples per signal period (4 SPP) (Archibald, 1991). Current research indicates that the reason for this optimum is tied to the conditioning of the data matrix. The sensitivity of the Least Squares (including Total Least Squares) solution to perturbations in the data, or noise, is very dependent on the matrix condition. If the sinusoid is sampled at a very high rate relative to the signal frequency, the matrix condition is degraded, and the solution becomes very sensitive to noise. Thus, poor parameter estimates can be obtained at high sample rates even for good signal to noise ratios.

Figure 2 shows the relationship between matrix condition number and signal period to sample points ratio. This figure will be described in detail in Chapter 3. It is clear that the optimum occurs at 0.25 periods per sample (4 samples per period). The larger condition numbers at very high and very low sample rates makes the solution much more sensitive to noise at these sample rates. This can pose significant problem if the data must be sampled at very high or low samples-to-period ratios. An alternative matrix definition

40

can substantially improve matrix condition, however. If each column of the data matrix is delayed by a delay factor equal to an integer number of sample intervals, the AR relationship of Eq. 2.5 is preserved, but the effective sample rate is lowered considerably. This results in satisfactory parameter estimates even at high sample rates. Sample rate considerations and matrix improvement methods will be presented in detail in Chapter 3.
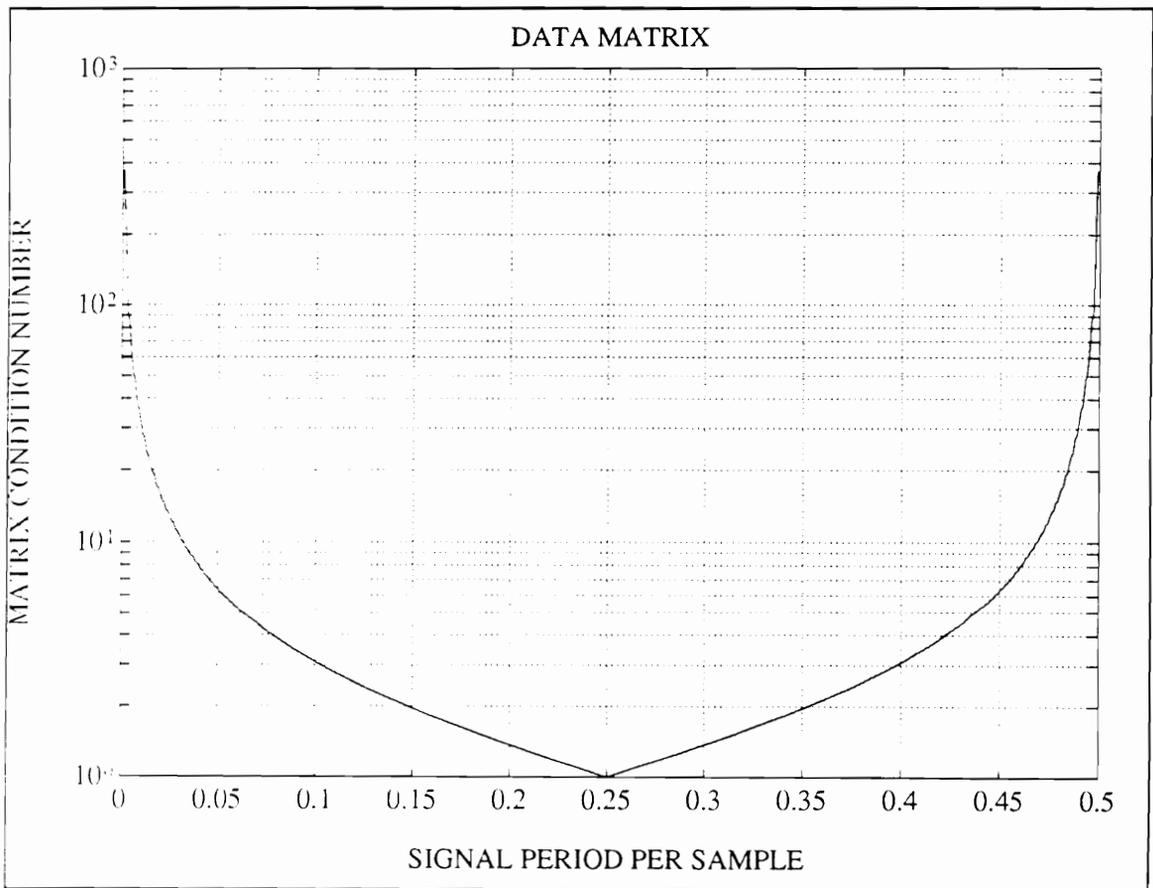
Figure 2 Data matrix condition number plotted versus signal period to samples ratio.

DYNAMIC ANALYSIS

VIBRATION OF BEAMS

The development of modal analysis methods require evaluation with physical structures. Beams are dynamically simple elements that are also very common models for many real-world applications. The lateral vibration of elastic beams is well understood. For these reasons, beams are often used to develop and test new modal analysis methods.

Classical beam theory, also known as Euler-Bernoulli beam theory, can be found in any basic vibrations text, such as Rao (1986) or Meirovitch (1975). The lateral vibration of a beam is a function of both time and location along the beam. As with all linear structures, beams vibrate in a linear combination of modes. Each mode has a characteristic mode shape comprised of sine, cosine, hyperbolic sine and hyperbolic cosine functions (complex and real exponential). Each mode vibrates sinusoidally at an associated natural frequency. The complete vibration can be expressed as

$$y(x,t) =$$

$$\sum_{j=1}^{m} [(C_{j,1}e^{\beta_j x} + C_{j,2}e^{-\beta_j x} + C_{j,3}e^{i\beta_j x} + C_{j,4}e^{-i\beta_j x})(C_{j,5}\sin(\omega_j t + \phi))] \qquad (2.14)$$

42

Timoshenko theory, or thick beam theory, takes into account the effects of rotatory inertia and shear deformation (Timoshenko, 1921). These adjustments shift the natural frequencies for beams that are thick compared to their length. Ebner and Billington (1968) have included the effects of damping on the vibration of Timoshenko beams.

The time-domain approaches outlined in previous sections involve analyzing the temporal function at each of several locations along the beam. The spatial function is then obtained from the resulting modal parameters. If spatial data is available, similar methods can be applied to the spatial function. This approach is called spatial modal analysis. An in-depth review of beam theory and development of spatial modal algorithms are presented in Chapter 4.

LASER VIBROMETERY

Vibration data is typically measured with piezoelectric accelerometers. If multiple response locations are desired, accelerometers must be placed on each location on the structure. It is very difficult to obtain high density spatial data with this method. A new instrumentation system utilizes a scanning laser vibrometer to measure the velocity of vibration at any location (subject to line-of-sight restrictions) on a structure. This enables high density spatial data to be easily obtained without physically attaching accelerometers

to the structure. This has the additional advantage that the structure is not mass-loaded by the instrumentation system.

The high density spatial data is crucial to spatial modal analysis. With this data, the spatial functions of vibrating structures can be fitted directly. Conventional algorithms for processing temporal modal data are not applicable for spatial domain analysis. New algorithms must therefore be investigated. Arruda, Sun and Mitchell have investigated spatial modal analysis using a singular value decomposition followed by a regressive discrete Fourier series analysis. (Arruda, et. al. 1992). Kochersberger has used a discrete Fourier transform - inverse Fourier transform method to extract angular velocities from spatial data (Kochersberger, et. al. 1991). Each of these methods rely on Fourier transforms, however, and can not be classed as parametric. West has investigated spatial beam analysis using Forsythe polynomials (West, et. al. 1993).

These new methods demonstrate the power of spatial modal analysis. A parametric spatial modal analysis should generate a modal model of the structure under investigation. The model should conform to all known theoretical constraints. Preferably, it should be based on the true form of the modal functions. New methods are developed in this research in an attempt to satisfy these requirements. Autoregressive methods appear to have much potential for spatial modal analysis of beams, because of their inherent AR nature. However, it is shown that difficulties arise with this method. A method based on

boundary condition analysis is shown to successfully meet the criteria. All theoretical constraints are included in the model, which is based directly on theory. It is a true spatial modal analysis method.

PARAMETRIC SPATIAL MODAL ANALYSIS OF BEAMS

The parametric spatial modal analysis of beams is possible only by the conjunction of the time series analysis methods, beam theory and scanning laser vibrometery. Time series analysis provides the foundation for the analysis technique, beam theory provides a knowledge of the underlying functions, and laser vibrometery provides the high spatial density data required. This research marks the first time these three have been combined in order to develop an algorithm for parametric spatial modal analysis.

To implement the method, operating shapes of beams are analyzed using time series techniques. Initially, this seems like a trivial task, however, a number of problems present themselves. The mode shapes of a beam can be inferred from Eq. 2.16 as

.

$$C_1e^{\beta x} + C_2e^{-\beta x} + C_3\sin(\beta x) + C_4\cos(\beta x)$$

Taking boundary conditions into account, the first mode of a beam consists of less than one period of a sine function (along with the exponential functions). Thus, optimum sampling is impossible. The problem is reduced for higher modes, but severe oversampling is always the case. Secondly, the presence of exponential functions has an additional negative impact on parameter estimation conditioning. The exponential components are most pronounced at the lower modes, and at the boundary of the beam. These two factors lead to an extremely ill-conditioned problem.

Three different methods are investigated. The first method is based on an AR model of the beam. The second method uses Newton's method for least squares approximation of the beam functions. Although the spatial-domain applications are unique, each of these approaches has close analogs in the time domain. Much of the background material presented in this chapter is used to develop these methods. They are presented in Chapter 5.

A third method is based on the unique capabilities of the scanning laser vibrometer along with classical beam theory. It is a method with no analog in time series analysis. It is an

entirely new method. As such, there is no supporting documentation in the literature. Chapter 6 is devoted to this method.

CHAPTER 3: SAMPLE RATE AND PARAMETRIC

SINUSOIDAL ESTIMATION

INTRODUCTION

Intuitive wisdom regarding choice of sample rate suggests that the higher the sample rate the better. It has been shown, however, that when the data is to be analyzed with algorithms that rely on difference equations, excessively high sample rates can be an impediment. Specifically, for sinusoidal analysis using autoregressive models, the optimum sample rate is four samples per period of the sinusoid. Sample rate to signal frequency ratios much higher or lower result in very poor estimates of the sinusoidal parameters. See Archibald and Wicks (1992, 1993) for a discussion of sample rate effects on parametric sinusoidal analysis.

This research demonstrates the link between the samples per sinusoid period ratio (SPP ratio) and the condition of the linear system used for the solution. This relationship is described and documented. The combined effects of noise and sample rate are investigated. The traditional matrix formulations are reviewed, and alternative

48

formulations are described. The use of a delay factor can reduce the effective sample rate without decimating the data. The efficacy of the delay factor is demonstrated for various signal-to-noise ratios. Also, a recursive algorithm is presented that enables successful analysis of sinusoidal signals with very broad-band content.

LINEAR SYSTEM SENSITIVITY AND CONDITION NUMBER

All of the sinusoidal estimation methods considered in this chapter involve solving a linear system of difference equations. The accuracy of the solution obtained by any of these methods depends on a number of factors, including signal-to-noise ratio and validity of assumptions. An additional factor that has a significant impact on solution accuracy is the condition of the linear system formed. The condition number of a linear system is a measure of the sensitivity of that system to permutations. If a system is well conditioned, the computed solution vector will most likely be close to the true solution. Conversely, if the system is poorly conditioned, the computed solution may vary considerably from the true solution. This can be true *even though the residual error is small* (Golub and Van Loan, 1989). The condition of a linear system is usually quantified in terms of the associated data matrix. Given the square linear system $Ax = b$, the matrix condition number, K, is defined for the matrix A as

$$K(A) = \|A\| \|A^{-1}\| \qquad\qquad (3.1)$$

where by definition $K(A) = \infty$ if A is singular. The condition number is a measure of the distance, in a consistent norm, to the set of singular matrices. Loosely, then, a high condition number indicates that a matrix is 'close' to being singular.

If $K(A)$ is large, A is said to be ill-conditioned. The solution vector x to the linear system $Ax = b$ will have few accurate digits. The relative error in the solution vector x can be $K(A)$ times as large as the relative errors in A and b. Thus, if the condition number is large, the solution vector is very susceptible to permutations in the data. In sinusoidal estimation, these permutations are assumed to be measurement noise. If the data matrix is well conditioned, i.e., $K(A)$ is small, then the solution vector x, which contains the autoregressive coefficients, will generally be very accurate even with very noisy data. This has been confirmed in practice, where frequencies have been accurately estimated from data with signal-to-noise ratios as small as 0 or -10dB. Conversely, if the system is ill-conditioned ($K(A)$ large) then large errors can be incurred in x even for very clean data. The residual error, defined as the quantity $\|Ax-b\|$, is often used to quantify the quality of the least squares model. However, the residual can be small for both well conditioned and ill-conditioned problems, despite the inaccuracy of the solution vector.

50

The magnitude of the residual is thus not sufficient for determining the quality of the model fit.

Note that the condition number is dependent on the matrix norm used. Any consistent norm is acceptable. In this chapter, only the 2-norm condition number will be used. It can be shown that the 2-norm condition number for square matrices is equal to the ratio of the largest and smallest singular values of A. Defining the matrix condition number as

$$K(A) = \frac{\sigma_1}{\sigma_n} \tag{3.2}$$

has several advantages. If A is $(n \times n)$, this definition is equivalent to Eq. 3.1 if the 2-norm is used (Golub and Van Loan, 1989). If A is $(m \times n)$, the definition in Eq. 3.2 is again equivalent to that in Eq. 3.1 provided that A^{-1} is replaced by the Moore-Penrose pseudoinverse. An additional advantage of Eq. 3.2 is that some of the sinusoidal estimation methods rely on singular value decomposition and thus no additional computation in involved in obtaining $K(A)$.

MATRIX FORMULATION

As stated above, all parametric sinusoidal estimation methods require the construction of a linear system of difference equations. These systems are based on the autoregressive nature of sinusoidal signals. It is shown in Appendix A2.1 that the discrete sinusoidal signal

$$y_k = \sum_{i=1}^{m} A_i \sin(\Omega_i k + \Phi_i) \qquad (3.3)$$

can be represented by the autoregressive difference equation

$$y_k = \sum_{i=1}^{2m} a_i y_{k-i} \qquad (3.4)$$

The relationship also holds for the autocorrelation function of sinusoids. This is easily confirmed by multiplying Eq. 3.4 by $y_{k+\tau}$ and taking the expectation. The result is a difference equation identical to Eq. 3.4 but with values of the autocorrelation function, that is

$$R_{yy}(\tau) = \sum_{i=1}^{2m} a_i R_{yy}(\tau - i) \qquad (3.5)$$

Equations 4 and 5 hold for any value of k and τ, respectively. Thus, they can be applied to any segment of the data vector or autocorrelation vector. Sequentially incrementing the index k through the data set generates a circulent system of equations, $Ya=y$. Y is the circulent data matrix, y is the right hand data vector, and a is the unknown vector of autoregressive coefficients. Likewise, if correlations are used, a similar circulent system $Ra=r$ is generated. The details for each case will be described. Throughout the discussion of these systems of equations, it is assumed that the data vector is of length N, and indexed from 1 to N (y_k, $k = \{1:N\}$).

Most of the early sinusoidal estimation methods used the autocorrelation function approach. These methods rely on the relationship in Eq. 3.5 to form the system $Ra=b$. The matrix thus formed, R, is circulent, and often Toeplitz. Because of the symmetry of the autocorrelation function, the matrix is generally, but not always, symmetric. The matrix constructed for Pisarenko Harmonic Decomposition is square, Toeplitz, and symmetric. Preservation of symmetry ensures that the poles lie on the unit circle. An example of such a matrix of dimension c is

$$
R = \begin{bmatrix}
R_{yy}(0) & R_{yy}(-1) & \cdots & R_{yy}(-(c-1)) \\
R_{yy}(1) & R_{yy}(0) & \cdots & R_{yy}(-(c-2)) \\
\vdots & & & \\
R_{yy}(c-1) & R_{yy}(c-2) & \cdots & R_{yy}(0)
\end{bmatrix}
$$

53

The vector **a** contains the unknown autoregressive coefficients of Eq. 3.5. Pisarenko Harmonic Decomposition involves the eigenanalysis of a homogenous system of equations. Thus, the right-hand vector **r** is the zero vector. For Example

$$a = \{ \ a_0 \ \ a_1 \ \ a_2 \ ... \ a_p \ \}^T$$

$$r = \{ \ 0 \ \ \ 0 \ \ \ 0 \ ... 0 \ \}^T$$

The autocorrelation approach is used by several methods in addition to Pisarenko Harmonic Decomposition (PHD) (Pisarenko, 1973). Some examples include the Levenson-Durbin algorithm and the Correlation Fit method (Cooper and Wright, 1989). Each of these methods use a correlation matrix. The exact matrix formulation varies from one method to the next. Pisarenko Harmonic Decomposition involves an eigenanalysis of a symmetric Toeplitz autocorrelation matrix. The autocorrelation lags range from $R_{xx}(-p)$ to $R_{xx}(p)$, where p is the autoregressive model order. (In the above example $p=c-1$.) Symmetry ensures that the resulting poles will lie on the unit circle. The correlation fit method performs a least squares fit of higher order autocorrelation terms using an overdetermined correlation matrix. The autocorrelation lags in this case range from $R_{xx}(\tau_i)$, $\tau_i > 0$ to $R_{xx}(\tau_j)$, where $(\tau_j - \tau_i)$ is greater than the model order p. The right-hand vector **r** is not zero, but contains the values of $R_{xx}(\tau)$. It can be used for either damped or

54

undamped sinusoids. However, it is possible to impose symmetry on the problem and thus force the poles to the unit circle.

Two new methods for estimating sinusoids in noise have been presented since 1985. Both the Oversize Total Least Squares (OTLS) (Archibald and Wicks, 1991) and Oversize Eigenmatrix Method (OEM) (Yang, 1985) fit the autoregressive relationship of Eq. 3.4 directly to the data. The autocorrelation function is not computed. The data matrix Y in each case is circulent and is not square. Both the OTLS and OEM approaches use singular value decomposition to solve a homogenous system of equations. The matrix Y has dimension $(r \times c)$, with $c \geq p$, and $r = (N-c)$. An example of the data matrix is

$$
Y = \begin{bmatrix}
y_c & y_{c-1} & y_{c-2} \cdots & y_1 \\
y_{c+1} & y_c & y_{c-1} \cdots & y_2 \\
y_{c+2} & y_{c+1} & y_c \cdots & y_3 \\
\vdots & & & \\
y_N & y_{N-1} & y_{N-2} \cdots & y_{N-c}
\end{bmatrix}
$$

The formulation of the data matrix or correlation matrix is important because it affects the conditioning of the matrix. In some situations, the above formulations are not

55

adequate. These situations are described, along with alternate formulations to improve matrix conditioning.

SAMPLE RATE AND MATRIX CONDITION

In dynamic analysis noise is often assumed to be additive, e.g.,

$$y_k = v_k + n_k.$$

If a pure sinusoid in additive noise is sampled at a rate much, much greater than the frequency of the sinusoid, none of the difference-equation based methods described above will provide accurate frequency estimates. This is true even for very high signal-to-noise ratios. In fact, in many such cases frequency estimates obtained by visual inspection of the data are much more accurate than those obtained from sinusoidal estimation algorithms. It has been noted that an optimum sample rate exists for parametric sinusoidal estimation. That sample rate is four samples per period of the sinusoid. At sample rates that are much higher (or much lower) than the optimum, very poor parameter estimates are usually obtained. The issue is one of sensitivity: as the sample rate diverges from the ideal, the system becomes much more sensitive to the effects of noise. This implies a relationship between sample rate and the conditioning of the system.

56

The sensitivity of all of the systems of equations described above can be characterized by a matrix condition number. This at first may seem incongruous for the several homogenous systems described. The matrix of a homogenous system is by definition singular, and the condition number of a singular matrix is infinity. However, the homogenous systems are actually constructed from non-homogenous systems of equations. For example, the homogenous system described above for OTLS and OEM can be derived from the system $Ya=y$.

$$Ya = y$$

or

$$[\; y_{k-1} \; y_{k-2} \; y_{k-3} \; \cdots \; y_{k-p}]a = y_k$$

An equivalent homogenous system can be formed by augmenting Y with y and a with 1 to obtain

$$[\; y_k \;/\; y_{k-1} \; y_{k-2} \; y_{k-3} \; \cdots \; y_{k-p}]\{1 \;/\; a\}^T = 0$$

or

$$Ya = 0$$

The condition number of the homogenous system is equivalent to the matrix condition number of the non-homogeneous system. The condition number is computed as the ratio of the largest to smallest singular values of the matrix Y or R, where these matrices are taken from the non-homogenous systems.

The condition number of the data matrix (or the correlation matrix) is a function of the sample rate to signal frequency ratio. This ratio is also known as the Samples Per (signal) Period ratio and is designated SPP. The reciprocal of this ratio is the signal period per sample ratio and is designated SPSR. These are significant quantities for describing the effects of matrix conditioning and sample rate.

The relationship between the condition numbers for both the data matrix and the correlation matrix formulations and the sample rate can be clearly seen in Figs. 3 and 4. These figures plot the matrix condition number for a data matrix and a correlation matrix versus the signal period per sample ratio (SPSR). Use of the SPSR for the horizontal axis results in a linear scale, and reveals the symmetry at high and low sample rates. These figures demonstrate how the character of the data and correlation matrices change with respect to sample rate. Both figures were generated by synthesizing a pure sinusoidal signal with no additive noise, sampled at 499 different rates. A circulent data matrix, as described above, was constructed for each sample rate. The matrix condition was

58

calculated by taking the ratio of the largest to smallest singular values. Figure 4 was

constructed using estimated correlations of the same sinusoidal data.
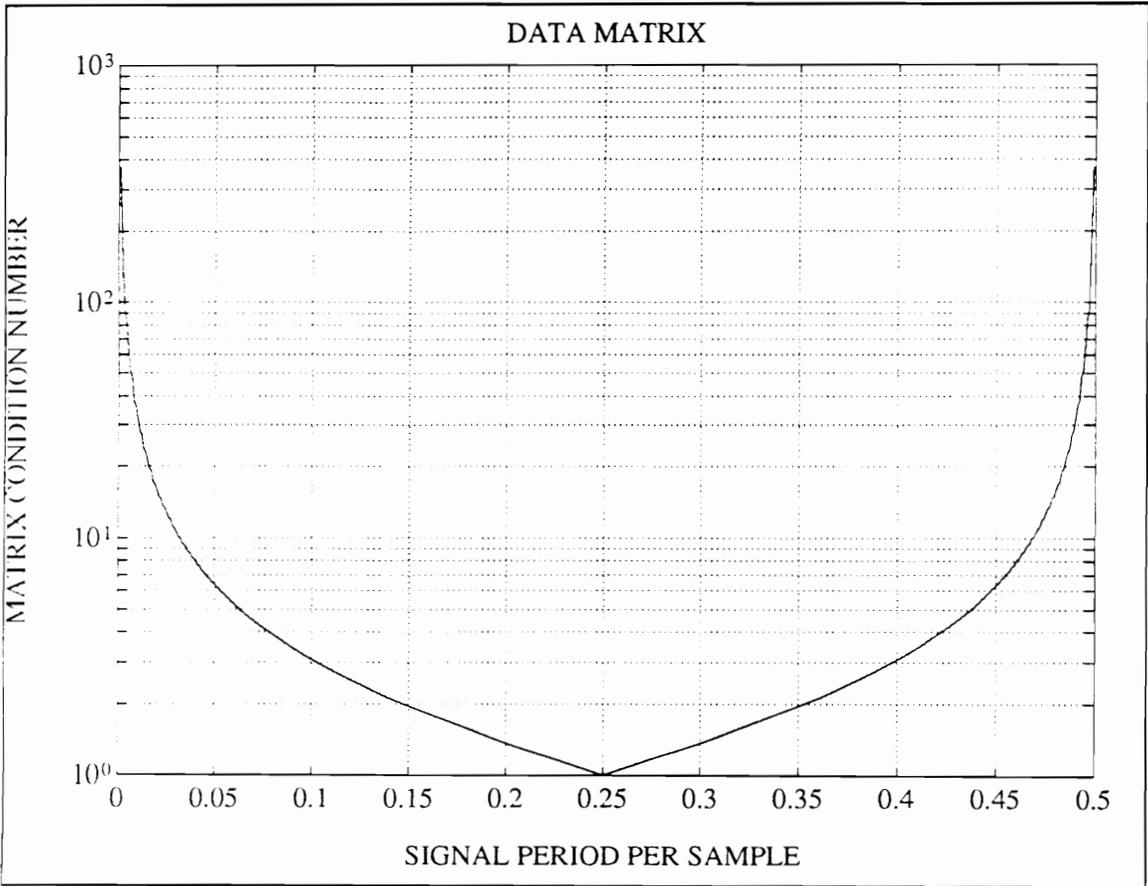
Figure 3 Data matrix condition number plotted versus signal period to samples ratio.

59
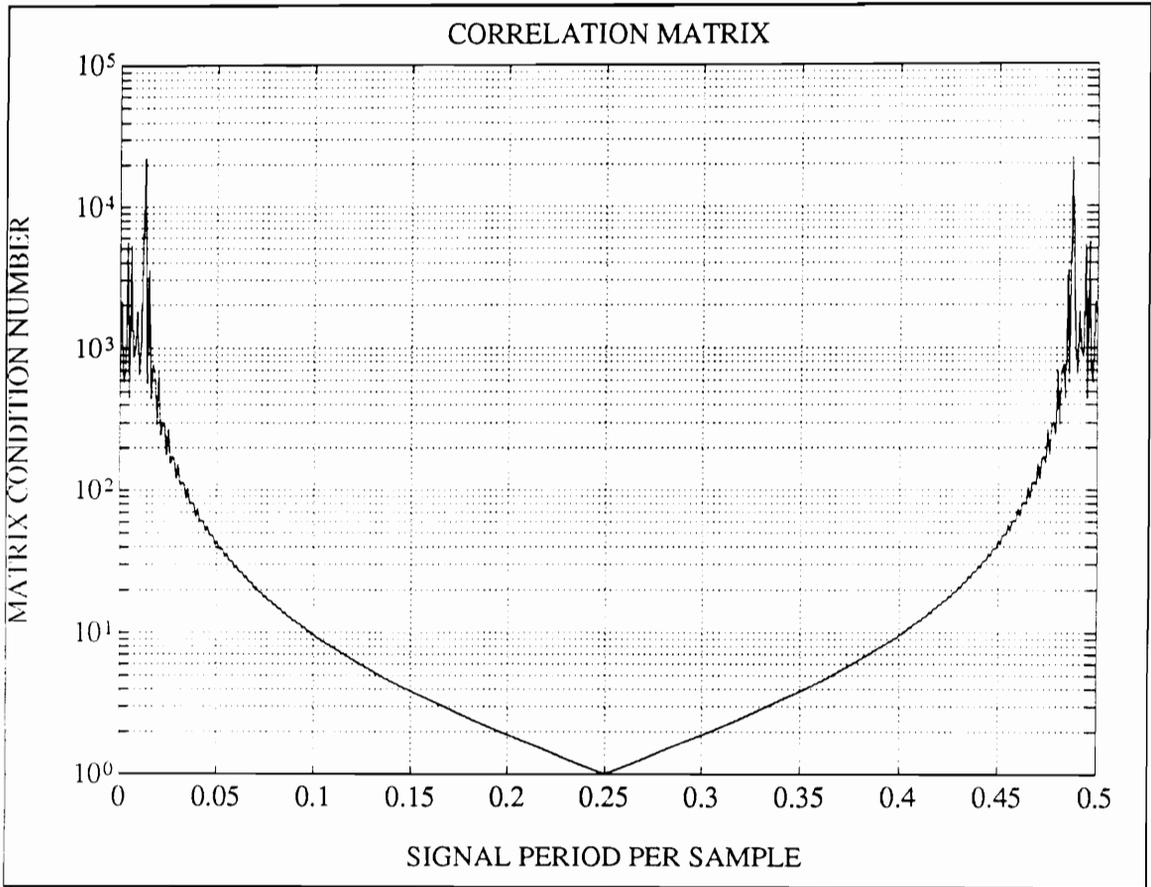
Figure 4 Correlation matrix condition number versus signal period to samples ratio.

Both figures show a distinct minimum at SPSR of 0.25. This corresponds to 4 samples per signal period. At very high and very low SPSR values, the condition number becomes large for both matrix types. The correlation matrix formulation indicates a more rapid increase in condition number with SPSR increasing/decreasing from 0.25. This indicates that the sinusoidal estimation problem is extremely sensitive to noise at high or low SPP values. This explains the poor results described above for sinusoids sampled at rates much, much greater than the sinusoidal frequency.

60

An intuitive explanation of this phenomena is easily provided. The increase in matrix condition number for extreme sample rates can be understood by considering the columns of the data matrix. The first column and the second column are each segments of the data vector. They are both sinusoids of equal magnitude and frequency, with a phase difference equal to one sample period. If the sample rate is very high compared to the period of the sinusoid, the phase difference is very small. Thus, the two columns are nearly identical. Figure 5 plots a sinusoid along with the first two columns of the data matrix constructed from that sinusoid. (Each column has an amplitude constant added to it to prevent the three plots from overlaying each other.) A relatively high sample rate of 50 samples per period (.02 SPSR) was used. It is readily seen that the two columns are very similar. Intuitively, when two columns of a matrix are nearly identical, they can be thought of as being 'close' to dependent. Thus the matrix is 'close' to being singular. This is exactly what the matrix condition number measures.

At very low sample rates a similar phenomena occurs, because of the periodic nature of sinusoids. At an SPSR ratio approaching 0.5 (the Nyquist frequency) the phase difference between the two columns is very close to 180°. Again, the columns are very similar with the difference of a sign change. The greatest difference between the columns will occur at a phase lag of 90°. This corresponds to 4 samples per signal period (0.25 SPSR). Based

61
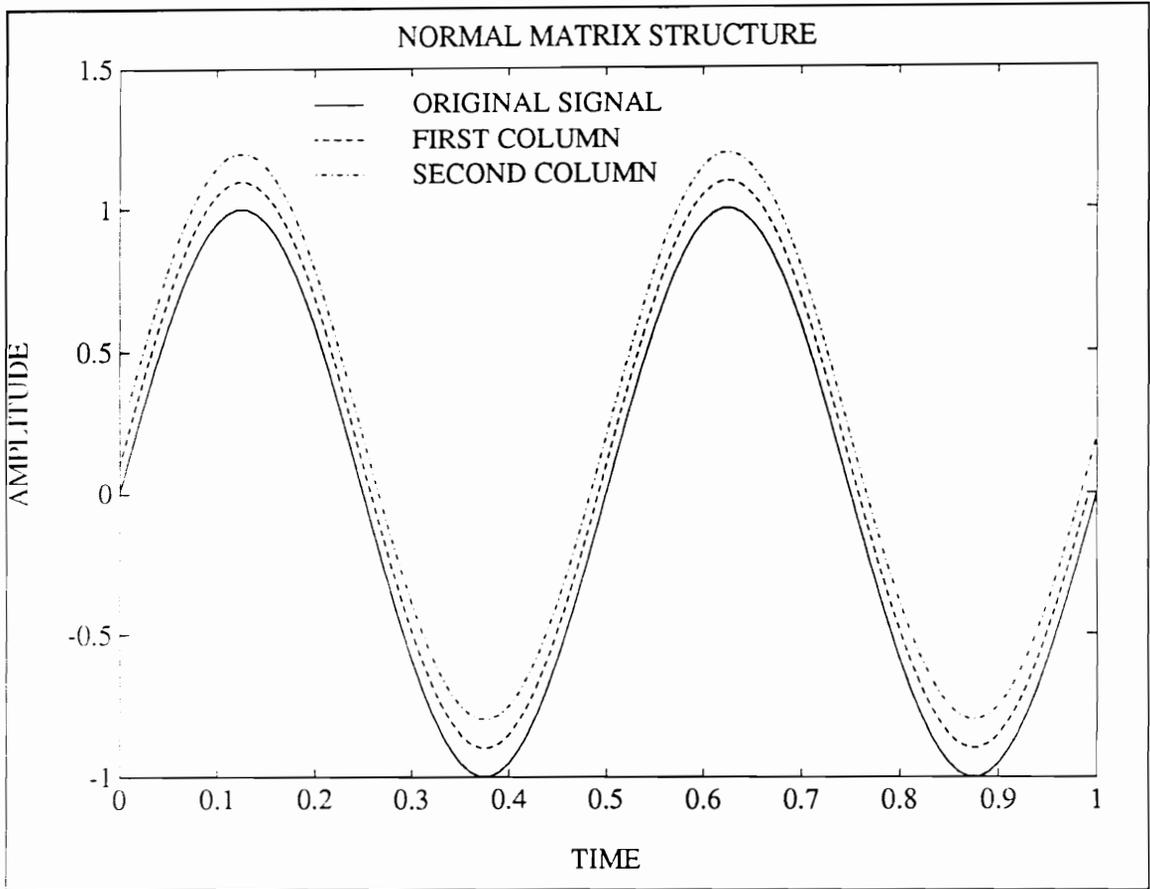
Figure 5 First and second columns of the data matrix of an oversampled sinusoid, showing the small phase lag.

on this logic, the optimum matrix condition is expected to occur at 0.25 SPSR. The figures and prior research indicate that this is, in fact, the case.

PARAMETER ESTIMATION

62

The objective of parametric sinusoidal estimation is to obtain accurate estimates of sinusoidal parameters from data that is corrupted by additive noise. Accurate parameter estimates depend in turn on accurate estimation of the autoregressive coefficients. This requires a system that is sufficiently well-conditioned so as to render it insensitive to measurement noise. The degradation of matrix condition with extreme sample rates suggests that poor estimates will be obtained at these sample rates. This has in fact been observed. Furthermore, the impact of matrix condition on parameter estimates is very noise dependent. As noise levels vary, the required sensitivity of the system varies. This is expected, since noise corrupts the sinusoidal data.

All measured data includes noise. It is assumed here that this noise is additive to the true, or deterministic, sinusoidal signal and that the noise is normally distributed. Given the measured sinusoid y_k, the true sinusoid v_k, and the random noise n_k, these assumptions can be summarized by

$$y_k = v_k + n_k$$

$$n \sim N(0, \sigma)$$

The noise tends to make the matrix columns more independent. Thus the condition number of the *measured* data matrix will be smaller than that of the true data matrix.

However, the noise also corrupts the data. The true data matrix condition number is a measure of the sensitivity of the problem to noise. Thus, accurate parameter estimation depends on the combination of sample rate and noise level. When the sinusoid is sampled near 4 samples per period (0.25 SPSR) parameter estimation is relatively insensitive to noise. However, as the sample rate increases or decreases, accurate parameter estimates become more dependent on high signal-to-noise ratios.

An experiment illustrates the combined effects of sample rate and noise on sinusoidal parameter estimation. The experiment involves determination of the variance in frequency estimates for each of 499 SPSR and 3 SNR values. The result indicates that the variance of frequency estimates is roughly proportional to both the noise level and the matrix condition number (as plotted in Fig. 1).

The experiment was implemented as follows:

    A.   For SPSR value from 0.001 to 0.499, in increments of 0.001,

        1.   Synthesize a discrete sinusoidal signal $v_k = sin(\Omega k)$

        2.   Generate a normally distributed, mean zero random series n_k.

3. Add v_k and n_k to produce the simulated measured series $y_k=v_k+n_k$.

4. Estimate signal frequency using Symmetric OTLS method. Save the result.

5. Repeat steps 2-4 50 times. Compute the variance and mean of the frequency estimates.

B. Repeat loop A for each of three SNR: 40, 20 and 0dB.

The experiment was performed using PC-Matlab software. A listing of the script file is included in appendix A3.1. Each sample rate and noise case was analyzed using the OTLS method. Symmetry was imposed in order to constrain the poles to the unit circle. The results are plotted in Fig. 6.

Inspection of Fig. 6 indicates results consistent with prior observations of matrix conditioning and SPSR value. The variance of the frequency estimates increases dramatically with increasing noise level. The change in frequency variance with SPSR
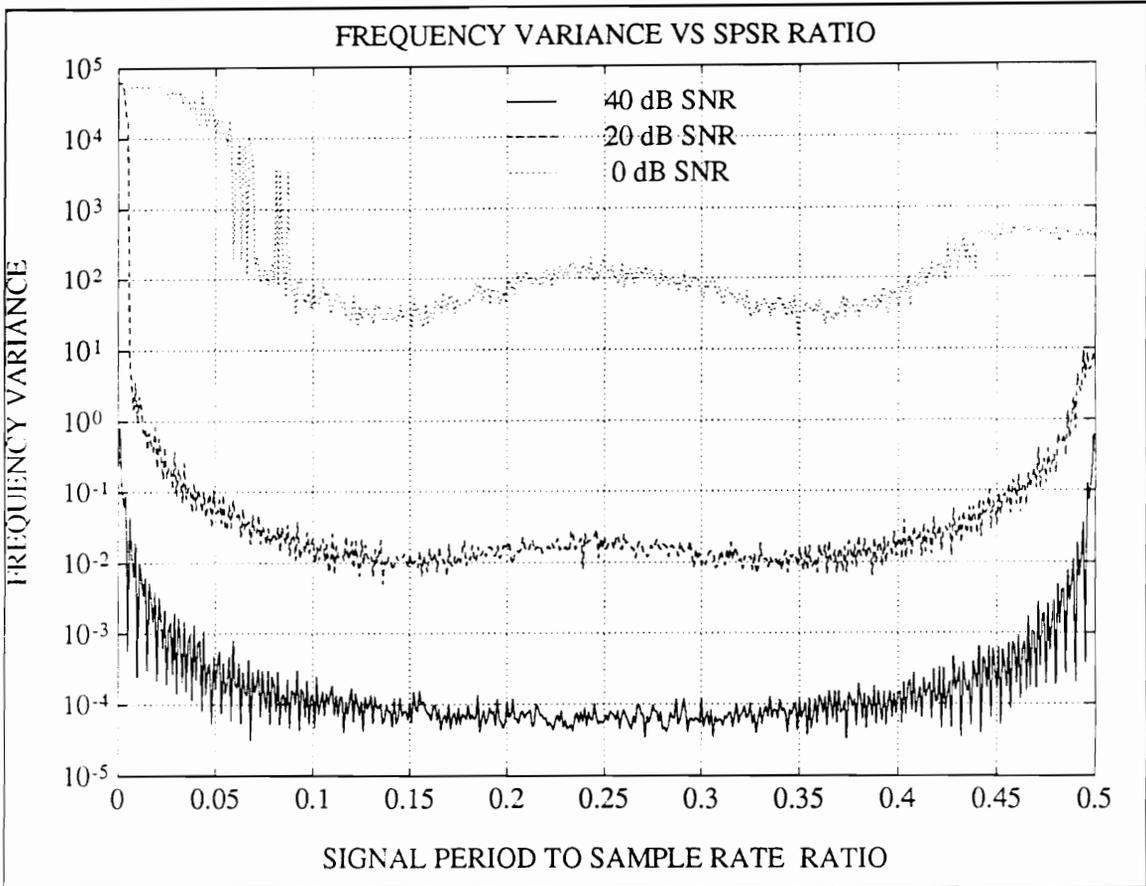
Figure 6 Frequency variance computed for different noise
levels and sample rates. Number of averages = 50.

follows reasonably well the change in matrix condition number with SPSR. However, a

slight increase in variance is observed near SPSR = 0.25 for the 20dB and 0dB noise

cases. The reason for this increase is unknown. The conclusion drawn from Fig. 6 is that

AR-based sinusoidal estimation methods have a dramatic increase in sensitivity to noise

as the SPSR diverges from the optimum of 0.25. Thus both signal-to-noise ratio and

sample points per signal period ratio are important parameters to keep in mind when

estimating sinusoidal signals.

DELAYED MATRIX FORMULATION

The ideal approach to parametric sinusoidal estimation is to sample at or near the optimum 0.25 SPSR. In some applications this is not possible, however. Sometimes sample rates many times greater than the signal frequency must be employed. Many of these applications are restricted by the data -- often only a few signal periods, or even less than one period of the signal is available. Examples of such cases may include transient signals, short-lived signals, or signals that are of such low frequency that data acquisition time becomes limiting. Another example is the shape of a vibrating beam. This application will be extensively treated in the following chapter. In all of these cases it is still possible to accurately estimate the sinusoidal signal, provided some modifications are made to the matrix formulations.

If sinusoidal data has been sampled at very high sample rates, accurate parameter estimates can still be obtained. This can be done by introducing a delay factor, D, into the data matrix formulation. The autoregressive relations in Eqs. 3.4 and 3.5 hold for any sample interval. (Although the values of the coefficients are dependent on the particular sample interval chosen). Thus if the delay factor is some positive integer D, then Eqs. 3.4 and 3.5 can be modified respectively as

$$y_k = \sum_{i=1}^{p} a_i y_{k-iD} \tag{3.6}$$

$$R_{xx}(\tau) = \sum_{i=1}^{p} a_i R_{xx}(\tau - iD) \tag{3.7}$$

These equations can be used, with proper choice of D, to improve the condition of the data and correlation matrices. The columns of the data matrix, instead of being separated by one sample, are separated by D samples. This increases the phase lag between columns. It also decreases the samples points per signal period ratio. The effective sample interval is the product of the delay factor and the original sample interval. For example, if the original, or natural, sample interval is Δ, the effective sample interval is $D\Delta$. In extracting frequencies from the system poles, the effective sample interval <u>must</u> be used. Improperly scaled frequencies will result if the natural sample interval is used.

The impact of the delay factor on matrix formulation is illustrated in Fig. 7. This figure is analogous to Fig. 5. The difference is that a delay factor of $D=12$ has been introduced. It can be seen that the two columns of the delayed data matrix are well separated and independent.

68
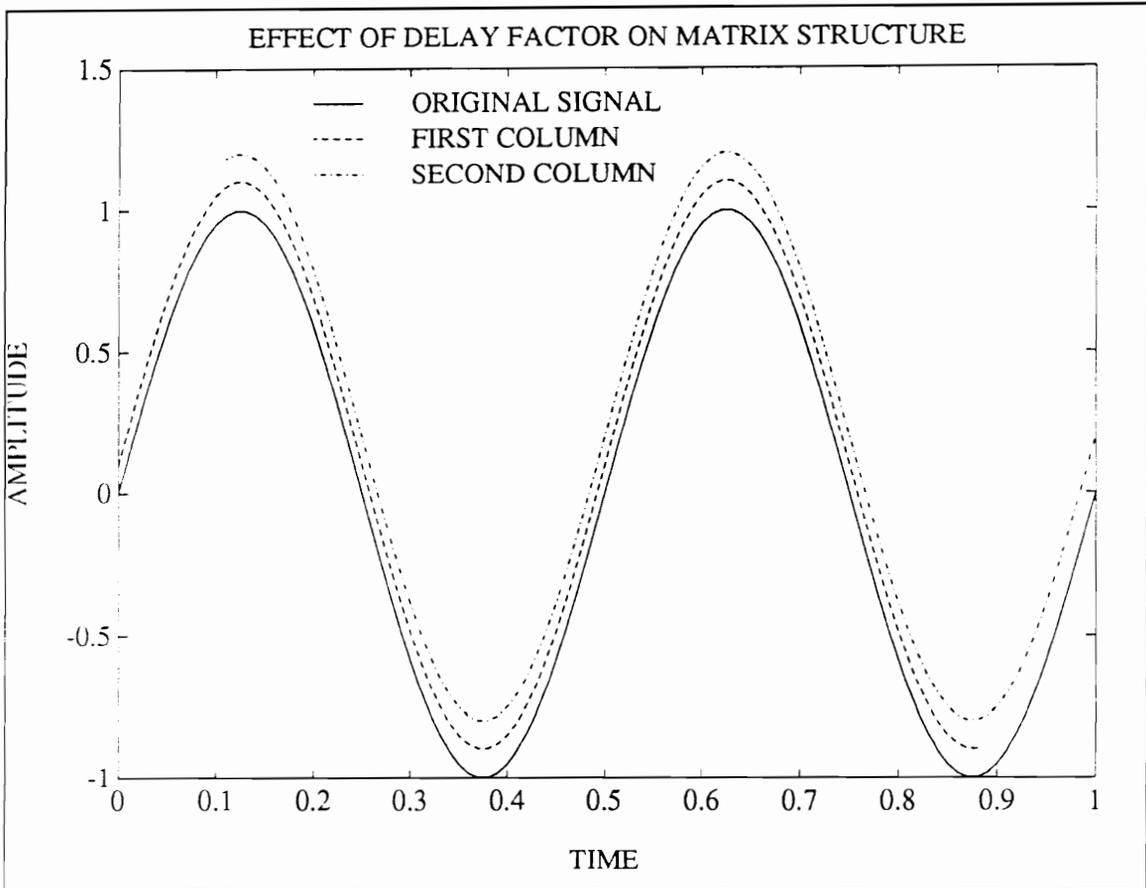
Figure 7 First two columns of a delayed data matrix.

The delayed matrix method is easily implemented. The delay factor should be chosen such that the effective SPSR is as close as practical to 0.25. The effective SPSR is given by

$$Effective\ SPSR = fD\Delta$$

where f is the signal frequency. In order to construct a delayed data matrix, the data vector is divided into a number of overlapping segments, each segment beginning D

69

samples after the preceding segment. If there are c columns, the length of each segment is $N-(c-1)D$. The resulting data matrix will have the following form:

$$\begin{bmatrix} y_{(c-1)D+1} & y_{(c-2)D+1} & \cdots & y_{D+1} & y_1 \\ y_{(c-1)D+2} & y_{(c-2)D+2} & \cdots & y_{D+2} & y_2 \\ y_{(c-1)D+3} & y_{(c-2)D+3} & \cdots & y_{D+3} & y_5 \\ \vdots & & & & \\ y_N & y_{N-D} & \cdots & y_{N-(c-2)D} & y_{N-(c-1)D} \end{bmatrix}$$

A delayed correlation matrix can likewise be constructed by using integer multiple of D lags i.e. $R_{xx}(0)$, $R_{xx}(D)$, $R_{xx}(2D)$, etc.

A dramatic improvement in parameter accuracy can be obtained using an appropriate delay factor. This improvement is illustrated by a second experiment. This experiment involves computing the variance in frequency estimates at each of 125 delay factors for a highly oversampled sinusoidal signal (SPP = 500). Results indicate that a substantial reduction in variance can be achieved by using an appropriate delay factor.

The experiment was conducted with the following steps:

70

1. Synthesize a discrete sinusoidal signal, $v_k = sin(\Omega k)$, with SPSR = 0.002.

2. Generate a normally distributed, mean zero random series n_k.

3. Add the sinusoidal component and the random component to generate a simulated measured signal $y_k = v_k + n_k$.

4. Estimate the sinusoidal frequency using OTLS method with a delay factor D.

5. Repeat step 4 125 times, for $D = 1:125$. Save the estimated frequencies.

6. Repeat steps 2-5 50 times and compute the variance of the frequency estimate for each delay factor value.

7. Repeat steps 2-6 three times, for SNR = 40, 20, and 0dB.

The results of this experiment are plotted in Fig. 8. This figure reveals that the frequency variance decreases rapidly for increasing D, particularly at high signal-to-noise ratios. The
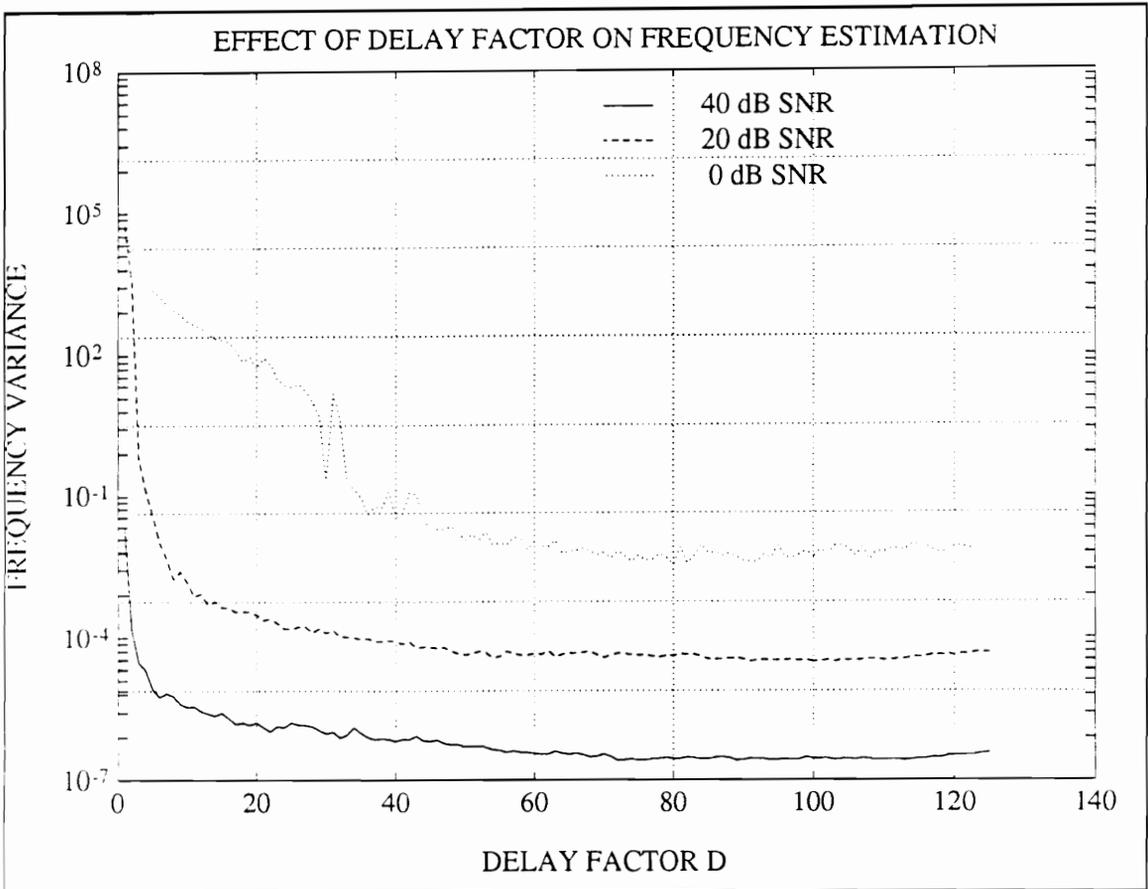
Figure 8 Effect of delay factor on frequency estimation. Number of averages = 50.

0dB case requires the highest delay factor, *D=40*. This is not unexpected. In all three noise cases, selection of a suitable delay factor results in satisfactory frequency estimation. Unpredictable estimates result if no delay factor is used. This illustrates the condition improvement provided by the delayed matrix formulation. It is essentially a method to decrease the noise sensitivity of the parametric sinusoidal estimation problem.

72

PARAMETRIC SINUSOIDAL ESTIMATION

The objective of parametric sinusoidal estimation is to obtain accurate estimates of the sinusoidal frequencies, amplitudes, and phases. The first step is frequency estimation. Amplitude and phase estimates are based on knowledge of frequency. However, it has been shown here that accurate frequency estimation is dependent on the sinusoidal frequency itself. This leads to an interesting paradox. The primary objective of these methods is estimating unknown frequencies, but accurate estimates depend on knowledge of those frequencies. How, then, is an appropriate sample rate to be chosen for unknown sinusoids? Several approaches can be taken.

In many applications, the unknown sinusoid lies within a known frequency bandwidth. Often, the bandwidth is narrow enough and signal-to-noise ratio high enough to preclude sample rate problems. A sample rate four times the center of the bandwidth is often satisfactory. This is the most common case. Any of the sinusoidal estimation methods mentioned can be used successfully with no modifications. The successful histories of these methods attest to the validity this approach.

Note that it is the presence of very low frequency signals that cause problems. In practice, most discrete data is obtained from sampling a continuous signal. Anti-aliasing filters are recommended for all sampling operations. Typically, filter cut-off frequencies are chosen

about 78% of the Nyquist frequency. Any signal content above this frequency is disregarded. This value corresponds to a SPSR of 0.4, which generally does not lead to enough ill-conditioning to impact parameter estimates (See Fig. 6). Thus, any time anti-aliasing filters are used, condition problems associated with high-frequency components (SPSR approaching 0.5) can be neglected.

If it is known a-priori that the component frequencies are much, much lower than the sample rate, use of the delay factor in matrix formulation is in order. This is typically the case when only very short (in terms of signal period) sinusoidal data segments are available. The best choice of the delay factor D depends on data record length and signal-to-noise ratio. Seldom is the optimum value of $D = 0.25/f\Delta$ either obtainable or necessary. As the delay factor is increased, the number of possible equations, and consequently the statistical degrees of freedom, decrease. This must be balanced against the beneficial effects of the delay. In practice, the best approach is to process the data using different values of D and check the frequencies for consistency. As Fig. 7 indicates, there is a broad range of acceptable values.

The most difficult case occurs if a signal contains multiple sinusoids with frequencies differing by several orders of magnitude. In this case, the higher frequency components may be accurately resolved without the use of a delay factor. However, the lower frequency components will only be resolved with an appropriate delay. Unfortunately, use

74

of the delay factor causes the higher frequency components to be aliased. It is impossible to determine if a component is aliased without additional information. The solution to this dilemma is incremental delay processing. This involves processing the data multiple times while incrementing the delay factor each iteration. This way the higher frequency components are identified first, and thus the aliases at higher delays can be tracked and identified.

Once frequency estimates are available, it is a simple task to determine if any of those frequencies will be aliased at the next higher delay factor. Specifically, a sinusoid with frequency f will be aliased if

$$f > \frac{1}{2D\Delta} \tag{7.2}$$

Furthermore, the aliased frequency will be

$$f_A = \begin{cases} \left(\dfrac{1}{2D\Delta} - f \right) & n \ odd \\ f & n \ even \end{cases} \tag{7.3}$$

75

At each iteration, all previously determined frequencies are checked using Eq. 3.8 to determine if they will be aliased in the next iteration. If so, the aliases frequencies are computed with Eq. 3.9. The delay factor is incremented, and the sinusoidal estimation method is again employed. The new estimated frequencies are compared with the aliases estimates previously computed. New sinusoids that are unaccounted for are considered to be low frequency components.

The method has several advantages and disadvantages. It can be very accurate and reliable. For the analysis of signals with sinusoidal components interspersed over a very broad frequency band, it may be the only method available that will accurately estimate all frequencies. It is very costly computationally, however. In general, unless it is known or suspected that broad-band sinusoidal components are present, it is probably best to use ordinary sinusoidal estimation techniques. An additional benefit is that no assumptions need be made regarding model order. As the frequencies are tracked, the number of occurrences of each can be tabulated. Any random, or spurious components will seldom occur more than once. However, true frequencies should reoccur at more than one iteration. Thus checking the frequency estimates against the number of occurrences provides a good estimate of the true sinusoidal components.

The INCremental Delayed Oversize Total Least Squares (INCDOTLS) algorithm is an implementation of the incremental delay method. It relies on the OTLS method for

frequency estimates. Any of the parametric sinusoidal estimation methods could be substituted, however. Following is a summary of the INCDOTLS algorithm:

INCDOTLS Algorithm for broad-band sinusoidal estimation.

1. Estimate first frequency set $\{f_1\}$ using OTLS method.

2. Increment delay factor D. Any reasonable increment may be used.

3. Check if any components in $\{f_1\}$ will be aliased at new delay using Eq. 3.8. Replace those components with their aliases, as computed by Eq. 3.9.

4. Estimate new frequency set $\{f_2\}$ using Delayed OTLS method.

5. Compare $\{f_1\}$ and $\{f_2\}$.

    If any frequencies compare within a pre-set tolerance, average old and new frequencies and compute true (unaliased) frequencies. Update f_1 and increment frequency counter.

If any frequencies do not compare within tolerance, add the new frequencies to f_1 and initialize frequency counter to 1.

6. Repeat steps 2-5 for remaining delay values.

7. Check frequency set $\{f_1\}$ and its counter for multiple occurrences of particular frequencies. Choose the most often occurring subset of $\{f_1\}$ as the true frequency set.

The INCDOTLS algorithm has been implemented in a PC-Matlab script file. A listing of this file is included in appendix A3.3.

EXAMPLE

An example will illustrate the problems and techniques described in this chapter. A sinusoidal signal with three components whose frequencies are widely spaced is used. A synthesized signal contains sinusoids of unit amplitude and zero phase at 7.00, 0.65, and 0.02 Hz. The signal is sampled at 20 Hz. This results is SPSRs of 0.35, 0.0325, and 0.001 respectively (2.86,30.8,and 1000 SPP). Normally distributed, mean zero random noise is added to the signal so as to obtain a signal-to-noise ratio of 20dB. This data is plotted in

Figure 9. Sinusoidal analysis using ordinary OTLS method, the delayed OTLS method, and the INCDOTLS algorithm reveals the differences and advantages of each.

Visual inspection of the data is often a good way to obtain a general idea of its content. The data in Fig. 9 shows definite sinusoidal content at high and intermediate frequencies. In addition a very low frequency drift is apparent, although visual inspection can not determine that this drift is sinusoidal.
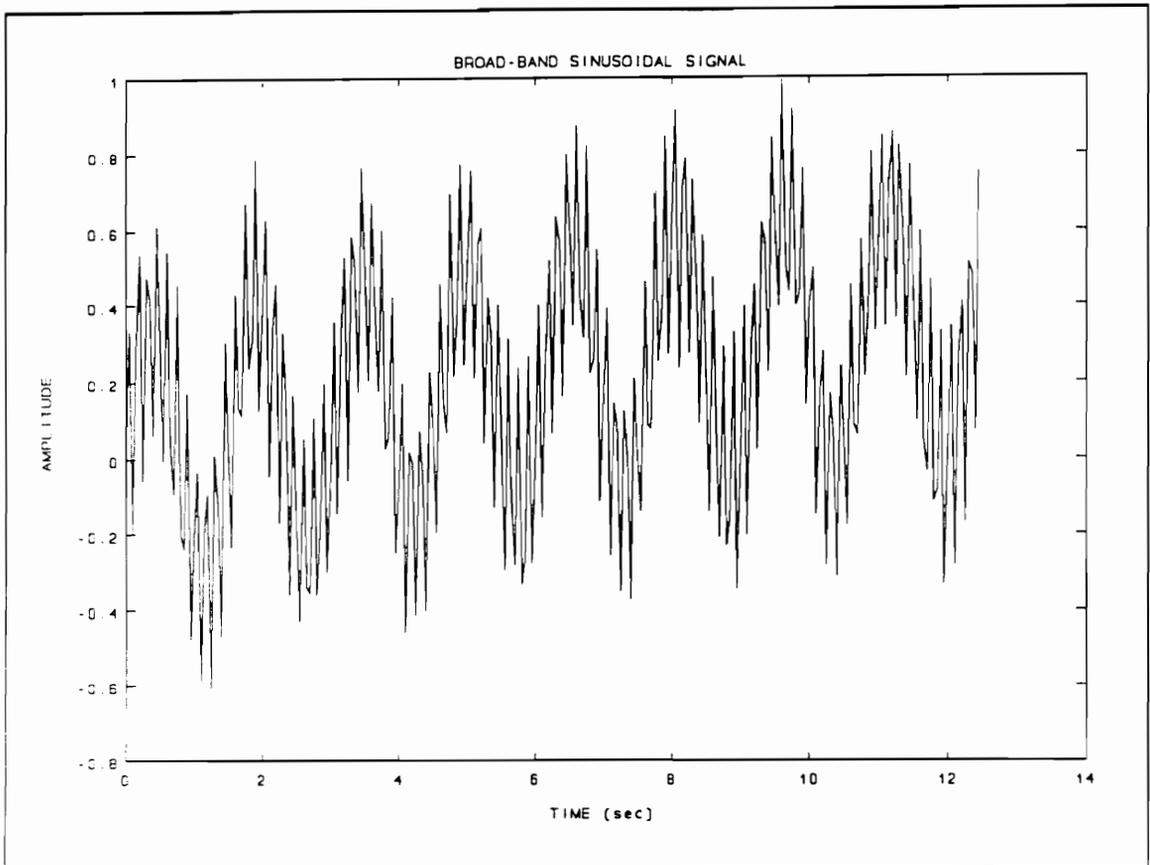
Figure 9 Broad-band sinusoidal data used in example.

The data is analyzed first with OTLS. This method only identifies the two highest frequencies, and one of them is in error by over 30%. However, the highest frequency, 7.0000 Hz is exact to 5 significant figures. It is not possible to resolve the very low frequency component. Numerical results are tabulated in Table I.

80

The delayed OTLS method yields much more accurate estimates of the intermediate and low frequency components. However, the high, and in one case the intermediate frequency is aliased. Several examples are given, each with a different delay factor. Some interesting observations can be drawn from the table. First, the low frequency component is difficult to estimate accurately, and requires a delay factor greater than 10. Second, without prior knowledge of the true frequencies, the aliased frequencies (denoted with a * in the table) would be incorrectly interpreted. Thirdly, in some cases the higher component frequencies drop out altogether. This is caused in the D=10 and D=20 cases because the true frequency is an integer multiple of the effective Nyquist frequency. Thus the apparent (aliased) frequency in these cases would be zero.

The frequency estimates show considerable improvement in the incremental delayed method. Again, several cases are included for comparison. The difference between the cases is the range of delay factor values used. The low frequency component is still not resolved nearly as accurately as the higher frequencies. However, all three frequencies are clearly present. It is possible that additional iterations could improve the accuracy of the low frequency component estimate.

This example reveals the problems associated with sinusoidal estimation of very widely spaced sinusoids. It also shows the advantages of the incremental delay method for identifying all of the sinusoidal components. Once these frequencies are known, the

amplitudes and phases can be found using a linear least squares procedure in the usual manner.

Table I Results of Broad-band sinusoidal analysis using various methods.

Method		Frequencies (Hz)			% Error		
True Values		7.0000	0.6500	0.0200	--	--	--
CTLS	D=7	7.0000	0.4511	--	0.00	-30.6	--
DTLS	D=5	6.9960*	0.6445	--	-0.40	-0.85	--
	D=10	--	0.6502	--	--	0.03	--
	D=15	6.3336*	0.6477	0.0199	0.09	-0.35	-0.05
	D=20	--	0.3500*	0.0140	--	0.00	-30.0
INCDTLS	D=1:20	7.0011	0.6480	0.0231	0.01	-.31	15.5
	D=1:25	7.0010	0.6485	0.0218	0.01	-0.23	9.00
	D=1:30	7.0007	0.6489	0.0224	0.01	-0.17	12.0

CONCLUSION

The research presented in this chapter documents the relationship between the sensitivity of parametric sinusoidal estimation methods and the sample rate to signal frequency ratio. At very large or very small values of this ratio, the estimation problem becomes very sensitive to noise. These findings are important to investigators using parametric time-domain approaches to modal analysis. They are also important to a wide range of other

82

applications. Sinusoidal estimation is used by scientists and engineers in many disciplines. The findings presented here are applicable and important to all of them.

It is hoped that the algorithms and comments presented here will prove useful to many researchers and analysts. The delayed matrix formulation and the incremental delay method are additional tools for the signal processing analyst. In those situations where they are applicable, they can be beneficial.

Parametric spatial modal analysis, described in detail in the following chapter, is one example in which these methods are required. The methods presented there would not be possible without this work.

As with most research, as many questions are raised as are answered. Further study should be applied to answer the following questions

What is the cause of the slight increase in frequency variance observed near SPSR = 0.25 in Fig. 6?

What is the effect on parameter estimation, if any, of phase variations of the sinusoids?

Is it possible to further improve the sensitivity of current algorithms?

These are just a few of the questions that should be addressed.

CHAPTER 4: REVIEW OF BEAM THEORY

INTRODUCTION

The objective of parametric spatial modal analysis is to derive a modal model of a vibrating structure directly from spatially distributed data. The technology enabling direct measurement of spatial data is quite new. High-quality, high-density spatial data has not been available prior to the advent of the scanning laser vibrometer. This technology allows measured data to be fitted directly to the spatial functions predicted by theory. In the case of laterally vibrating beams, this means that a measured operating shape can be fitted either to Euler-Bernoulli beam theory or Timoshenko beam theory. Several approaches are available. The theoretical beam shape functions satisfy an autoregressive relationship. Thus, autoregressive modeling is one approach. Multidimensional search methods, such as Newton's method, is another. It is also possible to use frequency-domain methods. Since this dissertation is concerned with parametric spatial modal analysis, only the first two approaches will be treated.

Euler-Bernoulli beam theory, or classical beam theory, disregards the effects of rotary inertia and shear deformation. It is applicable to the lower modes of slender beams. Timoshenko beam theory includes rotary inertia and shear deformation. These effects

must be included for short, stubby beams. Most of the beams considered in this research are slender, and thus the simpler Euler-Bernoulli theory is used for a theoretical basis.

This chapter describes both Euler-Bernoulli and Timoshenko beam theories. In subsequent chapters,different parametric spatial modal analysis methods are presented that are based on Euler-Bernoulli theory. Timoshenko theory is important for determining the applicability of these methods.

The spatial beam problem is very difficult. It will be shown that the data matrices are inherently ill-conditioned. In addition, the model is very sensitive to parameter accuracy. Thus, obtaining a meaningful model is numerically a daunting task. In fact, multi-mode analysis is too difficult to be feasible using the minimum residual models. However, excellent results can be obtained using the boundary condition analysis described in Chapter 6. Good result can also be obtained from single mode, or phase resonance, testing, using either of two minimum residual approaches.

The relative advantages and limitations of each method are discussed in subsequent chapters. Each method aims to derive a modal model, based on spatial data, that agrees with theory. The first method is based on an autoregressive model. It is very flexible in that excessive constraints are not placed on the model. However, it suffers limitations in accuracy. The second technique is based on a multi-dimensional Newton's method. It

provides higher accuracy, but care must be used to find suitable initial estimates for parameters. The two methods can be used together in that the autoregressive method can generate initial estimates that are subsequently 'polished' by Newton's method.

The boundary condition analysis is based directly on Euler-Bernoulli theory. It includes all constraints that are inherent in that theory. It is shown in Chapter 8 that the method is a powerful modelling tool. A solid foundation in classical beam theory is a prerequisite for understanding this method, however. It is therefore reviewed in some detail. Timoshenko theory is a higher-order beam theory. It is very useful for determining the applicability of the simpler, classical, theory. If both theories predict very similar natural frequencies, then it can be assumed that Euler-Bernoulli theory is sufficient. This may be an important check before using the boundary condition analysis. Thus, a brief review of Timoshenko theory is included as well.

BEAM THEORY - MODE SHAPES OF VIBRATING BEAMS

EULER-BERNOULLI BEAM THEORY

The dynamical characteristics of beams is an important topic for dynamicists. Simple beam theory is well understood, and is extensively used in mechanical design and

analysis. The simple beam has thus become a modeling element for design and analysis models. Many mechanical structures can be idealized as beams, facilitating dynamic analysis considerably. Finite element analysis makes extensive use of beam elements for analysis of many complex structures. Because simple beams are a fundamental dynamic element, they make good test beds for research involving new measurement and analysis tools. Parametric spatial modal analysis involves both innovative measurement methods, i.e., laser vibrometery, and new analysis methods. Thus, beams have been chosen for evaluation and development of these methods.

A review of beam theory is presented. Simple beam theory, also known as Euler-Bernoulli beam theory, is reviewed in some depth, particularly for the case of a harmonic exciting force. It is of interest to note that the mode shapes of a beam vibrating in accordance with simple beam theory are linear combinations of exponential functions. This is convenient from the parametric analyst's point of view, because exponential functions are easily analyzed. More advanced theories, attributed to Timoshenko, will also be discussed. These theories take into account rotatory inertia and shear deformation. A discussion of anticlastic effects of beams in bending will also be included. The inclusion of this effect forces the analyst to acknowledge the two-dimensional aspects of beam vibration.

SIMPLE BEAM THEORY: A simple theory of beam vibration can be developed from the Euler-Bernoulli theory of bending of beams. Since detailed derivations of the theory are abundant in the literature, only the important relations will be presented here. For more detail see, for example, Warburton (1964), or Rao (1986). Warburton also includes derivation for forced vibration of beams, while Rao includes derivations of Timoshenko theory. For Euler-Bernoulli theory of beam bending, see any basic mechanics text, such as Timoshenko and Gere (1984).

ASSUMPTIONS: The following assumptions are made in order to facilitate the theoretical development of the simple beam theory.

- The beam vibration is linear and elastic.
- The beam vibrates in one of its principal planes.
- Beam deflections are measured from the static equilibrium position.
- Rotary inertia and shear deformation are negligible.
- The beam is subject to pure bending loads (no axial loading).

These assumptions are reasonable in many cases. Most metals exhibit linear and elastic behavior provided the beam is not strained beyond the elastic limit of the material. If the beam is excited along a line that is parallel to the thickness dimension, vibration will be dominated by flexure, that is, deflection in a principal plane. In this case, out of plane

89

vibrations are minimized or eliminated. By measuring beam deflections from the static equilibrium position, gravitational effects can be neglected. Long, slender beams exhibit minimal rotary inertia and shear deformation effects. Meirovitch (1975) suggests that these effects can be neglected if the ratio of beam length to thickness is greater than 10. Although the case of combined bending and axial loading has been investigated, and is important in several applications, it, and other combined loading cases, are not treated here.

DEVELOPMENT: A derivation of the partial differential equation governing the lateral vibration of beams can be found in any good vibrations text, such as Rao (1986). The derivation involves dynamic analysis of a differential element of the beam coupled with Euler-Bernoulli beam theory. The resulting partial differential equation expresses the lateral beam deflection as a function of longitudinal position and time.

$$\frac{\partial^2}{\partial x^2}[EI\frac{\partial^2 w}{\partial x^2}] + \rho A \frac{\partial^2 w}{\partial t^2} = f(x,t) \qquad (4.1)$$

Equation 1 is valid for both uniform and non-uniform beams. A complete solution requires two initial conditions and four boundary conditions. The initial displacement and velocity are typically used for initial conditions. The end conditions of the beam provide boundary conditions in terms of beam deflection, slope, bending moment and shear force.

Rao provides a listing of specific boundary conditions for eight different ideal end conditions.

The mode shapes of a vibrating beam can be obtained from the free-vibration solution. For the special case where the beam is uniform and no forcing function is present Eq. 4.1 reduces to

$$\frac{EI}{\rho A}\frac{\partial^4 w}{\partial x^4} + \frac{\partial^2 w}{\partial t^2} = 0 \qquad (4.2)$$

Equation 2 can be solved by separation of variables by assuming a solution of the form

$$w(x,t) = Y(x)T(t) \qquad (4.3)$$

Substitution of Eq. 4.3 into Eq. 4.2 and rearranging leads to two ordinary differential equations describing the spatial function and the temporal function, respectively.

$$\frac{d^4 Y(x)}{dx^4} - \beta^4 Y(x) = 0 \qquad (4.4)$$

91

$$\frac{d^2T(t)}{dt^2} + \omega^2 T(t) = 0 \qquad (4.5)$$

where

$$\beta^4 = \rho A \frac{\omega^2}{EI} \qquad (4.6)$$

Equations 4.4 and 4.5 are well known forms, and have the following solutions

$$Y(x) = C_1 e^{\beta x} + C_2 e^{-\beta x} + C_3 e^{i\beta x} + C_4 e^{-i\beta x} \qquad (4.7)$$

$$T(t) = G e^{i\omega t} + G^* e^{-i\omega t} \qquad (4.8)$$

The asterisk indicates complex conjugation.

MODES OF VIBRATION AND MODE SHAPES Equations 4.7 and 4.8 are written for a single spatial frequency β and a single temporal frequency ω. In fact, an infinite set of distinct frequencies exits. The particular set of frequencies depends on the material and geometric properties of the beam as well as the boundary conditions. Each frequency corresponds to a mode of vibration of the beam. The modes are numbered consecutively

92

beginning with the lowest frequency. The mode shapes corresponding to each spatial frequency β are given by Eq. 4.7. Using the subscript n as a mode index, the nth mode shape of a beam in free vibration, designated $\phi_n(x)$, is given by

$$\phi_n(x) = C_{1,n}e^{\beta_x x} + C_{2,n}e^{-\beta_x x} + C_{3,n}e^{i\beta_x x} + C_{4,n}e^{-i\beta_x x} \qquad (4.9)$$

The constants $C_{1,n}$ through $C_{4,n}$ depend on the end conditions. If the end conditions are known, some of these constants can be eliminated. For example, the nth mode shape of a pinned-pinned beam, after appropriate substitution of trigonometric functions for complex exponential functions, is given by

$$Y_n(x) = C_n \sin(\beta_n x) \qquad (4.10)$$

The general form, using all four constants, allows for any arbitrary end conditions.

It is often convenient to normalize the mode shapes. Designating $\Phi_n(x)$ as the nth normalized mode shape, the following normalizing relation holds

93

$$\int_0^L [\Phi_n(x)]^2 dx = L \qquad (4.11)$$

The beam vibrates in a linear combination of its modes. The relative weighting of each mode is determined by the initial conditions, and is designated by a modal weighting factor, M_n. The complete solution for free vibration of a beam is given in terms of the modal weighting factor and the normal modes by

$$w(x,t) = \sum_{n=1}^{\infty} M_n \Phi_n(x) T_n(t) \qquad (4.12)$$

where $T_n(t)$ is given by Eq. 4.8 with $\omega = \omega_n$.

FORCED VIBRATION For the case of forced vibrations, generalized solutions to Eq. 4.1 exist only in terms of the normal mode shape functions and the convolution integral. This is a very awkward form for analysis. However, more attractive solutions are available for particular cases. The case of harmonic excitation of a single point on the beam is of particular interest in that 1) it is the common means of applying forcing in

spatial modal testing, and 2) the analysis is well known. A good derivation of forced vibration of beams is given by Warburton.

The beam is assumed to be uniform and to be exited by a harmonic force applied to a single point on the beam. Damping will be neglected in the analysis, however several observations regarding its effects are in order. First, damping will result in complex modes. Second, if steady-state vibration is assumed, the transient vibration term may be neglected. Thirdly, the forced vibration response will be similar to the undamped case with the exception of an additional factor resulting in finite resonant responses and slightly modified off-resonance response.

The undamped beam is excited by a steady state harmonic force $P\sin(\omega t)$ acting at the point $x = a$. The steady state response is given by

$$w(x,t) = \sum_n \frac{P\Phi_n(a)\Phi_n(x)\sin(\omega t)}{m(\omega_n^2 - \omega^2)} \tag{4.13}$$

In order to relate the theoretical beam response to data measured with the laser vibrometer, the velocity response must be obtained. The velocity response can be obtained by taking the partial derivative of Eq. 4.13 with respect to t. Thus

95

$$v(x,t) = \sum_n \frac{P\omega \Phi_n(a)\Phi_n(x)\cos(\omega t)}{m(\omega_n^2 - \omega^2)} \qquad (4.14)$$

The velocity amplitude, or velocity operating shape, is a function of position only, and is obtained by taking the time-independent terms in Eq. 4.14. It is expressed as

$$V(x) = \sum_n \frac{P\omega \Phi_n(a)\Phi_n(x)}{m(\omega_n^2 - \omega^2)} \qquad (4.15)$$

For a given excitation frequency, Eq. 4.15 can also be written in simple form as a linear combination of the normal modes of the beam. The parameters P, $\Phi_n(a)$, m, ω_n, and ω are independent of position, and can thus be combined in a single parameter M_n, called the modal weighting factor. With this substitution, Eq. 4.15 can be written as

$$V(x) = \sum_n M_n \Phi_n(x) \qquad (4.16)$$

The objective of spatial modal analysis is to estimate the normal mode functions, $\Phi_n(x)$, and the modal weighting factor, M_n, directly from the spatial data. The velocity amplitude function, $V(x)$ can thus be completely described in parameterized form.

96

The normal mode function, Eq. 4.9, is a continuous function of x. It is valid over the interval $x = \{0,L\}$, where L is the length of the beam. Measured data is always discretely sampled, however. A discretized representation of Eq. 4.9 is much more useful. Let Δx designate the spatial sampling interval and let the discrete spatial frequency $b_n = \beta_n \Delta x$. Substituting these values into Eq. 4.9 gives the discrete normal mode functions. Substitution again into Eq. 4.4 produces the general form of the discrete velocity amplitude, V_k.

$$ V_k = \sum_{n=1}^{m} C_{1,n} e^{b_n k} + C_{2,n} e^{-b_n k} + C_{3,n} e^{i b_n k} + C_{4,n} e^{-i b_n k} \qquad (4.17) $$

The nomenclature used is $x_k = k \Delta x$ where k is an integer in the range $k = \{0,1,...N-1\}$ and $N \Delta x = L$. The finite upper limit of the sum, m, represents the number of contributing modes. In theory, m is infinite. In practice, the number of significant contributing modes is finite and often small. If the beam is excited on resonance, that is if $\omega = \omega_n$, then the response is dominated by the excited mode.

The normal mode functions of Euler-Bernoulli beams are very sensitive to the coefficients in Eq. 4.17. This is demonstrated in a technical note by Chang and Craig (Chang and Craig, 1969). A change as small as 10^{-6} can lead to significant errors in the calculated

97

mode shape. This has significant impact on mode shape estimation, in that the modal coefficients must be estimated with high accuracy.

TIMOSHENKO THEORY

Euler-Bernoulli beam theory provides a very good model for the transverse vibration of slender beams. However, it is not sufficient for beams that have thick cross sections relative to the beam length. For such thick beams, the effects of rotatory inertia and transverse shear deformation become significant. These effects lower the natural frequencies of the beam and also affect the mode shapes. These effects are also significant for higher modes of thin beams. An improved beam theory is thus required for thick beams and for high modes of slender beams. Timoshenko beam theory (Timoshenko, 1921) includes the effects of rotary inertia and shear deformation on the lateral vibration of beams. It is applicable to a much wider range of beams than Euler-Bernoulli theory. However, as would be expected of a higher-order theory, it is much more complex than classical theory.

Timoshenko theory can also be used to test the limits of applicability of Euler-Bernoulli theory. For a given beam, it may be important to determine the errors incurred using the simpler theory. This is particularly true if experimental results are to be compared with

theory. Comparison of natural frequencies and mode shapes from both Timoshenko and Euler-Bernoulli theories provide this information. If a large discrepancy exists between the two, it can be assumed that Euler-Bernoulli theory is not applicable.

It should be noted that Timoshenko theory, though applicable to many more beams than Euler-Bernoulli theory, is still only an approximation. Exact beam solutions based on three dimensional solid mechanics are very difficult, and can only be obtained for certain cross sectional shapes, such as circular. Hutchenson (1981) compared various solutions for the transverse vibration of circular beams. He included, in addition to Euler-Bernoulli and Timoshenko theories, the exact solution and solutions due to Pochammer-Chree and Pickett. Included is a discussion of applicability for the various methods. Timoshenko theory is shown to provide excellent results until the diameter of the beam approaches the length. In a later paper (Hutchenson and Zillmer, 1986), Hutchenson compared Timoshenko solution to a plane-stress solution for beams with rectangular cross section. He concluded that both methods provided good accuracy for frequencies less than the fundamental frequency obtained by treating the thickness of the beam as the length dimension. The conclusion is that Timoshenko theory is applicable for a much wider range of beams than classical theory.

Timoshenko beam theory can be derived in a similar manner to Euler-Bernoulli theory, with the exception that additional terms appear due to rotatory inertia and shear

99

deformation. Derivations of the theory can be found in many vibration texts, such as Rao, 1986, or Warburton, 1964, and will not be included here. The theory leads to a pair of coupled partial differential equations describing the total transverse deflection of the beam, y, and the slope of the beam due solely to bending, ψ. These equations are

$$EI\frac{\partial^2\psi}{\partial x^2} + kAG\left(\frac{\partial y}{\partial x} - \psi\right) - I\rho\frac{\partial^2\psi}{\partial t^2} = 0$$

$$\rho A\frac{\partial^2 y}{\partial t^2} - kAG\left(\frac{\partial^2 y}{\partial x^2} - \frac{\partial \psi}{\partial x}\right) = 0$$

$$(4.18)$$

in which

G = Modulus of Rigidity

ρ = Density

k = Timoshenko Shear Coefficient

T. C. Huang has solved these equations for mode shapes and natural frequencies for a variety of boundary conditions (Huang, 1961). He investigated six common boundary conditions: pinned-pinned, free-free, fixed-fixed, pinned-free, fixed-pinned, and pinned free. Both the highly transcendental frequency equations and the normal mode functions

are given for each set of boundary conditions. These functions are presented in terms of

several non-dimensional parameters defined as

$$
\begin{aligned}
b^2 &= \frac{1}{EI}\rho A L^4 \omega^2 \\
r^2 &= \frac{I}{A L^2} \\
s^2 &= \frac{EI}{kAGL^2}
\end{aligned}
$$

(4.19)

and

$$
\begin{aligned}
\alpha &= \frac{1}{\sqrt{2}}\left\{-(r^2+s^2)+\left[(r^2+s^2)+\frac{4}{b^2}\right]^{\frac{1}{2}}\right\}^{\frac{1}{2}} \\
\beta &= \frac{1}{\sqrt{2}}\left\{(r^2+s^2)+\left[(r^2+s^2)+\frac{4}{b^2}\right]^{\frac{1}{2}}\right\}^{\frac{1}{2}}
\end{aligned}
$$

(4.20)

The general solution of Eq. 4.18 can be given in terms of the normal displacement and

bending functions Y and Ψ, and the non-dimensional length parameter ξ, as

101

$$Y = C_1\cosh(b\alpha\xi) + C_2\sinh(b\alpha\xi) + C_3\cos(b\beta\xi) + C_4\sin(b\beta\xi)$$

$$\Psi = \acute{C}_1\cosh(b\alpha\xi) + \acute{C}_2\sinh(b\alpha\xi) + \acute{C}_3\cos(b\beta\xi) + \acute{C}_4\sin(b\beta\xi) \tag{4.21}$$

The normal deflection mode shape is designated Y, and the normal bending slope function Ψ. Of particular interest is the function Y. This function can be used to fit spatial modal data to thick beams. Note that the coefficients of Y and Ψ are not independent.

It is assumed that the quantity in braces in Eq. 4.20 is non negative. If this is not the case, then α, as given by Eq. 4.20, is pure imaginary. In this case a real number α' can be defined as

$$\alpha = j\alpha'$$

where j is the square root of -1. The normal deflection and bending slope functions thus become

$$Y = C_1\cos(b\alpha'\xi) + jC_2\sin(b\alpha'\xi) + C_3\cos(b\beta\xi) + C_4\sin(b\beta\xi)$$

$$\Psi = j\acute{C}_1\sin(b\alpha'\xi) + \acute{C}_2\cos(b\alpha'\xi) + \acute{C}_3\sin(b\beta\xi) + \acute{C}_4\cos(b\beta\xi) \tag{4.22}$$

For any given boundary conditions, the coefficients in Eq. 4.21 can be evaluated. Also, the frequency equation, which gives the natural frequencies of the beam, can be found. For example, the frequency equation for free-free end conditions is given as

$$2 - 2\cosh(b\alpha)\cos(b\beta) +$$

$$\left(\frac{b}{\sqrt{1 - b^2 r^2 s^2}}\right)\left[b^2 r^2 (r^2 - s^2)^2 + (3s^2 - r^2)\right]\sinh(b\alpha)\sin(b\beta) = 0 \qquad (4.23)$$

This equation can be solved iteratively to obtain the frequency parameter b, and thence, by Eq. 4.19, the natural frequencies ω_n.

The normal mode functions are given in terms of the non-dimensional length parameters

103

$$\xi = \frac{x}{L}$$

$$\lambda = \frac{\alpha}{\beta}$$

$$\zeta = \frac{(\alpha^2 + r^2)}{(\alpha^2 + s^2)} = \frac{(\beta^2 - s^2)}{(\beta^2 - r^2)}$$

$$\delta = -\frac{\cosh(b\alpha) - \cos(b\beta)}{\lambda\sinh(b\alpha) - \xi\sin(b\beta)}$$

(4.24)

For free-free boundary conditions, Huang gives these functions as

$$Y = D\left[\cosh(b\alpha\xi) + \lambda\delta\sinh(b\alpha\xi) + \frac{1}{\zeta}\cos(b\beta\xi) + \delta\sin(b\beta\xi)\right]$$ (4.25)

$$\Psi = H\left[\cosh(b\alpha\xi) - \frac{\delta}{\lambda}\sinh(b\alpha\xi) + \zeta\cos(b\beta\xi) + \frac{1}{\delta}\sin(b\beta\xi)\right]$$ (4.26)

Equation 25 provides an accurate normal mode function for either thick or slender free-free beams. It also provides a theoretical model for comparison with experimental models.

104

A number of researchers have investigated the shear coefficient k. For beams of rectangular cross section, Timoshenko originally used a value $(5 + 5v)/(6 + 5v)$, where v is Poisson's ratio (Timoshenko, 1922). He later used a different value, however. Mindlin and Deresiewicz (1954) proposed a value of $\pi^2/12$. Cowper compared a number of different formulations for k for different cross sections. For rectangular beams he derived the formula $(10 + 10v)/(12 + 11v)$ (Cowper, 1966). In 1975 Kaneko reviewed over twenty values of shear coefficient for rectangular beams, and concluded that Timoshenko's original value best fit experimental data (Kaneko, 1975). Hutchinson and Zillmer (1986) compared several formulations with three-dimensional elasticity theory, and concurred with Kaneko for wavelengths longer than twice the beam depth. Otherwise, the shear coefficient becomes frequency dependent, and is better estimated with the formulation due to Mindlin. In this dissertation, Timoshenko's original expression for k is used. Thus, for beams with rectangular cross section,

$$k = \frac{(5 + 5v)}{(6 + 5v)} \tag{4.27}$$

CHAPTER 5: MINIMUM RESIDUAL MODELS

INTRODUCTION

Throughout modern history, scientists and engineers have used experimental data to develop models of physical phenomena. The task of the experimentalist is to find the most meaningful way to interpret or apply the measured data. One approach that is often used is to first choose a mathematical form for the model. This form contains parameters that are unknown. The model is defined by finding the values for the parameter set that minimizes the difference between the measured data and the model. The mathematical form is chosen based on knowledge of the underlying physics of the problem or some other appropriate criteria. For example, a particular set of data might be assumed to be a polynomial of some known or unknown order. In this case, the mathematical form would be a polynomial. The polynomial coefficients are then found such that the residual, or the difference between the data and the polynomial model, is as small as possible. This is a minimum residual approach.

The objective of minimum residual methods of modelling data is to minimize the difference between the measured data and the mathematical model. All least squares methods are minimum residual approaches. The underlying philosophy is that a particular set of measured data can be represented best by a mathematical model that most closely

approximates the data. It is important to note that no physical restrictions need be placed on the model. In other words, the model may have little or no relationship to the physical process that generated the data set. In some cases this is desirable. In other cases it can be a detriment. However, minimum residual methods are often the only way to develop any kind of meaningful model of the data.

All of the parametric modal analysis methods outlined in Chapter 2 are minimum residual methods. These methods have the advantage that the resulting model closely matches the measured data. Autoregressive and ARMA models in particular are powerful minimum residual modelling approaches that are often used where no knowledge of physical processes is available. In some of the modal methods, such as Pisarenko Harmonic Decomposition, some of the known physical constraints have been incorporated into the model.

Two minimum residual methods are presented in this chapter. The first method is based on the autoregressive nature of exponential functions. It is very similar to the AR methods used for time-domain analysis. The second method uses a multi-dimensional variation of Newton's method to fit a non-linear least squares model. Both of these approaches can generate models that closely fit the measured beam data. In applications where a good fit of measured data is all that is desired, these methods perform well. (There are some limitations and restrictions, which will be described.) However, because these models do

107

not incorporate all physical constraints of vibrating beams, the models may or may not reflect accurately the theoretical modal parameters.

The theory of each of these methods is presented in this chapter. An empirical error analysis appears in Chapter 7, and experimental verification is presented in Chapter 8.

AUTOREGRESSIVE MODELS

Spatial modal analysis involves the reduction of large amounts of spatial data to a relatively small modal model. This model accurately describes the vibration of a structure. The crux of the modeling task involves choice of a signal processing method. It has been shown that beam operating shapes can be described with complex exponential functions (recall that sin, cos, sinh, and cosh are exponential functions). It has further been shown that exponential functions can be modeled as self-exciting autoregressive systems. Hence an autoregressive approach is appropriate for fitting spatial models of beams. The oversize total least squares method (OTLS) is one such approach (Archibald and Wicks, 1991). It has advantages over other methods in that it is unbiased and has good numerical characteristics. It is a total least squares approach in which noise is assumed present on the entire data matrix.

OTLS THEORY

The OTLS method involves decomposition of a circulent data matrix such that a basis set of vectors spanning the noise space is obtained. This space, S_N, contains all solutions to the TLS problem. A method is developed to choose a vector in S_N such that all spurious, or noise poles are zero. System parameters are then obtained directly from that vector.

ASSUMPTIONS: The following assumptions are made.

1. The data is discrete.

2. The data consists of a purely deterministic component and a random component.

3. The random component is normally distributed, mean zero.

4. The deterministic component satisfies a pth order difference equation.

5. The deterministic component represents a linear system.

Assumptions 2. and 4. can be summarized by:

$$y_k = x_k + n_k$$

109

$$a_0 x_k + a_1 x_{k-1} + \cdots + a_p x_{k-p} = 0$$

DEVELOPMENT: If N measured data points, $y_0 \ldots y_N$, are available, the following matrix system of equations can be written:

$$[Y]a = [X+W]a = 0$$

The matrices X and W are circulent matrices containing the deterministic component and the random component, respectively. These matrices are not available to the analyst, however. Only Y is available. It is a circulent matrix of dimension (m,n) consisting of the measured (i.e., noise corrupted) data. This matrix has the form:

$$[Y] = \begin{bmatrix} y_{n\Delta} & y_{(n-1)\Delta} & y_{(n-2)\Delta} & \cdots & y_{\Delta} \\ y_{n\Delta+1} & y_{(n-1)\Delta+1} & y_{(n-2)\Delta+1} & \cdots & y_{\Delta+1} \\ y_{n\Delta+2} & y_{(n-1)\Delta+2} & y_{(n-2)\Delta+2} & \cdots & y_{\Delta+2} \\ \vdots & & & & \\ y_N & y_{N-\Delta} & y_{N-2\Delta} & \cdots & y_{N-n\Delta} \end{bmatrix}$$

110

The objective of the OTLS method is to minimize, in some sense, the noise matrix W, subject to the constraint that $[X+W]$ is singular. Stewart (1973) has shown that, given the singular value decomposition (SVD) of Y as

$$U^T Y V = S = diag\{s_1 \ s_2 \ ... \ s_n\}$$

with $\qquad s_1 >= ... >= s_p >= s_{p+1} = ... = s_n$

and U, V orthogonal,

then $\qquad s_n = minimum \ \|W\|_F$

$$rank[X] < n.$$

Here $\|W\|_F$ is the Frobenius norm of W, given by

$$\|A\|_F = \sum_i \sum_j |a_{ij}|^2.$$

Furthermore, the minimum is given by

$$[W'] = [Y]vv^T \qquad\qquad (5.1)$$

where v is any vector is the subspace S_N, defined by

$$S_N = span\{v_{p+1}\ v_{p+2}\ ...\ v_n\}.$$

Here v_i represents the ith column of V, the matrix of right singular vectors of Y. The implication is that the minimization problem can be solved in a reasonable sense by use of the SVD. Furthermore, the SVD exhibits two important and attractive features. First, the decomposition results, in some sense, in a segregation of the data into deterministic and random components. Second, the singular values provide realistic and practical information on the system model order.

Consider the case with $n > p$, that is, the number of columns of Y exceed the true model order of the system under investigation. Then the deterministic matrix, X is singular, and the last n-p singular values of X $\{s_{p+1}\ ...\ s_n\}$ are all equal to zero. Now consider measurement noise added to the data, i.e., $Y = [X+W]$. Wilkerson (1977) shows that for any matrix X perturbed by a small amount W, the singular values of Y are related to the singular values of the noise-free matrix X by

112

$$s_i(X) - s_1(W) \le s_i([X+W]) \le s_i(X) + s_1(W)$$

It can also be shown that the singular values of any matrix are all positive:

$$s_i >= 0 \qquad i = 1...n.$$

Thus, the first p singular values of Y will be bounded from above and below by the largest singular value of the noise matrix W, while the last n-p singular values will be bounded from below by 0 and from above by $s_1(W)$. Furthermore, if assumption 3. is considered, that is, if the noise is normally distributed, then it can be shown that in the expectation, $s_i(W) = C$, $i=1...n$, where C is a constant proportional to the standard deviation of the noise sequence, n_k. Thus if $s_i(Y)$ $i=1...p$ is sufficiently large compared with C, then inspection of the singular values of Y can provide information about both model order and noise variance.

It is clear from Eq. 5.1 that if n-$p > 1$, the TLS solution is not unique. Indeed, a solution can be written for any vector in S_N. The first p columns of V define the signal subspace, S_s. These vectors each satisfy the system difference equation. The columns in S_N are random vectors orthogonal to S_s. Thus, the roots of a polynomial with coefficients taken as elements of any column of S_N contain, as a subset, the poles of the deterministic component. In order to obtain the desired solution vector a, a vector, v_i, must be found

113

in S_N such that the last $n\text{-}(p+1)$ elements are identically zero. Since the roots of any vector in S_N contain the poles of the system under investigation, the roots of the first $p+1$ non-zero elements of v_t are the desired poles. No extraneous poles appear, since the remaining zero elements in v_t produce no poles. Since the last $n\text{-}p$ right singular vectors of Y span S_N, the desired vector v_t can be found as a linear combination of these vectors. This can be done by forming a system of equations from the last $n\text{-}p$ rows and columns of the matrix V. Form the system

$$[Wm]\{Co\} = \{Wv\}$$

where

$$\{Wv\} = [\ v_{p+2,n}\ v_{p+3,n}\ \cdots\ v_{n,n}\ ]^T$$
$$\{Co\} = [\ c_1\ c_2\ \ldots\ c_{n\text{-}(p+2)}\ ]^T$$

$$[W_m] = \begin{bmatrix} v_{p+2,p+1} & v_{p+2,p+2} & \cdots & v_{p+2,n-1} \\ v_{p+3,p+1} & v_{p+3,p+1} & \cdots & v_{p+3,n-1} \\ \vdots & & & \\ v_{n,p+1} & v_{n,p+2} & \cdots & v_{n,n-1} \end{bmatrix}$$

Once the coefficient vector Co is obtained, the vector v_t can be easily computed. Augment Co with 1 in the last row such that

114

$$\{Co'\} = [\ c_1\ c_2\ \dots\ c_{n-(p+2)}\ 1\ ]^T$$

Then the last n-p columns of V, multiplied by $\{Co'\}$, yield the desired vector v_t.

$$[\ v_{p+1}\ v_{p+2}\ \dots\ v_n\ ]\ \{Co'\} = \{v_t\}$$

$$\{v_t\} = [\ a_1\ a_2\ \dots\ a_p\ 0\ 0\ \dots\ 0\ ]^T = [\ \underline{a}^T\ \underline{0}^T\ ]^T$$

The vector a contains the coefficients of the system difference equation. The roots of this equation are the system poles.

If the deterministic signal is a discrete exponential function, i.e.,

$$x_k = \sum_{i=1}^{P} A_i e^{\lambda_i k}$$

then the system poles are given by

$$P_i = e^{\lambda_i \Delta}$$

where Δ is the sample interval. Once the poles have been determined, the constants A_i, $i = 1\ldots p$, can be computed by an ordinary linear least-squares procedure such as described in Patton, 1988.

The OTLS algorithm can be summarized by the following steps:

1. Form the circulent data matrix Y and perform the singular value decomposition $U^T[Y]V = S$.

2. Examine the singular values, $s_1\ldots s_n$. Determine an appropriate model order p, either by inspection or with a statistical test.

3. Construct the system of equations $[Wm]\{Co\} = \{Wv\}$ from the last $(n\text{-}p)$ rows and columns of the right singular vector matrix V, and solve for $\{Co\}$. Augment $\{Co\}$ with 1 to form $\{Co'\}$.

4. Multiply the last $(n\text{-}p)$ right singular vectors by $\{Co'\}$ to obtain $\{v_i\} = [\ a^T\ \underline{0}^T\ ]^T$. The coefficients of the deterministic difference equation are the elements of $\{a\}$ The roots of this polynomial are the poles of the deterministic process.

116

5. Compute the constant coefficients with a conventional least-squares method.

SPATIAL-DOMAIN CONSIDERATIONS

Theoretically, the OTLS method should be an effective tool for spatial modal analysis. However, a number of factors relevant to the spatial data affect the accuracy of parameter estimates. As a result, the OTLS method, and all ARMA-like methods, are limited in accurate pole estimation. These factors include sample-rate-to-signal-period ratio, unequal sample intervals, inadequacy of the model to incorporate constraints, and choice of model-fitting parameters. Additional considerations treated include model applicability and use of the residual function for model evaluation.

It is shown below that the beam mode shapes are very sensitive to parameter accuracy. This means that any estimation algorithm must be able to provide accurate parameter estimates. If this is not the case, the resulting model is meaningless. It will be shown that the autoregressive formulation of the beam problem is inherently ill-conditioned. This adversely impacts the ability of AR algorithms to model beam mode shapes. By using singular value decomposition, it is possible to obtain good results if on-resonance testing is used. In this case, only one mode is assumed present in the model. If multiple modes

117

are present, the problem is ill-conditioned to the extent that it is not feasible to use AR methods.

The factors that affect accuracy and conditioning are discussed in this section. An understanding of these factors enable the analyst to make rational, informed decisions regarding the quality and feasibility of the spatial beam analysis.

SPSR RATIO: The nature of beam mode shapes is such that the spatial data will always be oversampled for lower modes. The sample interval will be very small relative to the period of the constituent sinusoidal components. This effect is most pronounced at the lower modes. The SPSR Ratio can be found for a given mode by

$$SPSR = \frac{2\pi N}{\beta_i L}$$

Note that this quantity is dependent only on the number of samples (N) and the beam boundary conditions. The quantity βL is independent of beam geometry or material properties. As an example, the SPSR ratios for the first six modes of a free-free beam have been tabulated for various values of N. The results are shown in Table II. For a free-free beam, only the higher modes and short record lengths provide good SPSR Ratios. Boundary conditions other than free-free have comparable or even worse SPSR ratios.

118

The consequence of this oversampling is a poorly conditioned problem. The discussion on sample rate and matrix conditioning in Chapter 3 is pertinent here. The spatial beam problem is inherently ill-conditioned because of oversampling. This problem can be offset by using appropriate delay factors, as described in Chapter 3. Unfortunately, due to other factors discussed below, the ill-conditioning can not be entirely eliminated with delay factors.

Table II Example: SPSR Ratios for a free-free beam.

N	MODE 1	MODE 2	MODE 3	MODE 4	MODE 5	MODE 6
100	133	80	57	44	36	31
200	266	160	114	89	73	62
300	399	240	171	133	109	92
400	531	320	229	178	145	123
500	664	400	286	222	182	154

UNEQUAL SAMPLE INTERVAL: All of the ARMA-like methods rely on forming difference equations that fit the data. An inherent assumption is that the interval between samples is constant. In the case of spatial beam analysis, this implies that the spacing of the velocity measurements along the beam is even. If the coordinate along the longitudinal axis of the beam is x, then the ith sample should be taken at $x = x_{i-1} + \Delta x$, $i = 1:N$ and

119

Δ is constant. The scanning laser vibrometer is, at present, not able to provide equal spacing of samples along a beam.
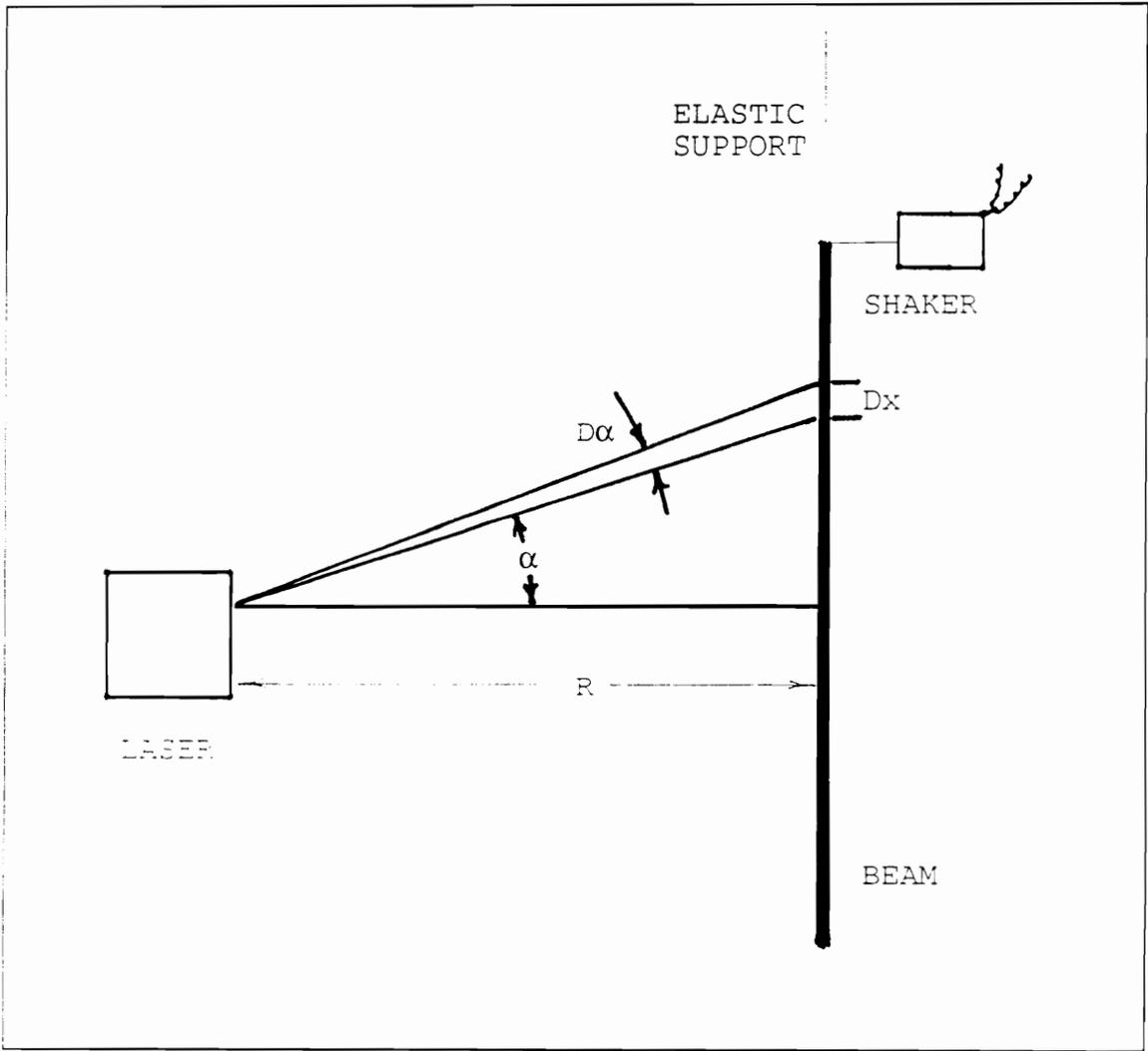
Figure 10 Schematic of Scanning Laser Vibrometer.

Figure 10 depicts a typical setup for scanning a beam. The laser is placed a distance R from the beam. The scan angle θ_x is defined as the angle between an imaginary line normal to the beam and the actual position of the laser. The scan increment is currently defined in terms of equal angles. That is, as the laser scans along the longitudinal axis of the beam, it moves in steps of equal angles $\Delta\theta_x$. Thus the spacing of the samples in the x-y coordinate system unequal. Specifically, the ith sample increment is given by $(x_{i+1} - x_i) = R(tan(\theta_{i+1}) - tan(\theta_i))$. This is a very non-linear change of coordinates, and is thus not amenable to correction.

Figures 11 through 14 show the effect of equal scan angles on sample interval. These figures plot the sample interval obtained from an actual beam scan. Each figure actually plots the effective sample interval associated with each entry in the data matrix versus the matrix row. The lines on each figure represent the effective sample intervals between the corresponding columns of the data matrix. The horizontal axis corresponds to the rows of the data matrix. The sample rate variations within each row can be seen by comparing the vertical differences between lines for a particular row. The variations between rows can be seen by comparing different horizontal slices of the plot. A significant difference between columns represents errors within a given equation, whereas sample rate differences between rows indicate errors between system equations. Either type of error leads to parameter estimation difficulties.

121
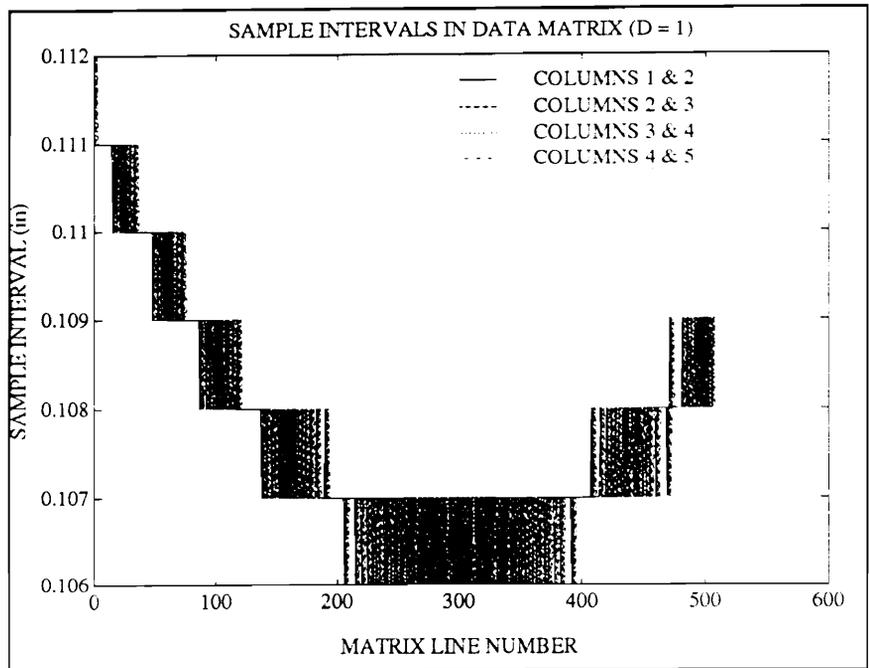
Figure 11 Effect of unequal sample interval, D = 1.
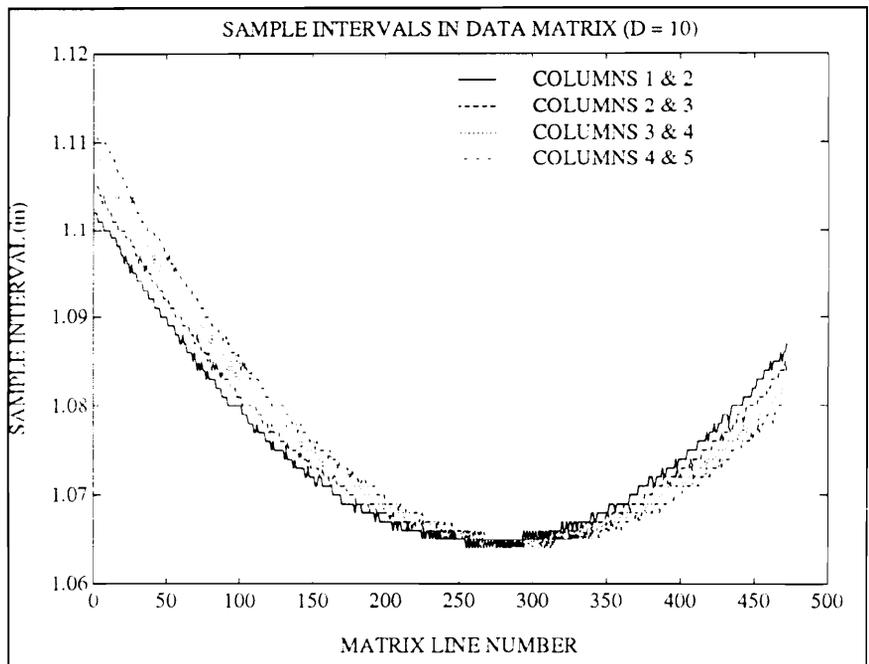
Figure 12 Effect of unequal sample interval, D = 10.

122
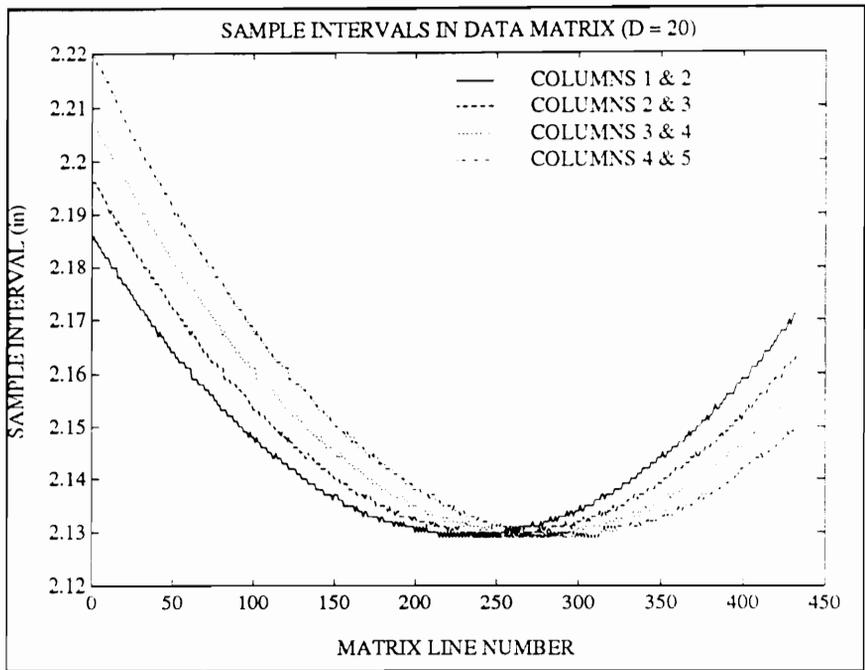
Figure 13 Effect of unequal sample interval, D = 20.
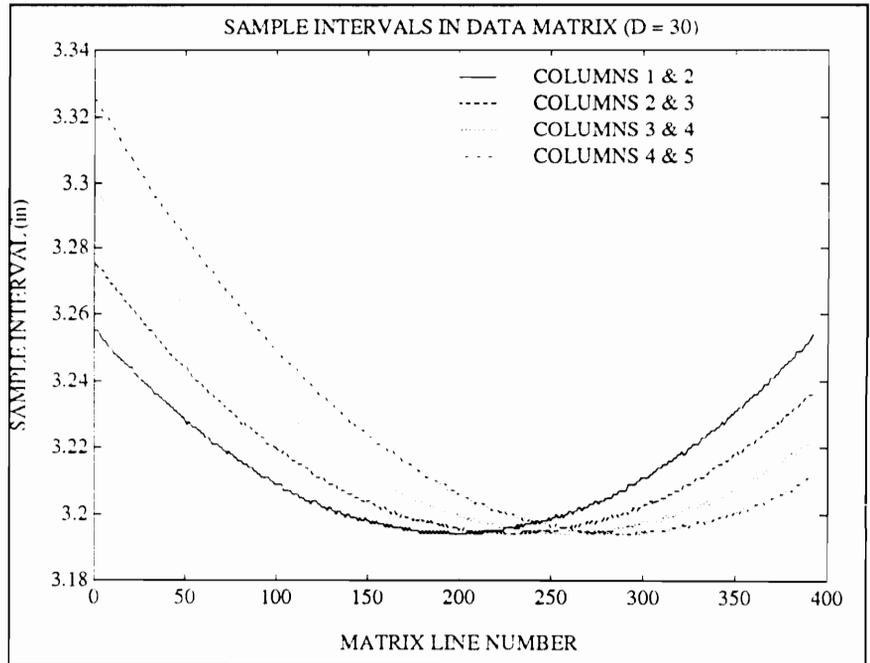
Figure 14 Effect of unequal sample interval, D = 30.

123

Inspection of the figures shows that the relative sample interval error is very dependent on the delay factor. With D=1, the difference is slight, both between and within columns. However, as the delay factor is increased, both errors become more pronounced. The discrepancy between rows can be seen by the curvature of each line. A uniform sample rate would result in a straight, horizontal line. The error between columns is indicated by the difference between the plotted lines. If the sample interval error were constant within equations, all column curves would be coincident.

The conclusion drawn from these figures is that The effects of unequal sample rate, for a given scan angle range, are strongly dependent on choice of delay factor.

If ARMA-like methods are used to process data obtained with the scanning laser vibrometer, errors will be incurred because of the unequal spacing. In some cases, these errors can be assumed to be small. If the velocity function does not change rapidly, then the change in velocity between the scan point and the assumed equal spaced point is small. For the same reason, errors are minimized by using a large number of data points. If N is large and the derivative of the velocity is small, then the unequal sample intervals can be assumed small. This has been observed in practice. Additionally, a relatively large delay factor has the effect of magnifying the errors. Thus, in order to minimize the impact of unequal spacing, delay factors should be chosen as small as possible. Unfortunately,

124

the requirement for large N and small D are contradictory. If highly accurate parameter estimates are desired, the violation of equal spacing could result in problems.

CONSTRAINTS: The theoretical beam mode shapes are well known. These mode shape functions are given in Eq. 4.9. The form of these functions is such that five parameters are required to fully describe the shape of each mode. Four of these parameters are coefficients of the exponential terms. The only constraint on these parameters is that $C_{3,i}$ and $C_{4,i}$ must be complex conjugates if the mode shape is a real-valued function. However, the fifth parameter is the spatial frequency β. This parameter occurs in the exponent of each of the four terms of the mode shape.

ARMA-like methods will produce spatial frequency estimates for each term included in the model. That is, if the selected model order is four, then four spatial frequencies will be produced. However, there is no constraint that these four frequencies will be related. If the poles are complex, the spatial frequencies will be complex conjugates of each other, as is desired, but for the real poles, no such constraints can be imposed. In a well conditioned problem, the estimates would be expected to approximate the known constraints. However, the spatial beam problem is not well conditioned, and often the exponent of the real terms bears no resemblance to that of the complex terms.

125

It is desired to impose constraints on the exponents such that they conform to those in Eq. 4.9. However, this is a very difficult task for ARMA-like models. No reasonable method for imposing these constraints is apparent. Furthermore, given the ill-conditioned nature of the problem, such constraints might not improve model accuracy. The inability to impose these constraints does pose difficulties in model interpretation. If more than one spatial frequency is estimated for a single mode, which one should be used? In general, the complex poles yield better frequency estimates than the real poles.

MODEL FITTING PARAMETER SELECTION: The OTLS method requires three model fitting parameter to be selected. The delay factor (D) and number of columns (c), as well as the model order (p), must be selected. Often it is not clear what values should be used for these parameters.

The delay factor D should be chosen based on approximate SPSR ratio and SNR. The theoretical SPSR ratio may be known for a given data vector length and boundary conditions. Uncertainties arise because of non-ideal or unknown boundary conditions and other deviations from theoretical results. The signal-to-noise ratio need not be known with any precision whatsoever. A visual inspection of the plotted data is often sufficient for estimation of the delay factor D. Considering the apparent noise level and estimated SPSR ratio narrows the band of likely values considerably. In general, the smallest delay that gives satisfactory results is desired.

126

Physical limits are imposed on D to ensure that the data matrix has more rows than columns. These limits are given by

$$1 < D < \left(\frac{N}{c} - 1\right)$$

If D is chosen too small, the dramatic increase in variance of the spatial frequency estimates leads to unreliable models. Likewise, if D is chosen too large, the effects of unequal sample intervals become detrimental.

The choice for number of columns is perhaps the most arbitrary of the model fitting parameters. If the number of modes is known or assumed, then the minimum column dimension is four times the number of modes. As a general rule, the value for c can be chosen roughly twice the estimated model order of the system. The limits on c are:

$$(p+1) < c < \left(\frac{N}{D-1}\right)$$

If p is chosen large enough to preclude bias error, the variations in spatial frequency estimates appear random. However, if p is chosen too small, a bias error occurs that is dependent on both c and D. Note that this parameter is only of concern for the total least

squares methods (OTLS, OEM). For other formulations, the column dimension is solely dependent on the model order.

In some cases the number of constituent modes is known a-priori. For example, in many cases, if the beam is excited on resonance, significant contributions can be expected from only the resonance mode. In these cases the model order should be four. Often the model order may not be known prior to analysis. In this case, inspection of the singular values will often shed light on the appropriate model order. An F-test, such as that described by Patton (Patton, 1988) can be used with the singular values to determine a parsimonious model order. Often, however, a visual inspection of the singular values leads to the same conclusion.

Theoretically, the model order is always a multiple of four. Sometimes, however, inspection of singular values indicates a model order of 2. If the data is processed at such a low model order, the spatial frequency estimates will be biased. In general, if the model order is underspecified, the model may exhibit bias errors. If the model order is overspecified, a very poor model could be obtained that still 'looks' good -- i.e., the residual may be small and normally distributed even though the model parameters are considerably in error.

It must also be noted that in practice, the number of spatial frequencies selected often differs from the chosen value of p. The number of poles, or spatial frequencies, obtained from the OTLS method is equal to the model order p. However, a subset of these frequencies is usually chosen for the final model.

The choice for model-fitting parameters is subjective and is not prone to exact analysis. If the beam model parameter estimates are insensitive to selection of model-fitting parameters, reliable models could be constructed for a variety of values of D, c, and p. Unfortunately, this is not the case. Different values of the delay factor, column dimension, and model order all yield different model parameter estimates. Even more distressing is the fact that no rigorous method exists to choose these values. A variety of cases can be tried and compared. Perhaps the best way to evaluate a particular model is the size of the residuals. For the same model order, the model that produces the smallest residual is the best model. This can become a trial and error process if numerous models must be fitted in order to determine the optimum model fitting parameters.

As an example of the variability of parameter estimates with respect to model-fitting parameters, a test case was run. Data simulating a free-free beam was synthesized. The contributions of six modes was included. Harmonic excitation very near resonance of the first mode was assumed. Thus the contributions of modes 2--6 was expected to be negligible. Random noise was generated and added to the signal to obtain a SNR of 40dB,

a rather clean signal. Table III shows the estimates obtained for the first spatial frequency

for various combinations of D and c, and for $p=2$ and $p=4$.

Table III Dependence of Parameter Estimates on model-fitting parameters.

Estimated Spatial Frequency **p = 2**

D	10	20	30	40	5.
c					
3	0.0746	0.0767	0.0828	0.0881	0.0928
4	0.0761	0.0828	0.0905	0.0964	0.1006
5	0.0788	0.0872	0.0954	0.0992	0.0998
6	0.0833	0.0910	0.0971	0.0971	0.0936
7	0.0842	0.0935	0.0960	0.0920	0.0861
8	0.0872	0.0944	0.0929	0.0856	0.0770
9	0.0884	0.0941	0.0889	0.0798	0.0704

Sum of squared residuals (ΣP^2)

D	10	20	30	40	50
c					
3	26.5372	21.1108	7.2838	1.3951	5.1175
4	22.4706	7.2758	1.9317	17.3094	45.1001
5	15.6175	1.7777	12.8498	34.2008	38.6356
6	8.4700	2.4053	20.6869	20.6582	7.1046
7	4.3913	6.7264	15.3484	3.7053	2.7052
8	1.5082	9.1905	5.2732	3.1694	20.3512
9	1.3289	8.2716	1.3043	13.6101	37.7027

Spatial Frequency Estimates **p = 4**

D	10	20	30	40
c				
3	0.0699	0.0842	0.0844	0.0858
4	0.0711	0.0735	0.0813	0.0823
5	0.0692	0.0888	0.0762	0.0837
6	0.0753	0.0888	0.0828	0.0829
7	0.0867	0.0788	0.0865	0.0900
8	0.0762	0.0885	0.0989	0.0969
9	0.0652	0.0826	0.0929	0.0939

Sum of squared residuals (ΣP^2)

D	10	20	30	40
c				
3	36.9808	5.0568	4.7177	3.0270
4	35.7442	23.4555	10.2161	8.2531
5	41.6477	31.7778	22.2532	5.8443
6	24.6647	1.3033	7.3430	7.2472
7	47.0526	15.8329	2.2935	1.6375
8	20.3395	1.6277	31.4701	19.6763
9	50.9631	7.6264	5.3628	7.8012

131

The results, tabulated in Table III, indicate the difficulty of correctly choosing model-fitting parameters. In both cases, the estimated frequency varies from the true spatial frequency of the first mode (0.0876) by up to 25%. Specifically, for the p=2 case, the lowest and highest frequency estimates are -19.76% and +14.82% below and above the true value. A trend can be detected that is due to the bias error. For the p=4 case, the maximum and minimum errors are -25.61% and +12.87%, respectively. However, many of the estimates were quite close. Estimates were obtained that were within 1% of the true value. The lack of a consistent pattern of estimation is the problem. However, inspection of the sum of residuals proves to be a good check for model accuracy. In all cases, those models in which the frequency estimate is close to the true estimate, the residual is relatively small. In contrast, in cases where the spatial frequency estimate is significantly in error, large residuals result. Comparing a few models and the resulting residual is the best option. Use of the residual is described in detail in the next section.

RESONANCE TESTING: A spatial modal test invloves exciting a structure and measuring the velocity response with a scanning laser vibrometer. The resulting velocity signal is referenced to the force signal, which is measured using a force transducer. Often, the excitation force, provided by an electromagnetic shaker, is harmonic. All data in this dissertation, both measured and synthesized, uses harmonic excitation. Resonance excitation occurs if the excitation frequency is the same as one of the natural frequencies

of the structure. Resonance excitation can be obtained by noting that at resonance, there will be either a 0° or 180° phase angle between the force and velocity signals. Near-resonance testing indicates that the excitation frequency is close to, but not exactly equal to, a natural frequency of the structure (within 2-3%).

If a structure with well spaced modes is excited on-resonance, the response will be dominated by the excited mode. The term unimodal strictly indicates that only one mode contributes to the response of the structure. The minimum residual methods described in this chapter require that the data be essentially unimodal. Often in this dissertation data is assumed to be unimodal. A single-mode analysis is one in which unimodal data is assumed. In fact, this is not true for physical beams. However, if the contribution of one mode is much, much larger than the remaining modes, only small errors are introduced by the unimodal assumption. Conversely, if several modes have significant contributions, then large errors occur.

USE OF RESIDUAL: Once a model has been obtained, it is prudent to evaluate the model for validity. Plots comparing the measured and fitted data have been used access the quality of the model. This is not a good method to use, however. In many cases, a model can be constructed that visually fits the measured data well, but in fact models the parameters very poorly. A better method is to investigate the nature and size of the

133

residual. If the measured data is given by y_k and the fitted model by v_k, then the residual is given by

$$R_k = y_k - v_k$$

A measure of the size of the residual is provided by an appropriate vector norm. The 2-norm will be used here to determine the size of the residual. Note that the least-squares solution to the spatial beam problem consists of those parameters that yield the minimum sum of squared residuals, or

$$LS \; Solution = minimum \sum_{k=1}^{N} (R_k)^2 \qquad (5.2)$$

This is precisely the definition of the 2-norm, squared. When comparing models, the one with the smallest sum of squared residuals most closely approximates the least squares solution.

This assumes that the estimated parameters are in the region of the true parameters. (However, if the estimated parameters are in error by large amounts, it is possible that a relatively small residual could reflect a local minima of the residual function.)

134

The residual may also be used for additional information about the model. A plot of the residual often reveals model inadequacies. If the system noise is assumed to be normally distributed, mean zero, then the residuals of a well-fitted model will also be normally distributed, mean zero. Deterministic trends in the residual can indicate frequency estimates in error or significant unmodeled contributions (such as significant contributions of unmodeled modes). If it is known that the measurement noise is not distributed normally, the residual should reflect what is known about that noise.

The size and nature of the residual are much better indicators of fitted model quality than plots of the measured and fitted data. As an example, two fitted models are presented, along with their residuals. The same simulated beam data was used for both models. Six modes were used in the simulation, with spatial frequencies of {0.0876, 0.1454, 0.2036, 0.2618, 0.3200, 0.3782}. Harmonic excitation very close to the first natural frequency was assumed $(\omega = 1.016\omega_n)$. This yielded an operating shape that could be modeled with one mode. (The modal weighting factors = {-19.7,-0.097,0.0227, -0.0081,0.0036,-0.0018}.) Random noise was added to the signal to simulate measured data with SNR of 40dB. The fitted model in Fig. 15 shows a model that was fitted well, with a spatial frequency of 0.088, and error of 0.457%. The model in Fig. 16 used a spatial frequency of 0.0800 (-8.676% error), resulting in a more poorly fitted model. Both figures 'look' relatively good. However, Figs. 17 and 18 plot the respective residuals. It readily apparent that the model in Fig. 17 is inferior to the model in Fig. 15. This is verified by the sum of

135

squared residuals. For the first model the sum of squared residuals is 0.0300. For the second model it is 0.0532, a 77% larger value. This indicates that the first model is superior to the second. As a comparison, the true noise variance (which is not known for measured data) is 0.0271. This figure is close to that of the first model, again confirming a good fit.
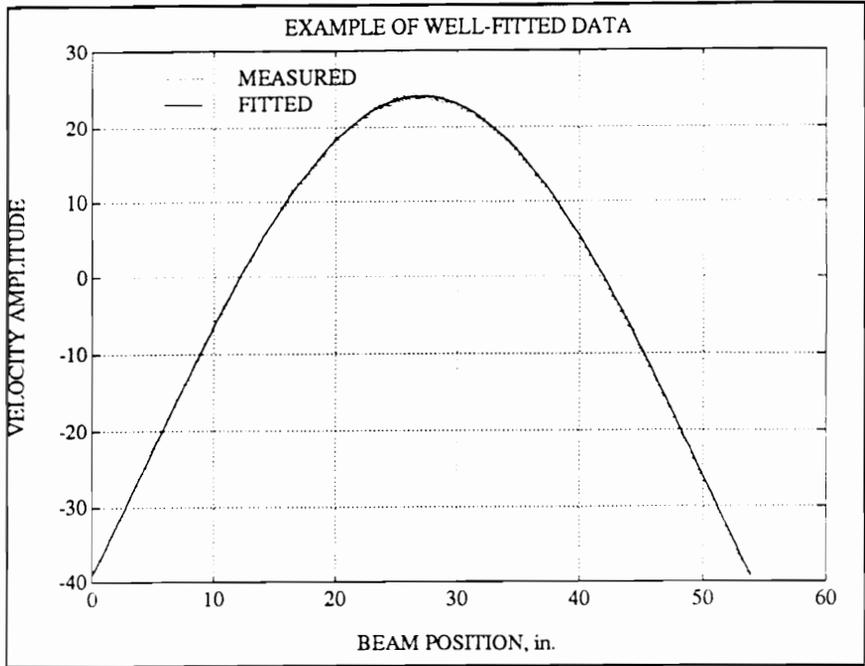
Figure 15 Example of good model fit.
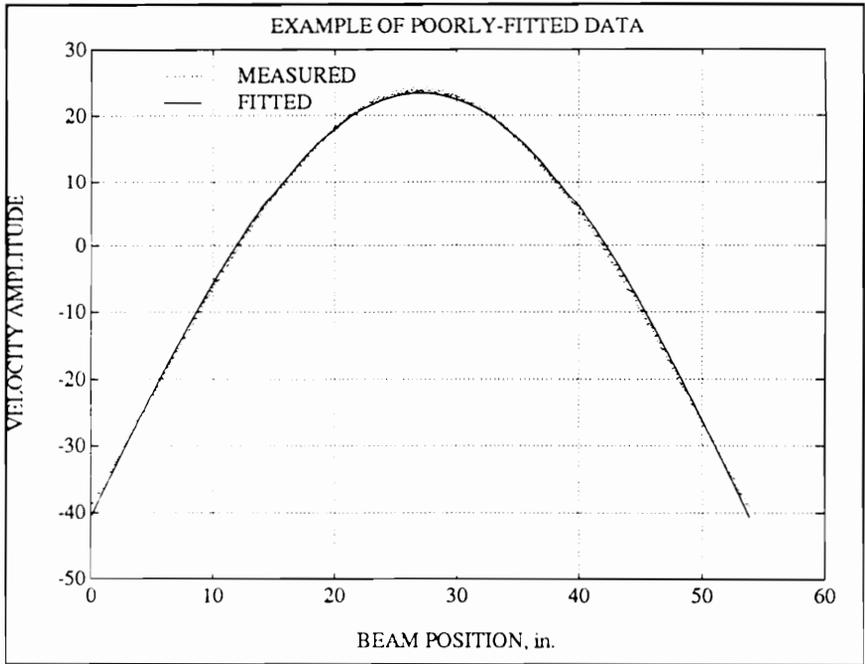
Figure 16 Example of poor model fit.

137
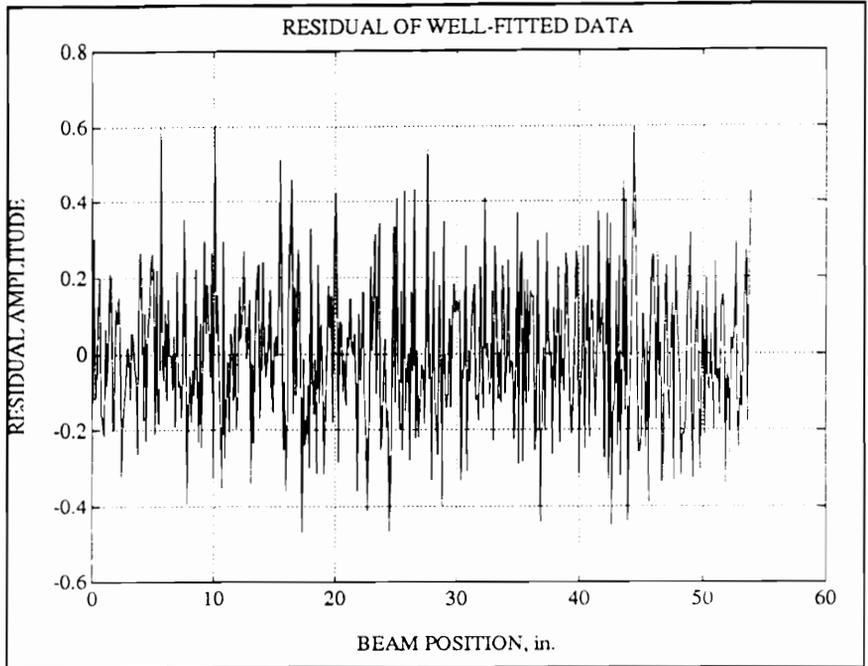
Figure 17 Residual for good model fit example.
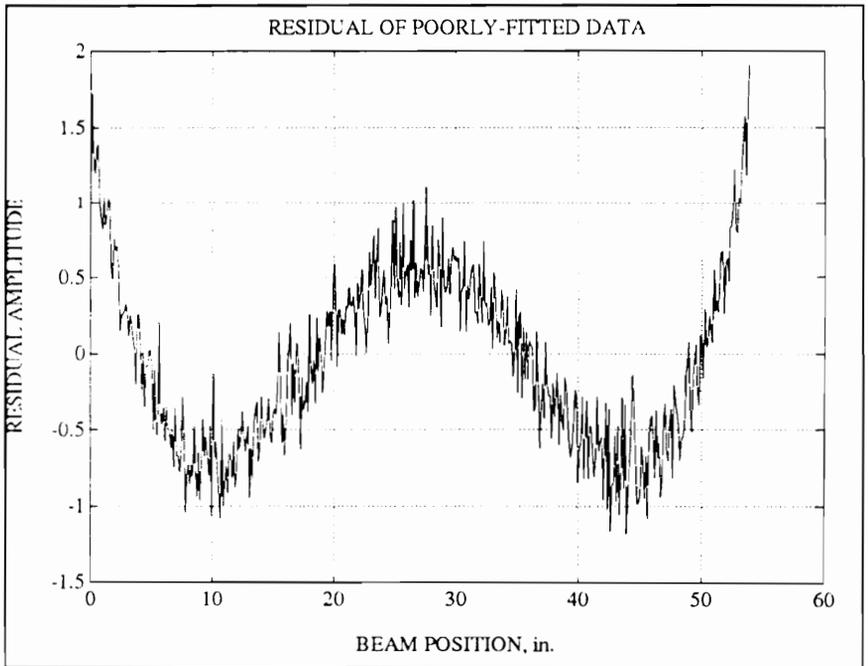
Figure 18 Residual of poor model fit example.

138

It must be kept in mind, however, that the above criteria for evaluating a model in terms of the residual apply only when comparing residuals of models of the same order. If the model order is overspecified, a small, normally distributed residual can result, even if the model parameters are grossly in error. As an example, the same simulated data used in Figs. 15 and 16 was fitted with a model using {0.04, 0.22} as spatial frequencies. These figures are not close to any of the true spatial frequencies of the simulated data. Figure 19 shows the fitted and simulated data, while Fig. 20 plots the resulting residual. Despite the fact that the estimated frequencies varied from the first mode by -54.3% and 151.1%, the fitted model closely matches the data, and the residual is small. In this case, the only indication that the model is deficient is the fact that the sum of squared residuals was 0.0300, the same value as the first model. A higher order model should yield a smaller residual. These examples indicate how the residual function can be used to evaluate the quality of a fitted model, and also some of the difficulties.
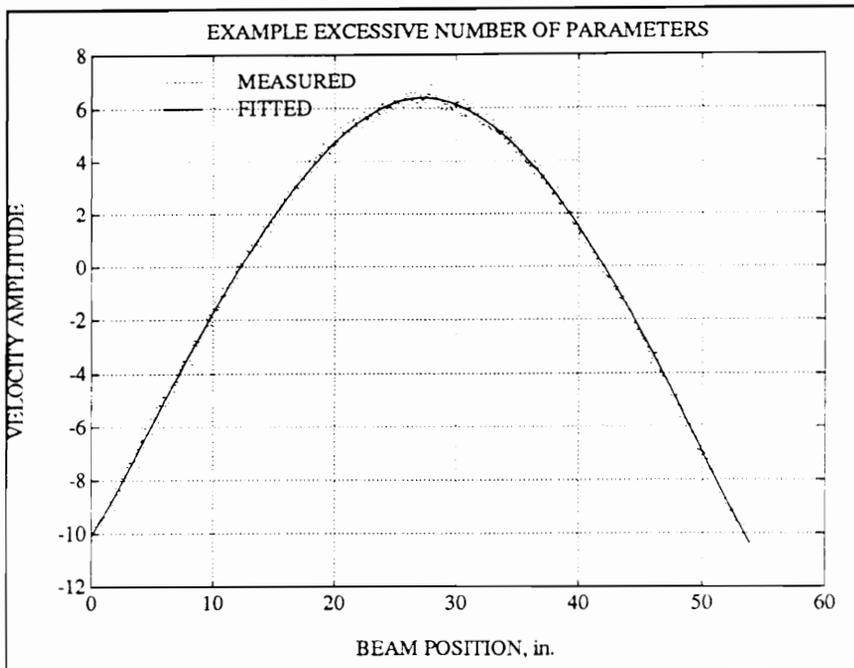
Figure 19 Example of a poorly fitted model with two modes.
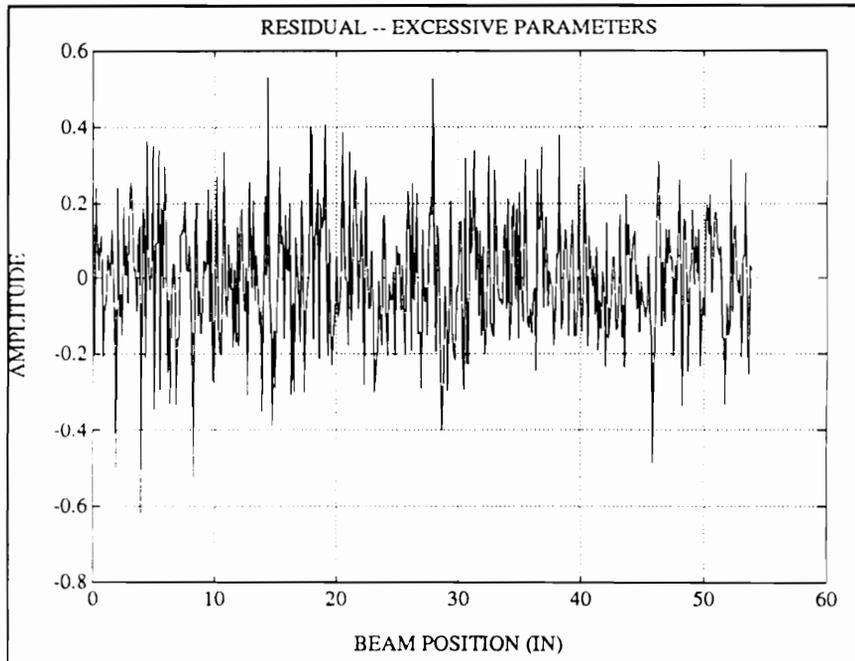
Figure 20 Residual of poorly fitted model with two modes.

140

CONDITION OF THE BEAM PROBLEM

The effect of high sample rate to signal frequency ratio on AR system condition is described in detail in Chapter 3. It is also pointed out above that the beam problem will always be oversampled. Thus the use of an appropriate delay factor is always in order. However, even with an acceptable delay factor, the beam problem continues to exhibit ill-conditioning for the lower modes. The presence of the hyperbolic functions summed with the circular functions decreases the system condition significantly with respect to either circular or hyperbolic functions. This leads to a poorly conditioned problem.

An example illustrates the condition the first six modes of a free-free beam. Data was generated using the following functions

$$y_1(x) = C_1 e^{\beta x} + C_2 e^{-\beta x} \qquad (5.3)$$

$$y_2(x) = C_3 e^{i\beta x} + C_4 e^{-i\beta x} \qquad (5.4)$$

$$y_3(x) = y_1(x) + y_2(x) \qquad (5.5)$$

141

The first two functions, $y_1(x)$ and $y_2(x)$ can be represented by an autoregressive function of second order, while $y_3(x)$ requires a model order of 4. Note that $y_3(x)$ is the same form as the spatial beam function. A data vector was generated from each of the three functions by evaluating each at 450 different, evenly spaced sample points. The condition number for delayed circulent matrices from each data vector was evaluated for a range of delay factors from $D = 1$ to 100. The first two vectors were formed into two-column matrices, while four columns were used for the third data vector. This was done for each of six cases, $\beta = \{0.0876, 0.1454, 0.2036, 0.2618, 0.3200, 0.3782\}$. The results are plotted in Figs. 21-26.

In each case, the condition number of the matrix constructed from $y_3(x)$ was much larger than the constituent functions. All functions indicated a noticeable drop in condition number as the delay factor is increased. The circular function has a distinct minimum, as demonstrated in Chapter 3. The hyperbolic function continues to decrease. In Figs. 24-26, the sharp peak on the right side of the plot indicates the Nyquist frequency. Despite the increase in the combined data condition number, with an appropriate delay acceptable conditioning is obtained in most cases. The first mode, however, poses a significant problem. Data taken from the first mode of a free-free beam can be considered ill-conditioned. This implies that reliable estimates of first mode spatial frequencies are very difficult.

These conclusions should be typical of all boundary conditions. The exception is pinned-pinned, in which the mode shapes consist only of circular functions. In that case, the same comments apply as in Chapter 2.
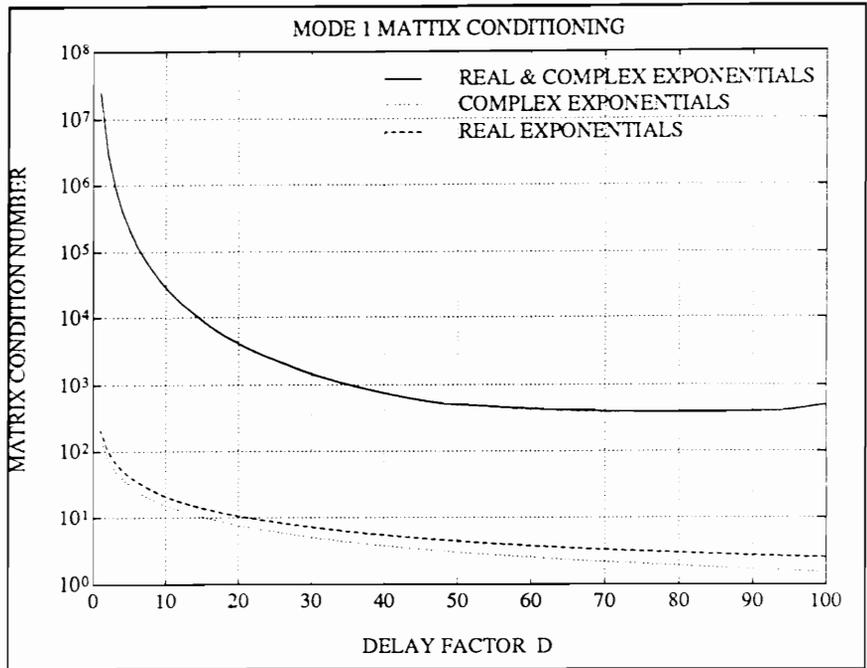
Figure 21 Theoretical matrix condition for mode 1.
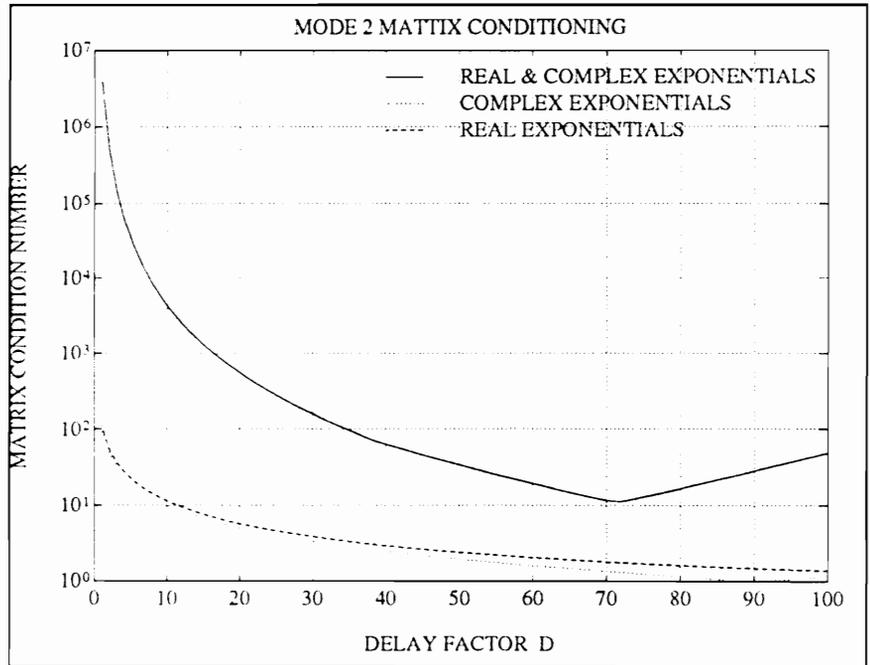
Figure 22 Theoretical matrix condition for mode 2.

144
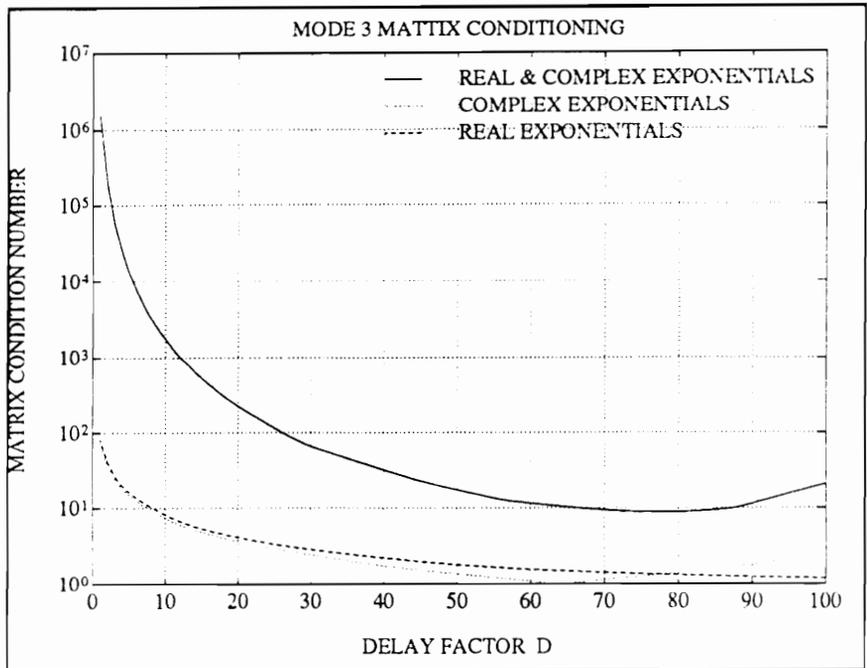
Figure 23 Theoretical matrix condition for mode 3.
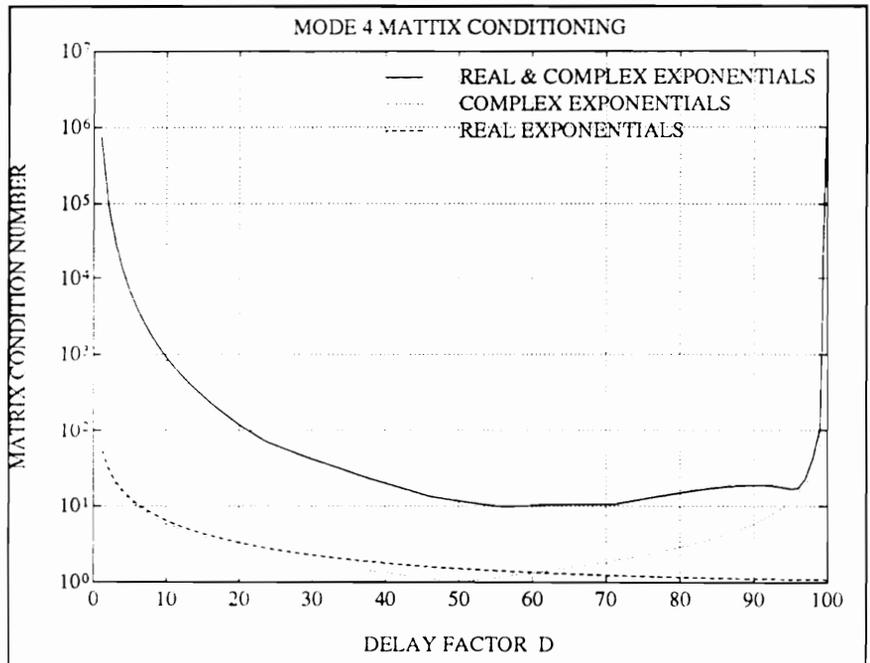
Figure 24 Theoretical matrix condition for mode 4.

145
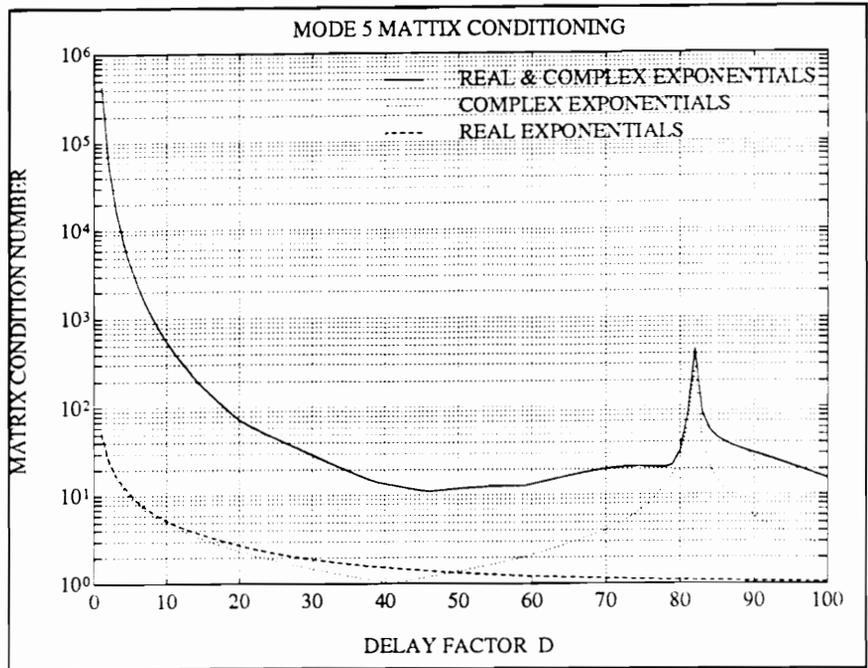
Figure 25 Theoretical matrix condition for mode 5.
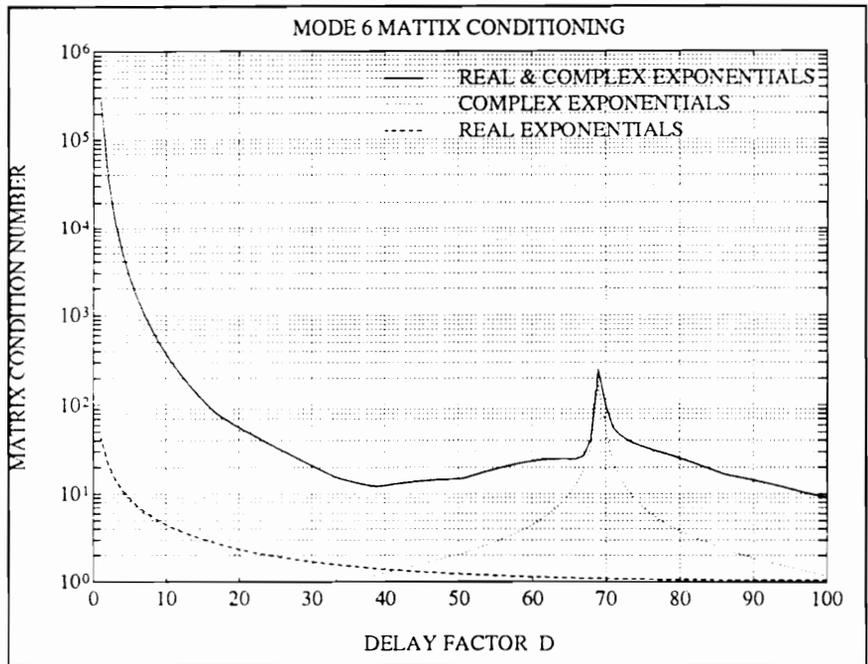
Figure 26 Theoretical matrix condition for mode 6.

146

An additional factor can contribute to the ill-conditioning of the beam problem. If the beam is excited near resonance, modes other than the resonance mode will contribute only a small amount to the operating shape of the beam. In these cases, the very small modal weighting of these modes will exacerbate the ill-conditioned nature of the problem. In such cases, the off-resonance modes may need to be neglected. If they are included, the model order may be correct theoretically, but the problem is severely ill-conditioned. Thus, unreliable parameter estimates will result. If these modes are neglected, the model order will be low, and will result in biased estimates. However, the bias error is usually much smaller than the errors resulting from a severely ill-conditioned problem. This, coupled with the results from the above section indicating the errors that can be masked by an overspecified model, suggest that the small bias error may yield the preferable model.

CONCLUSION

Despite several drawbacks, the AR methods can effectively model spatial beam data. It can be an efficient method for obtaining parameter estimates directly from the data. The residual function provides a useful indication of model quality, particularly when comparing models of the same order. The AR method is most effective for estimation of

147

higher modes. The first mode is the most poorly conditioned, and thus poses the most problems.

The AR approach is not without drawbacks, however. It can be difficult to choose the correct model fitting parameters, such as model order, column dimension, and delay factor. Models fitted with different values of these parameter will yield different model parameter estimates. Sometimes, the resulting model will be quite poor. If the model order is overspecified, it can be very difficult to detect a poorly fitted model. Also, limitations exist in terms of problem conditioning. The accuracy of parameter estimates is very dependent on signal-to-noise level. Other factors that contribute to inaccuracy are sample rate, and sample spacing, and the inability to impose theoretical constraints on the model.

NEWTON'S METHOD FOR SPATIAL BEAM ANALYSIS

The autoregressive method of spatial modal analysis of beams is an efficient way to estimate beam parameters. However, it is subject to drawbacks that limit the accuracy of parameter estimates. In an attempt to investigate other possibilities, Newton's method for spatial beam analysis was developed. Newton's method is an iterative approach, used to solve the non-linear least squares problem. Related techniques have been used for temporal analysis of free-vibration and impulse-response data (Smith, W.R., 1981; Smith, K.E., 1984). These time-domain methods have been shown to yield highly accurate

parameter estimates (Cooper & Wright, 1985). However, the computational effort is very high.

Application of Newton's method to spatial beam analysis is a considerably more difficult task than that faced by W.R. Smith. Many of the factors that make the AR problem ill-conditioned also make the minimizing function very flat in the search region. Thus, convergence is slow for multiple modes. However, rapid convergence and accurate parameter estimates are typical for single-mode analysis. Initial parameter estimates should be relatively accurate, within approximately 10% of the true value in most cases. Spatial frequency estimates obtained using the AR method will typically be quite satisfactory as initial estimates. A very reasonable approach to the beam problem is to first obtain parameter estimates via the AR method, and then 'polish' those estimates to the desired accuracy using Newton's method.

THEORY OF NEWTON'S METHOD

The spatial modal analysis problem is well defined for beams. High resolution spatial data is available with scanning laser vibrometery. Also, the operating shape of a beam vibrating laterally is well known from theory. This theory is presented in Chapter 4 of this dissertation. The combination of highly resolved measured data and a well known

theoretical model lead to the following question: What are the values of the parameters in the theoretical model that 'best fit' the measured beam velocities? Or, to cast the problem more rigorously: What values of parameters in the theoretical model will generate a function for which the sum of squared deviations from the measured velocity amplitude data is a minimum. This is simply the least squares problem for spatial beam data.

The difficulty in implementation of the least squares solution is the non-linearity of the unknown parameters. The AR method is attractive because it forces the non-linearity into a root-finding procedure, which is not a difficult problem. A different approach is to use an iterative solution for the non-linearity. This can be accomplished with a multi-dimensional Newton's method. This method involves finding the zeros of a function by iteration. In the one-dimensional case, this is accomplished by computing the slope of the tangent line at each iteration. The new value of the unknown variable is taken as that point where the tangent line is zero. For a linear function, this would be exact in one iteration. For nonlinear functions, the method converges quadratically to the correct solution. The multidimensional case is analogous, except that instead of replacing curves with tangent lines, the linearization involves replacing surfaces with tangent hyperplanes. A general implementation of the method is described by Forsythe and Moler, 1967. The method outlined below has been tailored to the spatial beam problem.

150

The formulation begins with basic beam theory. Recall that the equation for the operating shape of a beam in lateral vibration is

$$v(x) = \sum_{l=1}^{m} C_{1,l} e^{\beta_l x} + C_{2,l} e^{-\beta_l x} + C_{3,l} e^{i\beta_l x} + C_{4,l} e^{-i\beta_l x} \qquad (5.6)$$

Designate the measured velocity data y_k measured at locations x_k both for $k = 1:N$. The object is to find the least squares estimates for $C_{1,1} \dots C_{4,m}$ and $\beta_1 \dots \beta_m$. These values will be obtained with a model such that the sum of squared residuals is minimized. The residual function is given by

$$R_k = y_k - v(x_k, C_{1,1}, C_{2,1}, C_{3,1}, C_{4,1}, \beta_1, C_{1,2}, \dots \beta_m) \qquad (5.7)$$

The least squares solution requires that the sum of squared residuals be minimized. Thus, it is necessary to find

$$\min \sum_{k=1}^{N} (R_k)^2$$

This expression is minimized when all of the partial derivatives with respect to the unknowns are simultaneously equal to zero. Since there are 5 unknowns for each mode, this results in 5m simultaneous equations in 5m unknowns. These equations are

$$\left\{ \begin{array}{l} f_1 = \dfrac{\partial}{\partial \mathcal{C}_{1,1}} \displaystyle\sum_{k=1}^{N} (R_k)^2 = 0 \\[2mm] f_2 = \dfrac{\partial}{\partial \mathcal{C}_{2,1}} \displaystyle\sum_{k=1}^{N} (R_k)^2 = 0 \\[2mm] f_3 = \dfrac{\partial}{\partial \mathcal{C}_{3,1}} \displaystyle\sum_{k=1}^{N} (R_k)^2 = 0 \\[2mm] f_4 = \dfrac{\partial}{\partial \mathcal{C}_{4,1}} \displaystyle\sum_{k=1}^{N} (R_k)^2 = 0 \\[2mm] f_5 = \dfrac{\partial}{\partial \beta_1} \displaystyle\sum_{k=1}^{N} (R_k)^2 = 0 \\[2mm] \vdots \\[2mm] f_{5m-1} = \dfrac{\partial}{\partial \mathcal{C}_{m,4}} \displaystyle\sum_{k=1}^{N} (R_k)^2 = 0 \\[2mm] f_{5m} = \dfrac{\partial}{\partial \beta_m} \displaystyle\sum_{k=1}^{N} (R_k)^2 = 0 \end{array} \right\} \qquad (5.8a)$$

or, by taking the partial derivatives in Eq. 5.8a,

153

$$\left\{ \begin{array}{l} f_1 = \displaystyle\sum_{k=1}^{N} R_k e^{\beta_1 x} = 0 \\[2mm] f_2 = \displaystyle\sum_{k=1}^{N} R_k e^{-\beta_1 x} = 0 \\[2mm] f_3 = \displaystyle\sum_{k=1}^{N} R_k e^{i\beta_1 x} = 0 \\[2mm] f_4 = \displaystyle\sum_{k=1}^{N} R_k e^{-i\beta_1 x} = 0 \\[2mm] f_5 = \displaystyle\sum_{k=1}^{N} R_k \phi_{1,k} = 0 \\[2mm] \vdots \\[2mm] f_{5m-1} = \displaystyle\sum_{k=1}^{N} R_k e^{-i\beta_m x} = 0 \\[2mm] f_{5m} = \displaystyle\sum_{k=1}^{N} R_k \phi_{m,k} = 0 \end{array} \right\} \qquad (5.8b)$$

The quantity $\Phi_{i,k}$ in Eq. 5.8b is the partial derivative of $v(x)$ with respect to β_i. In continuous space it is given by the relation

$$\Phi_l = \frac{\partial y}{\partial \beta_l} = \qquad\qquad (5.9)$$
$$x C_1 e^{\beta_l x} - x C_2 e^{-\beta_l x} + ix C_3 e^{i\beta_l x} - ix C_4 e^{-i\beta_l x}$$

The non-linearities of the exponential functions in Eq. 5.8b preclude use of conventional linear system methods. The problem is well posed for Newton's method however. First,

154

initial values for the unknowns, $P = \{C_{1,1}, C_{2,1}, C_{3,1}, C_{4,1}, \beta_1, \ldots, C_{4,m}, \beta_m\}$ must be assumed. The initial values can be the parameter estimates obtained from an AR analysis, or they can be obtained from theory. Except for the first mode, they need not be very accurate. The initial values are designated $P^0 = \{C^0_{1,1}, C^0_{2,1}, C^0_{3,1}, C^0_{4,1}, \beta^0_1, \ldots, C^0_{4,m}, \beta^0_m\}$. The functions in Eq. 5.8b can now be approximated by the first two terms of Taylor's Series for multiple variables. Let f^*_j be the function f_j evaluated at the true parameters P. Also let f^0_j be the function f_j evaluated at the initial parameters P^0. Then the truncated Taylor's Series is given by

$$f^*_j = f^0_j + \sum_{l=1}^{m} \left(\frac{\partial f^0_j}{\partial P_l} \right) (P^*_l - P^0_l) \tag{5.10}$$

The group of 4m equations formed from Eq. 5.10 for $j = 1{:}4m$ can be written in matrix form as

$$f = f^0 + J(P^0)(P - P^0) \tag{5.11}$$

The $(5m \times 5m)$ matrix $J(P^0)$ is the Jacobian matrix of the system $f(P)$. It is given by

155

$$J(P) = \begin{bmatrix} \left(\dfrac{\partial f_1}{\partial C_{1,1}}\right) & \left(\dfrac{\partial f_1}{\partial C_{2,1}}\right) & \left(\dfrac{\partial f_1}{\partial C_{3,1}}\right) & \left(\dfrac{\partial f_1}{\partial C_{4,1}}\right) & \left(\dfrac{\partial f_1}{\partial \beta_1}\right) & \cdots & \left(\dfrac{\partial f_1}{\partial \beta_m}\right) \\[2ex] \left(\dfrac{\partial f_2}{\partial C_{1,1}}\right) & \left(\dfrac{\partial f_2}{\partial C_{2,1}}\right) & \left(\dfrac{\partial f_2}{\partial C_{3,1}}\right) & \left(\dfrac{\partial f_2}{\partial C_{4,1}}\right) & \left(\dfrac{\partial f_2}{\partial \beta_1}\right) & \cdots & \left(\dfrac{\partial f_2}{\partial \beta_m}\right) \\[2ex] & & & \vdots & & & \\[2ex] \left(\dfrac{\partial f_5 m}{\partial C_{1,1}}\right) & \left(\dfrac{\partial f_5 m}{\partial C_{2,1}}\right) & \left(\dfrac{\partial f_5 m}{\partial C_{3,1}}\right) & \left(\dfrac{\partial f_5 m}{\partial C_{4,1}}\right) & \left(\dfrac{\partial f_5 m}{\partial \beta_1}\right) & \cdots & \left(\dfrac{\partial f_5 m}{\partial \beta_m}\right) \end{bmatrix} \qquad (5.12)$$

Each row of J contains the partial derivative of one of the functions in Eq. 5.8b. Each column is composed of the partial derivatives of the functions with respect to one of the unknown parameters in P. For example, the first term in the first row is the partial derivative of f_1 with respect to $C_{1,1}$. It is given by

$$\frac{\partial f_1}{\partial C_{1,1}} = \frac{\partial}{\partial C_{1,1}}\left(\sum_{k=1}^{N} R_k e^{\beta_1 x_k}\right) = -\sum_{k=1}^{N} e^{\beta_1 x_k} e^{\beta_1 x_k} \qquad (5.13)$$

Likewise, the fifth entry on the first row is given by

$$\frac{\partial f_1}{\partial \beta_1} = \frac{\partial}{\partial \beta_1}\left(\sum_{k=1}^{N} R_k e^{\beta_1 x_k}\right) = -\sum_{k=1}^{N} (R_k x_k - \Phi_{i,k}) e^{\beta_1 x_k} \qquad (5.14)$$

156

The Jacobian matrix J can be written in block form as an $(m \times m)$ matrix of (5×5) submatrices. The diagonal blocks, or submatrices, contain the single-mode terms, i.e., all terms in the diagonal blocks contain only parameters from one mode. The remaining blocks contain cross-mode terms -- each element contains parameters from two modes. The two types of blocks are of different forms. Using the block notation that J_i is the ith diagonal submatrix and J_{ij} is the submatrix in row i and column j, the Jacobian can be written as

$$J = \begin{bmatrix} J_1 & J_{1,2} & J_{1,3} & \cdots & J_{1,m} \\ J_{2,1} & J_2 & J_{2,3} & \cdots & J_{2,m} \\ \vdots & & & & \\ J_{m,1} & J_{m,2} & J_{m,3} & \cdots & J_m \end{bmatrix} \qquad (5.15)$$

The diagonal, or single-mode, blocks have the form of Eq. 5.16. Similarly, the cross-mode, or off-diagonal, blocks have the form of Eq. 5.17.

157

$$J_l = -\sum_{k=1}^{N} \begin{bmatrix} e^{\beta_k r_k} e^{\beta_j r_k} & e^{-\beta_k r_k} e^{\beta_j r_k} & e^{i\beta_k r_k} e^{\beta_j r_k} & e^{-i\beta_k r_k} e^{\beta_j r_k} & (\Phi_{l,k} - R_k \chi_k) e^{\beta_j r_k} \\ e^{\beta_k r_k} e^{-\beta_j r_k} & e^{-\beta_k r_k} e^{-\beta_j r_k} & e^{i\beta_k r_k} e^{-\beta_j r_k} & e^{-i\beta_k r_k} e^{-\beta_j r_k} & (\Phi_{l,k} + R_k \chi_k) e^{-\beta_j r_k} \\ e^{\beta_k r_k} e^{i\beta_j r_k} & e^{-\beta_k r_k} e^{i\beta_j r_k} & e^{i\beta_k r_k} e^{i\beta_j r_k} & e^{-i\beta_k r_k} e^{i\beta_j r_k} & (\Phi_{l,k} - iR_k \chi_k) e^{i\beta_j r_k} \\ e^{\beta_k r_k} e^{-i\beta_j r_k} & e^{-\beta_k r_k} e^{-i\beta_j r_k} & e^{i\beta_k r_k} e^{-i\beta_j r_k} & e^{-i\beta_k r_k} e^{-i\beta_j r_k} & (\Phi_{l,k} + iR_k \chi_k) e^{-i\beta_j r_k} \\ (\Phi_{l,k} - R_k \chi_k) e^{\beta_j r_k} & (\Phi_{l,k} + R_k \chi_k) e^{-\beta_j r_k} & (\Phi_{l,k} - iR_k \chi_k) e^{i\beta_j r_k} & (\Phi_{l,k} + iR_k \chi_k) e^{-i\beta_j r_k} & (\Phi_{l,k} \Phi_{l,k} - R_k \Theta_{l,k}) \end{bmatrix} \tag{5.16}$$

$$J_{l,j} = -\sum_{k=1}^{N} \begin{bmatrix} e^{\beta_k r_k} e^{\beta_j r_k} & e^{-\beta_k r_k} e^{\beta_j r_k} & e^{i\beta_k r_k} e^{\beta_j r_k} & e^{-i\beta_k r_k} e^{\beta_j r_k} & \Phi_{l,k} e^{\beta_j r_k} \\ e^{\beta_k r_k} e^{-\beta_j r_k} & e^{-\beta_k r_k} e^{-\beta_j r_k} & e^{i\beta_k r_k} e^{-\beta_j r_k} & e^{-i\beta_k r_k} e^{-\beta_j r_k} & \Phi_{l,k} e^{-\beta_j r_k} \\ e^{\beta_k r_k} e^{i\beta_j r_k} & e^{-\beta_k r_k} e^{i\beta_j r_k} & e^{i\beta_k r_k} e^{i\beta_j r_k} & e^{-i\beta_k r_k} e^{i\beta_j r_k} & \Phi_{l,k} e^{i\beta_j r_k} \\ e^{\beta_k r_k} e^{-i\beta_j r_k} & e^{-\beta_k r_k} e^{-i\beta_j r_k} & e^{i\beta_k r_k} e^{-i\beta_j r_k} & e^{-i\beta_k r_k} e^{-i\beta_j r_k} & \Phi_{l,k} e^{-i\beta_j r_k} \\ \Phi_{j,k} e^{\beta_j r_k} & \Phi_{j,k} e^{-\beta_j r_k} & \Phi_{j,k} e^{i\beta_j r_k} & \Phi_{j,k} e^{-i\beta_j r_k} & \Phi_{j,k} \Phi_{l,k} \end{bmatrix} \tag{5.17}$$

This form of the Jacobian matrix can be called the modal form. Each element in the matrix of Eq. 5.15 represents the influence of the modal parameters of one mode on those of another. However, for computational purposes, a different form is preferred. Equations 16 and 17 can be written in block form as

$$J_{lj} = \begin{bmatrix} E_{lj} & PE_{lj} \\ EP_{lj} & P_{lj} \end{bmatrix} \quad \begin{cases} E \rightarrow (4x4) \\ PE \rightarrow (4x1) \\ EP \rightarrow (1x4) \\ P \rightarrow (1x1) \end{cases} \tag{5.18}$$

Where E, is the upper left $(5x5)$ submatrix of J_{lj}, PE is the upper right $(4x1)$ submatrix, EP is the lower left $(1x4)$ submatrix, and P is the lower right $(1x1)$ submatrix.

The rows and columns of J can be rearranged to place all like blocks into a larger submatrix. When this is done, the set of unknown parameters will also need to be rearranged. Let P be the rearrangement of set P. Then $P = \{C_{1,1},C_{2,1},C_{3,1},C_{4,1},...,C_{4,m},\beta_1,...,\beta_n\}$. The corresponding rearrangement of J is

159

$$
J = \begin{bmatrix}
\begin{vmatrix}
E_{1,1} & E_{1,2} & \cdots & E_{1,m} \\
E_{2,1} & E_{2,2} & \cdots & E_{2,m} \\
\vdots & & & \\
E_{m,1} & E_{m,2} & \cdots & E_{m,m}
\end{vmatrix} &
\begin{vmatrix}
EP_{1,1} & EP_{1,2} & \cdots & EP_{1,m} \\
EP_{2,1} & EP_{2,2} & \cdots & EP_{2,m} \\
\vdots & & & \\
EP_{m,1} & EP_{m,2} & \cdots & EP_{m,m}
\end{vmatrix} \\
\begin{vmatrix}
PE_{1,1} & PE_{1,2} & \cdots & PE_{1,m} \\
PE_{2,1} & PE_{2,2} & \cdots & PE_{2,m} \\
\vdots & & & \\
PE_{m,1} & PE_{m,2} & \cdots & PE_{m,m}
\end{vmatrix} &
\begin{vmatrix}
P_{1,1} & P_{1,2} & \cdots & P_{1,m} \\
P_{2,1} & P_{2,2} & \cdots & P_{2,m} \\
\vdots & & & \\
P_{m,1} & P_{m,2} & \vdots & P_{m,m}
\end{vmatrix}
\end{bmatrix} \tag{5.19}
$$

Or simply

$$
J = \begin{bmatrix} E & EP \\ PE & P \end{bmatrix} \qquad
\begin{cases}
E \to (4m \ \times \ 4m) \\
EP \to (4m \ \times \ m) \\
PE \to (m \ \times \ 4m) \\
P \to (m \ \times \ m)
\end{cases} \tag{5.20}
$$

This form of the Jacobian reveals something about its nature, as well. The submatrices E and P are symmetric. The matrix PE is the transpose of the matrix EP. Thus, the Jacobian is a symmetric matrix. The submatrix E represents the linear least squares fit of the constants $\{C_{1,1}, C_{2,1}, C_{3,1}, C_{4,1}, ..., C_{4,m}\}$. The matrix P, on the other hand, represents the application of Newton's method to the non-linear least squares fit of the spatial frequencies.

160

In Smith's Least Squares Time-Domain method, analogous matrices were formed to fit free-response time-domain data. In his analysis, the evaluation of the two different sets of constants, amplitude and phase versus frequency and damping ratio, is conducted in two distinct steps. In each iteration the linear least squares problem was solved first by ordinary means, and only then was Newton's method applied to obtain frequency and damping updates. For the damped sinusoidal data this approach works well. However, because the beam problem has more parameters, convergence rate is impeded by use of the two-step method. The submatrix PE provides a feedback between the non-linear and the linear terms. This dramatically improves convergence rate. However, the stability of the system is reduced -- that is, the initial guesses P^0 must be closer to the true values in order to ensure that the method will converge. Without the feedback, the procedure is very stable, but convergence is extremely slow.

The updated parameters can be obtained from Eq. 5.11 by solving for P. Thus, the parameter estimates for each iteration, P^i, are computed based on the previous parameter set P^{i-1} by the following relation

$$P^i = P^{i-1} + (J_{i-1})^{-1} f_{i-1} \qquad (5.21)$$

The vector f is obtained by evaluating Eq. 5.8b at P^{i-1}.

161

Equation 21 is solved at each iteration. The parameter set P^i typically converges rapidly to correct version. However, no definitive criteria for determining convergence exists. The objective is to minimize the residual function. This suggests that convergence be assumed when the residual is smaller than some pre-set tolerance. However, the residual is related to the noise on the signal. Thus, it will always be larger for noisy data than for clean data. Hence, the convergence criteria will depend heavily on the SNR of the data being analyzed. This is not an acceptable alternative. A related convergence criteria is for the difference between the residuals of two consecutive iterations to be below a prescribed tolerance. As the method converges to the true parameters, the residual will approach a value proportional to the noise variance. The residual difference between consecutive iterations will therefore be small. This method produces very satisfactory results. It is reliable, and stable. No cases of false convergence have been noted for single mode analysis. Mathematically, this criteria can be stated as

$$\left(\sum_{k=1}^{N} (R_k^i)^2 \ - \ \sum_{k=1}^{N} (R_k^{i-1})^2 \right) < \textit{tolerance}$$

CONVERGENCE ANALYSIS

Newton's method is iterative in nature. As with any iterative analysis, questions of convergence must be addressed. Will the method converge to the 'correct' answer? Under what conditions will the method converge? Under what conditions will it not converge? How rapidly will the method converge? What criteria will be used to determine convergence? These questions can be answered either by analytical or empirical analysis.

Several convergence tests are presented in order to address different convergence concerns. Theoretical univariate and bivariate convergence analyses are presented to determine the convergence of spatial frequencies given known modal coefficients. Also, the results of empirical analyses using both simulated and measured data are presented. A limited multivariate analysis considering only spatial frequency estimates for multiple modes is also presented.

THEORETICAL ANALYSIS: The theoretical convergence of Newton's method with respect to spatial frequency is investigated. Both a univariate case, in which only one mode is modeled, and a bivariate case, in which two adjacent modes are modeled, are considered. Univariate analyses are much simpler to perform and to evaluate than multivariate analyses. The multivariate case provides valuable information about practical implementation of Newton's method. A comparison of both cases gives insight into the nature of the LSSD problem.

163

These analyses investigate convergence only with respect to spatial frequency. Thus, assumptions must be made regarding the modal coefficients. Two assumptions were made, and each was investigated for both the univariate and multivariate analyses. These assumptions are:

1. The modal coefficients are known exactly.

2. The modal coefficients are computed using a linear least squares method.

For the univariate case, it is further assumed that the data can be modeled with only one mode. Likewise, the bivariate case implicitly assumes that the data can be modeled with two modes.

Accurate spatial frequency estimates are critical to building a meaningful model. The theoretical basis will be developed based on a multivariate model in which the only unknown parameters are the spatial frequencies for each mode. In implementation, only one mode or two modes will be modeled.

The operating shape of a vibrating beam is given as a linear combination of the normal mode functions. According to Euler-Bernoulli theory, the operating shape has the form

$$y = \sum_{i=1}^{m} \left\{ C_{1,i} e^{\beta_i x} + C_{2,i} e^{-\beta_i x} + C_{3,i} e^{j\beta_i x} + C_{4,i} e^{-j\beta_i x} \right\} \qquad (5.22)$$

Newton's method is a way of fitting measured data obtained from a beam to the model in Eq. 5.22. The objective is to find the parameters $C_{i,j}$ and β_i that minimizes the sum of squared residuals. More rigorously, this objective can be stated as:

Given the discrete, measured spatial series Y_k, $k=1{:}N$, measured at the discrete locations x_k, find the parameter set $P=\{C_{1,1},C_{1,2},...C_{m,4},\beta_1, \beta_2,... \beta_m\}$ that minimizes

$$S(P) = \sum_{k=1}^{N} R_k^2 \qquad (5.23)$$

where R_k is the residual function given by

$$R_k = Y_k - y_k \qquad (5.24)$$

with Y_k the measured data and y_k is the beam model given by Eq. 5.22 with $y_k = y(x_k, P)$.

In order to investigate the convergence of Newton's method it is necessary to investigate the residual and the derivatives of the residual. In general, this is a difficult problem for a multivariate analysis. However, some insight can be gained by a limited analysis. Equation 22 is linear in the modal coefficients. The non-linear nature of the modeling problem is associated with estimation of the spatial frequencies. If it is assumed that the modal coefficients are known, then the fitted model becomes a function of only the non-linear spatial frequencies β_i and the independent coordinate x_k. That is, $y = y(x_k, \beta_1, \beta_2, \ldots \beta_{ni}) = y(x_k, Q)$ where Q is a subset of the parameter set P which contains only the spatial frequencies.

An objective function can be defined in terms of $S(Q)$ as

$$S(Q) = \sum_{k=1}^{N} (Y_k - y_k(Q))^2 \tag{5.25}$$

The partial derivative of $S(Q)$ with respect to β_i is then given by

$$D_i(Q) = \frac{\partial S(Q)}{\partial \beta_i} = -2 \sum_{k=1}^{N} (Y_k - y_k(Q)) \Phi_i \tag{5.26}$$

166

where

$$\Phi_i = \frac{\partial y(Q)}{\partial \beta_i} = x\left[C_{1,i}e^{\beta_i x} - C_{2,i}e^{-\beta_i x} + jC_{3,i}e^{j\beta_i x} - jC_{4,i}e^{-j\beta_i x}\right] \qquad (5.27)$$

It is desired to investigate the behavior of $S(Q)$ and $D_i(Q)$ in the neighborhood of the true spatial frequencies β_i. This can be done considering any number of modes. However, interpretation of the results is clearest for the univariate case -- that is, only one mode included in the model. A bivariate analysis, in which two modes is considered, is also useful if two-dimensional mesh plots are used to interpret the data. However, analyses considering more than two modes are of little value, because a) the bivariate case is considered representative of the more general multivariate case, and b) multi-dimensional results are difficult to present in a meaningful manner. For these reasons, only the univariate and bivariate cases are investigated here.

The analysis can be performed by evaluating Eqs. 25 and 26 for a range of spatial frequencies in the neighborhood of the true frequencies. The true operating shape is synthesized using the program BEAMSIG. This program simulates a free-free Euler-Bernoulli beam subject to harmonic excitation. In order to more accurately reflect the behavior of a true beam, the influence of six modes was considered in synthesizing the data. For the univariate analysis, excitation frequencies were chosen very close to the

167

natural frequencies of the simulated beam. Data for the simulated beam is provided in Table IV. The simulation parameters for the univariate analysis are tabulated in Table V, while those for the bivariate case are presented in Table VI. The true parameters are taken to be those parameters used to synthesize the data.

Table IV True parameters for simulated beam data.

Width		3.00 in
Height		0.25 in
Length		54.00 in
Modulus of Elasticity		27.7e6 psi
Specific Weight		0.28 lb/in^3

MODE	1	2	3	4	5	6
β	0.0876	0.1454	0.2036	0.2618	0.3200	0.3782
ω	108.3	298.4	585.0	967.1	1444.7	2017.7

Table V Test parameters for univariate convergence analysis.

MODE	1	2	3	4	5	6
FREQ ω	110	300	590	970	1450	2010
MODAL	-19.748	-0.261	-0.120	-0.071	-0.047	-0.034
WEIGHT	-0.097	21.691	0.155	0.078	0.049	0.035
FACTOR	0.023	0.081	-6.888	-0.110	-0.056	-0.037
	-0.008	-0.024	-0.069	11.718	0.085	0.044
	0.004	0.010	0.023	0.058	-6.384	-0.070
	-0.002	-0.005	-0.011	-0.021	-0.050	-4.393
MIN β	0.0701	0.1163	0.1629	0.2094	0.2560	0.3025
$\Delta\beta$	0.0004	0.0006	0.0008	0.0010	0.0013	0.0015
MAX β	0.1051	0.1745	0.2443	0.3142	0.3840	0.4538

169

Table VI Test parameters for bivariate convergence analysis.

MODES i & j	1 & 2	2 & 3	3 & 4	4 & 5
FREQUENCIES	200	400	700	1200
MODAL WEIGHT FACTORS	-0.4820	-0.1838	-0.0997	-0.0573
	-0.2778	0.3842	0.1190	0.0605
	0.0451	0.1496	-0.3229	-0.0745
	-0.0152	-0.0352	-0.1071	0.1620
	0.0067	0.0141	0.0299	0.1264
	-0.0034	-0.0070	-0.0133	-0.0311
MIN β_i^s	0.0701	0.1163	0.1629	0.2094
$\Delta\beta_i^s$	0.0014	0.0023	0.0033	0.0042
MAX β_i^s	0.1051	0.1745	0.2443	0.3142
MIN β_j^s	0.1163	0.1629	0.2094	0.2560
$\Delta\beta_j^s$	0.0023	0.0033	0.0042	0.0051
MAX β_j^s	0.1745	0.2443	0.3142	0.3840

UNIVARIATE ANALYSIS: The univariate analysis assumed that only one spatial frequency parameter, β_i, is unknown. The residual function was evaluated for values of β_i in the neighborhood of the true value. The objective function S is thus a function of only one parameter, and only one derivative, D, exists. If the approximate value of β_i is given by β^o, then these Eqs. 25 and 26 become

170

$$S(\beta_i^o) = \sum_{k=1}^{N} \left(Y_k - y_k^*\right)^2$$

$$y_k^* = y_k\big|_{\beta_i = \beta_i^o}$$

(5.28)

$$D_i(\beta_i^o) = -2\sum_{k=1}^{N} \left(Y_k - y_k^*\right)\Phi_i^*$$

$$\Phi_i^* = \Phi_i\big|_{\beta_i = \beta_i^o}$$

(5.29)

The asterisk simply indicates that the function is to be evaluated with the assumed value β^o. Equations 28 and 29 can be easily evaluated for a range of β_i^o. For this analysis, 100 different values of β^o were used, ranging from 80% to 120% of the true spatial frequency. The procedure is

1. Simulate the series Y_k, $k=1{:}N$.

2. For $\min(\beta^o)$ to $\max(\beta^o)$ step($\Delta\beta^o$),

    Compute the residual R using Eq. 5.24 with $y(P) = y^*$

    Compute the partial derivative Φ^* using Eq. 5.27

    Compute the sum of squared residuals S using Eq. 5.40

    Compute the derivative function D using Eq. 5.41

3. Plot S and D versus β^o

171

This procedure was used for modes 1 through 6. In each case, the excitation frequency was chosen such that the mode of interest was the dominant mode. The results are plotted in Figs. 27 through 32. The computed values of S and D for each mode often differed by more than an order of magnitude. Thus, both the residual function S and the derivative D have been normalized by the formulas

$$
\begin{aligned}
S &= \frac{S}{\|S\|_2} \\
D &= \frac{D}{\|D\|_2}
\end{aligned}
\qquad (5.30)
$$

Figures 27 through 32 show that the residual function S is concave upward. When $\beta^o = \beta$, the residual is minimum, and that minimum is zero, as it should be. For the first mode, the function is almost symmetric, however as the mode of interest increases, the left half of the curve becomes flatter and the right half becomes steeper. The derivatives, except for first mode, all show a minimum at approximately 90% of the true spatial frequency. The right half of all derivative curves smoothly increases in magnitude and slope. Newton's method uses the derivative to estimate improved values of β. For convergence, local maxima and minima should not be present. The slope of the residual function should remain negative for $\beta^o < \beta$ and positive for $\beta^o > \beta$. Figures 27 through 32 show that this is indeed true for all cases. Thus, based on known modal coefficients, Newton's method,

in the univariate case, should converge efficiently for any $0.8\beta < \beta^o < 1.2\beta$. The small slope for higher modes in the region $\beta^o < \approx 0.9\beta$ may cause slower convergence, however.
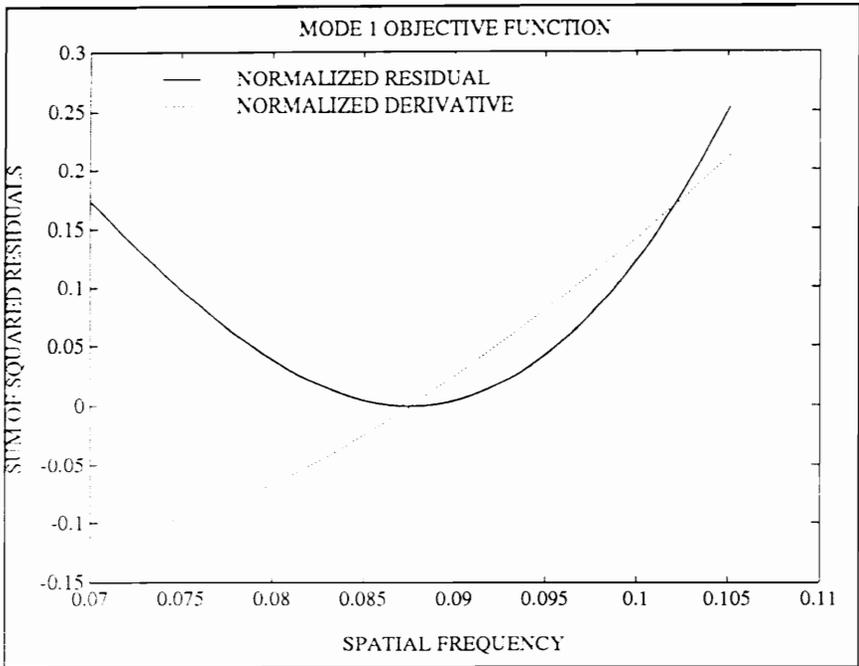
Figure 27 Residual function and derivative for mode 1 using exact coefficients.
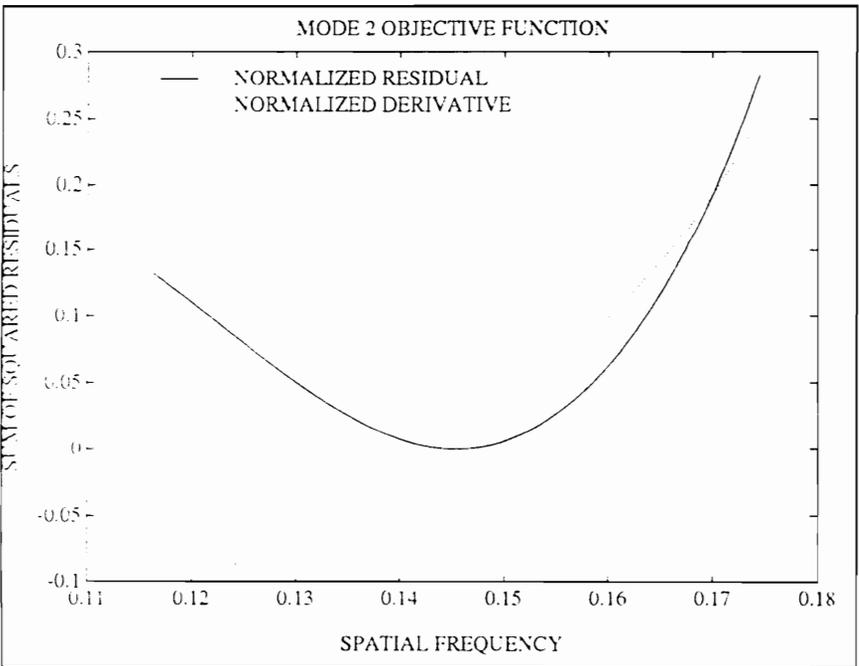
Figure 28 Residual function and derivative for mode 2 using exact coefficients.
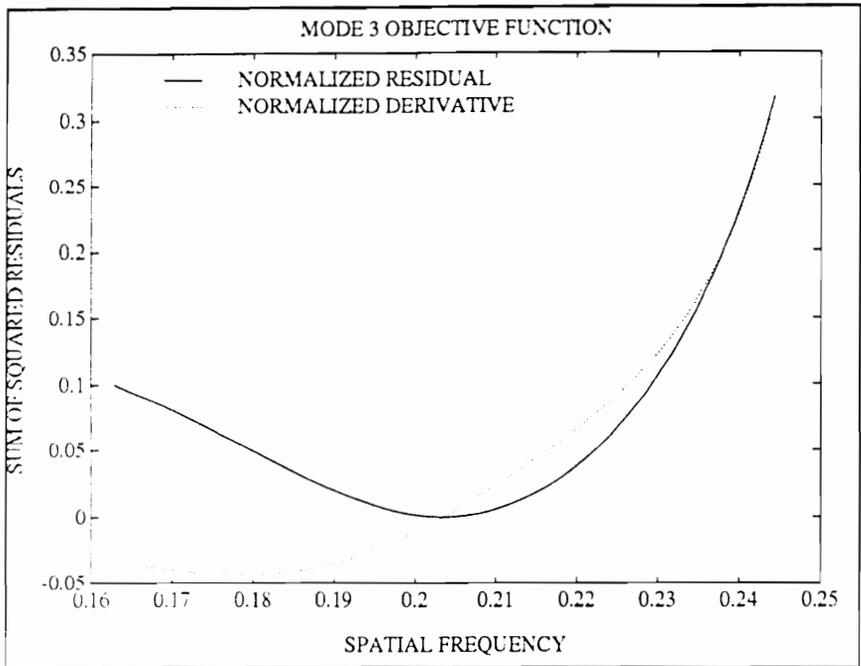
Figure 29 Residual function and derivative for mode 3 using exact coefficients.
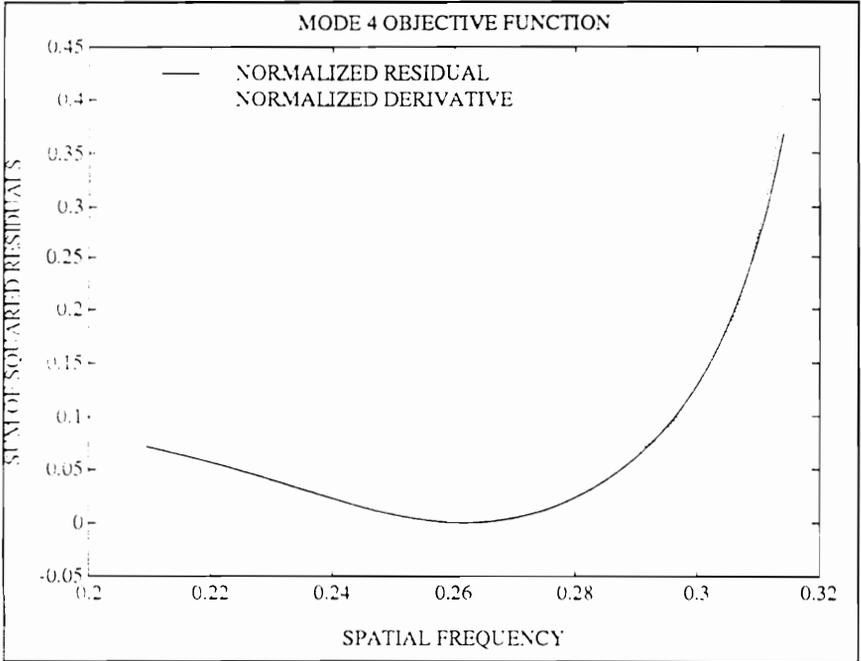
Figure 30 Residual function and derivative for mode 4 using exact coefficients.

175
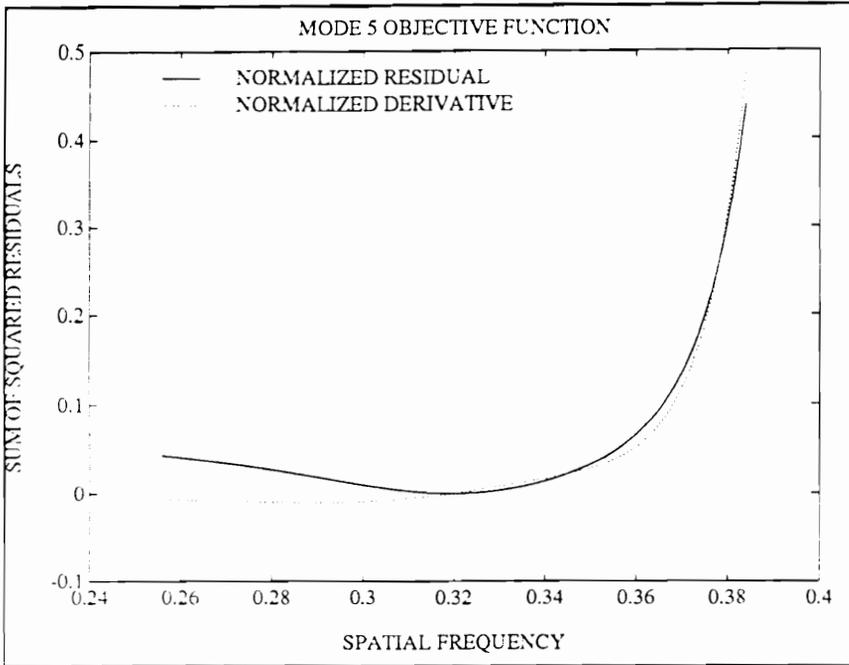
Figure 31 Residual function and derivative for mode 5 using exact coefficients.
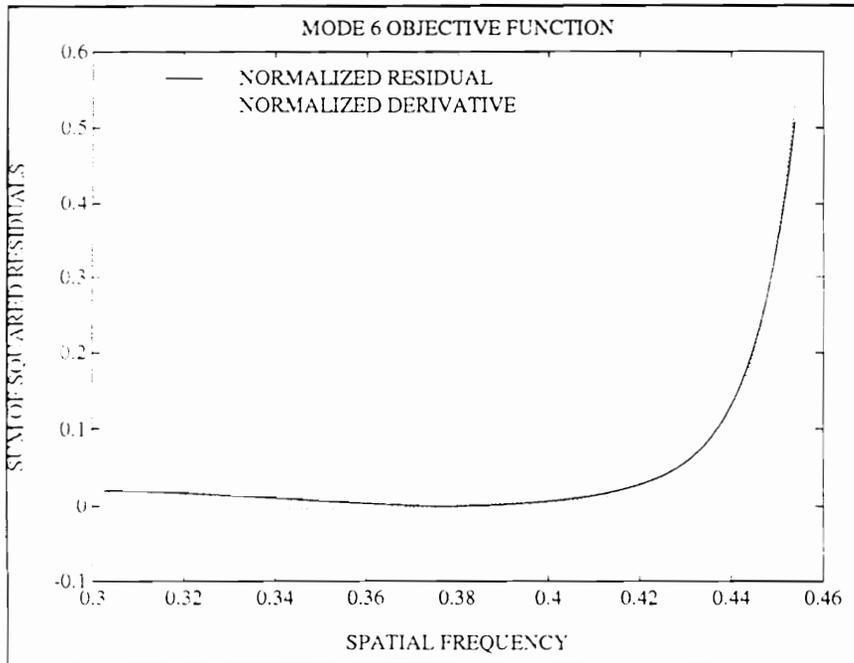
Figure 32 Residual function and derivative for mode 6 using exact coefficients.

176

The foregoing analysis assumed that the modal coefficients were known exactly. A more realistic approximation can be obtained by using the coefficients that give the best single-mode approximation to the true (simulated) data for each $\beta = \beta^o$. That is, at each assumed spatial frequency, the modal coefficients are found by a linear least squares fit of Eq. 5.22.

This requires an investigation of the residual and derivative in the neighborhood of β when C_1, C_2, C_3, and C_4 are estimated by a linear least squares method. As before, the operating shape y is synthesized using contributions from 6 modes. This data will be modeled with a single mode approximation (as is commonly done in practice). The least squares fit is accomplished by forming the matrix

$$ E = \left[e^{\beta^o x} \quad e^{-\beta^o x} \quad e^{j\beta^o x} \quad e^{-j\beta^o x} \right] $$

where $e^{\beta^o x}$ is a column vector of length N ($x = x_k$, $k=1:N$). Then the least squares coefficients can be found by solving the linear system $EC = y$. The function y^* is then simply $y^* = EC$. The residual function S is computed as before with Eq. 5.28. Likewise, the derivative is computed with Eq. 5.29. Note that in this case, the asterisk indicates that the function is evaluated with $\beta = \beta^o$, and the least squares C_i's.

The results of this analysis are presented in Figs. 33 through 38. Note that the residual in all cases exhibits a distinct concave upward curvature. The derivative of the higher modes indicates the presence of an inflection point in the residual function at approximately 85% and 115% of the true spatial frequency. Otherwise, both functions are well behaved in all the figures. The presence of the inflection points indicate that outside the region plotted, Newton's method should not be expected to converge. However, within the range of the analysis, good convergence should be expected. The minimum value of the residual function S is found, as it should be, at $\beta = \beta^o$. Thus, the method should converge to the correct value (e.g. no bias error is expected).

NOTE: Caution must be used in interpreting all figures in this section. The methods used are not exact but are heuristic in nature. They are, however, expected to shed light on the behavior of Newton's method.
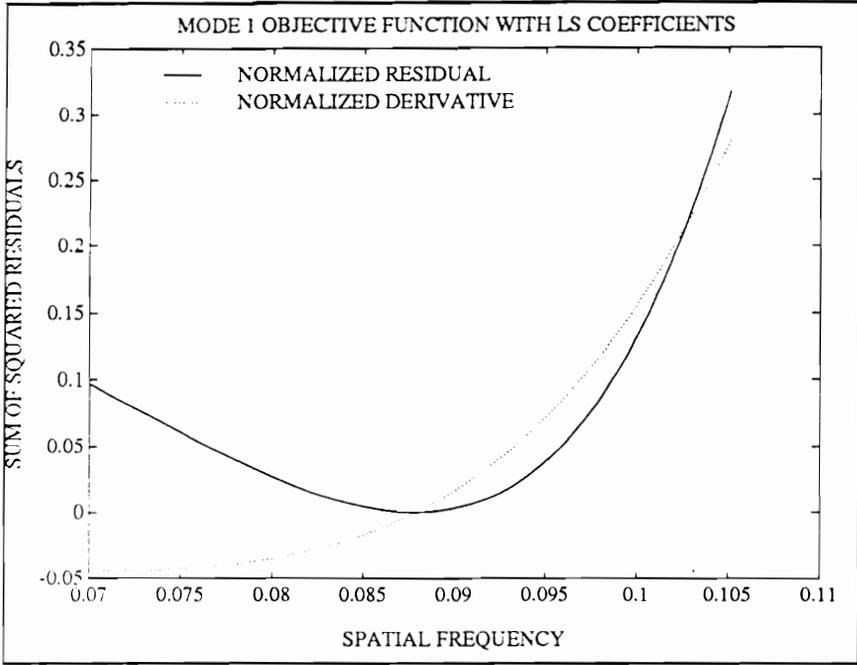
Figure 33 Residual function and derivative for mode 1 using least squares coefficients.
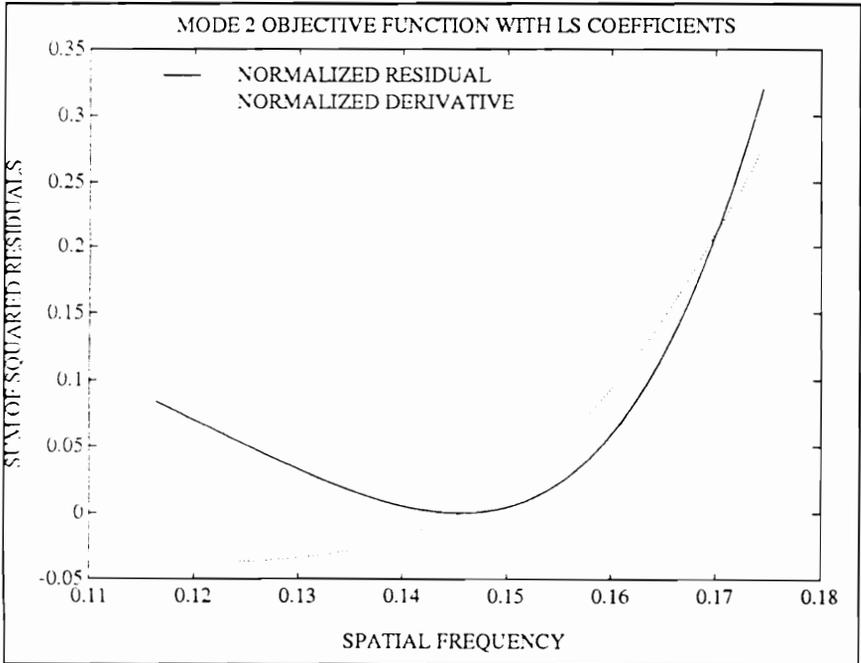
Figure 34 Residual function and derivative for mode 2 using least squares coefficients.

179
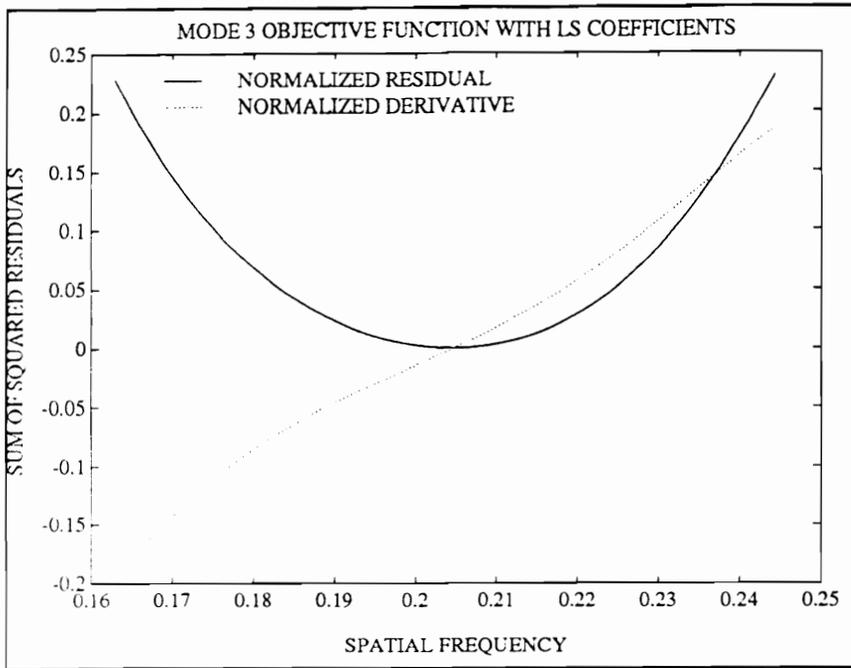
Figure 35 Residual function and derivative for mode 3 using least squares coefficients.
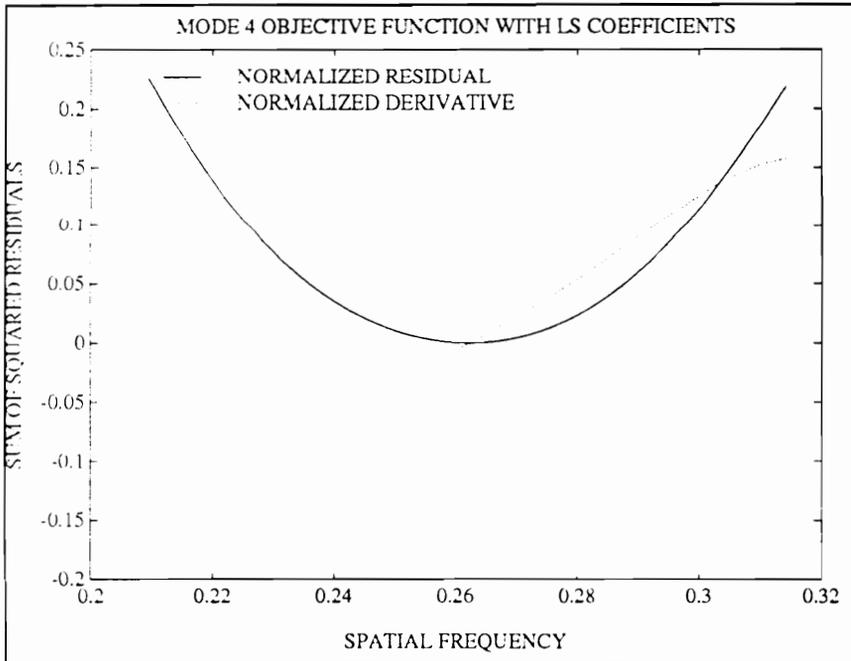
Figure 36 Residual function and derivative for mode 4 using least squares coefficients.

MODE 5 OBJECTIVE FUNCTION WITH LS COEFFICIENTS
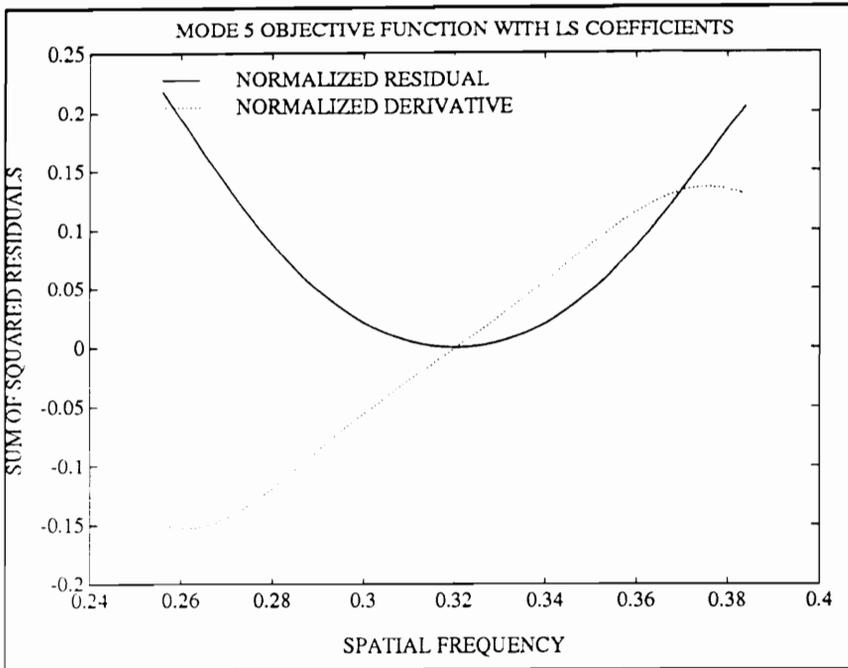
Figure 37 Residual function and derivative for mode 5 using least squares coefficients.

MODE 6 OBJECTIVE FUNCTION WITH LS COEFFICIENTS
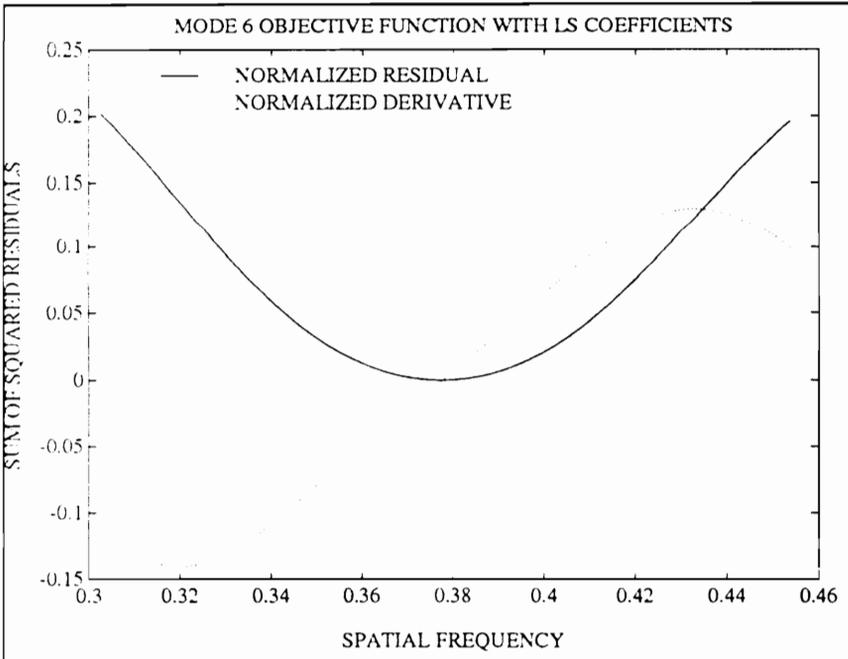
Figure 38 Residual function and derivative for mode 6 using least squares coefficients.

181

BIVARIATE ANALYSIS: The theory behind the bivariate analysis is similar to that for the univariate case. It is complicated by the fact S is a function of two variables, and two residual functions must be evaluated. The simulation data for the bivariate case is summarized in Table VI. The excitation frequencies were chosen so that two modes contributed significantly to the operating shape. The residual function was investigated in the neighborhood of the two corresponding spatial frequencies.

If i and j represent the two modes of interest, then the analysis involves investigation of $S(\beta_i^o, \beta_j^o)$, where β_i^o is in the neighborhood of β_i and β_j^o is in the neighborhood of β_j. The residual function S is evaluated as in Eq. 5.28, where the asterisk now indicates that the associated function is to be evaluated at (β_i^o, β_j^o). The derivatives are given by Eq. 5.29. Note that there are two derivatives for each of the two spatial frequencies.

These functions were evaluated for 26 values of each β^o, ranging again from 80% to 120% of the true spatial frequency. The resulting (26x26) matrices were displayed as a mesh plot. In order to aid visual interpretation of the two derivative plots, a fourth plot was generated. The slope magnitude, designated D_A, provided a means of evaluating the total slope at each point in the spatial frequency grid. It was calculated by

$$D_A(\beta_i^o, \beta_j^o) = \sqrt{D_i^2 + D_j^2} \qquad (5.31)$$

The procedure was repeated using the least squares coefficients, as described in the univariate section. In this case, the simulated operating shape, again containing contributions of six modes, was modeled with the best fit two mode model (for each pair of spatial frequencies). The matrix E contained eight columns instead of four, and eight coefficients were estimated with the least squares procedure.

The results of the multivariate analysis are markedly different than that of the univariate case. The results were plotted in a series of mesh plots, in which the objective function S is plotted as a height above a plane whose coordinate axes are β_i^o and β_j^o respectively. Derivative plots were generated in a similar manner.

Figures 39 and 40 show the functions S, D_1, D_2, and D_A for modes of interest 1 and 2. Figure 39 was generated using exact coefficients, whereas Fig. 40 used the least squares coefficients. The residual plot in Fig. 39 shows a smooth, concave function with a single minimum. Although it is not clear from the plot, inspection of the data shows that the minimum is indeed at the point (β_1, β_2). The derivatives D_1 and D_2 each show well behaved derivatives. A valley in the slope magnitude mesh shows that the derivative functions are appropriately signed. Thus, Fig. 39 indicates that Newton's method should

183

converge rapidly to the correct spatial frequencies, given the modal coefficients. However, the residual generated with the least squares coefficients, Fig. 40a, shows a very different pattern. The residual is very flat along one boundary. No distinct minimum is present, and the actual minimum occurs on the boundary. This indicates that use of the least squares coefficients may not converge, and certainly will not converge to the correct spatial frequencies. The three derivative plots corroborate this conclusion.

The trends described for the modes 1 & 2 data also hold for modes 2&3, 3&4, 4&5. Figures 41 through 46 present data for these modes. Inspection of these figures shows in all cases similar behavior. The cases in which exact coefficients are used indicate very satisfactory convergence is to be expected. However, if the coefficients are estimated via least squares, poor convergence and strong bias errors are likely to result. In practice, the true coefficients are not known, and must be estimated.

The univariate and bivariate convergence analyses, while not exact, provide good indications of the expected convergence of Newton's method. In all cases, when exact modal coefficients are used, favorable convergence indications are seen. However, for the bivariate case, the use of least squares coefficients leads to poor convergence and bias error. It can be concluded that Newton's method will yield unsatisfactory parameter estimates if the model contains more than one mode.

184
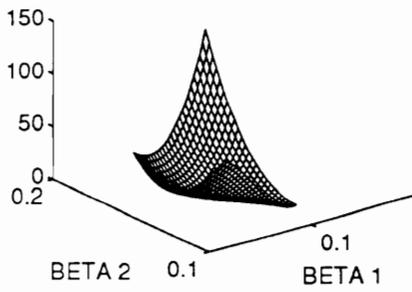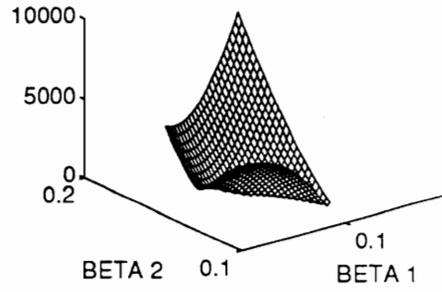
Figure 39 Residual analysis for modes 1 and 2 using exact coefficients.

185
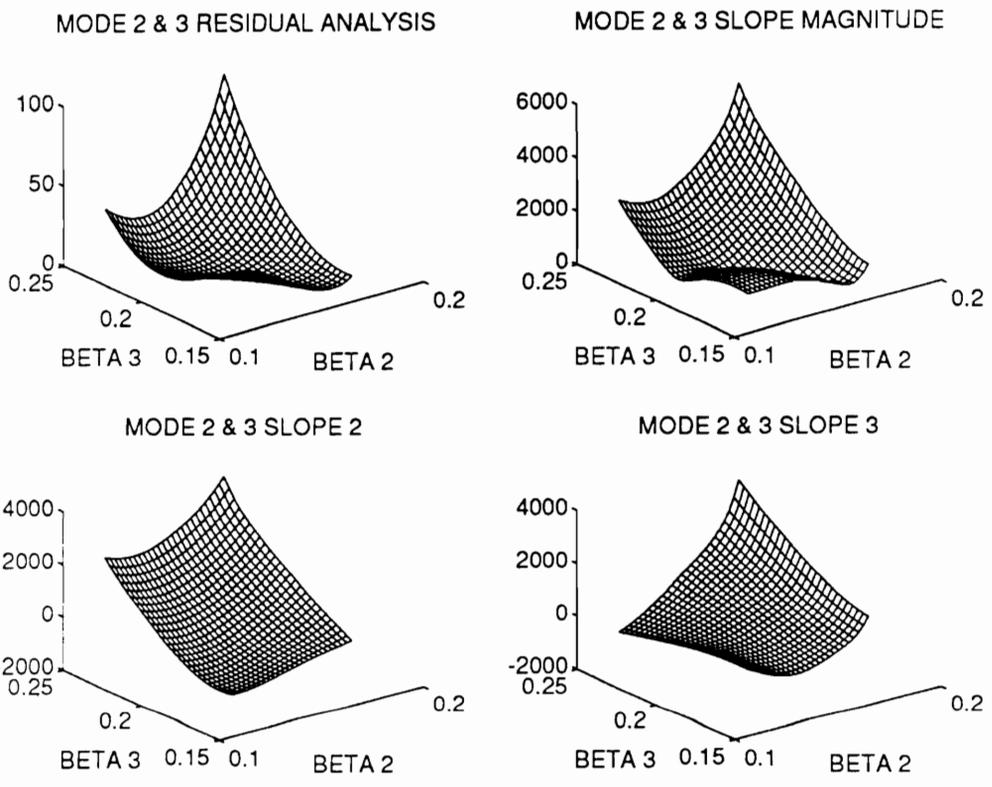
Figure 40 Residual analysis for modes 2 and 3 using exact coefficients.

186
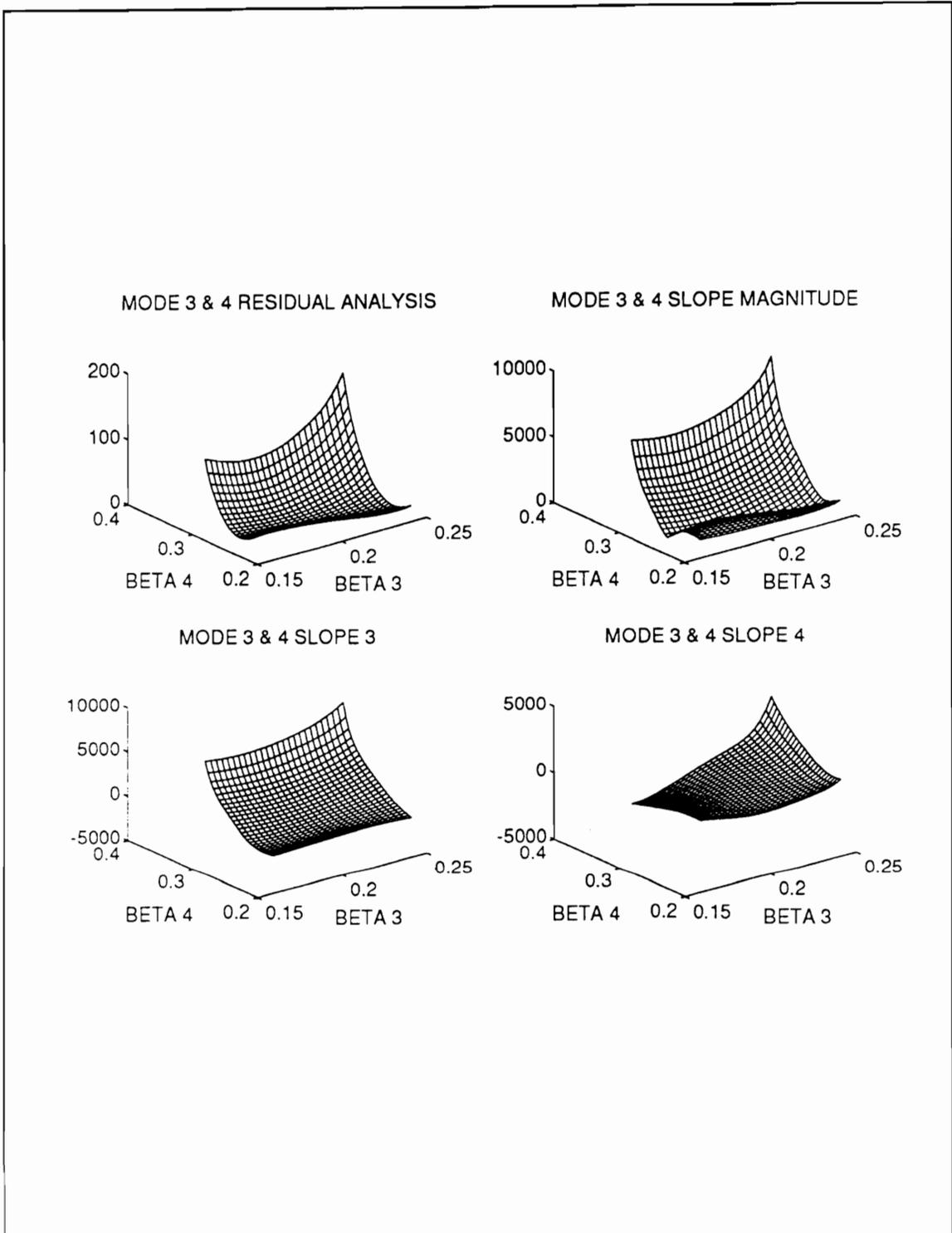
Figure 41 Residual analysis for modes 3 and 4 using exact coefficients.
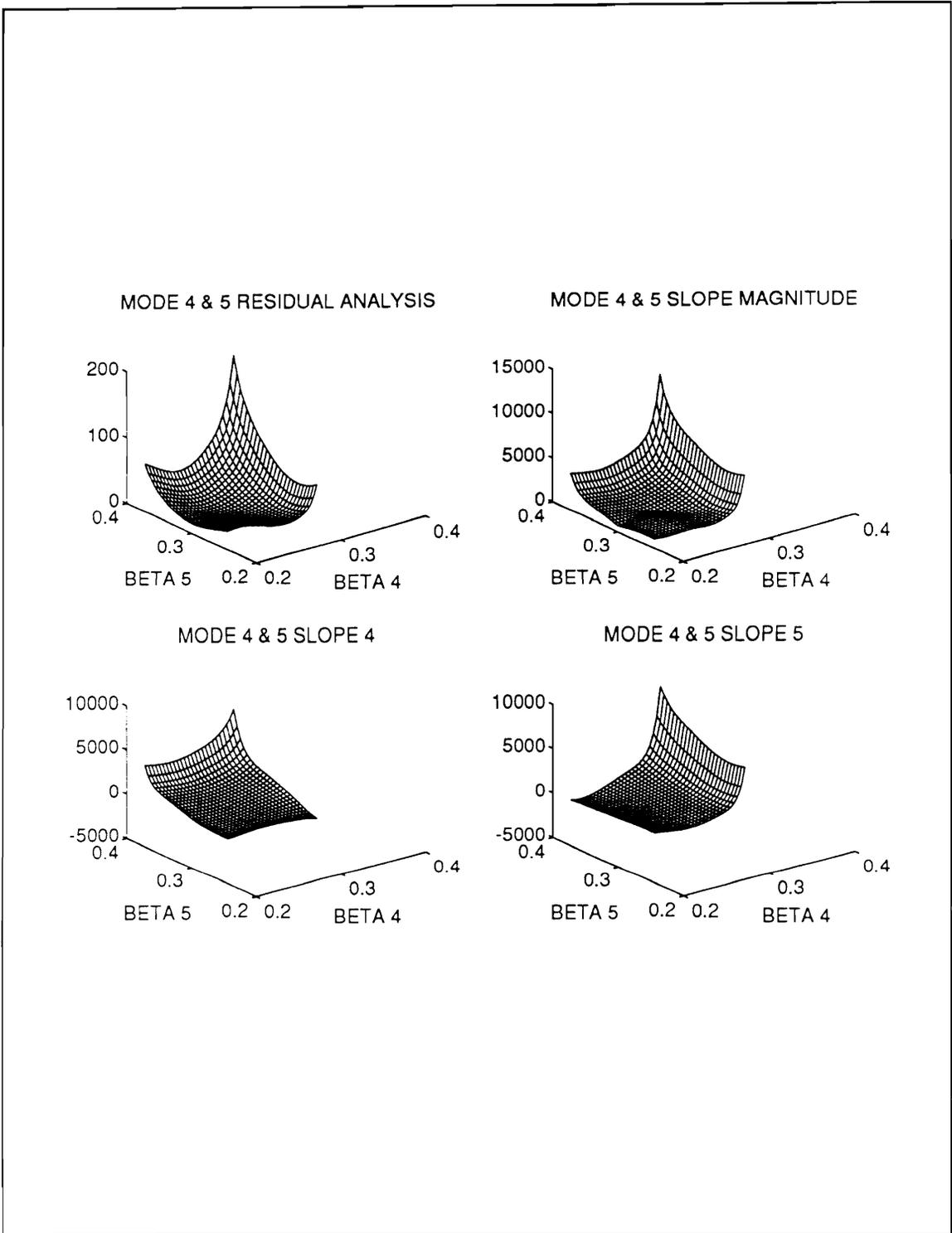
Figure 42 Residual analysis for modes 4 and 5 using exact coefficients.

188
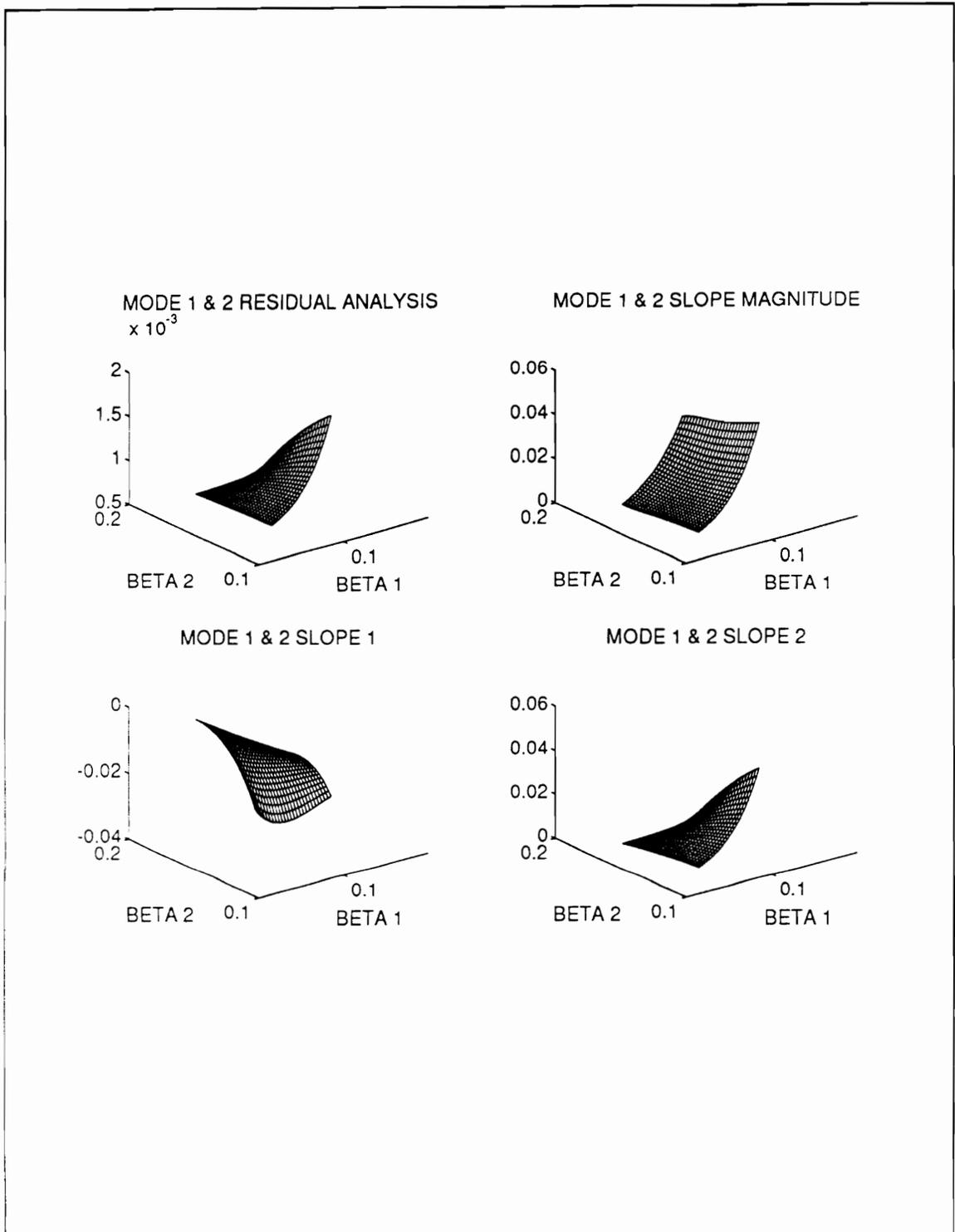
Figure 43 Residual analysis for modes 1 and 2 using least squares coefficients.
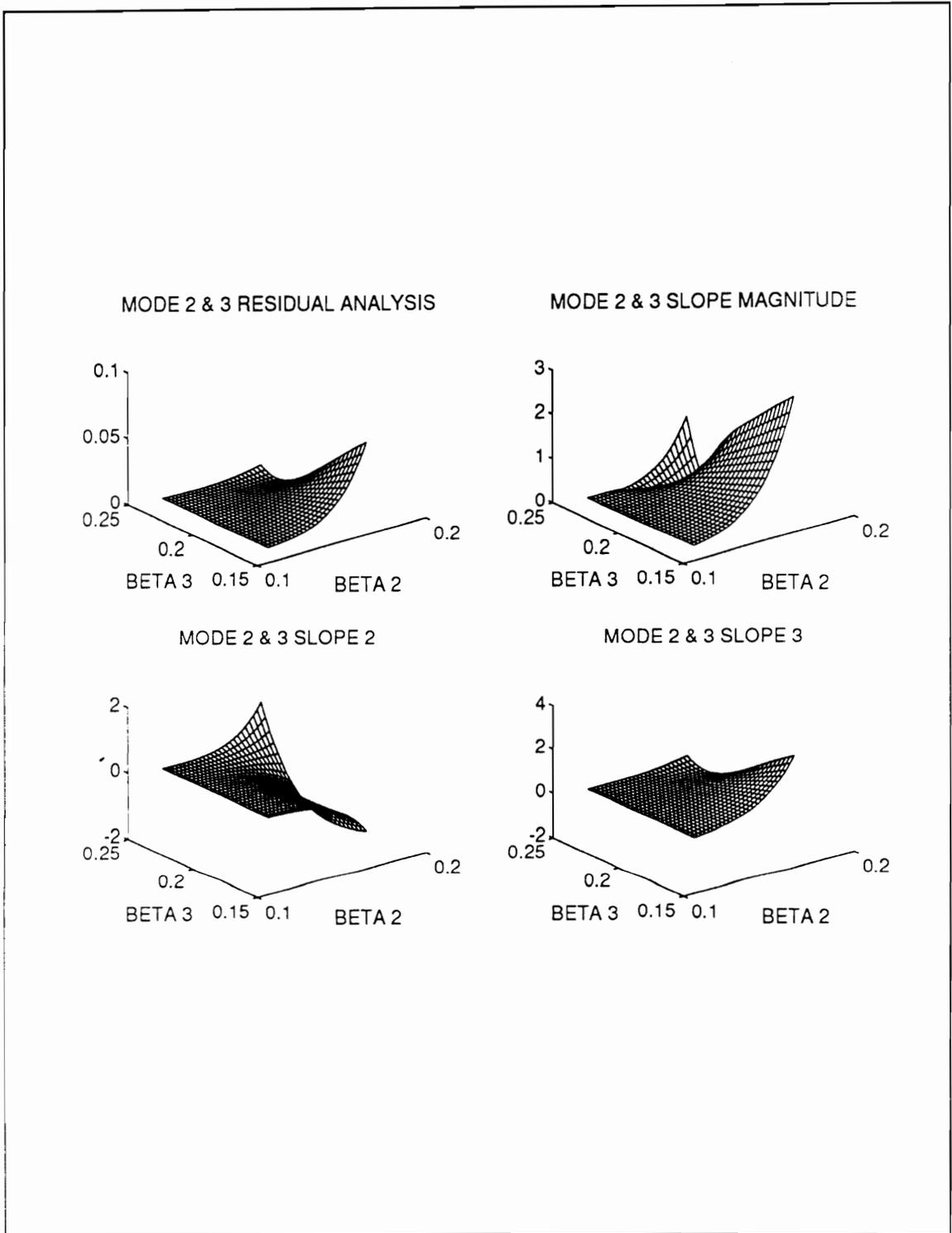
Figure 44 Residual analysis for modes 2 and 3 using least squares coefficients.

190
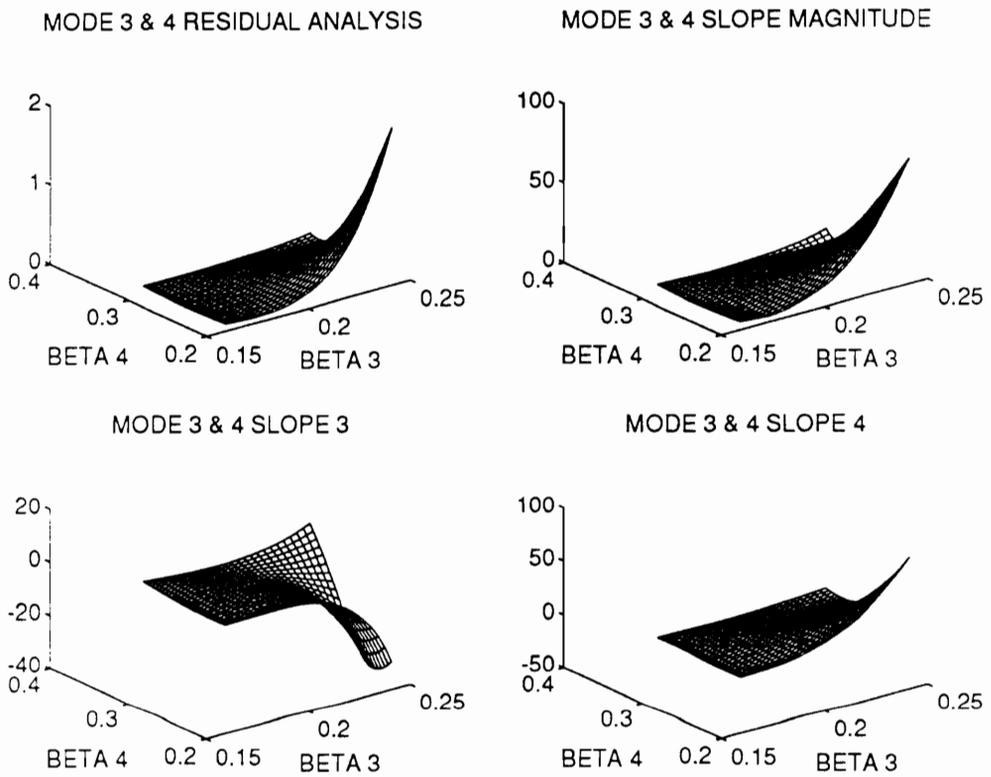
Figure 45 Residual analysis for mode 3 and 4 using least squares coefficients.

MODE 4 & 5 RESIDUAL ANALYSIS

MODE 4 & 5 SLOPE MAGNITUDE

MODE 4 & 5 SLOPE 4

MODE 4 & 5 SLOPE 5
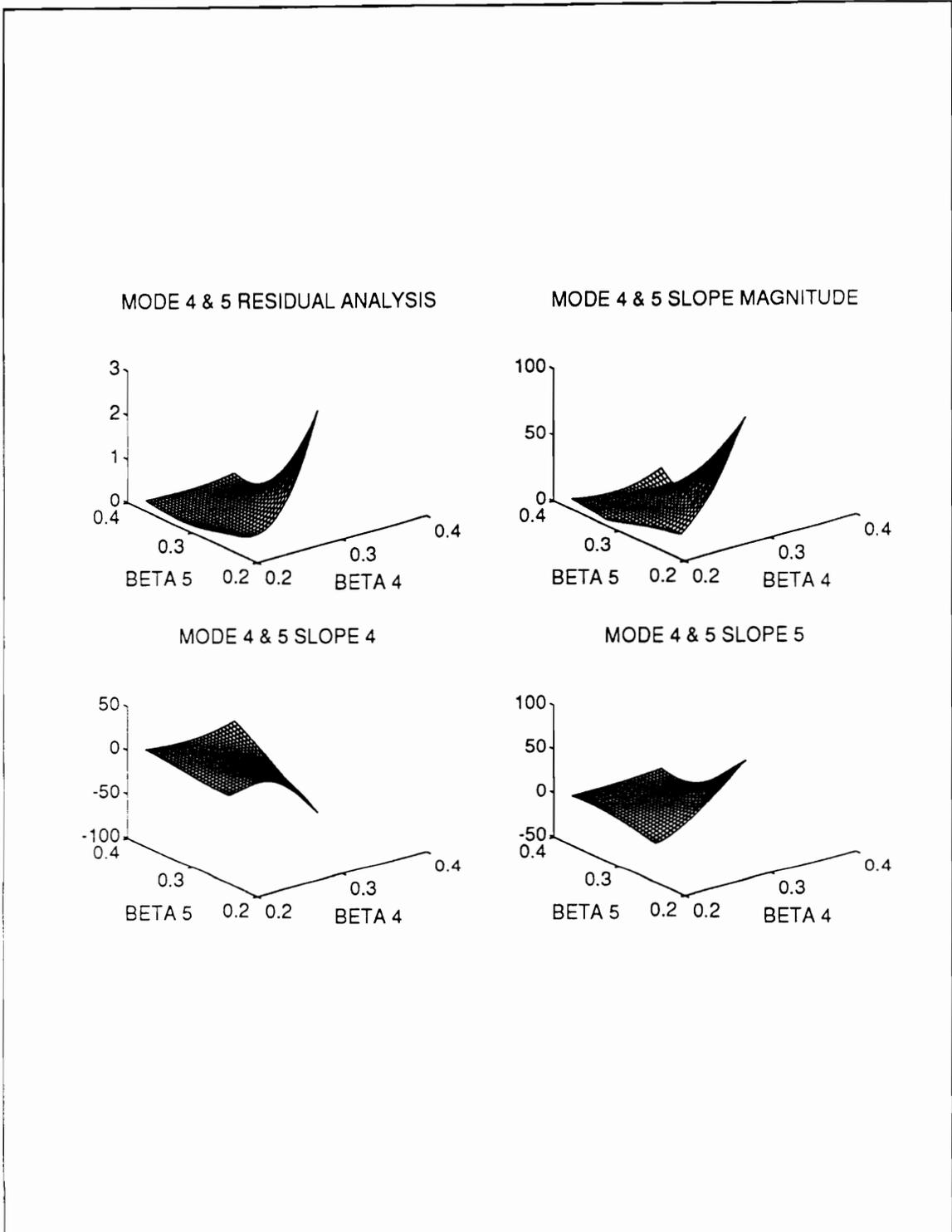
Figure 46 Residual analysis for modes 4 and 5 using least squares coefficients.

192

EMPIRICAL CONVERGENCE ANALYSIS

The analytical convergence investigation provides useful and pertinent information about potential performance of the LSSD method. A different approach involves experimentally determining the maximum and minimum values of β^o for which the method converges. It has been observed that in the neighborhood of β, LSSD converges to the same model parameters regardless of the initial value. If the initial parameter guess is outside this neighborhood, convergence will either not occur or occur very slowly. This fact can be utilized to find the bounds of convergence. This method, while not providing the insight of the analytical approach, provides more direct and practical information regarding convergence.

An empirical analysis of synthesized beam data has been performed. The experiment involved generating the operating shape of a vibrating beam and finding the lowest and highest values of the initial spatial frequency guess, β^o, for which the algorithm converged. The synthesized data contained contributions from six modes. Six excitation frequencies were chosen such that for each simulation, one of the modes was dominant -- that is, near resonance excitation was used. This resulted in six operating shapes. Normally distributed random noise was added to each operating shape to simulate measurement errors. Three noise levels were used, 20, 30 and 40dB SNR. The lowest and highest spatial frequency guesses that led to convergence were found by a sieve search

method. These values were reported in percent of the true spatial frequency. The search terminated when the limits of convergence were found to within one percentage point accuracy.

The simulated beam parameters are identical to those described previously. The simulated natural frequencies and excitation frequencies are presented in Table VII.

Table VII Convergence experiment simulation parameters.

	RESONANT MODE					
	1	2	3	4	5	6
NAT. FREQ.	108.3	298.4	585.0	967.1	1444.7	2017.7
EXCIT. FREQ.	110.0	300.0	590.0	970.0	1450.0	2020.0

Note: Frequency in radians/second

The specific steps involved in the experiment are:

1. Simulate a harmonically excited operating shape of a beam using BEAMSIG.

2. Add normally distributed, mean zero noise to obtain the desired SNR.

194

3. Use a sieve search to find the lowest value of β° for which the LSSD method converges.

4. Non-convergence is assumed after 20 iterations.

5. Use a sieve search to find the highest value of β° for which the LSSD method converges.

6. Increase the SNR and repeat Steps 2 - 5.

7. Repeat Steps 1 - 6 for each excitation frequency.

RESULTS: The results of this experiment indicate that the range of convergence may be more limited than the theoretical analysis indicates. The lower limits are more restrictive than the upper limits. This is in agreement with the theoretical univariate analysis.

The results of this experiment, expressed as percent of true spatial frequency, are tabulated in Table IV. All but the third mode require an initial parameter estimate within 11% of the true spatial frequency. However, only one mode, the sixth, required a higher limit within 10% of the true value. Neither the high nor the low limit appears dependent

195

on the noise level. Only slight, apparently random, differences appeared with respect to the three noise levels. The lower limits do not show any apparent dependence on mode number. The higher limits, on the other hand, show a distinct decrease as the mode number increases.

Table VIII LSSD empirical limits of convergence for simulated Free-Free beam (modes 1-6).

MODE	40dB low	40dB high	30dB low	30dB high	20dB low	20dB high
1	91^1	151	92	152	92	152
2	93	132	94	132	94	132
3	72	121	72	119	72	119
4	96	115	94	116	94	115
5	89	112	95	112	95	112
6	91	109	96	109	96	109

1 Results expressed in % of true spatial frequency.

CONCLUSIONS

Both the univariate theoretical convergence analysis and the empirical analysis indicate that convergence can be expected when the initial parameter estimate is in the neighborhood of the true parameter. In some cases, the lower limit is quite narrow, however. This implies that if a band of possible initial estimates are available, use of the

largest estimate has the best chance of leading to convergence. The range of convergence

narrows with increasing mode number, but is relatively unaffected by noise.

CHAPTER 6: BOUNDARY CONDITION BEAM ANALYSIS

INTRODUCTION

The term spatial modal analysis implies that measured data can be decomposed into vibrational modes. The boundary condition beam analysis (BCBA) method does just this. It is a true spatial modal method. This is in sharp contrast to the minimum residual models presented in Chapter 5. The BCBA method is based directly on simple beam theory. It includes all theoretical constraints. It is based on the ability to estimate general boundary conditions for the beam. If the boundary conditions can be estimated, the spatial frequencies, and mode shapes for any desired modes can be found.

THEORY

The fundamentals of Euler-Bernoulli beam theory are presented in Chapter 4. The boundary condition beam analysis is based directly on this theory. The following assumptions are made:

- Euler-Bernoulli theory is applicable.

- The beam is uniform (E,I,A = Constant).

- The beam is subject to harmonic point excitation.

Equation 4.2 is the differential equation describing the free vibration of such a beam. It is repeated here for clarity.

$$\frac{EI}{\rho A}\frac{\partial^4 w}{\partial x^4} + \frac{\partial^2 w}{\partial t^2} = 0 \tag{6.1}$$

As in Chapter 4, a solution can be obtained by separation of variables. The solution can be represented by Eqs. 4.7 and 4.8. The first of these is the spatial function, and represents the mode shapes of the beam. This function is given by

$$V(x) = C_1 e^{\beta x} + C_2 e^{-\beta x} + C_3 e^{j\beta x} + C_4 e^{-j\beta x} \tag{6.2}$$

The coefficients C_1, C_2, C_3, and C_4 must be determined from the boundary conditions. In addition, the frequency equation, leading to both the spatial frequencies β and the natural frequencies ω can be obtained from the boundary conditions. Thus, if the boundary conditions can be estimated, the frequencies and coefficients of any desired modes can

199

be computed. This is the basis for the Boundary Condition Beam Analysis (BCBA) method.

A variety of possible boundary conditions exist. The end of a beam may be fixed rigidly such that both deflection and slope of the beam are zero at the boundary. The end could be free, in which case the shear force and the bending moment will be zero, but the deflection and slope are not restricted. Or the end could be pinned such that the deflection and bending moment are zero. These are the three so-called simple boundary conditions.

In general, the end of a beam may be subject to stiffness, damping, or inertial effects. Five general boundary conditions exist, which are sufficient to describe any of the simple or general conditions. These general boundary conditions and their corresponding symbols are:

- linear spring k

- rotational spring K_t

- damping (viscous) c

- concentrated mass m

- concentrated moment of Inertia J

In terms of the general boundary conditions, a fixed end could be described as having an infinite mass and an infinite moment of inertia. A pinned end has an infinite end mass, and a free end has all stiffnesses, damping and inertias identically equal to zero.

The boundary conditions are applied at each end of the beam. Defining the coordinate system as shown in Fig. 47, it is clear that the ends of the beam occur at $x = 0$ and at $x = L$.
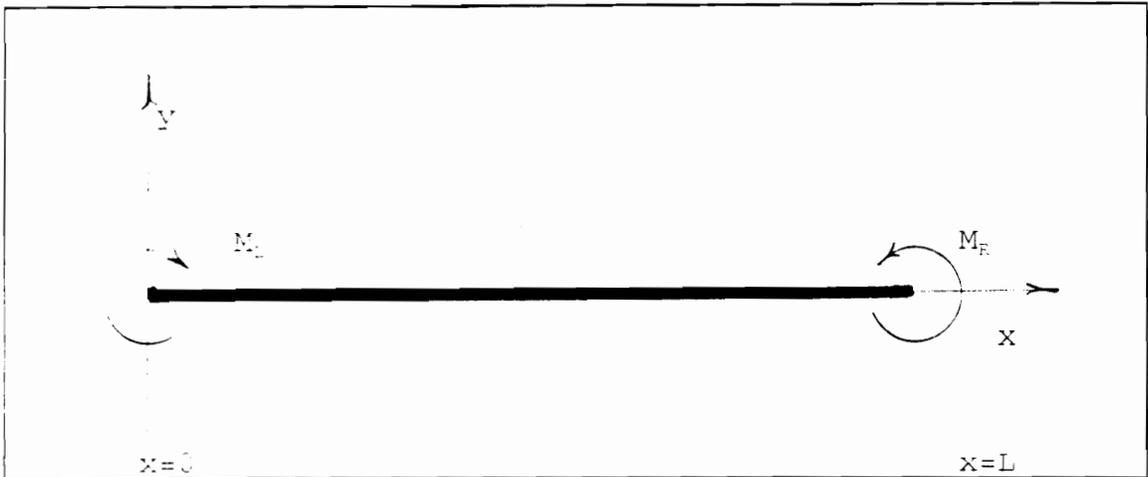
Figure 47 Beam coordinate system and sign convention for bending moments.

The general boundary conditions can be related to the deflection, slope, bending moment, and shear force at the ends of the beam. These relationships are defined in Table IX. For simplicity, define the following nomenclature for the left end of the beam. Similar

relations can be written for the right end of the beam using the subscript 1 for the right end and o for the left end. This nomenclature is used both in Table IX and in the remainder of this chapter.

$$V_o \doteq w(0,t)$$

$$V_o' \doteq \left. \frac{\partial w}{\partial x} \right|_{x=0;t}$$

$$V_o'' \doteq \left. \frac{\partial^2 w}{\partial x^2} \right|_{x=0;t} \tag{6.3}$$

$$V_o''' \doteq \left. \frac{\partial^3 w}{\partial x^2} \right|_{x=0;t}$$

Table IX General Boundary Conditions and their relation to deflection, slope, bending moment and shear force at the ends of a beam.

BOUNDARY TYPE	LEFT END (x=0)	RIGHT END (x=L)
K_t	$EIV_o'' = K_{t,o}V_o'$	$EIV_1'' = -K_{t,1}V_1'$
J	$EIV_o'' = -J_oV_o'\omega^2$	$EIV_1'' = J_1V_1'\omega^2$
k	$EIV_o''' = -k_oV_o$	$EIV_1''' = k_1V_1$
c	$EIV_o''' = -jc_oV\omega$	$EIV_1''' = jc_1V_1\omega$
m	$EIV_o''' = m_oV_o\omega^2$	$EIV_1''' = -m_1V_1\omega^2$

The derivatives for the left boundary $(x=0)$ are

$$
\begin{aligned}
C_1 + C_2 + C_3 + C_4 &= V_o \\
\beta C_1 - \beta C_2 + j\beta C_3 - j\beta C_4 + &= V_o' \\
\beta^2 C_1 + \beta^2 C_2 - \beta^2 C_3 - \beta^2 C_4 &= V_o'' \\
\beta^3 C_1 - \beta^3 C_2 - j\beta^3 C_3 + j\beta^3 C_4 &= V_o'''
\end{aligned}
\tag{6.4}
$$

Likewise, the derivatives at the right boundary $(x=L)$ are

203

$$e^{\beta L}C_1 + e^{-\beta L}C_2 + e^{j\beta L}C_3 + e^{-j\beta L}C_4 = V_l$$

$$\beta e^{\beta L}C_1 - \beta e^{-\beta L}C_2 + j\beta e^{j\beta L}C_3 - j\beta e^{-j\beta L}C_4 = V_l'$$

$$\beta^2 e^{\beta L}C_1 + \beta^2 e^{-\beta L}C_2 - \beta^2 e^{j\beta L}C_3 - \beta^2 e^{-j\beta L}C_4 = V_l''$$ (6.5)

$$\beta^3 e^{\beta L}C_1 - \beta^3 e^{-\beta L}C_2 - j\beta^3 e^{j\beta L}C_3 + j\beta^3 e^{-j\beta L}C_4 = V_l'''$$

The shear and moment at each end of the beam can be related to the boundary conditions. These relationships can be obtained directly from Table IX. The rotational stiffness and moment of inertia relate the slope to the second derivative, whereas the mass, damping, and linear stiffness relate the deflection to the third derivative. Specifically, these relationships at the left and right ends of the beam are:

$$V_o'' = \frac{1}{EI}\left(K_{t_o} - J_o\omega^2\right)V_o'$$

$$V_o''' = \frac{1}{EI}\left(m_o\omega^2 - jc_o\omega - k_o\right)V_o$$ (6.6)

$$V_l'' = \frac{1}{EI}\left(J_l\omega^2 - K_{t_l}\right)V_l'$$

$$V_l''' = \frac{1}{EI}\left(k_l + jc_l\omega - m_l\omega^2\right)V_l$$

Equation 6.6 can be substituted into Eqs. 6.4 and 6.5 to eliminate V_o, V_o', V_l, and V_l'. The result is a 4x4 matrix containing the unknown coefficients C_1, C_2, C_3, and C_4, and the unknown spatial and natural frequencies β and ω. Prior to writing this matrix, however, it is convenient to define some terms.

204

First, a relationship exists between the spatial and natural frequencies. This relationship is

$$\beta^4 = \frac{\rho A \omega^2}{EI} \tag{6.7}$$

or, by defining

$$e = \sqrt{\frac{EI}{\rho A}} \tag{6.8}$$

we have

$$\omega = e\beta^2 \tag{6.9}$$

Now, define the following

205

$$\gamma = \frac{EI\beta^3}{(m_o e\beta^4 - jc_o e\beta^2 - k_o)} \qquad (6.10)$$

$$\delta = \frac{EI\beta}{(K_{t_o} - J_o e\beta^4)} \qquad (6.11)$$

$$\epsilon = \frac{EI\beta^3}{(k_l + jc_l e\beta^2 - m_l e\beta^4)} \qquad (6.12)$$

$$\xi = \frac{EI\beta}{(J_l e\beta^4 - K_{t_l})} \qquad (6.13)$$

With these definitions, substitute Eq. 6.6 into Eqs. 6.4 and 5. Then, by eliminating the boundary conditions and arranging the result in matrix format, we get the 4x4 matrix equation

206

$$\begin{bmatrix} (1-\gamma) & (1+\gamma) & (1+j\gamma) & (1-j\gamma) \\ (1-\delta) & -(1+\delta) & (j+\delta) & (-j+\delta) \\ e^{\beta L}(1-\epsilon) & e^{-\beta L}(1+\epsilon) & e^{j\beta L}(1+j\epsilon) & e^{-j\beta L}(1-j\epsilon) \\ e^{\beta L}(1-\xi) & -e^{-\beta L}(1+\xi) & e^{j\beta L}(j+\xi) & e^{-j\beta L}(-j+\xi) \end{bmatrix} \begin{Bmatrix} C_1 \\ C_2 \\ C_3 \\ C_4 \end{Bmatrix} = \begin{Bmatrix} 0 \\ 0 \\ 0 \\ 0 \end{Bmatrix} \qquad (6.14)$$

Equation 14 can be written symbolically as

$$\Lambda c = 0$$

This is a homogenous system of equations that is linear in the coefficients and non-linear in the spatial frequencies. This equation can only be satisfied for non-trivial c if Λ is a singular matrix. In other words,

$$DET(\Lambda) = 0 \qquad\qquad (6.15)$$

Equation 15 is the frequency equation for a beam with general boundary conditions. Its roots are the beam spatial frequencies. There are an infinite number of roots, corresponding to the theoretically infinite number of modes. The finite set containing the spatial frequencies of interest, β_1, β_2,...,β_m, can be obtained by finding only the desired roots.

207

Once the desired spatial frequencies are known, the mode shape corresponding to any spatial frequency β_i may be found by solving Eq. 6.14 for c after substituting β_i for β. The mode shapes thus obtained can be normalized in any reasonable manner. For example, it may be desired to normalize the mode shapes for the length of the beam.

If a beam is excited by a harmonic force acting at a single point on the beam, the resulting response will also be harmonic. The operating shape of the beam is the shape obtained by plotting the amplitude of displacement versus the axial position along the beam. The operating shape is composed of a linear combination of the normal mode shapes. The weights corresponding to the normal modes are called the modal weighting factors.

The modal weighting factors corresponding to any measured data set can be found by a least squares fit of the normal mode shapes to the data. The normal mode shapes are properties of the beam itself, and are not dependent on type or location of excitation. Thus, any operating shape of the beam can be fitted with the normal mode shapes. The only requirement is that sufficient mode shapes be computed to model the actual vibration.

NUMERICAL IMPLEMENTATION

Beam theory with general boundary conditions can be used to find the spatial frequencies and mode shapes for any uniform beam. Implementation requires estimation of the deflection and spatial derivatives at the beam ends. This can be done using high-density spatial data. Use of a scanning laser vibrometer ensures that sufficient spatial data is available to do this. The boundary conditions and subsequently the spatial frequencies and mode shapes of the beam can then be estimated. This approach has several advantages. All theoretical constraints are included in the model. Since any arbitrary linear boundary conditions will be modeled, a structure composed of uniform beams can be modeled.

The analysis procedure involves several steps. These are:

1. Estimate the deflection and spatial derivatives at each beam boundary. (V_o, V_o', V_o'', V_o''' V_l, V_l', V_l'', and V_l''')

2. Compute the Boundary Conditions (J, K_l, m, c, k) at each of the beam boundaries.

3. Solve the frequency equation $\Lambda c = 0$ for all frequencies of interest.

4. Compute the coefficients and the mode shapes corresponding to each mode of interest.

5. For each data set, compute the modal weighting factors and the operating shape.

ESTIMATION OF DERIVATIVES

The first step is to estimate the deflection and the spatial derivatives of the measured data. This is critical for the successful estimation of frequencies and mode shapes. The deflection at the boundary is easy to obtain. However, the derivatives pose problems. Numerical differentiation is possible. Indeed, the laser vibrometer capabilities allow great flexibility in terms of quantity and quality of data available. High order numerical differentiation schemes could be developed based on this data. However, numerical differentiation is notoriously inaccurate in the presence of any measurement noise. Despite large quantities of accurate data, some noise will always be present. Hence, other alternatives should be investigated.

A better approach consists of modeling the data with a differentiable function. If such a function can be found that fits the data well, the derivatives can be readily obtained from

210

the fitted function. The PSMA and LSSD algorithms described in Chapter 5 do provide good models for the beam data in terms of small residual. They also produce a model that is easily differentiable. This suggests that significantly improved estimates of the derivatives can be obtained by modeling the beam data using either PSMA or LSSD. The model thus obtained can then be differentiated at the boundaries to obtain the desired derivatives. This approach yields superior derivative estimates as compared to numerical differentiation.

In practice, this has proved to be a very satisfactory method of estimating the derivatives. One drawback is the difficulty of minimum residual models to fit off-resonance data. In order to obtain a good model, both LSSD and PSMA require resonance excitation. The boundary condition analysis is independent of excitation frequency. However, if PSMA or LSSD is used for estimation of derivatives, then effectively the procedure is restricted to resonance excitation. Two additional comments are in order here. First, if off-resonance data is available, it is certainly possible to fit that data with a differentiable function using methods other than PSMA or LSSD. Any model that can provide accurate estimates of the derivatives at the ends of the beam is satisfactory. Secondly, if both resonance and off-resonance data are available, the resonance data sets may be used to estimate the normal mode shapes, which will still apply to the off-resonance data. Thus, modal models may be built for more data sets than are used for estimation of the modal parameters.

211

(Modal weighting factors will be found for all data sets based on the modes computed from the resonance data sets.)

If resonance excitation is used, PSMA or LSSD are good choices for the initial model. The model so obtained has the form of Eq. 6.2. This form and its first three derivatives with respect to x are:

$$V(x) = C_1 e^{\beta x} + C_2 e^{-\beta x} + C_3 e^{j\beta x} + C_4 e^{-j\beta x}$$

$$V'(x) = \frac{dV}{dx} = \beta C_1 e^{\beta x} - \beta C_2 e^{-\beta x} + j\beta C_3 e^{j\beta x} - j\beta C_4 e^{-j\beta x}$$

$$V''(x) = \frac{d^2 V}{dx^2} = \beta^2 C_1 e^{\beta x} + \beta^2 C_2 e^{-\beta x} - \beta^2 C_3 e^{j\beta x} - \beta^2 C_4 e^{-j\beta x} \quad (6.16)$$

$$V'''(x) = \frac{d^3 V}{dx^3} = \beta^3 C_1 e^{\beta x} - \beta^3 C_2 e^{-\beta x} - j\beta^3 C_3 e^{j\beta x} + j\beta^3 C_4 e^{-j\beta x}$$

These functions, evaluated at $x=0$ and at $x=L$ provide estimates of V_o, V_o', V_o'', V_o''' V_l, V_l', V_l'', and V_l'''.

.

BOUNDARY CONDITION ESTIMATION

The second step involves estimating the boundary conditions. There are five unknown boundary conditions at each end of the beam. These must be estimated from the

212

derivatives computed in step 1. These boundary conditions are physical properties of the beam system, and are independent of excitation frequency. The deflections and spatial derivatives are, however, highly dependent on excitation frequency. Thus, if multiple data sets, each obtained using a different excitation frequency, are available, the boundary conditions estimated from each set should be identical.

It is known from theory that the bending moment in a beam is proportional to the second derivative and the shear force proportional to the third derivative. (Recall the assumption of a uniform beam.) In both cases the constant of proportionality is the modulus of elasticity - area moment of inertia product, EI.

Referring to Table IX, it is clear that the moment acting on the beam at either end is determined by a combination of the rotational spring stiffness, K_r, and the mass moment of inertia, J. Likewise, the shear force is determined by a combination of the mass m, the linear stiffness k, and the damping, c. These relationships are defined explicitly in Eq. 6.6. It is thus impossible to determine these parameters from only one data set. Because three terms appear in the shear equation, a minimum of three data sets is required.

The right hand side of Eq. 6.6 is a quadratic polynomial in ω, the response frequency. For harmonically excited linear structures, the response frequency can be taken as the excitation frequency. If three data sets are available, each taken with different, and

known, excitation frequencies, Eqs. 6.6 can be solved for the boundary conditions. If more than three data sets are available, the boundary conditions can be found using a least squares method. Assuming that q data sets are available, each taken using a different excitation frequency, the following matrix equations can be formed:

$$
\begin{bmatrix}
V'_{o1} & -V'_{o1}\omega_1^2 \\
V'_{o2} & -V'_{o2}\omega_2^2 \\
\vdots & \\
V'_{oq} & -V'_{oq}\omega_q^2
\end{bmatrix}
\begin{Bmatrix} K_{t_o} \\ J_o \end{Bmatrix} \frac{1}{EI}
=
\begin{Bmatrix}
V''_{o1} \\
V''_{o2} \\
\vdots \\
V''_{oq}
\end{Bmatrix}
\tag{6.17}
$$

$$
\begin{bmatrix}
V_{o1}\omega_1^2 & -jV_{o1}\omega_1 & -V_{o1} \\
V_{o2}\omega_2^2 & -jV_{o2}\omega_1 & -V_{o2} \\
\vdots & & \\
V_{oq}\omega_q^2 & -jV_{oq}\omega_q & -V_{oq}
\end{bmatrix}
\begin{Bmatrix} m_o \\ c_o \\ k_o \end{Bmatrix}
=
\begin{Bmatrix}
V'''_{o1} \\
V'''_{o2} \\
\vdots \\
V'''_{oq}
\end{Bmatrix}
\tag{6.18}
$$

$$
\begin{bmatrix}
-V'_{l1} & V'_{l1}\omega_1^2 \\
-V'_{l2} & V'_{l2}\omega_2^2 \\
\vdots & \\
-V'_{lq} & V'_{lq}\omega_q^2
\end{bmatrix}
\begin{Bmatrix}
K_{t_l} \\
J_l
\end{Bmatrix}
\frac{1}{EI}
=
\begin{Bmatrix}
V''_{l1} \\
V''_{l2} \\
\vdots \\
V''_{lq}
\end{Bmatrix}
\tag{6.19}
$$

$$
\begin{bmatrix}
-V_{l1}\omega_1^2 & jV_{l1}\omega_1 & V_{l1} \\
-V_{l2}\omega_2^2 & jV_{l2}\omega_1 & V_{l2} \\
\vdots & & \\
-V_{lq}\omega_q^2 & jV_{lq}\omega_q & V_{lq}
\end{bmatrix}
\begin{Bmatrix}
m_l \\
c_l \\
k_l
\end{Bmatrix}
=
\begin{Bmatrix}
V'''_{l1} \\
V'''_{l2} \\
\vdots \\
V'''_{lq}
\end{Bmatrix}
\tag{6.20}
$$

In Eqs. 6.17 through 20, the displacement and derivative terms use two subscripts. The first subscript indicates the left or right boundary -- o for left and l for right. The second subscript indicates the data set from which the term was obtained. The subscripts on ω also indicate the corresponding data set.

For a stable, physically realizable system, the quantities K_t, J, m, c, and k should all be non-negative. Numerical solution of Eqs. 6.17 through 20 using conventional least squares approaches do not prevent these quantities from becoming negative. Errors in estimation of the spatial derivatives (Step 1) can lead to negative solutions. This is particularly true in cases such as a free end in which the boundary conditions are theoretically zero.

215

In order to ensure that the boundary conditions are non-negative, this constraint must be included in the solution of Eqs. 6.17 through 20. Lawson and Hanson (1974) present an algorithm for Non-Negative Least Squares (NNLS). This algorithm has proved successful in practice. Preventing negative boundary conditions greatly improves the computed mode shapes and spatial frequency estimates. It is strongly recommended that algorithm NNLS, or an equivalent algorithm, be used for solution of the boundary conditions.

FREQUENCY ESTIMATION

Computation of the spatial frequencies by solution of the frequency equation is the third step. As many spatial frequencies as desired can be found, including out-of-band spatial frequencies. This is part of the power of the boundary condition analysis. The primary limitation will be the applicability of Euler-Bernoulli beam theory. That is, spatial frequencies and mode shapes may be found that agree well with classical beam theory. However, as was pointed out in Chapter 4, this theory is in error for high modes due to invalid assumptions of negligible shear deformation and rotatory inertia. Care must therefore be exercised to extract only those modes for which Euler-Bernoulli theory is valid.

216

The frequency equation (Eq. 6.15) may be solved by considering DET(Λ) as a non-linear function of β. The multiple roots of this function are the spatial frequencies of the beam. The function is highly unstable and may contain singularities. It is thus difficult to find the roots. The recommended approach is to initially use a grid search to bound the roots, followed by a bisection search.

The determinant can be evaluated once the quantities γ, δ, ε, and ξ are computed. This is accomplished by using Eqs. 6.10-6.13. These quantities are functions of the boundary conditions, the spatial frequency, and the beam properties. The boundary conditions are available from Step 2. The quantity e, containing physical properties of the beam, must be provided. In most cases the beam dimensions and material properties are available, and e is readily available. (From the experimentalist's viewpoint, it is attractive to be able to construct a modal model using only the measured data. However, in this case, that is not possible.) The spatial frequency is the independent variable used in the grid or bisection search.

Once γ, δ, ε, and ξ are computed, the matrix Λ can be formed as in Eq. 6.14. The determinant is computed. If the grid search is used, a plot of DET(Λ) versus β will highlight the regions in which roots can be isolated. The step size should be sufficiently fine to ensure that no roots are missed. The required step size will vary considerably,

217

depending on beam length, boundary conditions, and material properties. Theoretical values, if available, may be used as a guide for determining step size.

The grid search identifies bounds around each root of interest. Some type of efficient search method can then be used to locate the root. The bisection method is one such approach. It is not the fastest method, but it is guaranteed to converge (provided one root actually has been bounded). Because of the nature of the determinant as a function of β, such a dependable method is desirable, even at the cost of a little more computation time. Grid search and bisection methods, as well as many other root-finding approaches, can be found in any good numerical methods text. One such reference is Press, et. al. (1988).

It should be noted here that the spatial frequency estimates <u>must</u> be computed with as much accuracy as possible. Small errors in spatial frequency can lead to a much larger error in the corresponding mode shape. Ensuring maximum accuracy and use of double precision arithmetic will help improve spatial frequency estimates and mode shape estimates. One advantage of the bisection search is that it can be programmed to terminate with an arbitrarily high accuracy.

A final note on rooting the frequency equation concerns singularities in the frequency function. Singularities in which the functional value is infinite can occur. The bisection search method can not distinguish between such a singularity and a true root. It is

incumbent on the analyst to ensure that each bound contains a true root and not a singularity. If a sufficiently fine grid search is conducted first, this is generally not a problem. However, if no grid search is conducted (bounds assumed) or too coarse of a grid is used, a singularity may be confused with a root.

MODE SHAPE ESTIMATION

The fourth step in the boundary condition analysis is to compute the coefficient vector c and the normal mode shape for each mode. Once the spatial frequencies for each mode of interest have been determined, Eq. 6.14 can be solved to obtain the coefficients. As with identification of the spatial frequencies, computation of the modal coefficients must be effected with high accuracy. Chang and Craig (1969) have demonstrated that large errors can occur in the mode shape if these coefficients are not accurate.

Numerically, the most accurate method of solving Eq. 6.14 is by singular value decomposition (Golub and Van Loan, 1980). If the singular value decomposition of Λ is given by

$$USV^T = \Lambda$$

219

and if

$$\Lambda c = 0$$

then c can be obtained directly from the last column of the matrix V. If $[v_1 \ v_2 \ v_3 \ v_4]$ is a column partition of V, then

$$v_4 = c$$

is a solution to Eq. 6.14.

With c known, the mode shapes can be found. Let ϕ_i represent the mode shape corresponding to the ith mode. Then

$$\phi_i = C_{1,i}e^{\beta_i x} + C_{2,i}e^{-\beta_i x} + C_{3,i}e^{j\beta_i x} + C_{4,i}e^{-j\beta_i x} \qquad (6.21)$$

Equation 21 can be evaluated at any x in the range $x=0$ to $x=L$. It is convenient to designate a vector x containing the x coordinates corresponding to the measured data set. In this case, the modes can be compared directly with the measured data. This will be important in the next step. If this approach is used, a vector containing $\phi_i(x)$ is obtained.

220

It is often desirable to normalize the mode shapes. If the modal weighting factors for any data set are to be determined, it is mandatory. One approach is to normalize with respect to length. Numerically, this is quite easy to accomplish. If the normalized mode shape is designated Φ, then length normalized mode shape vectors conform to

$$\Phi^T \Phi = L$$

To compute Φ from ϕ, first calculate the sum of squares of ϕ, designated q.

$$\phi^T \phi = q$$

Then the scale factor to be used for length normalization is given by $sqrt(L/q)$, such that

$$\Phi_i = \phi_i \sqrt{\frac{L}{q_i}} \qquad (6.22)$$

The modal index i has been used in Eq. 6.22 to indicate that the normalization procedure must be independently performed for each mode.

221

MODAL WEIGHTING FACTORS

Steps 1 through 4 are based on simultaneous use of data from each of the several data sets. The spatial frequencies and mode shapes obtained are characteristics of the beam, and are independent of excitation frequency. In contrast, the operating shape of the beam subject to harmonic excitation is very dependent on frequency. Each data set will have a characteristic mode shape that is comprised of a linear combination of the normal mode functions. The modal weighting factors, v_i, describe the contribution of each mode to the operating shape.

Mathematically, the operating shape can be represented by

$$v(x) = \sum_{i=1}^{m} v_i \Phi_i(x) \qquad (6.23)$$

The modal weights can be found for each data set by using a least squares procedure. Let M be a matrix containing the normal mode shapes. That is, $M = [\Phi_1 \ \Phi_2 \ ... \ \Phi_m]$. Also let v be a vector of the unknown modal weighting factors. Then if y is a vector containing the measured operating shape, the modal weights can be found by solving

222

$$Mv = y \qquad (6.24)$$

for v. Any standard least squares method may be used. The matrix M is orthogonal, and thus Eq. 6.24 is well conditioned.

With the modal weighting factors known, a complete dynamic analysis of the beam has been completed. The constituent modes and their associated spatial and natural frequencies are known. The contribution of each mode to a particular operating shape is also known. The method is a direct implementation of classical beam theory, made possible by the high density spatial data obtained from a scanning laser vibrometer.

Experiments utilizing the boundary condition beam analysis method have indicated that mode shapes thus obtained correlate well with theory. These experiments are detailed in Chapter 7.

BCBA IMPLEMENTATION CONSIDERATIONS

The BCBA analyst must make several important decisions. These include the number of data sets to be used in the analysis and the excitation frequencies of those data sets. The number of data sets required is highly dependent on the quality of the spatial derivatives

that can be obtained from the data. This in turn depends on the noise level in the data and the excitation frequency. Three data sets are always required. The following comments can be made regarding choice of number of data sets and excitation frequencies.

- · If the LSSD method is used to estimate spatial derivatives, excitation frequencies must be chosen as close to resonance as possible.

- · If the LSSD model residual from any data set indicates a difference between the model and the measured data near the boundaries, use additional data sets.

- · If the data contains much noise, particularly near the boundaries, use additional data sets.

FUTURE RESEARCH IN BCBA

The BCBA method produces a modal model based solely on spatial data. The boundary conditions and mode shapes are automatically computed as part of the analysis procedure. This gives the method great potential for expanded applications. One such application is the ability of the BCBA method to be used for analyzing structures composed of systems

224

of beams. Future research should investigate this possibility. Another topic that should receive attention is estimation of beam damping.

SYSTEMS OF BEAMS

Many complex structures can be modeled as systems comprised of beam elements. If the constituent beam elements can be assumed uniform, the BCBA method can potentially be used to analyze the structure. The beam elements must be visible in order to facilitate the laser scan. Each beam element can then be analyzed using the BCBA method. This gives dynamic information and boundary condition information for each element. The boundary conditions for two contiguous elements must be compatible. These joints at which the beam elements are connected are automatically modeled by the BCBA algorithm.

In order to extend the BCBA method to systems of beams, a procedure must be developed to consolidate the individual beam element models into a larger, structural dynamical model. This is not a trivial task. However, such a method has great potential for building dynamical models of complex structures.

DAMPING ESTIMATES

Damping in a beam does not affect the mode shapes of the beam. However, it does affect the beam response. Using time-based measurements, and processing vibration data in the time or frequency domain, damping estimates are readily available. With spatial data, damping is much more difficult to estimate.

The modal weighting factors are affected by the beam damping. It should thus be possible to obtain damping estimates from the modal weighting factor estimates. It should be kept in mind, however, that estimation of the modal weighting factors are the final step in the BCBA method. If errors are cumulative, then these quantities are the least reliable estimates obtained by that method. Thus it may be difficult to obtain the requisite accuracy for damping estimates.

This research did not include computation of damping estimates from spatial models. This is a topic well worth investigation, however. It is recommended that future research be conducted in this area.

CONCLUSIONS

The BCBA method is a true spatial modal analysis method. Unlike the minimum residual models, it generates a modal model that is completely compatible with Euler-Bernoulli beam theory. All theoretical constraints are incorporated. The method produces a modal decomposition of the measured spatial data.

The critical step is estimation of the deflection and spatial derivatives at the ends of the beam. The LSSD method can be used for near-resonance data sets. However, for off-resonance excitation, difficulties may be encountered. This is true even for exceptionally noise-free data. The capabilities of the scanning laser vibrometer to provide as much data as required and at the desired locations (i.e. near the ends of the beam) suggests that new algorithms for obtaining the derivatives may be developed.

The remaining steps in the BCBA method follow a logical progression. The general boundary conditions are estimated, followed by the spatial frequencies and mode shapes. Modal weighting factors corresponding to any measured data set can then be found. Operating shapes based on the model can be compared directly with measured data.

Several recommendations for future research are in order. It is recommended that:

227

- Algorithms should be developed to obtain accurate derivatives at the boundaries of the beam regardless of the excitation frequency. (This will remove the restriction of resonance excitation.)

- The feasibility of the BCBA method to extract damping estimates should be investigated.

- The ability of the BCBA method to model a structure composed of beam elements should be investigated.

CHAPTER 7: ERROR ANALYSES

The utility of any modeling method is dependent on the confidence that is placed in the estimated parameters. Ideally, the estimates should accurately reflect the true parameters being estimated. This is the case only if the estimates are unbiased and have a small variance. If the method is unbiased, the expected values of the estimates are equal to the true values. A small variance indicates that the estimates differ from the true values by only a small amount.

Three algorithms for spatial analysis of beams are presented in Chapters 5 and 6 of this dissertation. The PSMA algorithm relies on the self-exciting autoregressive nature of exponential functions. The LSSD approach utilizes a variation of a multivariate Newton's method. Both of these methods can be classed as minimum residual approaches. The BCBA method presented in Chapter 6 is a true spatial modal analysis. None of these algorithms are amenable to exact statistical analysis. Thus, bias and variance determination must be accomplished empirically. This chapter presents tests for each method used to determine the quality of the resulting parameter estimates. Results indicate that the minimum residual models are biased unless the excitation frequency corresponds to a resonance of the beam. The BCBA method is unbiased if accurate spatial derivatives

can be obtained. If either LSSD or PSMA is used in conjunction with BCBA, then resonance excitation must be used to prevent bias error.

BEAM SIMULATION

In order to facilitate the error analyses presented in this chapter, a computer program was developed to simulate the operating shape of a free-free beam. The program used theoretical spatial frequencies and an analytic derivation of the modal constants to obtain the normal mode shapes. Harmonic excitation was assumed. The modal weighting factors and the beam operating shape were then computed.

The computer code was written for PC-Matlab, and named BEAMSIG. A listing of the script file appears in the appendix of this chapter. The program prompted the user for Signal-to-Noise ratio and excitation frequency. It then computed the operating shape with additive, normally distributed random noise. The BEAMSIG program was used with all the analyses described in this chapter.

PSMA ERROR ANALYSIS

230

The PSMA method was evaluated for bias and variance of spatial frequency estimates. Since no definitive method exists for determining optimum delay factor and column dimension, the study also investigated variations in mean and variance between different combinations of model fitting parameters.

OBJECTIVE

The objective of the PSMA analysis is twofold.

1. To determine the bias and variance of modal parameters obtained using the PSMA algorithm.

2. To determine the effect of column dimension and delay factor on parameter estimates.

IMPLEMENTATION

The PSMA algorithm requires three model fitting parameters to be selected. These are the data matrix column dimension c, the delay factor D, and the model order p. The algorithm estimates the spatial frequencies of the beam by finding the poles of the associated

231

autoregressive system. The modal coefficients are subsequently found by a linear least squares procedure. Because the modal coefficients are entirely dependent on the spatial frequency estimates, a study of the statistical nature of the estimated parameters can be restricted to investigation of the quality of the spatial frequencies. Such a study must include the effects of the column dimension c and the delay factor D.

An empirical analysis was conducted to investigate these factors. This involved generating a synthesized beam operating shape and performing a Monte Carlo analysis for a variety of values of c and D. Mean values and standard deviations of the parameter estimates were computed. This provided indication of bias error and variability. The synthesized data was based on near resonance harmonic excitation. This experiment did not investigate off-resonance cases.

The program BEAMSIG was used to generate the simulated operating shape. The effects of six modes of the beam were included in order to more accurately reflect reality. Twenty five realizations of a random noise series were generated. These were added to the simulated beam operating shape to reflect measurement noise. The resulting simulated signals were processed using the DOTLS method (the principal component of the PSMA algorithm). The spatial frequencies for each noise realization were computed and averaged. Also, the standard deviation was computed.

The analysis was repeated for a variety of delay factors and column dimensions. Three different signal-to-noise ratios were used. This provided data covering the spectrum of normal beam analysis parameters. The specific values for these parameters are shown in Table X.

Table X Modeling parameters for PSMA error analysis.

PSMA Modelling Parameters:

Delay Factors:	$D = \{1,4,7,10,13,16,19,22,25,28\}$
Column Dimensions:	$c = \{5,6,7,8,9,10,11,12,13,14\}$
Number of Averages:	25

Beam Simulation Parameters:

Excitation Frequencies:	$\{110,300,590,970,1450,2020\}$
Natural Frequencies:	$\{108,298,585,967,1445,2018\}$
Signal-to-Noise Ratios:	$\{40,30,20\}$ dB

RESULTS

The results of this numeric experiment indicated that the spatial frequency estimates are much more sensitive to column dimension than to delay factor. Variability in parameter estimates is also dependent on noise level (as is expected) and mode number. For near-

resonance excitation slight bias is observed. Specifically, the experiment produced the following results :

- Variability increased with increasing noise.

- Variability decreased with increasing mode number (Recall resonance excitation was used).

- Variability was very large for small column dimensions.

- Variability was independent of matrix delay factor.

- Slight bias error was observed.

The experiment produced eighteen sets of data, each with mean values and standard deviations for 100 combinations of column dimension and delay factor. Presentation of this prodigious amount of data was difficult. The format chosen for presentation was mesh plots. A 10x10 grid was constructed for the ten delay factor values and the ten column dimension values. The mean or standard deviation was then plotted as the vertical displacement of this grid. The result was a mesh plot for the mean values and for the standard deviations.

A total of eighteen such plots were generated, one for each of the six excitation frequencies and the three signal-to-noise ratios. Each plot depicts a mesh of the mean spatial frequency estimate and the standard deviation of the spatial frequency estimates. The six plots corresponding to the 30dB SNR cases are reproduced in Figures 48 through 53. The 20dB and 40dB cases are similar, differing only by an decrease in variability with decreasing noise.

Inspection of Figs. 48 through 53 shows that as the dominant mode's frequency increases, the variability of the spatial frequencies decreases. Figure 48, corresponding to the first mode, shows a high degree of variability. The mean value mesh becomes progressively smoother for Figs. 49 through 52. The data corresponding to mode 6, shown in Fig. 53, is quite smooth except in the region where the column dimension is small.

Each of the figures shows a marked increase in variability for small column dimension. This indicates that for near-resonance testing, the minimum column dimension should be approximately 9. It can also be seen that the variability does not change in with respect to the delay factor.

The presence of bias error is not apparent in the figures. An additional check was performed to determine bias. The true spatial frequency of the simulated data that corresponded with the resonance mode was compared with the estimated spatial

235

frequency. If the true value lay within two standard deviations of the estimated value, it was assumed that no bias error was present. This test was performed on all data sets and all combinations of column dimension and delay factors. In a small percentage of cases, a bias was observed. It is significant to note that the bias was noted where the standard deviation was small. This suggests the possibility that a small bias could be masked in many cases by large variance.

MEAN SPATIAL FREQUENCY - MODE 1

STANDARD DEVIATION - MODE 1
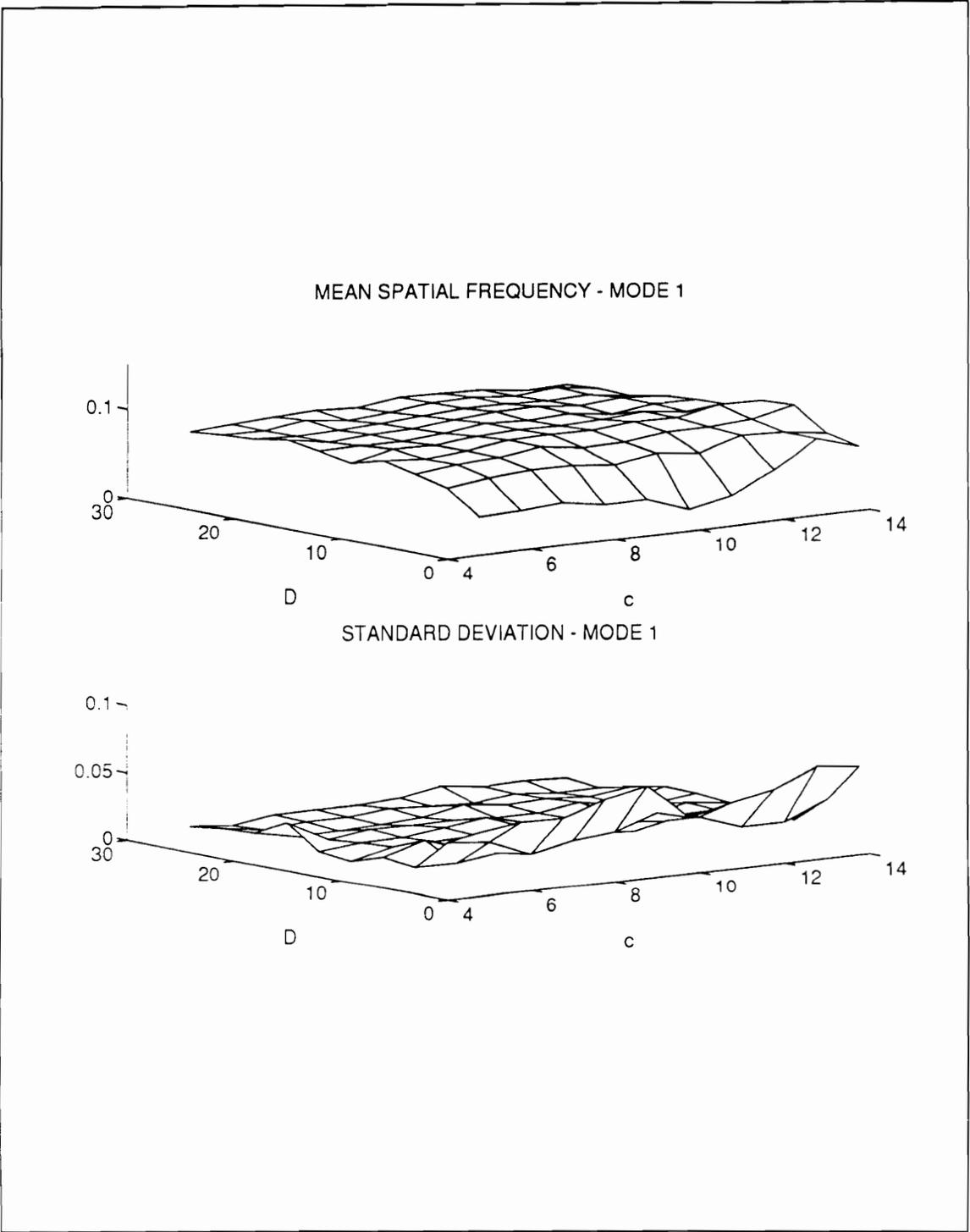
Figure 48 Spatial frequency estimate mean and standard deviation versus column dimension and delay factor. **Mode 1 30dB SNR**

237

MEAN SPATIAL FREQUENCY - MODE 2

STANDARD DEVIATION - MODE 2
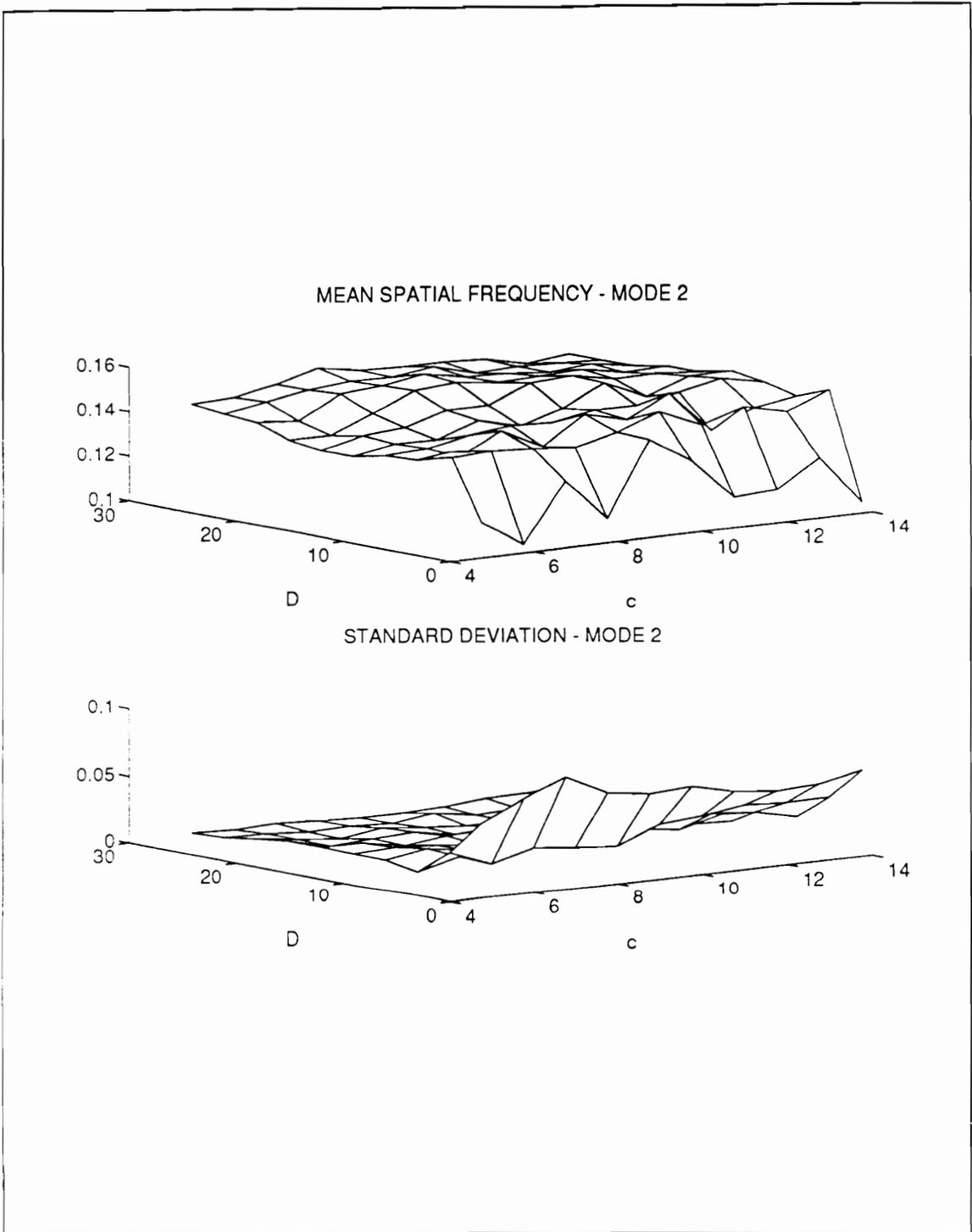
Figure 49 Spatial frequency estimate mean and standard deviation versus column dimension and delay factor. **Mode 2, 30dB SNR**
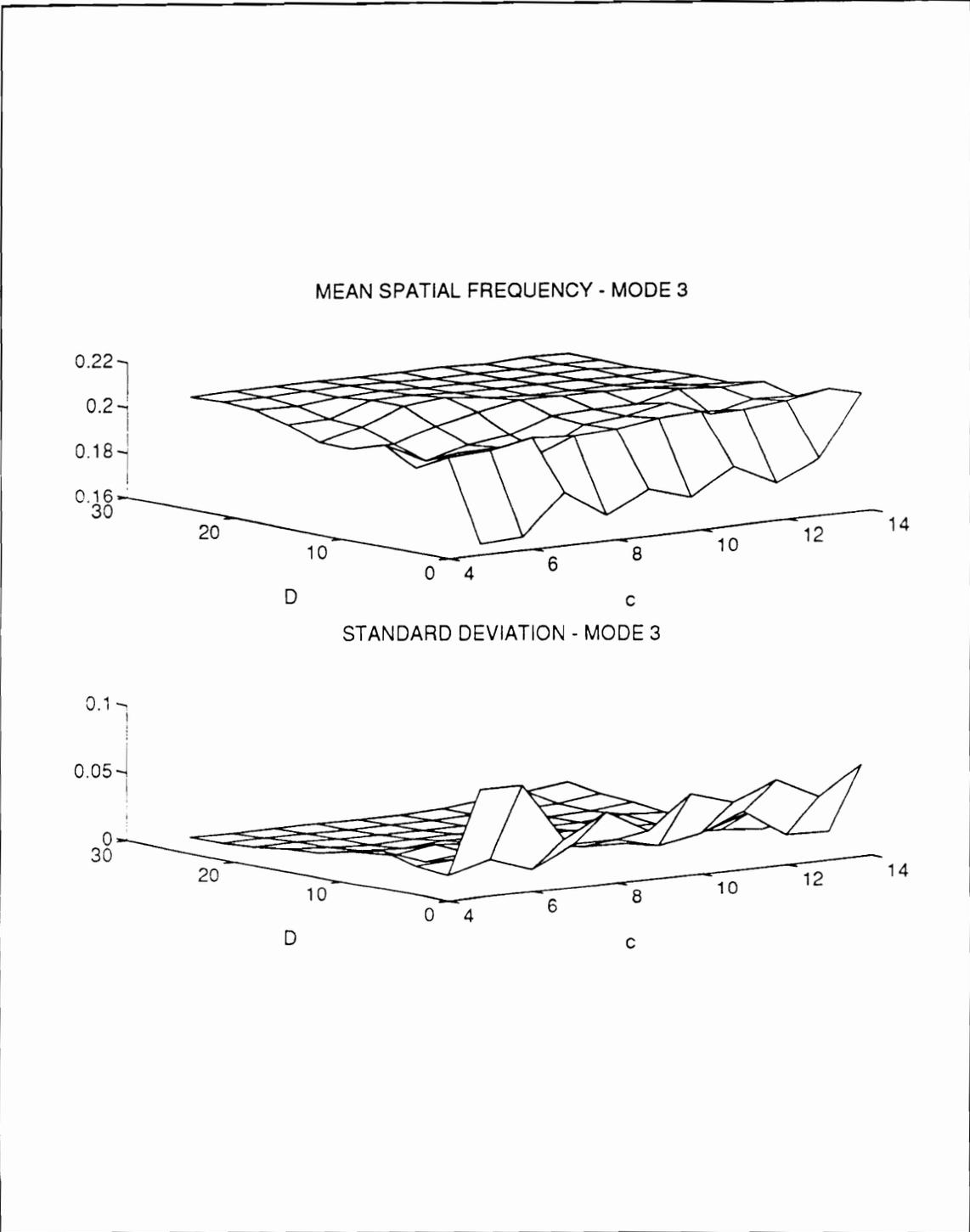
Figure 50 Spatial frequency estimate mean and standard deviation versus column dimension and delay factor. **Mode 3, 30dB SNR**
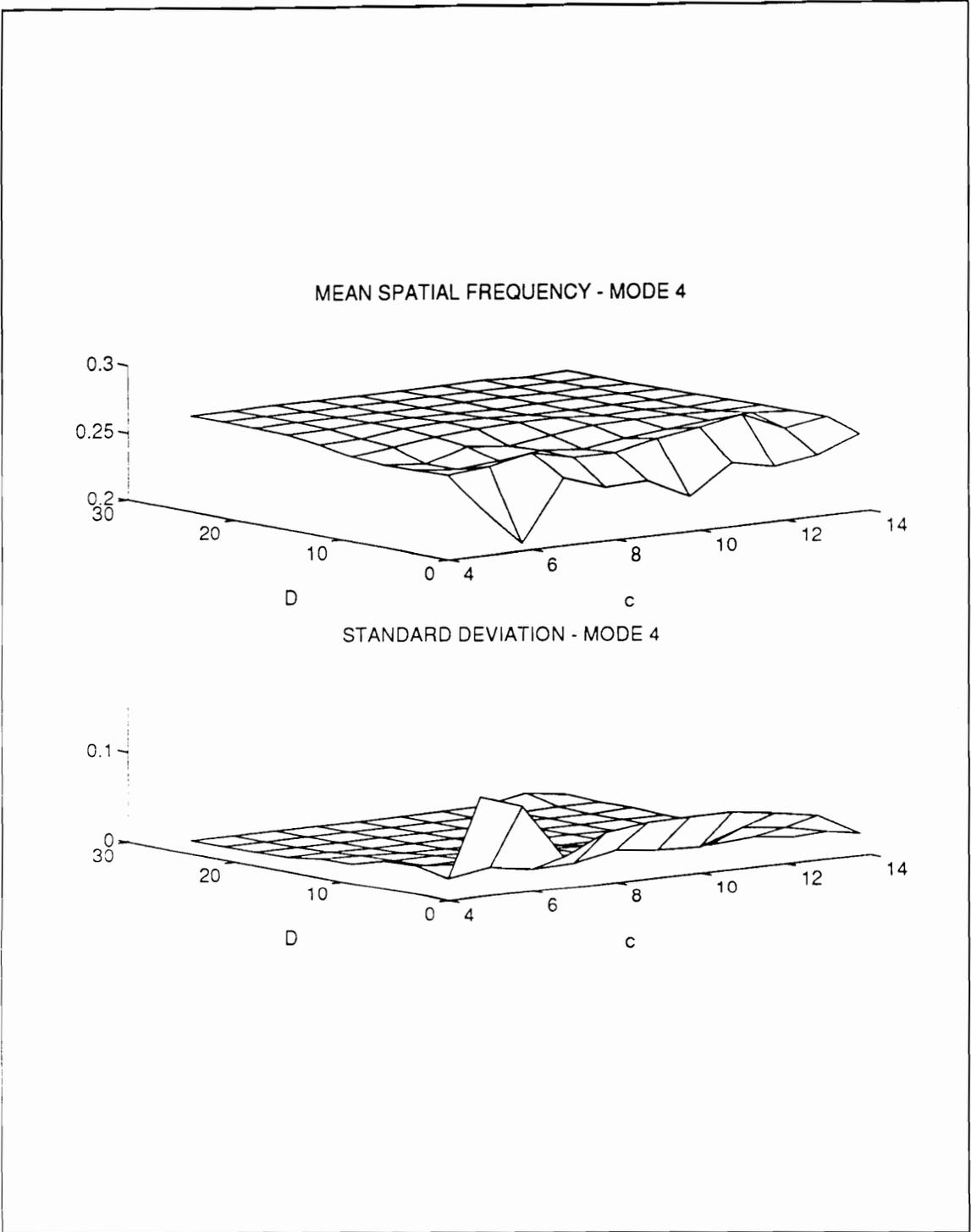
Figure 51 Spatial frequency estimate mean and standard deviation versus column dimension and delay factor. **Mode 4, 30dB SNR**

240

MEAN SPATIAL FREQUENCY - MODE 5

STANDARD DEVIATION - MODE 5
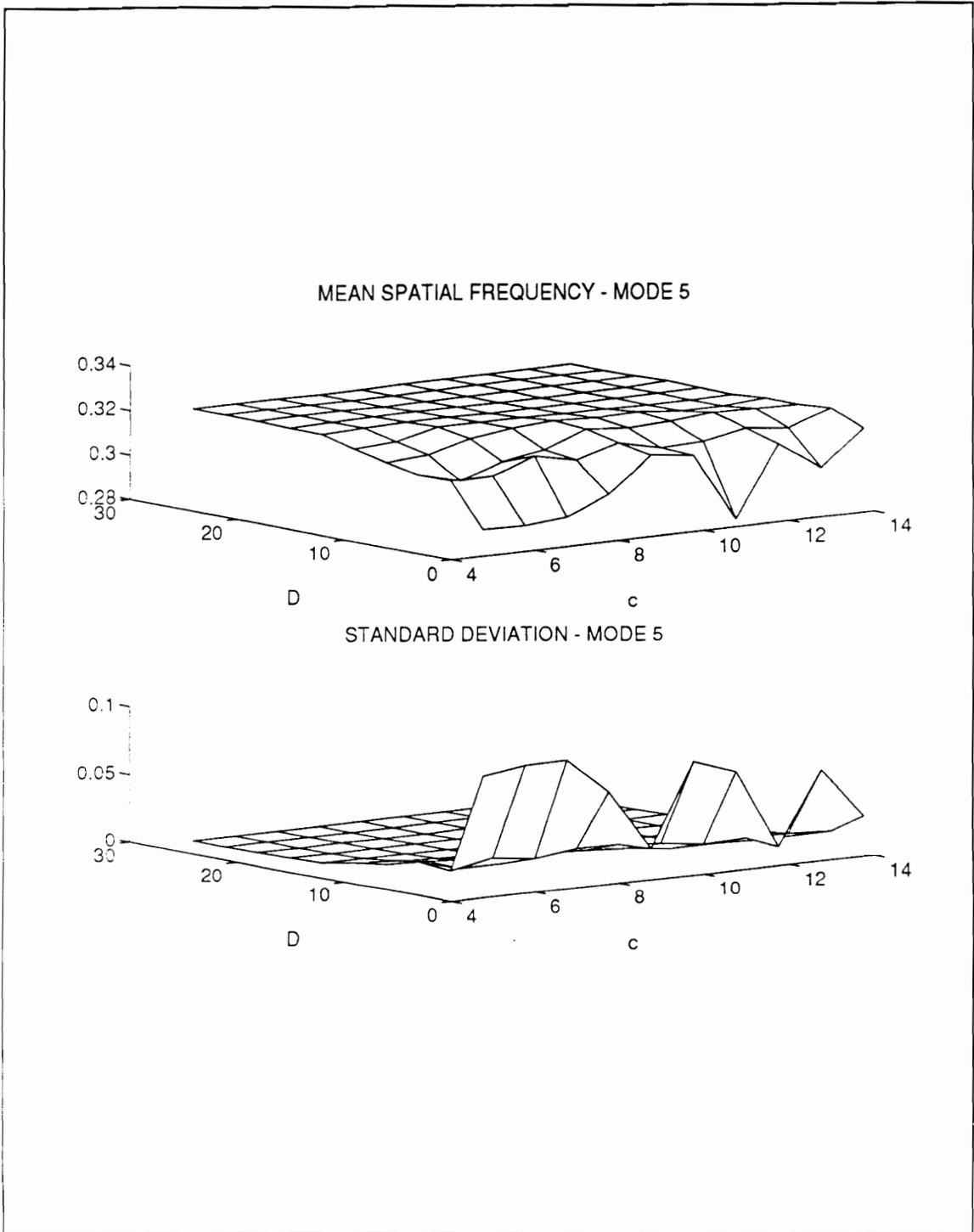
Figure 52 Spatial frequency estimate mean and standard deviation versus column dimension and delay factor. **Mode 5, 30dB SNR**
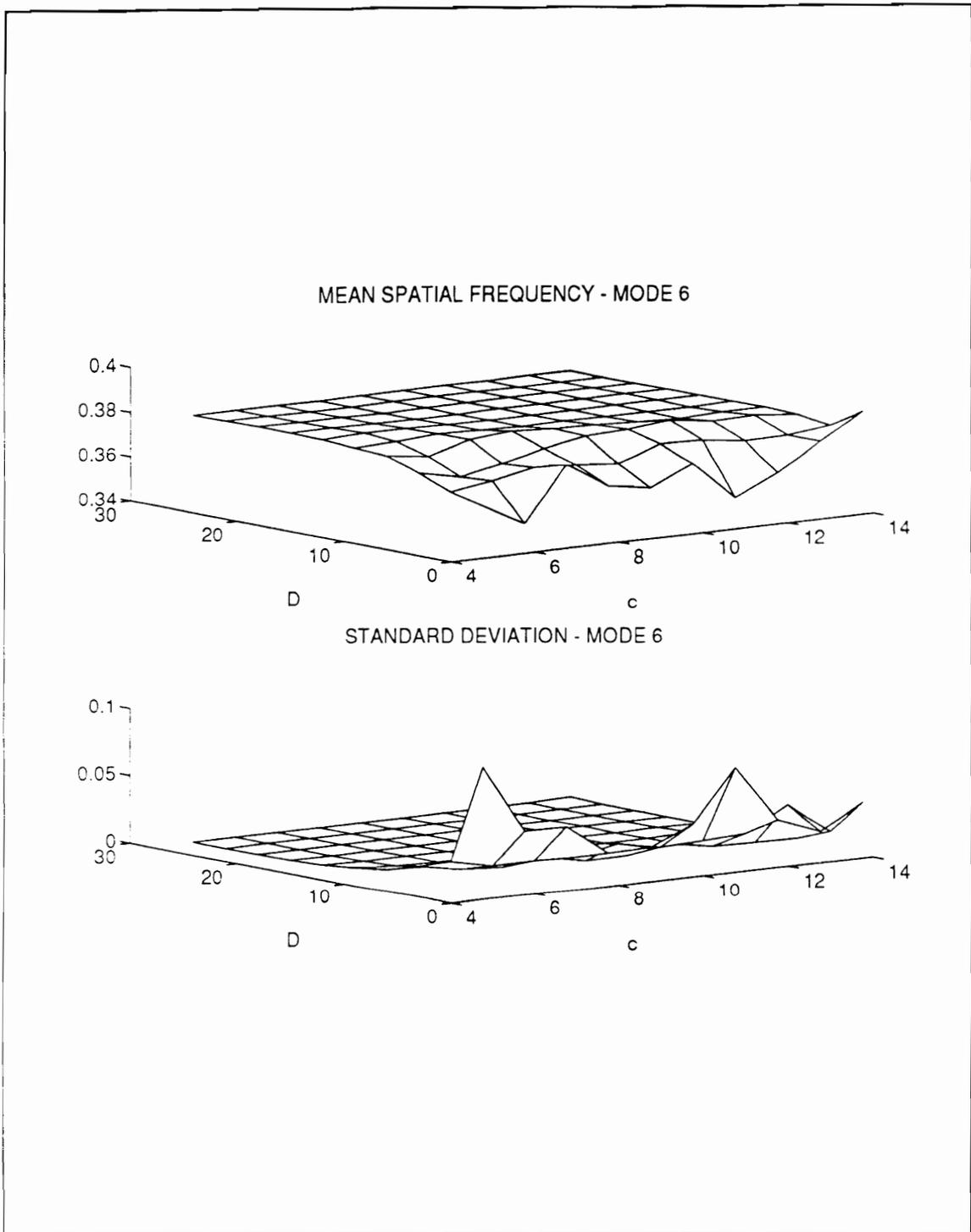
Figure 53 Spatial frequency estimate mean and standard deviation versus column dimension and delay factor. **Mode 6, 30dB SNR**

242

CONCLUSIONS

The following conclusions can be drawn from the PSMA error analysis:

- Additional study is required to determine bias errors.

- For resonance testing, the column dimension should be chosen greater than approximately 9.

- The matrix delay factor has little bearing on spatial frequency estimation. It should therefore be chosen as small as possible.

- Spatial frequency variance decreases with mode number for PSMA analysis of resonance data.

LSSD ERROR ANALYSIS

An investigation of the variability and bias of parameter estimates obtained using the LSSD method was performed. The LSSD method simultaneously solves for the spatial

243

frequencies and the modal constants. Thus the mean value and variance for β, C_1, C_2, C_3, and C_4 were computed.

OBJECTIVE

The objective of the LSSD error analysis was to:

- Determine bias error and variance for modal parameter estimates obtained using the LSSD method.

IMPLEMENTATION

The simulated beam data was obtained in exactly the same manner as for the PSMA analysis. Simulation parameters were identical. Refer to Table X for the specific values. For each excitation frequency and noise level, the data was analyzed using the LSSD method. Since resonance testing was used, only one mode was extracted. The parameter estimates for β, C_1, C_2, C_3, and C_4 for the mode of interest were computed. The mean value and standard deviation were computed for 25 different noise realizations.

244

RESULTS

The results of this experiment reveal that a slight spatial frequency bias error is present in all cases. The modal coefficients do not indicate any bias. Variance decreases with noise levels. It is worth noting that the variance of the spatial frequency estimates was much smaller than with the PSMA analysis.

The mean value of each parameter was plotted along with two standard deviation bounds. The true value used in the simulation was also plotted. This enabled rapid determination of bias and variance. Data from each of the three noise levels was plotted on a common graph.

Figures 54 through 59 show the mean value and two standard deviation bounds for the spatial frequency estimates of the six modes. Figure 54 depicts the data for mode 1. The standard deviation bounds decrease with decreasing noise levels, as is to be expected. Of greater interest, it can be seen that the mean value is offset from the true value in all three noise cases. Furthermore, the mean value was constant for all noise levels. Although the mean values all lie within the two standard deviation bounds, the constant offset suggests a possible bias error.

The spatial frequency data for mode 2 (Fig. 55) is similar to that of mode 1. However, Fig. 56 shows that for mode 3, a very noticeable bias error is present. Figures 57 through 59 show a similar phenomenon. In all cases the mean value is offset from the true values. The offset is constant with respect to noise levels. This supports the hypothesis that a bias error is present in all data sets. In some cases, such as the mode 1 data, the bias error is small enough to be statistically insignificant.
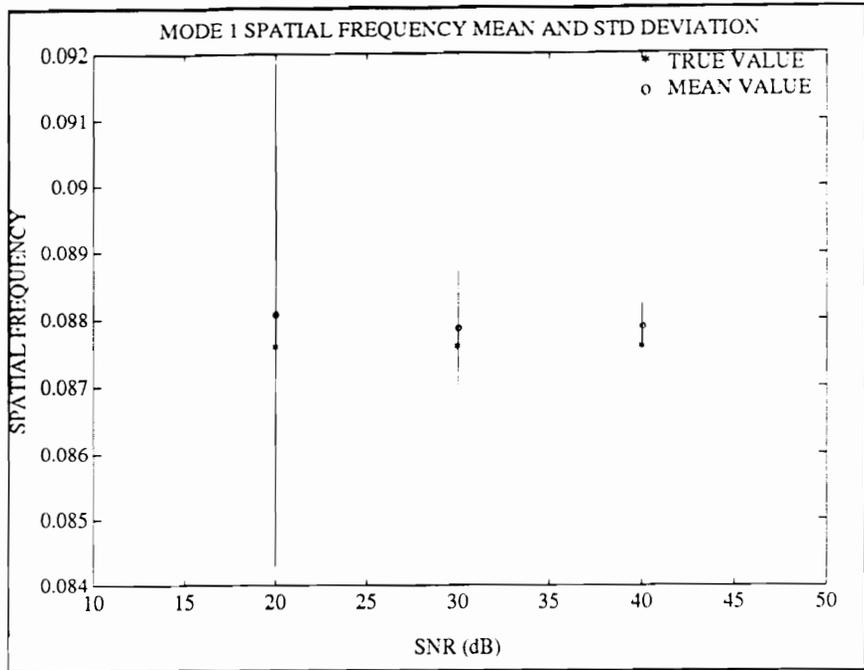
Figure 54 LSSD Statistical analysis for β -- Mode 1.
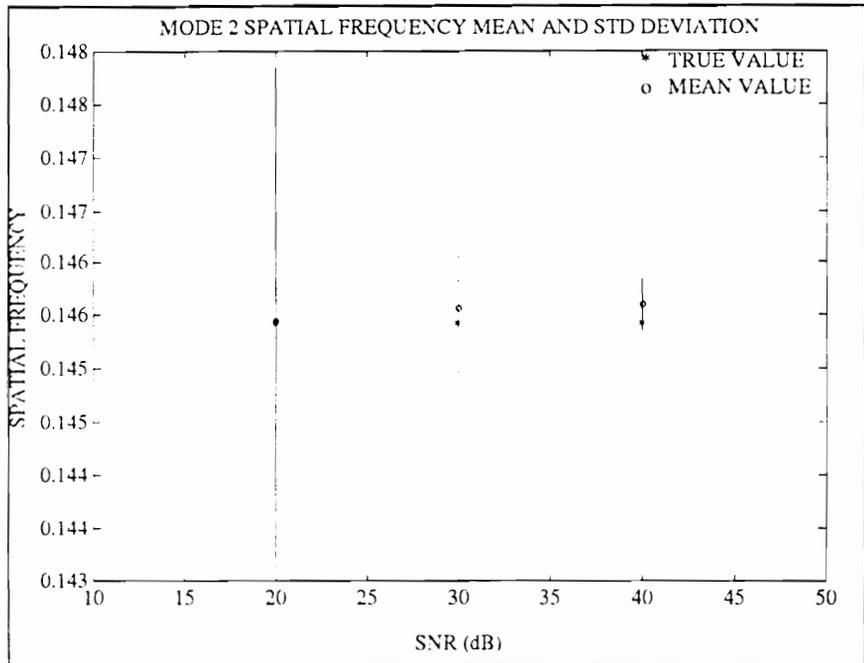
Figure 55 LSSD Statistical analysis for β -- Mode 2.

247
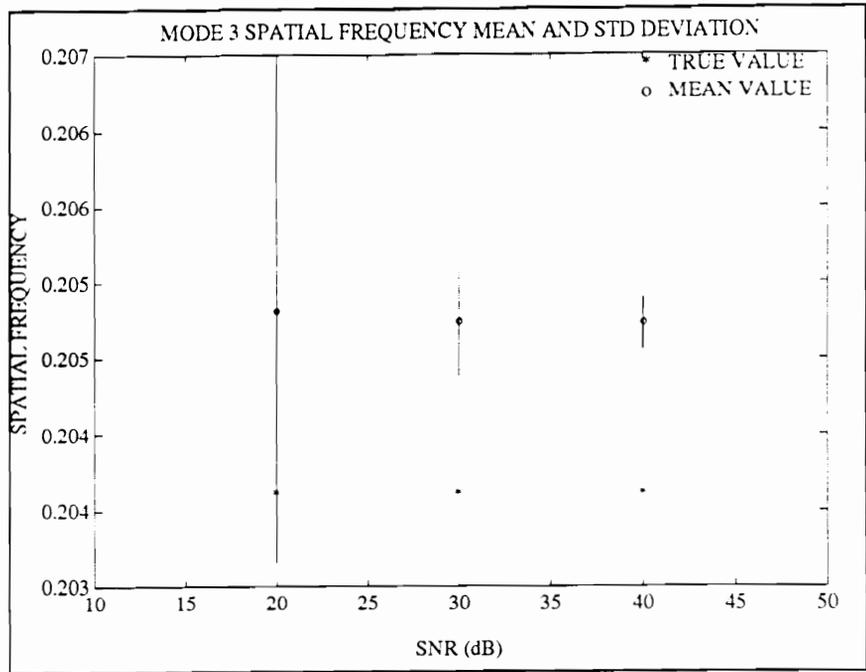
Figure 56 LSSD Statistical analysis for β -- Mode 3.
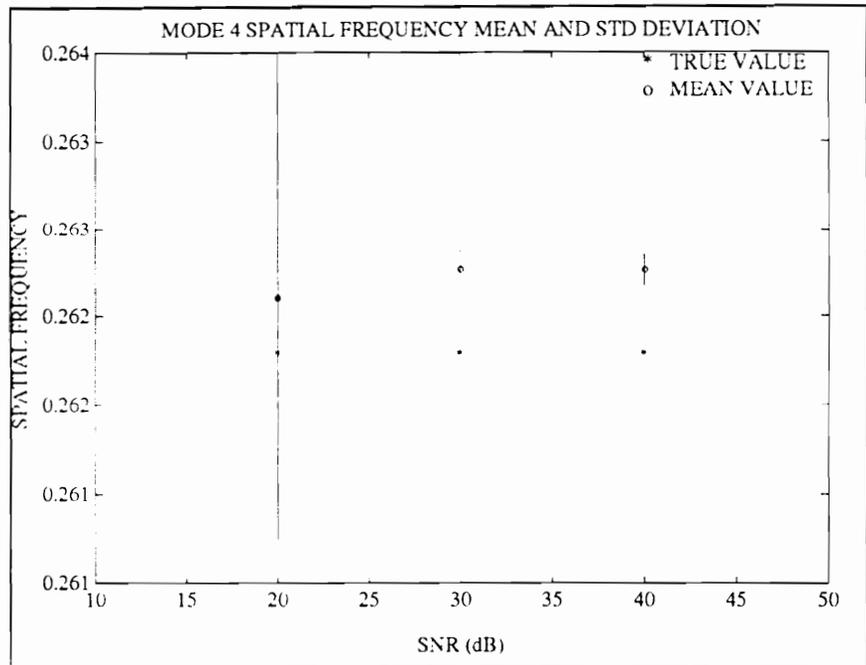
Figure 57 LSSD Statistical analysis for β -- Mode 4.

248
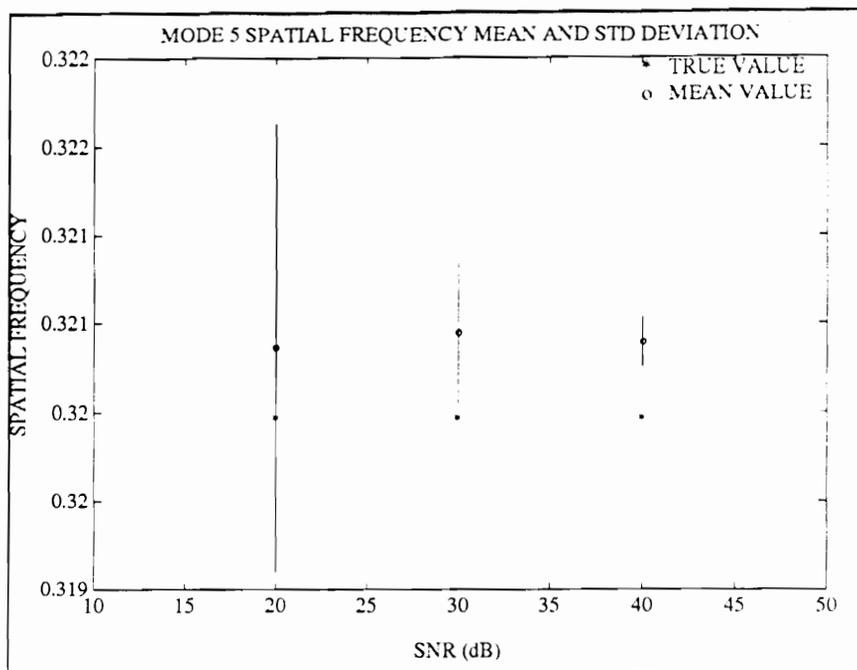
Figure 58 LSSD Statistical analysis for β -- Mode 5.
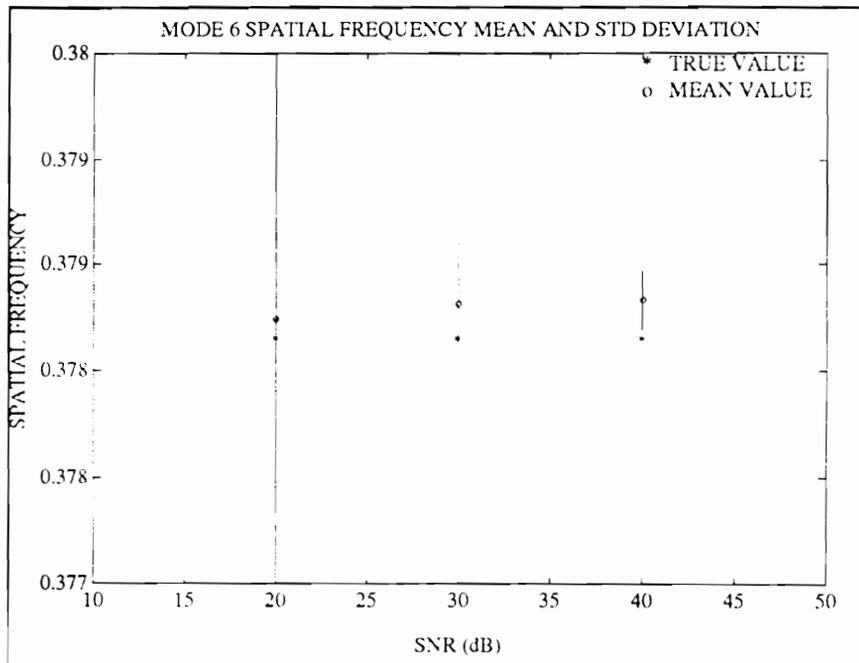
Figure 59 LSSD Statistical analysis for β -- Mode 6.

249

The modal coefficients, C_1, C_2, C_3 and C_4, did not indicate the bias that was apparent in the spatial frequency estimates. In general, the mean values corresponded very well with the true values. The most sensitive parameter appeared to be the real part of C_3. Figures 60 through 65 show the results of the analysis for this parameter. Inspection of Fig. 60 shows that the true values and the mean values of $Re(C_3)$ for mode 1 data are collocated. This indicates no bias error. However, the two standard deviation bounds are much larger than for the spatial frequencies. Thus expected values may not be biased, but they will have large variability.

Figure 61, presenting data for the mode 2 excitation case, is very similar to Fig. 60. Large variance and no bias error are indicated. Figure 62 shows the results for mode 3 data. In this case a possible bias is indicated. It should be noted that the 40dB mode 3 analysis for $Re(C_3)$ is the only case in which the mean value of any of the modal coefficients lies outside the two standard deviation bounds. Figures 63, 64, and 65 are similar to Figure 62, with the exception that smaller differences between true and mean values are noted. The plots for C_1, C_2, and $Im(C_3)$ all appear very similar to Figure 60, and are thus not reproduced here. These plots indicate large variance and no apparent bias error.
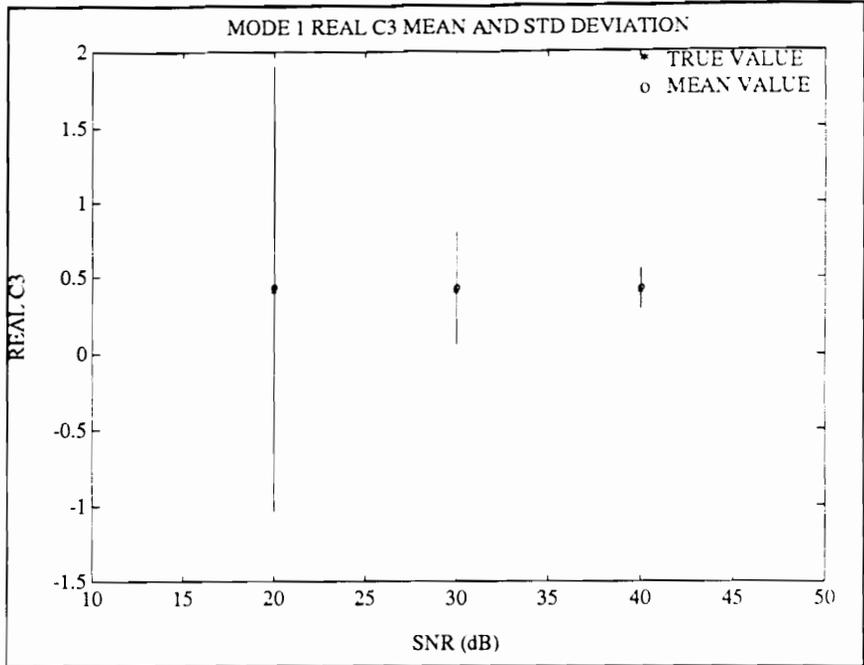
Figure 60 LSSD Statistical analysis for real part C_2 -- **Mode 1.**
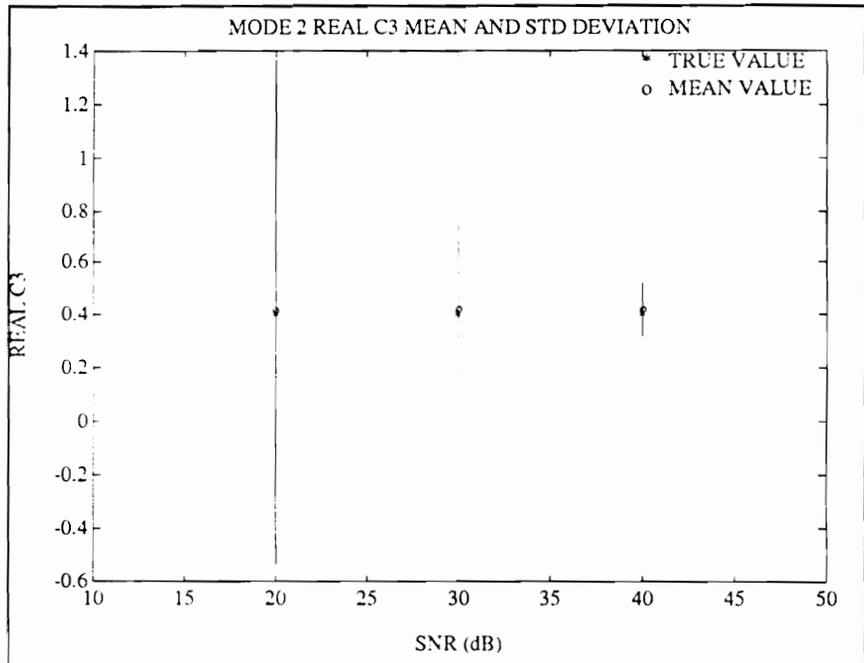
Figure 61 LSSD Statistical analysis for real part C_2 -- **Mode 2.**

251
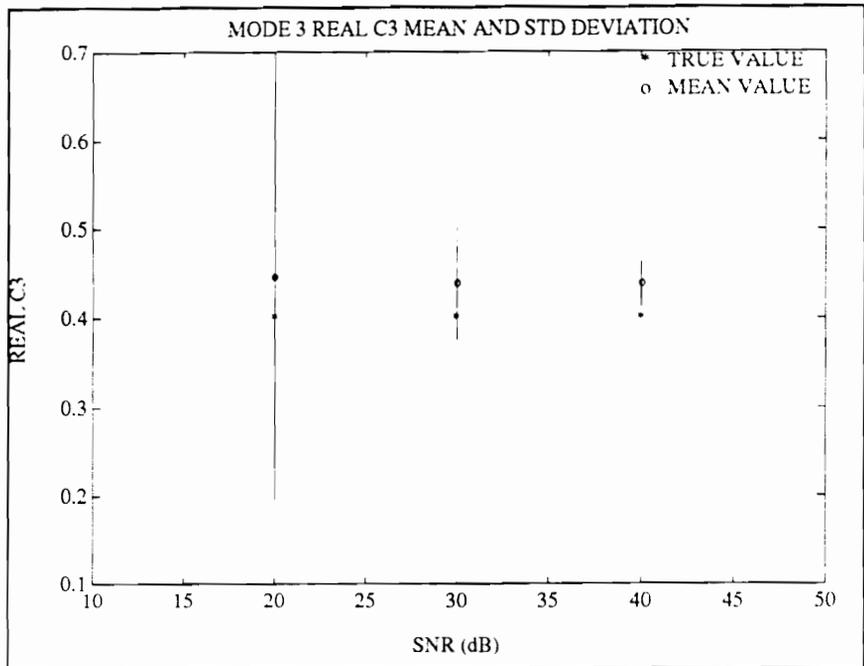
Figure 62 LSSD Statistical analysis for real part C_3 -- **Mode 3.**
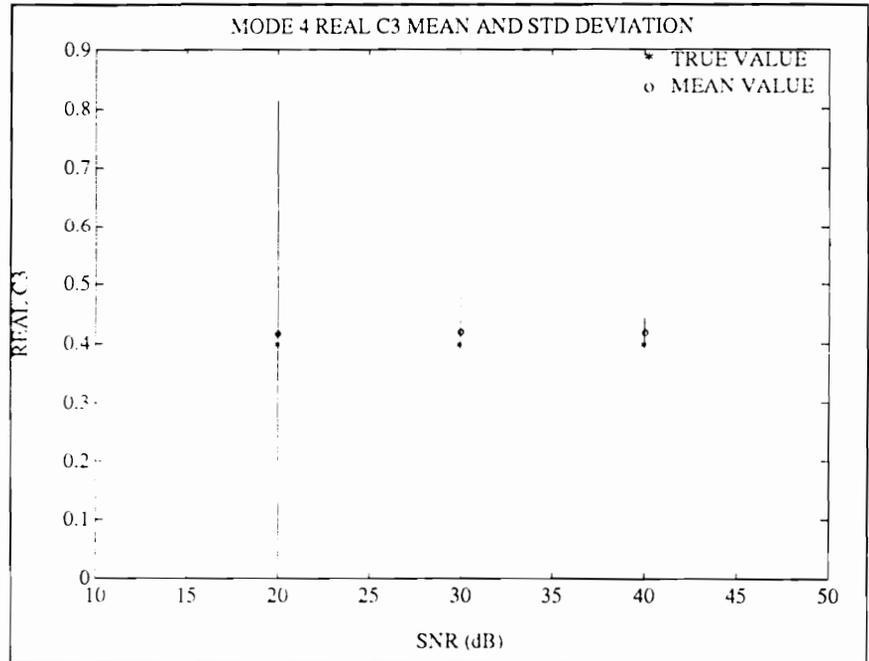
Figure 63 LSSD Statistical analysis for real part C_3 -- **Mode 4.**

252
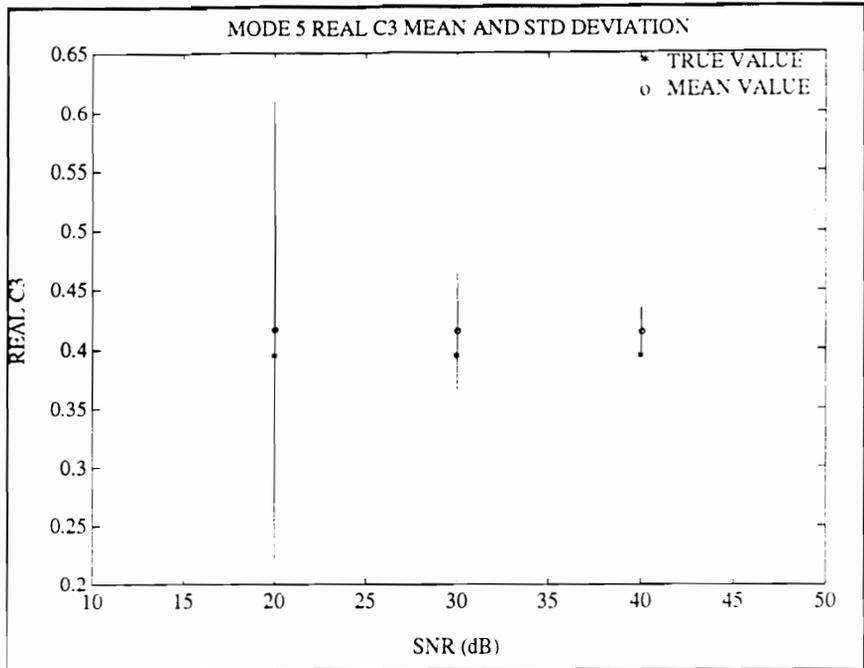
Figure 64 LSSD Statistical analysis for real part C_2 -- **Mode 5.**
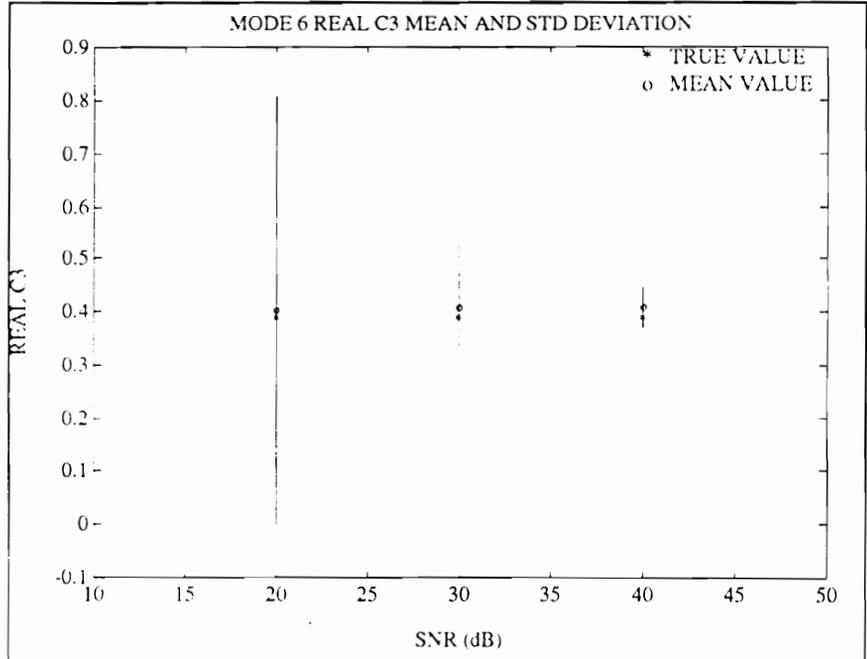
Figure 65 LSSD Statistical analysis for real part C_2 -- **Mode 6.**

253

CONCLUSIONS

The following conclusions can be drawn from the LSSD error analysis:

- Spatial frequency estimates are biased.

- Coefficient estimates exhibit large variance.

- Additional investigation into the nature of the bias error is warranted.

Since both the LSSD and the PSMA methods are minimum residual approaches, it is possible that the bias errors noted with the LSSD analysis are also present in the PSMA case. The mean values of both analyses were very close. The larger variance observed in the PSMA analysis could mask small bias errors.

Note: Strictly speaking, from a statistical perspective, the two standard deviation bounds provide a means of determining bias error with a 95% probability. The spatial frequency estimates for mode 1 excitation, as depicted in Fig. 54, could be said to be not biased with 95% probability. The hypothesis that a bias error does indeed occur is thus not strictly supported by the data. However, the consistency of the estimates regardless of

noise, coupled with trends seen in the remaining data sets, give credence to the possibility of a bias error.

BIAS ERROR STUDY

The importance of determining the nature and extent of the bias observed in the LSSD and PSMA analyses led to an additional study. It was desired to confirm the presence of the bias and to gain some insight into its characteristics. It was observed that the data sets which exhibited the largest bias error also had the greatest difference between excitation frequency and natural frequency. Perhaps a relationship existed between the bias error and excitation frequency.

OBJECTIVE

The objective of the bias study was to:

- Determine if a relationship existed between excitation frequency and estimated frequency bias.

· Quantify such a relationship, if it exists.

IMPLEMENTATION

As with the previous analyses, the beam simulation program BEAMSIG was used to simulate operating shapes of a free-free beam. The contributions of six modes were included in the synthesized data. In this case, the excitation frequency was not restricted to near resonance. Over two hundred operating shapes, each containing contributions of six modes, were synthesized. The excitation frequencies ranged from 10 rad/s to 2050 rad/s in increments of 5 rad/s. This band ranged from well below the first resonance to slightly above the sixth. A relatively high signal-to-noise ratio of 40 dB was chosen. Since only the bias error was of interest, higher noise levels were not required.

Both the LSSD and the PSMA methods are minimum residual approaches. Both are restricted in practice to single-mode analysis. The bias error could be due to this limitation. It was thus assumed that the bias error should be common to both methods. This assumption was supported by observations of the performance of both methods. For the bias study, only the LSSD method was used, since the spatial frequency variance is much smaller than with the PSMA method.

256

The bias study experiment thus used only single-mode analysis, even for those cases in which the excitation frequency was quite distinct from any resonance frequency. This approach provided insight into the nature of the bias error. The resulting spatial frequency estimates were plotted against the excitation frequency. The true natural frequencies of the simulated beam were also plotted.

RESULTS

The results indicate a very distinct bias that is strongly dependant on excitation frequency. At resonance, no bias is noted. However, as the excitation frequency deviates from resonance, errors become quite large. These results are plotted in Figure 66. Inspection of the figure shows the biased trend. Theoretically, the spatial frequencies should have discrete values corresponding to the true simulated spatial frequencies, regardless of the excitation frequency. Thus, the figure should indicate a set of discrete frequencies. However, this is not the case. If the excitation frequency does not correspond to a natural frequency, a single, biased spatial frequency is observed. This is seen in Fig. 66 by the continuous line, as opposed to a discrete set of spatial frequencies.

The LSSD and PSMA analyses were conducted with near-resonance excitation frequencies. This explains the small bias errors seen in those studies. Had the excitation

257

frequencies been chosen farther from resonance, the bias would have been much more pronounced.
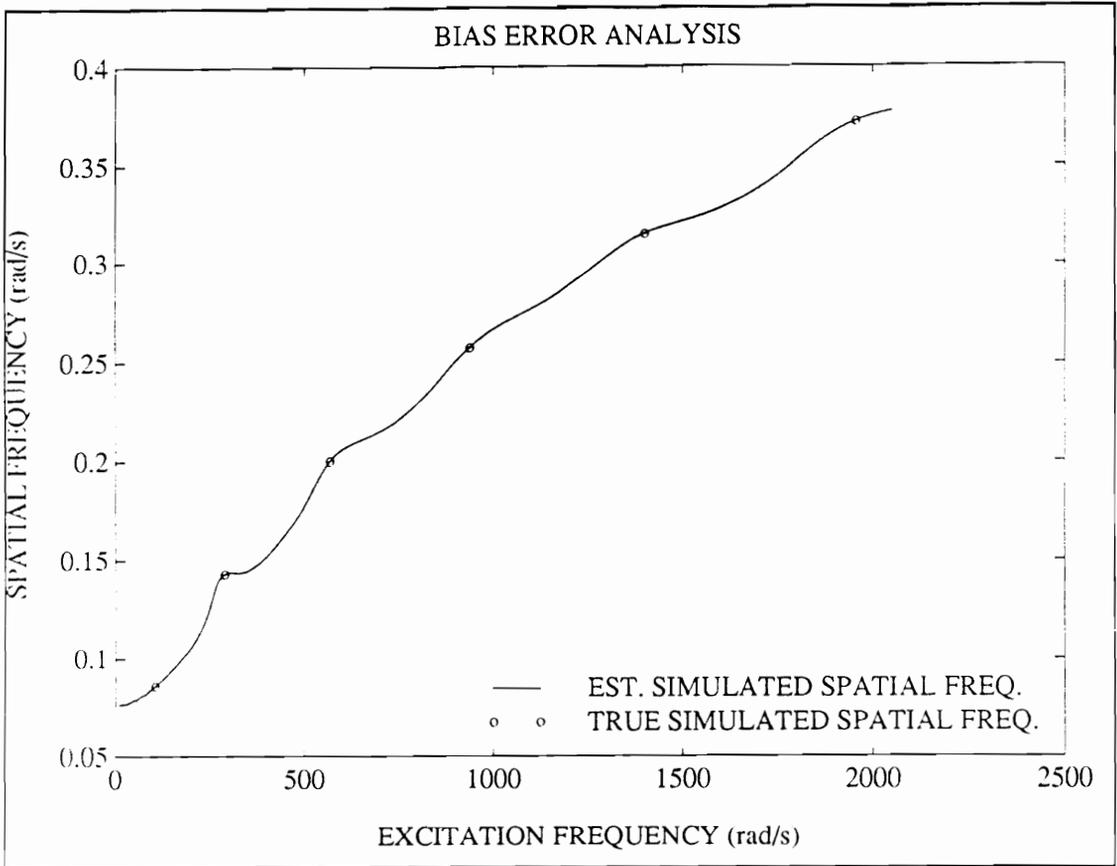
Figure 66 Bias of spatial frequency estimates from minimum residual models versus beam excitation frequency.

CONCLUSIONS

It can be seen in Fig. 66 that the estimated spatial frequency is equal to the true spatial frequency only when the excitation frequency is equal to one of the natural frequencies of the beam. This reflects the inability of minimum residual methods to fit a true modal model. Contributions from other modes distort the spatial frequency estimate. Recall that

259

the BEAMSIG program does not include damping. It is possible that for a damped beam, all cases would exhibit a bias.

The conclusion to be drawn from this study is that:

- Minimum residual approaches must only be used with resonance excitation.

- Significant bias errors exist for off-resonance excitation.

BCBA ERROR ANALYSIS

The BCBA method represents an approach to spatial modal analysis that is distinctly different from the minimum residual methods. It is a progressive analysis in that it consists of a number of steps that must be completed in sequence. The first step is estimation of the deflection and spatial derivatives at the ends of the beam. If these quantities were known exactly, the only error in the remaining steps would be attributed to round-off error or numerical computation inaccuracies. It is therefor important to be able to characterize the quantity of the derivative estimates. This analysis involves estimating the mean value and standard deviation of deflection and spatial derivative estimates at the beam boundaries.

260

OBJECTIVE

The objective of the BCBA error analysis was to:

- Investigate the bias error and variability of deflection and spatial derivative estimates used in the BCBA method.

IMPLEMENTATION

The deflection and spatial derivatives at the boundaries of a beam may be estimated in a number of different ways. One method that has worked well in practice is to model the data using the LSSD method. The derivatives may then be easily obtained. A significant limitation of this approach is the restriction to near resonance excitation. Despite this drawback, the LSSD model is the best option unless specialized differentiation algorithms are developed.

This study investigates the ability of the LSSD modeling method to provide accurate spatial derivative estimates. The BEAMSIG program is used to generate a simulated operating shape of a beam. Excitation frequencies are chosen that range from 10% below to 10% above the third natural frequency. Random noise is added to the signal to produce

a SNR of 30dB. Derivative estimates are averaged over 50 realizations of the noise sequence. The standard deviation is also computed.

RESULTS

The results of the BCBA error analysis indicate that:

.

- · The variance of the deflection and spatial derivative estimates was in all cases very small.

- · A bias error is incurred when LSSD is used to estimate the derivatives.

- · The absolute magnitude of the bias error is small.

The analysis provided information on the deflection and the first three spatial derivatives at each end of the simulated beam. This resulted in eight sets of data. Mean values were compared with true values (obtained from the simulated model) for each case. The estimates were considered biased if the mean value differed from the true value by more than two standard deviations.

262

These results were plotted against the excitation frequency. The data points coinciding with resonance excitation were omitted from the plots. The BEAMSIG program does not include damping, and the resulting resonance data point were several orders of magnitude larger than all the remaining data points. The resulting graphs thus include ten data points below the third resonance frequency, and ten above.

These plots are reproduced as Figures 67 through 74. Figures 67 and 68 depict the deflection estimates at the right and left ends of the beam, respectively. A slight bias is apparent in the data for the left end. The two standard deviation bounds are almost coincident with the mean value. Note that the deflection bias tends toward zero as the excitation frequency approaches resonance.

The slope at each end of the beam is presented in Figs. 69 and 70. These resemble the deflection plots. The bias error is slightly more pronounced, however.

The second and third derivatives are of most importance for a free boundary condition. In theory, the moment and shear, and consequently these derivatives, are zero at the beam boundaries. In general, the estimated second and third derivatives are not equal to zero. This error is not unexpected, considering the limitations of the LSSD method. The absolute values were small, however, validating the utility of the approach.

263

Figures 71 and 72 depict the second derivative at the left and right ends of the beam. Figure 71 shows a marked, although small, bias error at the left beam boundary. This bias could lead to small errors in boundary condition estimation. It is worth noting that the omitted data point, using excitation almost at resonance, was statistically unbiased. The right end of the beam indicated less bias error. If excitation frequency is within approximately 5% of the resonance frequency, no bias is observed. See Fig. 72.

The third derivatives at the right and left ends are shown in Figs. 73 and 74, respectively. Similar behavior is observed in these figures. The bias is an order of magnitude smaller than that of the second derivative. Nonetheless, it is still very apparent in both figures.
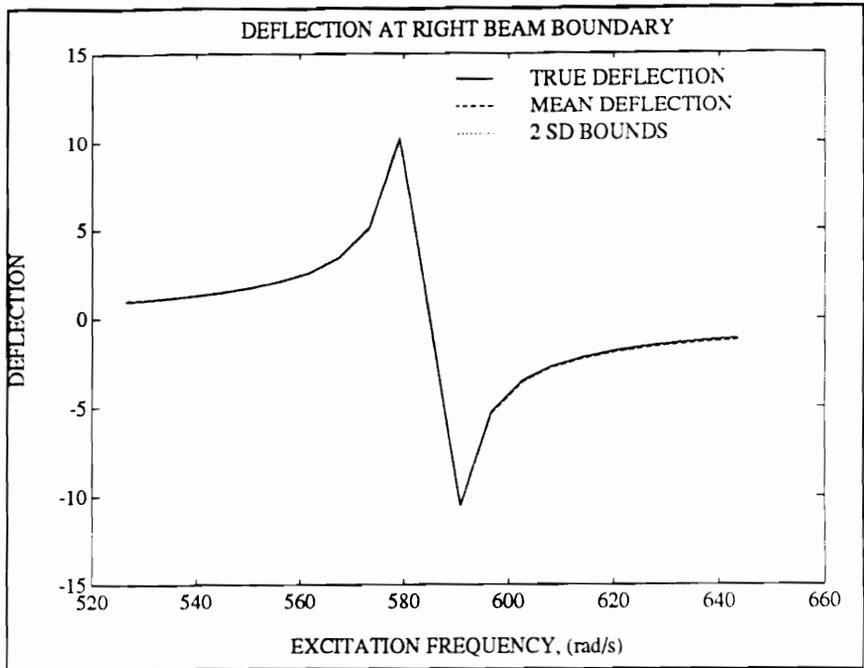
Figure 67 Deflection at right beam boundary
true simulated value, mean value, and two
standard deviation bounds.
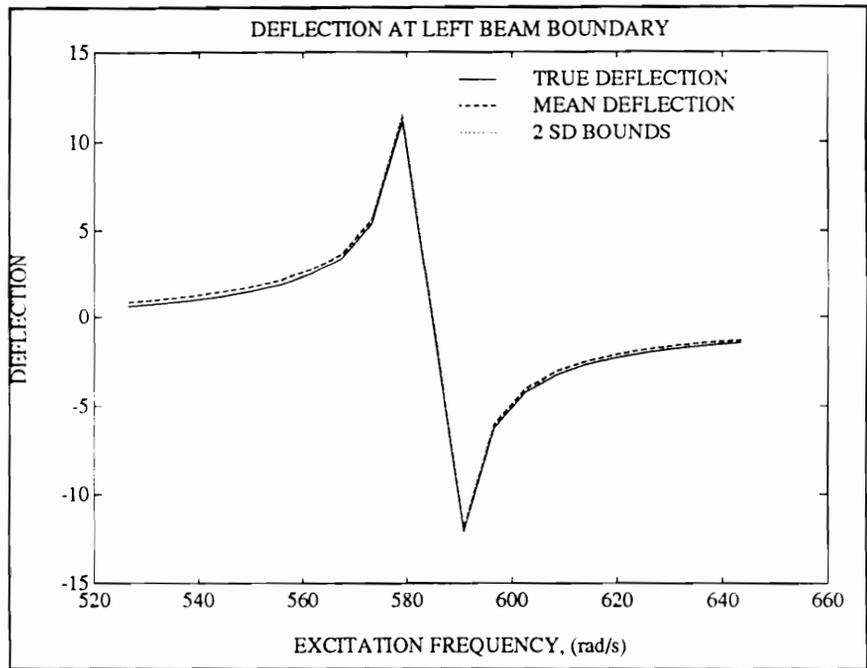
Figure 68 Deflection at left beam boundary
true simulated value, mean value, and two
standard deviation bounds.

265
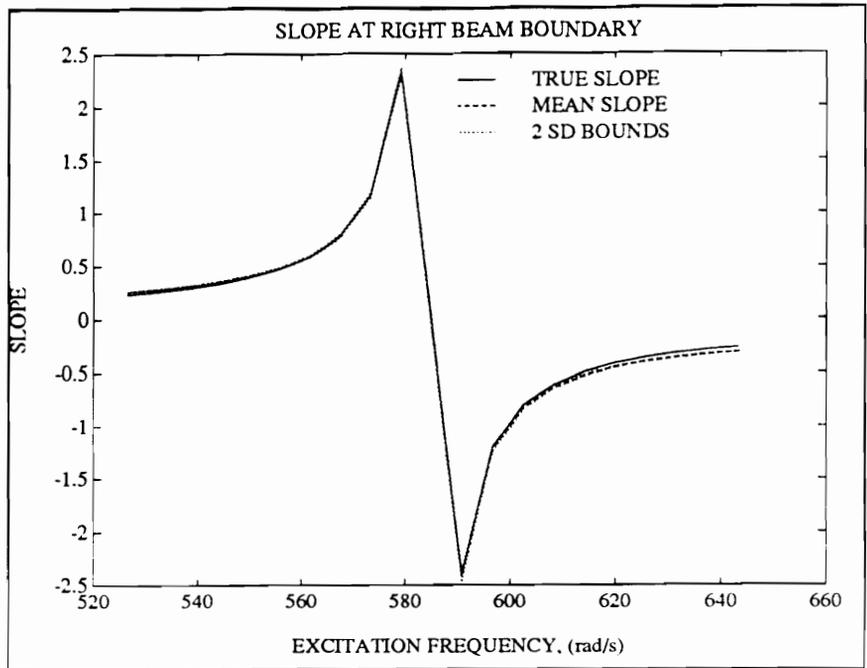
Figure 69 Slope at right beam boundary true
simulated value, mean value, and two standard
deviation bounds.
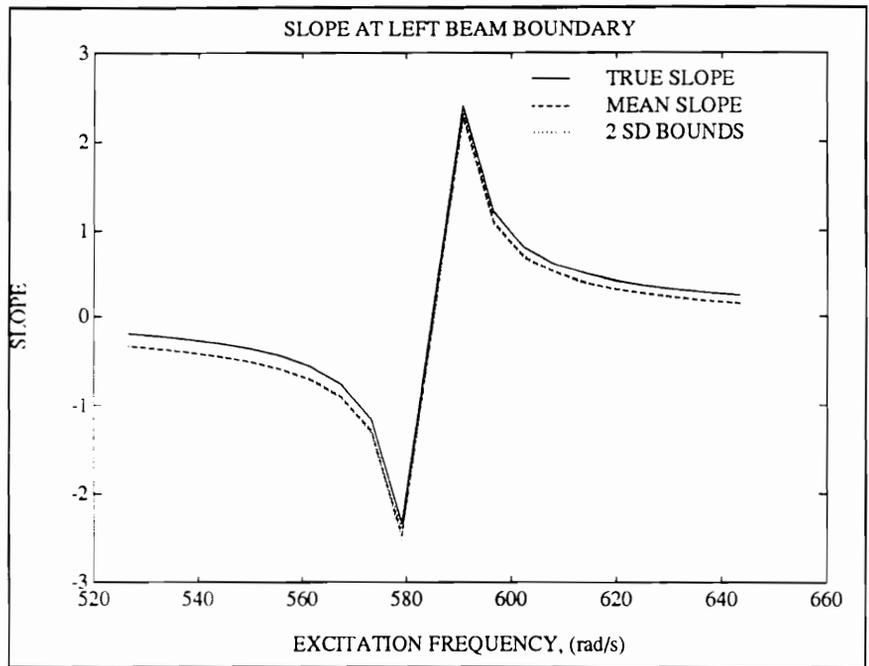
Figure 70 Slope at left beam boundary true
simulated value, mean value, and two standard
deviation bounds.

266
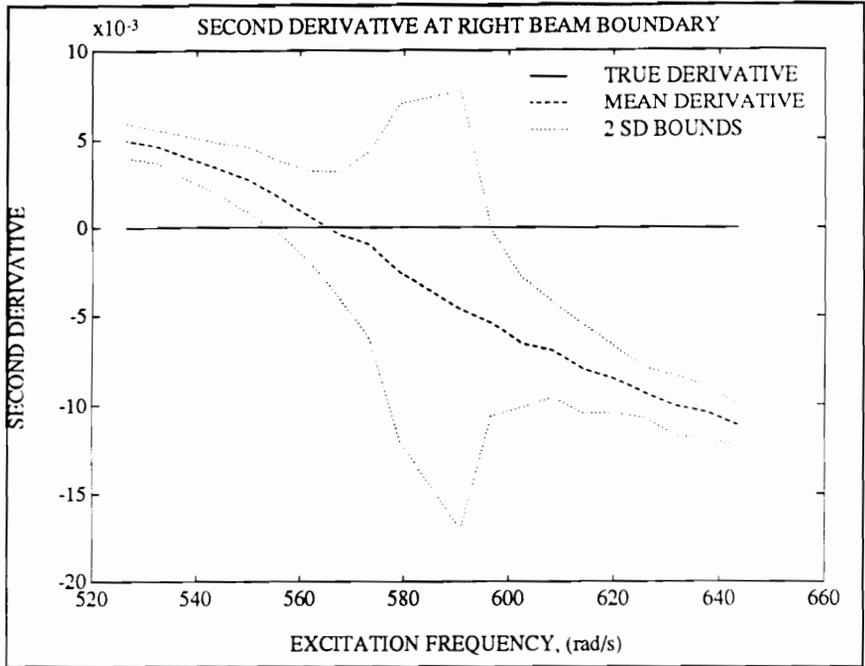
Figure 71 Second derivative at right beam boundary true simulated value, mean value, and two standard deviation bounds.
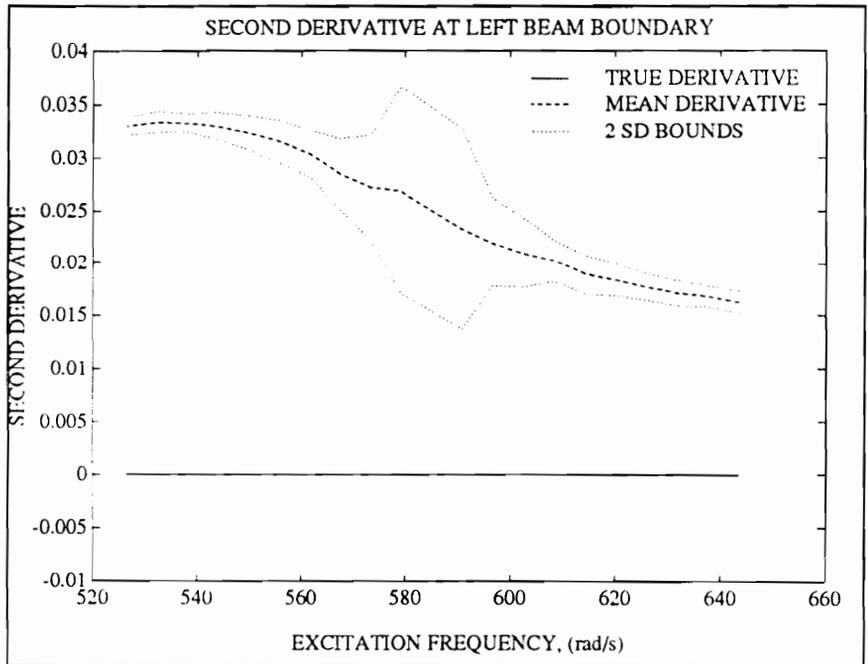
Figure 72 Second derivative at left beam boundary true simulated value, mean value, and two standard deviation bounds.

267
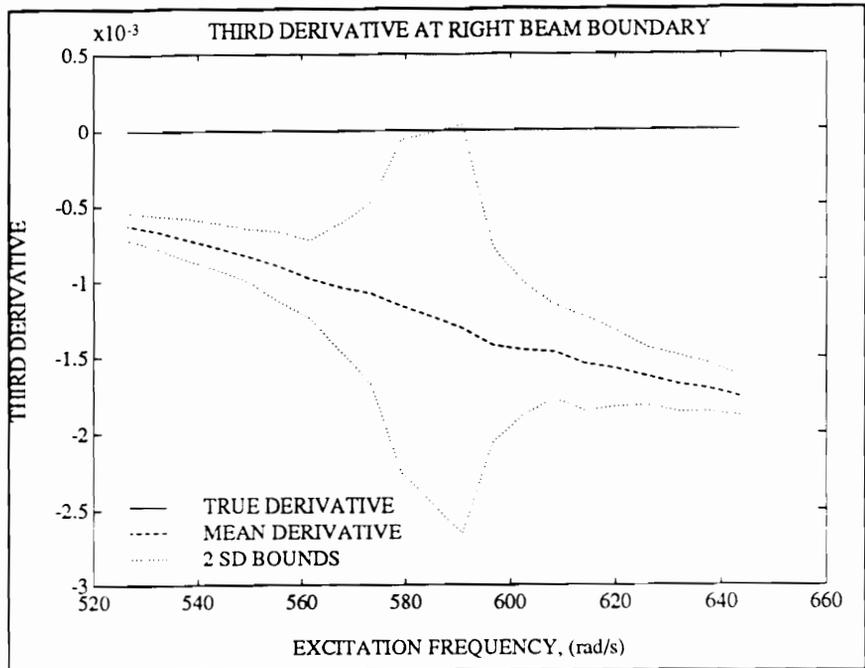
Figure 73 Third derivative at right beam boundary true simulated value, mean value, and two standard deviation bounds.
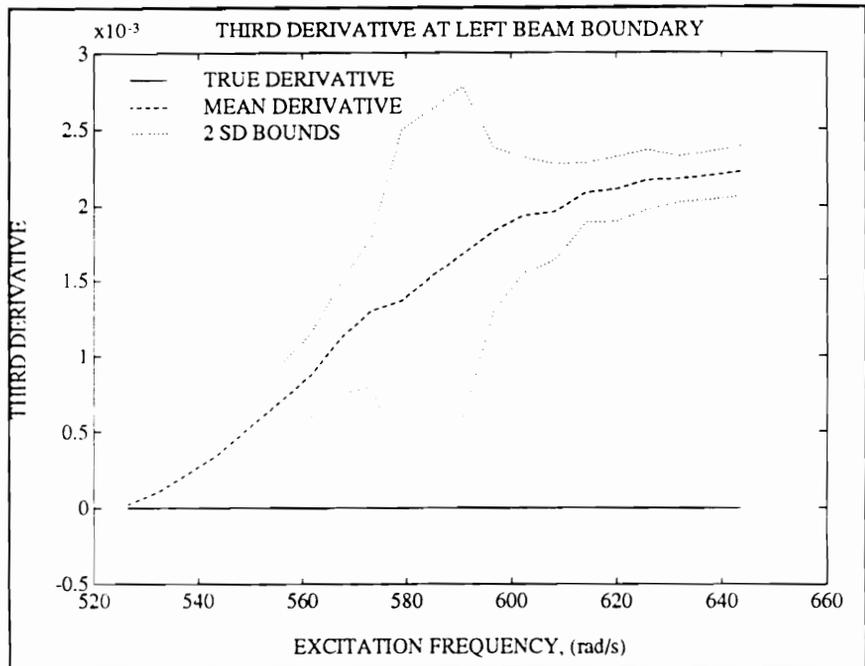
Figure 74 Third derivative at left beam boundary true simulated value, mean value, and two standard deviation bounds.

CONCLUSIONS

The boundary condition error analysis indicated that estimates of the deflection and spatial derivatives can be biased if the LSSD method is used. This result is not surprising, as the bias inherent in the LSSD method has been demonstrated. It is significant that the bias was in all cases small in absolute numbers. It thus is possible to obtain reasonably accurate estimates of the derivatives despite this bias.

The following conclusions can be drawn from this study.

- Deflection and spatial derivative estimates are biased if LSSD is used.

- The bias is minimized or eliminated if resonance excitation is used.

- The bias is sufficiently small that the deflection and derivative estimates from LSSD can still be used.

CHAPTER 8: EXPERIMENTAL VERIFICATION

Experiments have been conducted using physical beams. This was necessary to validate theoretical simulation results. The first experiment involved analyzing a slender beam using both PSMA and LSSD algorithms. The results were compared with each other and with classical beam theory. In the second experiment, the same data was analyzed using the BCBA method. Results are compared to theory. The third experiment involved using the LSSD method to analyze a wide beam with significant two-dimensional effects. The three experiments confirmed the ability of PSMA and LSSD algorithms to smooth spatial data, and of BCBA to generate an accurate modal model based on spatial data.

MINIMUM RESIDUAL MODELS

The first experiment involved the analysis of a slender free-free beam. The first six modes were investigated. Both PSMA and LSSD algorithms were used, and the results compared. The experiment demonstrated the feasibility of either method to perform spatial modal analysis. The differences between the two approaches -- the advantages and disadvantages of each -- were also highlighted by the experiment. Both methods yielded spatial frequency estimates that differed from theory by less than 2%. The AR method

270

(PSMA) was more flexible and informative, but also required much more analyst interaction. Newton's method (LSSD) yielded solutions with smaller residuals and required no analyst interaction, but did require suitable initial estimates for convergence. Computation time for LSSD was much greater than for a single PSMA analysis. However, the interactive nature of PSMA required multiple analyses in order to obtain and to verify a solution. The overall computation time was actually less for the LSSD method. A combination approach in which an abbreviated PSMA analysis is used to obtain initial estimates for LSSD was shown to combine the advantages of each method.

OBJECTIVE

The objective of this experiment was to:

- Determine the feasibility of PSMA and LSSD algorithms for spatial modal analysis of a slender beam

- Investigate the performance of these algorithms with respect to accuracy, speed, and ease of implementation.

IMPLEMENTATION

The experiment involved analyzing data taken from a slender stainless steel beam using a scanning laser vibrometer. The beam was suspended from one end so as to simulate free-free boundary conditions. Harmonic excitation was provided by a small electromagnetic shaker attached to one end of the beam. Spatial vibrational data was obtained by scanning the beam with a laser vibrometer. This data was subsequently analyzed using both LSSD and PSMA algorithms.

Experimental parameters are given in the following tables. Table XI describes beam dimensions. Table XII provides information about the experimental setup, and Table XIII gives the excitation frequency used for each data set. The excitation frequencies were arbitrarily chosen very close to the theoretical natural frequencies of the beam. The theoretical natural frequencies for each mode are also included in Table XIII for comparison.

Table XI BEAM PARAMETERS

BEAM DIMENSIONS	MATERIAL
Length 54.875in Width 3.000in Thickness 0.260in	Stainless Steel

Table XII EXPERIMENT 1 SETUP PARAMETERS

BEAM SUSPENSION
        Type   Elastic, Vertical Support
        Location   Upper Terminus of Beam

EXCITATION
        Type   Harmonic; On-Resonance
        Method   Electromagnetic Shaker
        Force Transmittal   Stinger
        Location   Upper Terminus of Beam

FORCE MEASUREMENT
        Type   Force Transducer
        Attachment   Screw Fitting
        Location   Upper Terminus of Beam,
                                              Between Stinger and Beam

LASER SCAN SAMPLE SPACING
        Axial   512 Sample Points
        Lateral   3   Sample Points[1]
        Axial Spacing   Equal Angles

SCAN DISTANCE
        Laser to Beam   153in

[1] Mode 1 data taken with 7 lateral sample points

Table XIII EXPERIMENT 1 -- EXCITATION FREQUENCIES

DATA SET	EXCITATION FREQUENCY (Hz)	NATURAL FREQUENCY (Hz)
MODE1	17.0	16.82
MODE2	47.0	46.36
MODE3	93.0	90.89
MODE4	154.0	150.25
MODE5	230.9	224.45
MODE6	323.2	313.48

AUTOREGRESSIVE ANALYSIS: The beam data was first processed using the autoregressive method. The delayed oversize total least squares method was used, as described in the PSMA algorithm. Because of the inherent variability in parameter estimates with respect to model fitting parameters c, D, and p, a number of analyses were completed for each data set. The procedure used for each analysis was:

1. Prepare the data set for processing (y, x, Δ).

2. Choose column dimension and delay factor (c, D).

3. Invoke PSMA algorithm.

   a. Choose p based on singular values.

274

b.   Identify spatial frequency β from system poles.

c.   Inspect/Evaluate residual, fitted model, and sum of squared residuals (res).

4.   If warranted, repeat steps 3b and 3c for different p.

5.   Based on information from steps 3 and 4, choose new c, D.

6.   Repeat steps 3-5 until acceptable model is obtained.

The autoregressive approach requires a high level of analyst interaction. It may be helpful to describe the implementation details of each of the above steps.

DATA PREPARATION: Data obtained from the laser vibrometer must be manipulated in order to obtain the requisite velocity information. Velocity data is provided as a complex Nxm matrix, where N is the number of axial data points and m is the number of transverse data points. The axial coordinate of each point is also available. The data vector is prepared by:

1.   Computing the signed magnitude of the velocity matrix.

2.   Computing the mean value of the m transverse data points.

The result is a real-valued velocity vector of length N. Averaging the transverse data points is based on the assumption that beam vibration does not vary transversely.

It has been pointed out that the sample spacing for laser data is not uniform. The AR methods require a sample increment value. An approximate sample increment was computed by taking the mean of the sample increments over the data set. That is,

$$\Delta = \left(\frac{1}{N-1}\right)\sum_{i=1}^{N-1}(x_{i+1}-x_i) \tag{8.1}$$

Errors such as those described in Chapter 5 result from this approximation. However, if the delay factor is small, these errors will also be small. It was assumed that the errors due to unequal sample interval were negligible. Results tended to support this assumption.

MODEL FITTING PARAMETER CHOICE: The initial choice of column dimension was based on the ability to estimate model order. The known theoretical model order for a single-mode analysis was $p=4$. Therefore, the minimum value of c was 5. However, often increasing the column dimension tends to improve the ability to determine model

276

order from the singular values. For this experiment, the initial value of c was always taken as 9. This value proved satisfactory.

The delay factor was initially chosen as $D=1$. For optimum results, D should be as small as possible. Even though it was unlikely that a unit delay would yield acceptable results, this initial value ensured that the lowest possible delay would be realized.

The initial choice for model order was based on visual inspection of the singular values. In most cases, this proved as satisfactory approach. If c is much larger than p, the $(c-p)$ trailing singular values will be very close in magnitude. The first p singular values will be noticeably larger. This informal method worked well for the beam data.

Once the initial model fitting parameters were chosen, the AR coefficients, and subsequently the system poles, were found. The spatial frequency β, and the modal coefficients C_i, were determined as described in Chapter 4. This preliminary model was evaluated for quality of fit. This was done by computing the sum of squared residuals, and by plotting both the residual and of the fitted model.

The model fitting parameters c,D,p, along with estimated model parameters β and ΣR^2, were recorded. Comments regarding the residual and fitted model plots were also recorded. In order to compare models, new values of c,D, and p were chosen, and the

model fitting process was repeated. A table was constructed containing information on each model. This allowed rapid comparison of the various models, and provided a basis for determining the relative quality of fit of a particular model. After several models had been fitted and tabulated, the best model (or models), could be selected. Performing a comparison in this fashion minimized the possibility that a deficient model would be selected.

As an example, the model fitting table for mode 6 is given in Table XIV. The table illustrates the procedure of validating a model. Each row in the table represents one trial solution. A shorthand notation was used for comments on the plot of the residual and of the fitted data. The abbreviations used in this column are defined in Table XV. The comment DCR, for example, stands for deterministic content in the residual plot. This is indicative of a poor fit. In general, comments about the residual are more important than comments about the fitted model. As was pointed out in Chapter 5, a very poor model can still exhibit good visual fit. However, if the fitted model shows even slight visual discrepancies, the model should, in general, be rejected.

The final choice of model in the example is highlighted in Table XIV by bold type. It was selected based primarily on the size of the residual, along with observations of the residual and fitted model plots. In this case the sum of squared residuals was very small - - 0.2976. The plot of residuals showed only slight deterministic content, and the apparent

278

fit of the model was good. Models for which the spatial frequency was clearly inconsistent (based on previous trials) were not analyzed for residual. These cases are represented by blank entries in Table XIV.

Table XIV Example of AR method model fitting table.

c	D	p	b	res	comments
9	1	2	0.3103	87.844	DCR - VPAF
		4	0.3652	0.5060	DCR - AGAF
9	**3**	**2**	**0.3670**	**0.2976**	**SDCR - GAF**
		4	0.3593	2.4295	DCR - PAF
		6	0.3766	1.9937	DCR - NGAF
9	5	2	0.3756	1.6232	DCR - NGAF
		4	0.3489		
9	10	4	0.3665	0.3417	SDCR - AGAF
		2	0.3713	0.4573	DCR - AGAF
5	5	2	0.3739		
		4	0.3733		

Table XV AR fitting table comment definitions.

GAF	Good Apparent Fit
AGAF	Almost Good Apparent Fit
NGAF	Not Good Apparent Fit
PAF	Poor Apparent Fit
VPAF	Very Poor Apparent Fit
GR	Good Residual
VSDCR	Very Slight Deterministic Content in Residual
SDCR	Slight Deterministic Content in Residual
DCR	Deterministic Content in Residual
LDCR	Large Deterministic Content in Residual

NEWTON'S METHOD: The implementation of Newton's method involved direct application of the LSSD algorithm described in Chapter 5. Initial spatial frequency estimates were obtained by an abbreviated AR analysis. Only one mode was assumed present. In all cases, convergence was rapid. The velocity data vector was obtained by averaging transverse data points on the beam, as was done for the AR analysis.

ASSUMPTIONS

The following assumptions were made with respect to the measured data:

- The beam vibrated in accordance with Euler-Bernoulli theory.
- The beam vibrated in only one dimension.
- Each data set contained only one significant mode.
- Measured data contained additive random content.
- The random content was distributed $n \sim N(0, \sigma^2)$.

The first assumption was justified by the dimensions of the beam. Meirovitch (1975) states that Euler-Bernoulli theory is valid if the ratio of length to height of the beam is greater than 10, and if the beam does not become too "wrinkled" due to bending. The beam used in the experiment had a length to height ratio over 200, much greater than 10.

281

Also, only the first six modes were investigated. The "wrinkling" effects are more pronounced at higher modes. In addition, theoretical natural frequencies were computed for the beam based on both Timoshenko and Euler-Bernoulli theories. Both theories predicted nearly identical frequencies. This is further evidence of the validity of Euler-Bernoulli theory.

Euler-Bernoulli theory is one-dimensional. Thus, it was assumed that the vibration of the beam varied only with respect to the axial coordinate, and was constant across any lateral section. This assumption is valid if beam length is large compared to beam width. The beam used had a length to width ratio of 18.3, sufficient to neglect two-dimensional effects.

The assumption that only one mode contributed significantly to the data was based on resonant excitation. It is known that other modes will actually contribute to the vibration of the beam. However, because the structure was excited very near resonant frequencies, contributions of other modes was minimized.

A deterministic form of vibration was assumed, based on Euler-Bernoulli theory (Assumption 1). It is further assumed that the process of measuring the vibrational data introduces random errors that are added to the deterministic signal. This assumption stems

from the philosophy that the quantity under investigation is a deterministic, and not a chaotic process. This assumption is consistent with assumption 1.

The noise associated with laser data is known to not be normally distributed. Errors tend to be biased toward zero as a result of dropouts. In addition, the noise amplitude increases in regions of high curvature of the beam. Thus, the assumption of normality is known to be invalid. However, both PSMA and LSSD algorithms are based on normally distributed noise, hence the assumption. The invalidity of this assumption leads to errors in parameter estimates. These errors are manifest in the residual functions. It is assumed, however, that such errors are small.

RESULTS

The spatial data was processed using both LSSD and PSMA methods. The spatial frequency estimates obtained by both methods were comparable, and also compared favorably to theoretical values. In all cases the difference between theoretical and estimated spatial frequencies was less than 2%. The sum of squared residuals, indications of model fit, were small, and comparable, using both methods. Estimates of modal coefficients and beam constants obtained by each method were also comparable, although these values differed from theory much more than the spatial frequencies.

283

The discrepancy between theory and model for the coefficients may be due to non-ideal boundary conditions, the presence of rigid body modes, invalid noise assumptions, and errors in spatial frequency estimates. For these reasons, the beam constants were not expected to agree with theory to the extent that spatial frequencies did. However, the difference between the modal coefficients obtained from the two modelling methods was in general much less than the difference from theoretical values. This lends credence to the hypothesis that the discrepancy with respect to theory could be due to non-ideal boundary conditions or the presence of unmodeled content.

The estimated and theoretical spatial frequencies are tabulated in Table XVI. The sum of squared residuals, ΣR^2, and the spatial frequency error (with respect to the theoretical value) are also included. Results from both the PSMA and LSSD analyses are included.

Table XVI Spatial frequency estimates and sum of squared residuals for PSMA and LSSD analyses of slender beam.

PSMA ANALYSIS

MODE	β THEORY	β EST.	RESIDUAL	% ERROR
1	8.6197e-02	8.7885e-02	4.9676e-02	1.9589
2	1.4311e-01	1.4468e-01	1.6683e+00	1.0951
3	2.0038e-01	1.9802e-01	1.3073e-01	-1.1731
4	2.5762e-01	2.5366e-01	4.7458e-01	-1.5408
5	3.1487e-01	3.1187e-01	7.3102e-01	-0.9542
6	3.7212e-01	3.6697e-01	2.9763e-01	-1.3863

LSSD ANALYSIS

MODE	β THEORY	β EST.	RESIDUAL	% ERROR
1	8.6197e-02	8.6173e-02	4.3012e-02	-0.0273
2	1.4311e-01	1.4423e-01	1.6631e+00	0.7806
3	2.0038e-01	1.9794e-01	1.3031e-01	-1.2165
4	2.5762e-01	2.5423e-01	4.5804e-01	-1.3190
5	3.1487e-01	3.1122e-01	6.7707e-01	-1.1606
6	3.7212e-01	3.6841e-01	2.4276e-01	-0.9983

The modal coefficients are presented in Tables XVII through XIX. These tables include C_1, C_2, and the real and imaginary parts of C_3. Since C_4 is the complex conjugate of C_3, this includes all pertinent information. In all cases, the coefficients were normalized. The coefficients for a free-free beam based on Euler-Bernoulli theory are presented in Table XVII. The normalized coefficient estimates obtained from the PSMA analysis are tabulated, along with the percent errors, in Table XVIII. The LSSD results are tabulated similarly in Table XIX.

Table XVIII Modal coefficients estimates obtained from PSMA slender beam analysis.

MODE	C1 % error	C2 % error	Re C3 % error	Im C3 % error
1	6.0675e-03 -15.802	7.9066e-01 -3.1605	4.7010e-01 14.147	3.9221e-01 -3.0694
2	-2.3102e-04 -27.172	7.0633e-01 -13.493	5.6649e-01 38.814	4.2449e-01 3.9391
3	-1.3688e-05 -0.0662	-7.8910e-01 -3.3552	-4.5068e-01 10.392	-4.1738e-01 2.2381
4	-6.5243e-07 10.223	7.9900e-01 -2.1423	4.3181e-01 5.7710	4.1849e-01 2.5086
5	-2.6221e-08 2.5098	-7.6819e-01 -5.9163	-4.7741e-01 16.941	-4.2657e-01 4.4881
6	-1.2156e-09 9.9745	7.9965e-01 -2.0634	4.4163e-01 8.1775	4.0684e-01 -0.3440

Table XVII Modal coefficients predicted by Euler-Bernoulli beam theory.

THEORETICAL MODAL COEFFICIENTS

MODE	C1	C2	Re C3	Im C3
1	7.2062e-03	8.1646e-01	4.1184e-01	4.0463e-01
2	-3.1721e-04	8.1650e-01	4.0809e-01	4.0841e-01
3	1.3697e-05	8.1650e-01	4.0826e-01	4.0824e-01
4	-5.9192e-07	8.1650e-01	4.0825e-01	4.0825e-01
5	2.5579e-08	8.1650e-01	4.0825e-01	4.0825e-01
6	-1.1054e-09	8.1650e-01	4.0825e-01	4.0825e-01

286

Table XIX Modal coefficient estimates from LSSD slender beam analysis.

MODE	C1 % error	C2 % error	Re C3 % error	Im C3 % error
1	6.8314e-03 -5.2015	8.0521e-01 -1.3781	4.3704e-01 6.1196	4.0073e-01 -0.964
2	-2.4065e-04 -24.137	7.1602e-01 -12.306	5.5339e-01 35.604	4.2553e-01 4.1929
3	-1.3794e-05 0.70914	-7.9208e-01 -2.9898	-4.4633e-01 9.3268	-4.1640e-01 1.9984
4	-6.2437e-07 5.4821	7.9026e-01 -3.2133	4.4672e-01 9.4249	4.1944e-01 2.7403
5	-2.7606e-08 7.9226	-7.7969e-01 -4.5075	-4.5935e-01 12.517	-4.2553e-01 4.2333
6	-1.0808e-09 -2.2237	7.7587e-01 -4.9759	4.8072e-01 17.753	4.0857e-01 0.0800

Normalization was accomplished by dividing each constant by dividing each constant by the norm of the vector comprised of the four constants. That is

$$ C_{i\ normalized} = \frac{C_i}{\sqrt{C_1^2 + C_2^2 + real(C_3)^2 + imag(C_3)^2}} \tag{8.2} $$

287

The percent errors in all the tables are based on differences from Euler-Bernoulli theory.
They were computed with

$$\% \ error = \left(\frac{\Psi_{ESTIMATED} - \Psi_{THEORY}}{\Psi_{THEORY}} \right) x100 \qquad (8.3)$$

Where Ψ is any model parameter. The fitted AR models, along with their residuals, are plotted in Figs. 75-80. These figures show the good apparent fit and the residual characteristics for each mode. Figures 81-86 plot the fitted models and residuals obtained from Newton's method. Inspection of these figures shows good correlation between the two methods.
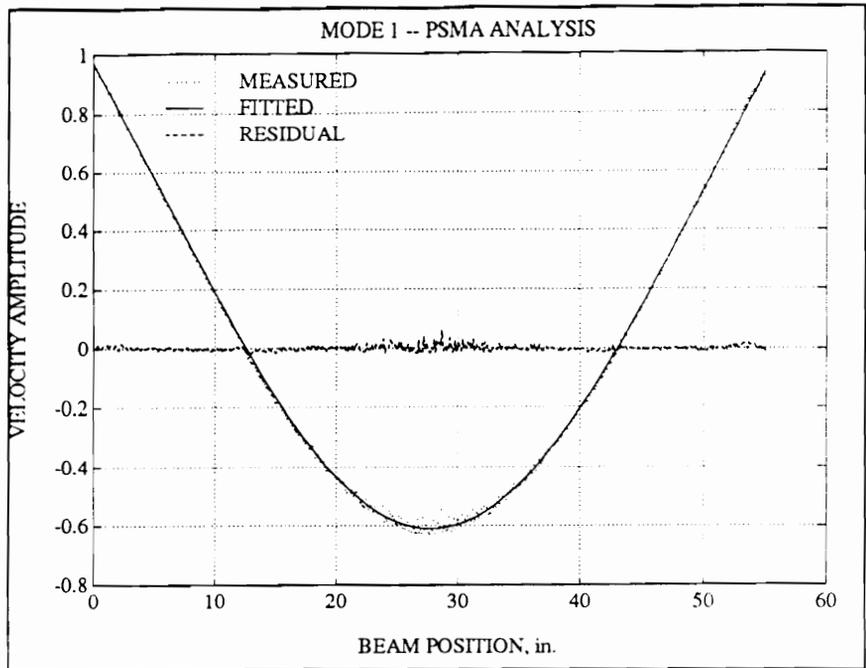
Figure 75 Fitted model and residual from PSMA analysis of mode 1.
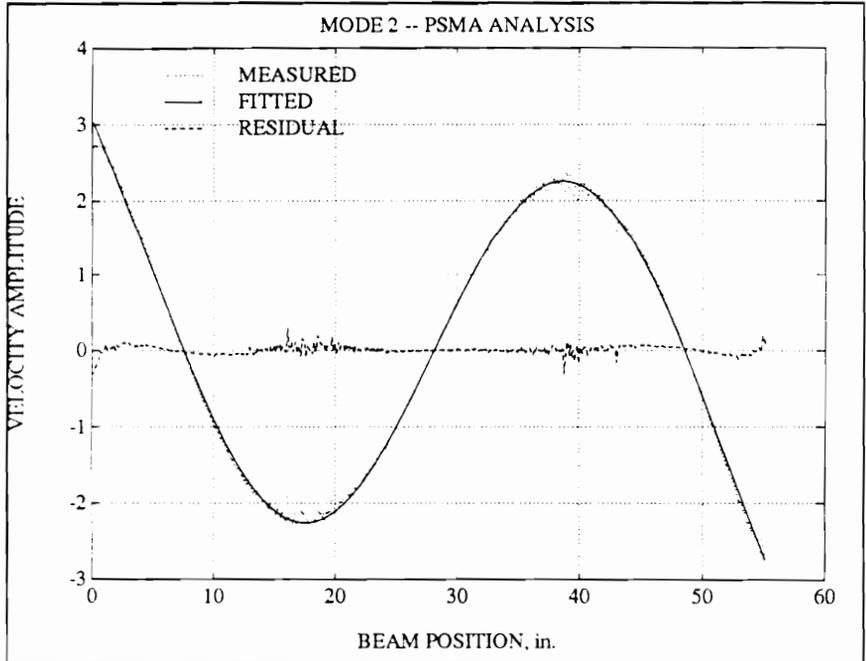
Figure 76 Fitted model and residual from PSMA analysis of mode 2.

289
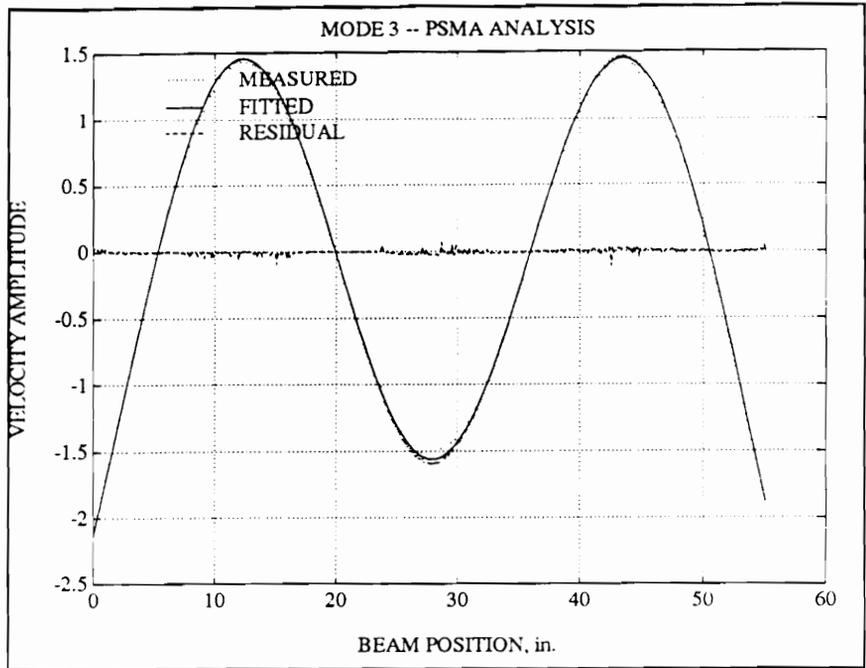
Figure 77 Fitted model and residual from PSMA analysis of mode 3.
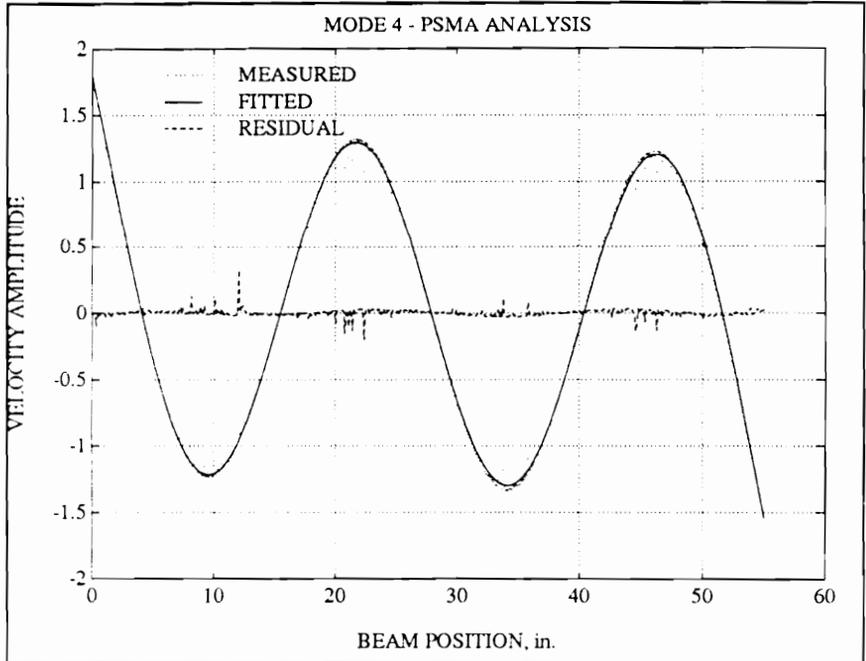
Figure 78 Fitted model and residual from PSMA analysis of mode 4.

290
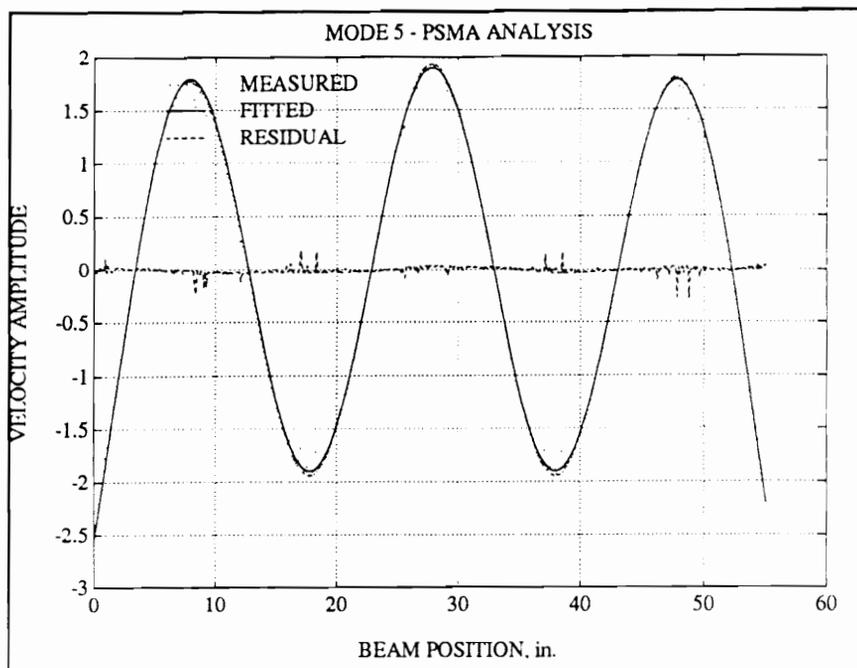
Figure 79 Fitted model and residual from PSMA analysis of mode 5.
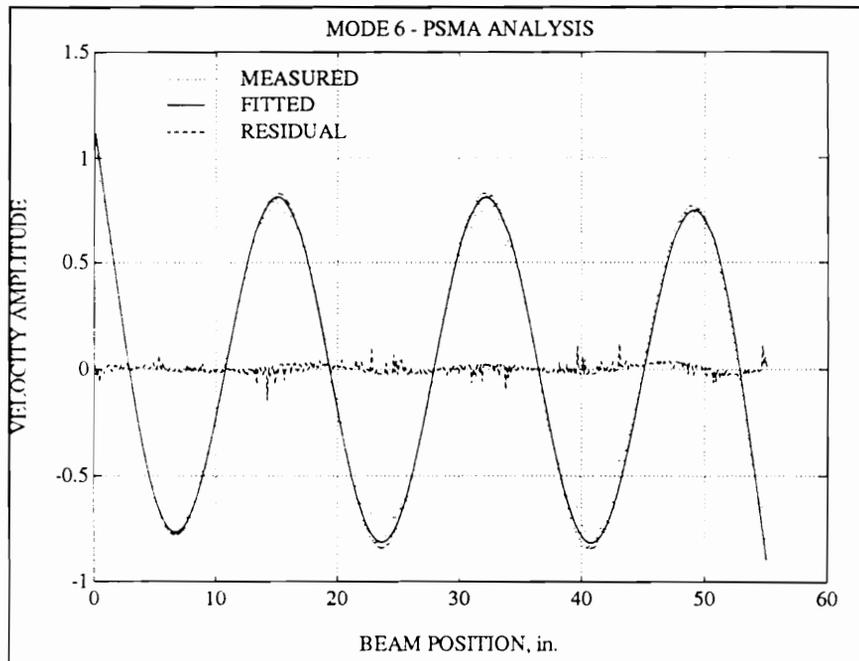
Figure 80 Fitted model and residual from PSMA analysis of mode 6.

291
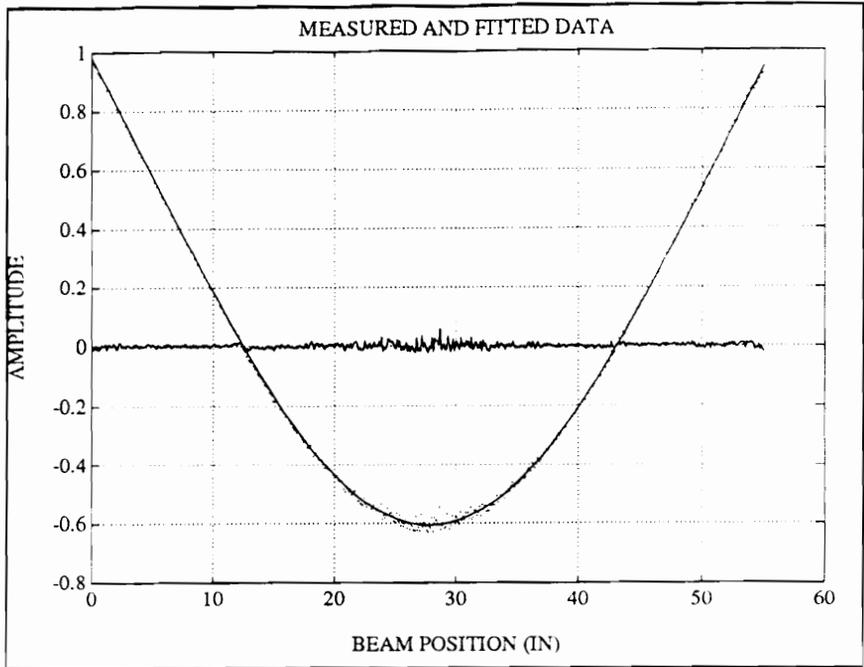
Figure 81 Fitted model and residual from LSSD analysis for mode 1.
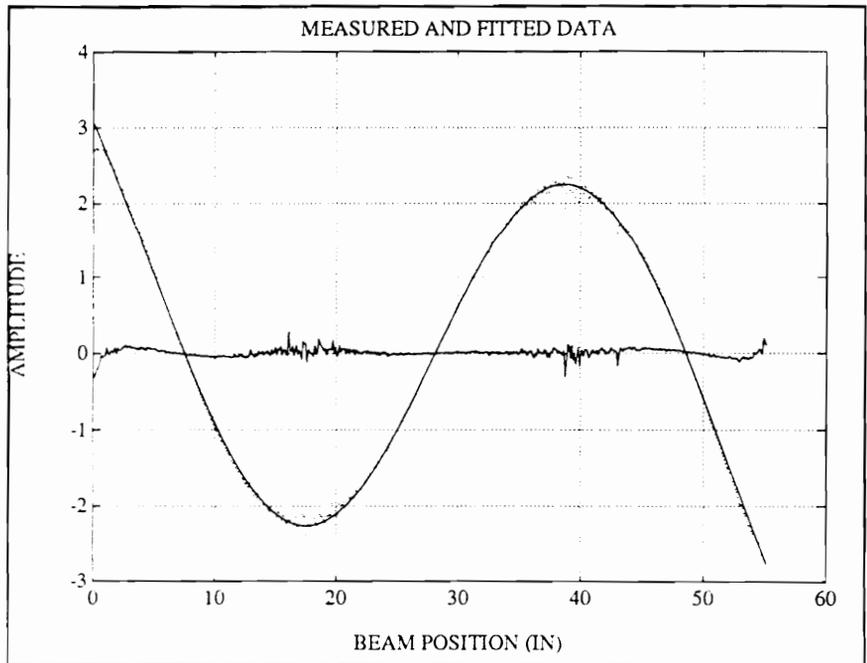
Figure 82 Fitted model and residual from LSSD analysis for mode 2.

292
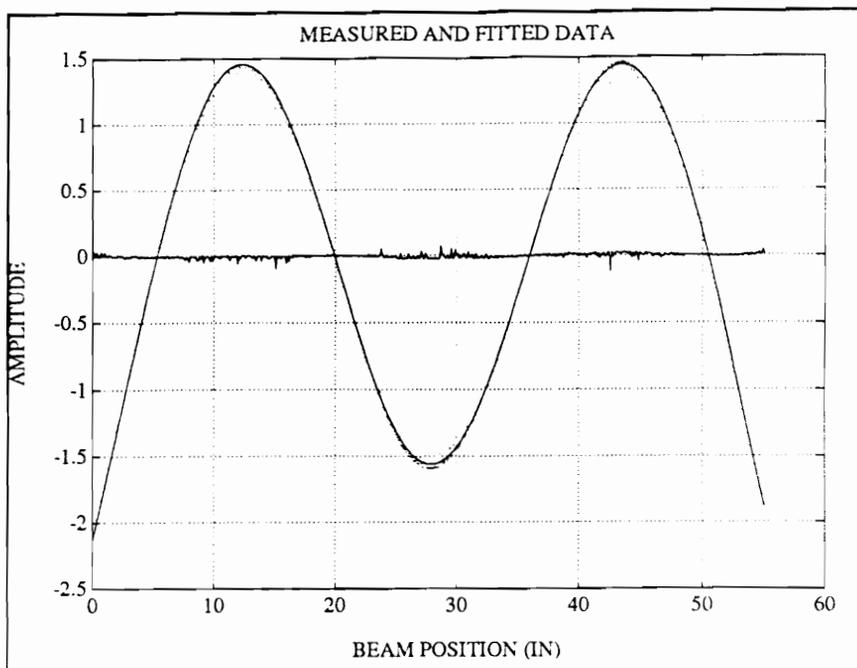
Figure 83 Fitted model and residual for LSSD analysis of mode 3.
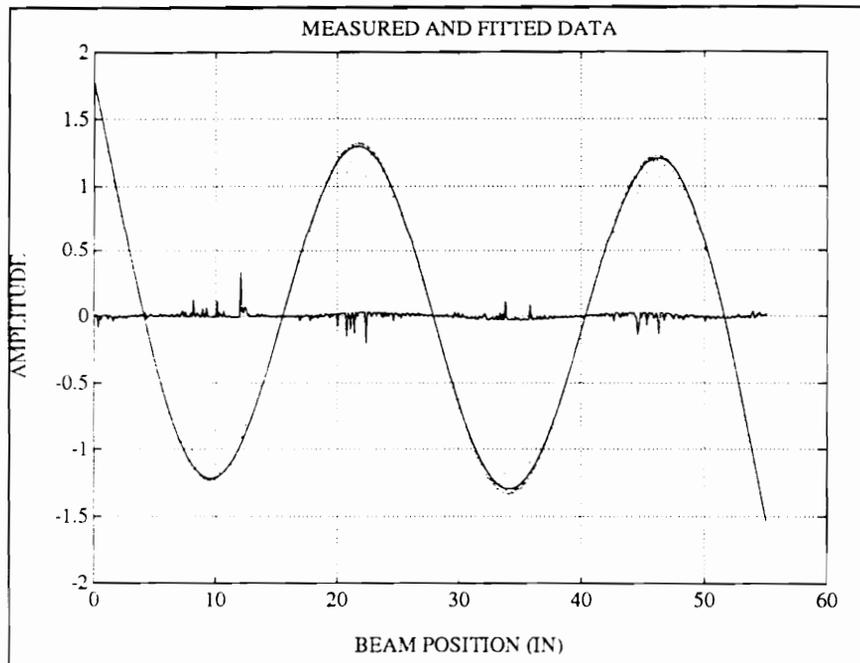
Figure 84 Fitted model and residual from LSSD analysis of mode 4.

293
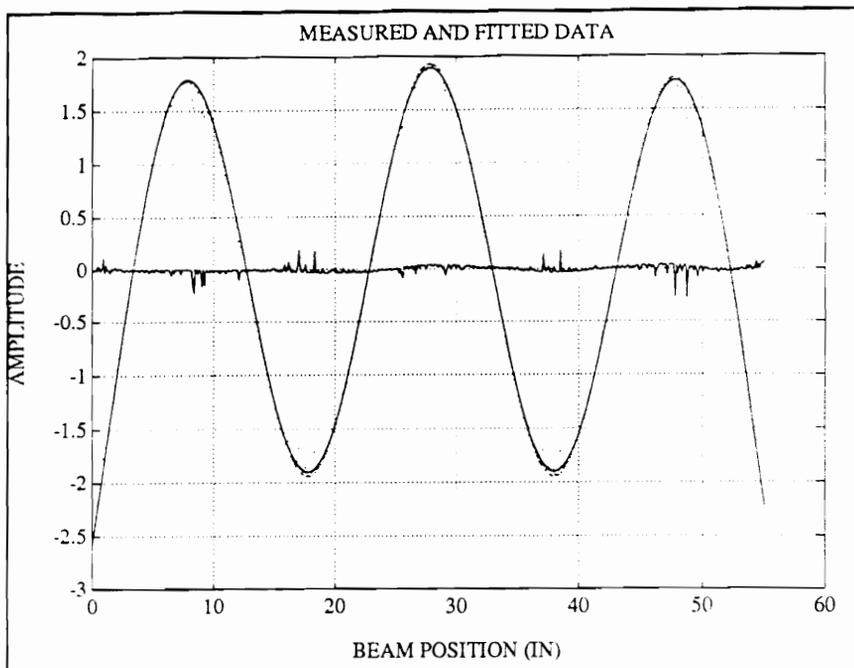
Figure 85 Fitted model and residual from LSSD analysis of mode 5.
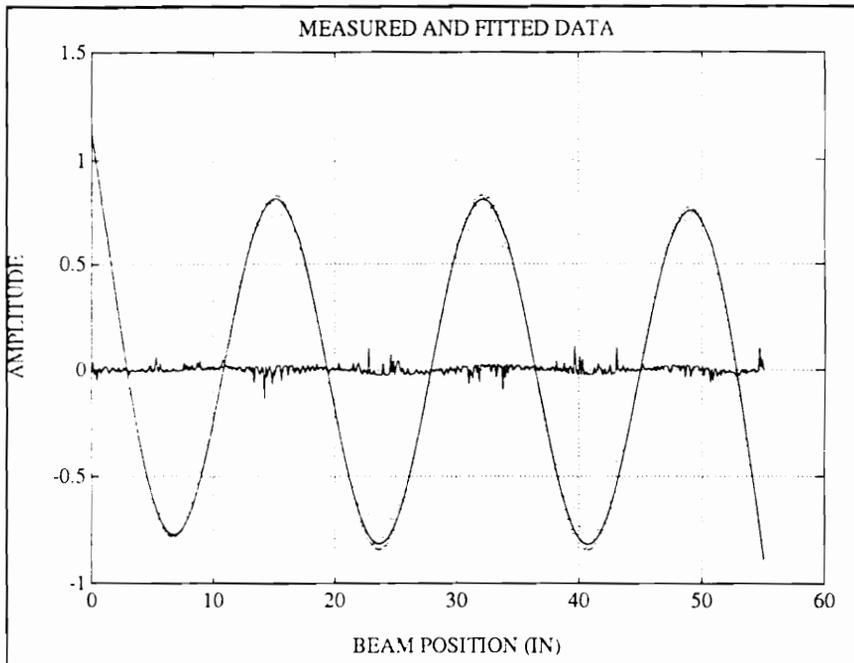
Figure 86 Fitted model and residual from LSSD analysis of mode 6.

294

CONCLUSIONS

This experiment verified the ability of both the AR method and Newton's method to successfully model mode shapes of slender beams. Spatial frequencies can be identified with high accuracy. Modal coefficients can be successfully identified as well. The following points highlight the differences between the two methods.

- Newton's method produced slightly smaller residuals.

- In most (but not all) cases, Newton's method produced estimates slightly closer to theoretical results.

- The AR method required much more analyst interaction.

- Preliminary spatial frequency estimates produced by the AR method often make good initial guesses for Newton's method.

From these observations, the following conclusions can be drawn:

295

- If a-priori information about the spatial frequencies is available, use Newton's method.

- If no information is available, use the AR method.

- An alternative is to use an abbreviated AR method followed by Newton's method.

BOUNDARY CONDITION BEAM ANALYSIS (BCBA) EXPERIMENTS

Experiments have been conducted to document the performance of the BCBA algorithms. These experiments verified the ability of the BCBA method to generate a modal model of a vibrating beam. They also provided some insight as to the performance of the method with respect to such variables as number of data sets required and excitation frequency selection. In all, four experiments were conducted, all using a slender free-free beam. The four experiments were designed together, and will be presented together. The results confirm that the BCBA is a powerful and versatile spatial modal technique.

OBJECTIVE

The objectives of the BCBA experiments are twofold:

1. To verify the feasibility of BCBA to model slender beams.

2. To determine the effects of number of data sets and excitation frequencies on the BCBA model.

IMPLEMENTATION

The experiment involved analyzing spatial modal data obtained from a slender beam. The beam was suspended by an elastic support at one end so as to approximate free-free boundary conditions. Harmonic excitation was provided by an electromagnetic shaker attached to the upper end of the beam via a stinger and force transducer. The response velocity amplitude was measured with a scanning laser vibrometer. This data was then used to construct a BCBA model of the beam.

The BCBA experiments utilized the same data as the slender beam experiments. Beam parameters and descriptions of the data sets were described in previous sections, and will

297

not be repeated here. Refer to Tables X, XI, and XII for data descriptions. Three

additional data sets were collected, using off-resonance excitation. These data sets, along

with the previous six, provided nine data sets available for analysis. For convenience, the

data sets are numbered according to excitation frequency. Throughout this section,

references to each data set will be made by number. Table XIX summarizes the nine data

sets and the corresponding excitation frequencies:

Table XX BCBA experiment data set definitions and excitation frequencies.

DATA SET	FREQ. (Hz)	COLUMNS	RESONANCE
1	17.0	5	1
2	47.0	3	2
3	50.0	5	(2)
4	93.0	3	3
5	120.2	5	NO
6	154.0	3	4
7	230.9	3	5
8	250.0	5	NO
9	323.2	3	6

The number of columns shown in Table XIX represents the number of vertical scans of

the beam obtained for each data set. As with the LSSD and PSMA experiments, these

were averaged to obtain the operating shape for each data set.

298

Different combinations of the data sets were used to generate four BCBA modal models. Recall that the BCBA algorithm requires a minimum of three data sets. The first test used the six resonance data sets and a least squares procedure to determine the boundary conditions. The remaining four tests used three data sets each. The second test used only the first three resonance data sets, while the third test used only the last three. In each of these cases, the intent was to determine the ability of the BCBA method to model out-of-band modes. The fourth test utilized only three data sets, but these were distributed over the bandwidth of interest. A fifth test, using the non-resonance data, was not completed, for reasons described later. The data sets used for each test are listed in Table XX.

Table XXI Data sets used for each test.

EXPERIMENT	DATA SETS USED
TEST 1	1,2,4,6,7,9
TEST 2	1,2,4
TEST 3	6,7,9
TEST 4	1,4,7

The analysis procedure for each test followed that in Chapter 6. The steps were:

1. Estimate the deflection and spatial derivatives at the boundaries of the beam.

2. Estimate the beam boundary conditions from the spatial derivatives.

3. Compute the spatial frequencies based on the estimated boundary conditions.

4. Compute the normal mode shapes for all modes of interest.

5. Compute the modal weighting factors for each data set.

ESTIMATION OF DERIVATIVES: Each data set in Tests 1-4 used resonance excitation. The LSSD method was used to construct a preliminary model. The deflection and spatial derivatives were obtained directly from differentiating the LSSD model. This proved to be a satisfactory method, far superior to numerical differentiation.

According to Euler-Bernoulli theory, the moment and shear, and hence the second and third spatial derivatives, should be zero at the beam boundaries. Numerically, this is, of course, not expected to occur. However, using LSSD modeling, the second and third derivatives were typically one to two, and in some cases three, orders of magnitude smaller than the first derivative. Numerical differentiation, in contrast, often produced very large second and third derivatives.

Accurate estimation of the derivatives for the off-resonance data sets proved difficult. As has been demonstrated in previous chapters, minimum residual models for off-resonance data yields very poor results. Thus, LSSD or PSMA methods could not be used. Likewise, numerical differentiation is unreliable. Hence no apparent method was available for accurate estimation of the derivatives. This does not imply that such methods may not be developed. Given the capabilities of the scanning laser vibrometer, is probable that such methods can be developed. However, current methods in conjunction with the measured data do not provide adequate estimates. For this reason, the off-resonance data sets (numbers 3,5,and 8) were not used for boundary condition estimation. They were used for fitting mode shapes estimated from the resonance data sets, however.

BOUNDARY CONDITION ESTIMATION: The general boundary conditions were estimated using the methods described in Chapter 6. Equations 6-17 through 6-20 were solved for J, K_t, m, c, k at each end of the beam. For test 1, with six data sets, $q=6$. For the remaining tests, $q=3$. In order to ensure non-negativity of the boundary conditions, algorithm NNLS was used for the solution.

The boundary conditions were not expected to be identically equal to the theoretical values of zero. However, in all cases the parameters were very small, and in several cases the estimates were indeed equal to zero. The presence of an end damper results in

301

complex modes. Since real mode shapes were used, the values for c at each end of the beam were identically equal to zero.

SPATIAL FREQUENCY COMPUTATION: The spatial frequencies were found, once the boundary conditions were known, by solving the frequency equation (Eq. 6-15). The spatial frequencies corresponding to modes 1 through 6 were desired. Initially, a grid search was conducted. The initial grid spanned a range from 0 to .05 in steps of 0.0005. The resulting value of the determinant of Λ was plotted against the grid. Roots were identified by the zero crossings of the function. Each root was bracketed, and a bisection method was used to find the roots to a precision of 14 digits.

In order to obtain the desired spatial frequencies, additional grids had to be searched. Grids from 0.05 to 0.10, 0.10 to 0.15, etc. were searched using the same method. This was repeated until six roots were obtained.

In all tests, either one or two rigid-body modes were present. The corresponding spatial frequencies for these modes was not identically zero, as is predicted in theory. Thus, more than six spatial frequencies had to be determined in order to obtain the first six non-rigid-body modes. The presence of rigid-body modes is not apparent when finding the spatial frequencies. However, these modes become obvious when the mode shapes are calculated.

302

NORMAL MODE SHAPES: The mode shapes corresponding to each spatial frequency can be found by solving Eq. 6-14. This was done using singular value decomposition, as described in Chapter 6. This method ensures maximum accuracy of the modal coefficients. Once the modal coefficients were estimated, the mode shape was computed from Eq. 6-21, and normalized for length. The x-coordinate used corresponded to the actual x-coordinate of the measured data. This enabled direct comparison with the various data sets. The mode shapes, including the rigid-body modes, were saved in a matrix form.

MODAL WEIGHTING FACTORS: Modal weighting factors were computed for each data set and for each model. Since four tests were completed, and nine data sets were available, this resulted in 36 sets of modal weighting factors. The method used in each case was to perform a least squares fit of the modal matrix (obtained from each of the four tests) to each of the measured data sets.

In each case, the modal weighting factors were used to construct a complete modal model for each data set. The mode shape matrix **M**, described in Chapter 6, multiplied by the estimated modal weighting factors v, gives the fitted model operating shape. That is

$$y_{fitted} = Mv \qquad (8.4)$$

The residual is given by the difference between the fitted model and the measured data. It is given by:

$$R = y_{measured} - y_{fitted} \qquad (8.5)$$

In all 36 cases, both the fitted model and the residual were computed and plotted along with the measured data. In all cases, good agreement between measured and fitted models was obtained.

RESULTS

The results of the BCBA experiment indicated that true spatial modal analysis is possible and feasible. Spatial frequencies and mode shapes compared favorably with theory. Small residuals were obtained in all cases. The effects of out-of-band modes can be seen and accounted for.

The five steps of the BCBA experiment are described in the preceding section. Each step produces a quantifiable result, with theoretical or ideal values available for comparison. The results are thus presented here in the same order as the steps in the analysis.

304

DEFLECTION AND SPATIAL DERIVATIVES AT THE BEAM BOUNDARIES:

Step one of the analysis was estimation of the deflection and the spatial derivatives of the operating shape evaluated at the ends of the beam. The beam used in the experiment was suspended so as to simulate free-free boundary conditions. Thus, the estimated derivatives were compared with those for an ideal free-free beam.

Simple mechanics theory dictate that a free-free beam must have zero bending moment and zero shear force at the ends. The bending moment and shear force are proportional to the second and third derivative of deflection with respect to the axial coordinate x. Therefore, an ideal free-free beam must have second and third derivative at the boundaries identically equal to zero.

The estimated deflection and derivatives for each of the four tests are shown in Tables XXII and XXIII. Table XXII presents the derivatives at the left end of the beam, whereas Table XXIII presents data from the right end. Numerically, the second and third derivatives are not expected to be zero. However, they are expected to be small in comparison to the deflection and slope. Inspection of the tables reveals that this is indeed the case. The second and third derivatives at each end of the beam are one to two orders of magnitude smaller than the first derivative. This lends credence to the hypothesis that

305

the LSSD method can be used effectively for estimation of derivatives when resonance excitation is used.

Table XXII Deflection and spatial derivatives at the left boundary (for resonance data sets).

DATA SET	V_o	V_o'	V_o''	V_o'''
1	0.9835	-0.0804	-0.0003	0.0000
2	3.0709	-0.3809	-0.0137	0.0007
4	-2.1347	0.4069	0.0053	-0.0004
6	1.7780	-0.4374	-0.0070	0.0008
7	-2.5730	0.7689	0.0204	-0.0033
9	1.1213	-0.3788	-0.0163	0.0013

Table XXIII Deflection and spatial derivatives at the right boundary (for resonance data sets).

DATA SET	V_1	V_1'	V_1''	V_1'''
1	0.9450	0.0818	-0.0002	-0.0000
2	-2.7534	-0.4161	0.0090	0.0020
4	-1.8789	-0.4304	-0.0005	0.0028
6	-1.5316	-0.4693	-0.0038	0.0055
7	-2.2249	-0.8444	-0.0103	0.0159
9	-0.8834	-0.4180	-0.0040	0.0147

BOUNDARY CONDITION ESTIMATES: Boundary conditions for the beam were estimated from the spatial derivatives. The boundary conditions include a linear and rotational stiffness, mass and moment of inertia, and damping at each end of the beam. For an ideal free-free beam, these quantities should be identically zero. As with the spatial derivatives, numerical computation of these quantities is not expected to yield exactly zero results. However, in several cases this is precisely what has occurred.

The boundary conditions obtained at each end of the beam for each of the four tests are presented in Table XXIV. It can be seen that the results from all four tests are similar. In all cases, the quantities are very small. In some cases they are, in fact, identically equal to zero. The first test used the largest number of data sets, and has the maximum number of zero entries, e.g., 5. However, Test 3 also produced 5 zero boundary conditions. Recall that Test 3 involved data sets corresponding to resonance excitation of modes 4 through 6. These data sets produced the best LSSD models (as described in the LSSD experiment). Thus, the high number of zero estimates in this case may result from better modeling of these data sets.

SPATIAL FREQUENCY ESTIMATES: Once the boundary conditions were estimated, the spatial frequencies could be computed. In general, these agreed closely with

Table XXIV Boundary condition estimates obtained from Tests 1 through 4 at each beam boundary.

	TEST 1		**TEST 2**	
	LEFT (TOP)	RIGHT (BOT)	LEFT (TOP)	RIGHT (BOT)
$K_?$	2.5991e-002	3.9141e-003	4.0882e-002	2.7864e-002
J	0	5.7338e-009	8.0511e-008	8.4554e-008
m	4.7544e-010	3.6674e-009	8.2675e-010	4.7962e-009
c	0	0	0	0
k	0	0	0	0

	TEST 3		**TEST 4**	
	LEFT (TOP)	RIGHT (BOT)	LEFT (TOP)	RIGHT (BOT)
$K_?$	2.6914e-002	0	2.3389e-002	8.8942e-004
J	0	4.2426e-009	0	6.2081e-009
m	4.7148e-010	3.9498e-009	6.0349e-010	3.4178e-009
c	0	0	0	0
k	0	6.9784e-004	3.4597e-006	0

Note: Units for the boundary conditions are: $K_?$ lb-in/rad, J lb-in-s^2/rad, m lb-s^2/in, c lb-s/in, and k lb/in. However, the numerical values are not scaled correctly.

theoretical values for a free-free beam. It is significant to note that one or two quasi-rigid body modes appeared in each test. The initial indication of these modes was the presence of low spatial frequencies that did not correlate with theory. These frequencies were puzzling until the corresponding mode shapes were computed. At that time it became clear that they represented rigid body modes.

The theoretical and estimated spatial frequencies, along with the percent difference between the two, are presented in Table XXV. The first and fourth tests provide the most accurate results relative to theory. This is consistent with observations made in the preceding section on boundary condition estimates. Again, the high accuracy of the first

308

test may be attributable to the larger number of data sets used in that test. The fourth test, again, used data sets that yielded excellent LSSD models.

The largest discrepancy occurs in Test 3. In this case, the first mode spatial frequency estimate differs from theory by nearly 20%. However, for the higher modes excellent agreement with theory was obtained. Test 3 used data sets corresponding to modes 4, 5, and 6 only. This error in the first mode could be due to lack of inclusion of low modes in the constituent data sets.

The percent error presented in the table was computed by the formula

$$error(\%) = \left[\frac{\beta_{estimated} - \beta_{theory}}{\beta_{theory}}\right]100\% \qquad (8.6)$$

The theoretical spatial frequency corresponding to the rigid body modes is zero, and thus no percent errors were computed for these modes.

MODE SHAPES: The mode shapes corresponding to the spatial frequencies found in the preceding step were computed and plotted. This was done for each test. The mode shapes

309

Table XXV Spatial frequency estimates for modes 1-6 obtained from each BCBA experiment. Numbers in parentheses are errors, in percent, from Euler-Bernoulli theory.

E-B THEORY	EXPERIMENTAL TEST-1	TEST-2	TEST-3	TEST-4
0	0	0	1.2611	0.8419
0	1.9396	2.3524	3.8621	1.8835
4.7300	4.9826 (**5.1**)	5.2318 (**9.6**)	5.8524 (**19.2**)	4.9411 (**4.3**)
7.8532	8.0292 (**2.2**)	8.2204 (**4.5**)	8.2562 (**4.9**)	7.9980 (**1.8**)
10.9956	11.1276 (**1.2**)	11.2788 (**2.5**)	11.2007 (**1.8**)	11.1036 (**1.0**)
14.1372	14.2428 (**0.7**)	14.3673 (**1.6**)	14.2719 (**0.9**)	14.2233 (**0.6**)
17.2787	17.3667 (**0.5**)	17.4723 (**1.1**)	17.3794 (**0.6**)	17.3504 (**0.4**)
20.4203	20.4957 (**0.4**)	20.5872 (**0.8**)	20.5010 (**0.4**)	20.4817 (**0.3**)

were compared with theoretical mode shapes for free-free boundary conditions. In general, the estimated mode shapes compared well with theory. The magnitude of the deviations from theoretical shapes corresponded with the error in spatial frequency estimates. Thus, the largest deviations occurred for Test 3. Mode shapes from Tests 1 and 4 showed the best agreement with theory.

The estimated normal mode shapes for modes 1-6, along with differences from theoretical mode shapes, are plotted in Figs. 87-98. Viewed as a set, it is clear that as the mode

number increases, the estimated mode shapes more closely approximate the theoretical mode shapes. Again, this is in agreement with the spatial frequencies.

Inspection of Fig. 87 shows that most estimated mode shapes match the theoretical shape. However, one estimated shape, corresponding to mode 1 obtained from Test 3, is noticeably in error. Figure 88 plots the difference from the theoretical mode shape. It is clear that the largest difference occurs with Test 3. It is also significant to note that the differences from theory in all other cases is less than an order of magnitude smaller than the normal mode shapes. This is additional confirmation of the agreement between theory and estimated.

Figures 89 and 90 show the second mode shapes and the difference from theory. In this case, closer agreement between theory and estimated is obtained. All differences are smaller than an order of magnitude below the normal mode shapes.

Figures 91 through 96 reveal the continuing improvement in estimated mode shapes with respect to theory. The normal mode shape plots for each test become indistinguishable. The differences from theory remain less than an order of magnitude smaller than the mode shapes. In all cases, the results of Tests 1 and 4 show the best agreement with theory. Test 3 results show the largest difference from theory.

The sixth mode and its differences from theory are shown in Figs. 97 and 98. The same trend is evident here. Estimated mode shapes from all tests are very close to theoretical shapes. The differences are less than an order of magnitude below the mode shapes. Tests 1 and 4 showed the best agreement with theory. The errors appear to be frequency based, an observation that is in agreement with the correlation between mode shape errors and spatial frequency errors. The peaks in the difference plots occur at nearly the same x-coordinate for each test. The differences between tests is principally one of magnitude. This is perhaps due to the difference between the estimated boundary condition effects and the ideal effects for a free-free beam.
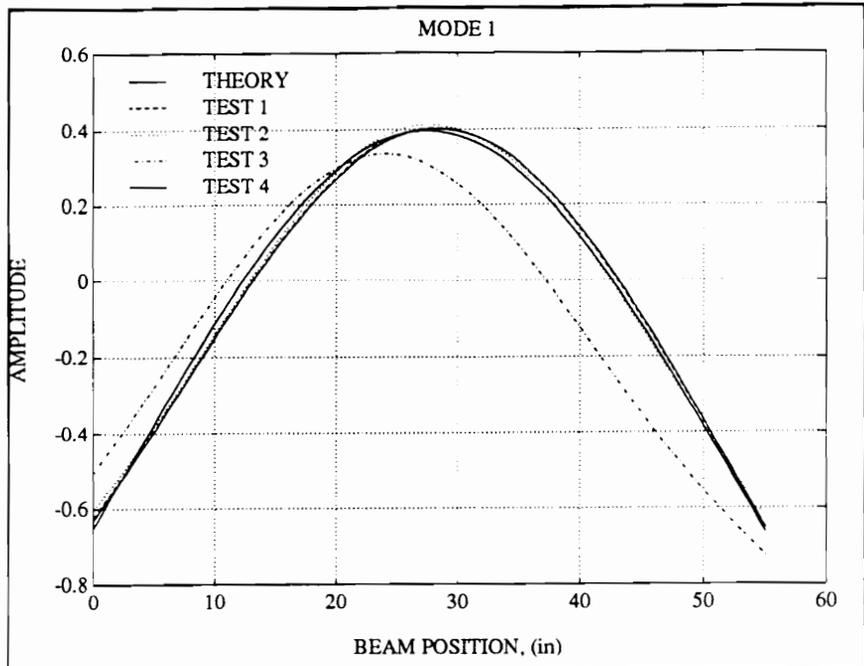
Figure 87 BCBA estimated mode shape from tests 1 through 4 and theory for mode 1.
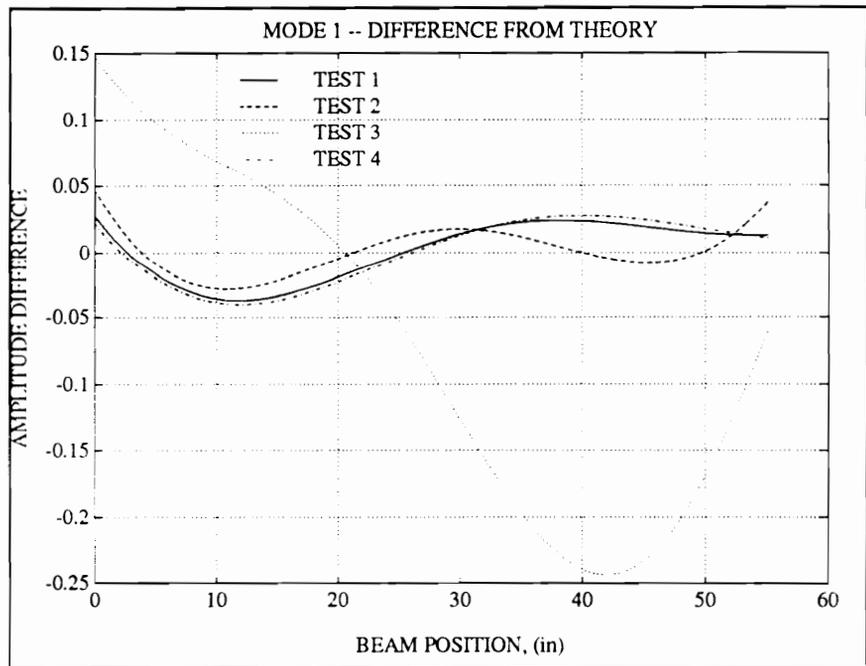
Figure 88 Difference between theoretical mode shape and mode shape estimates from tests 1 through 4 for mode 1.

313
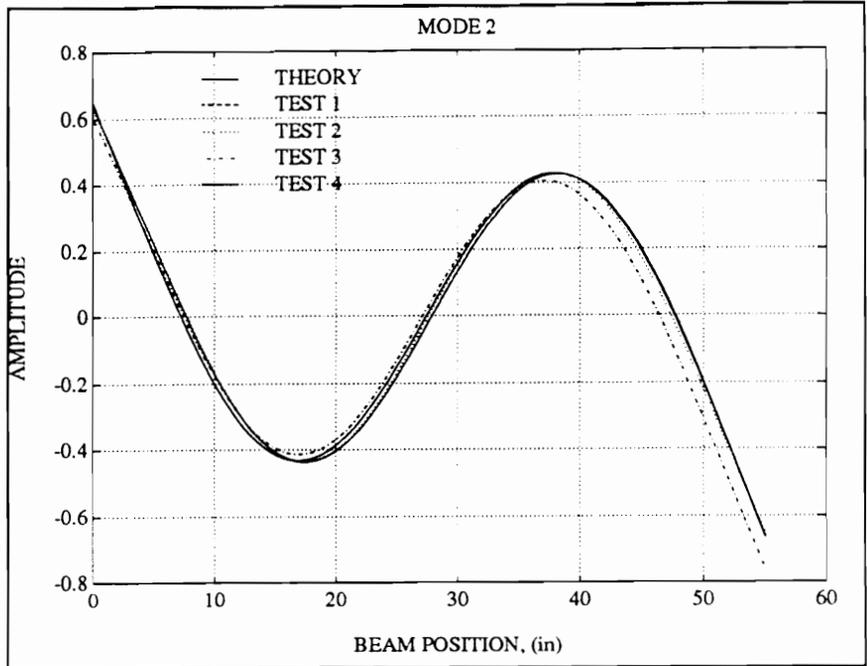
Figure 89 BCBA estimated mode shape from tests 1 through 4 and theory for mode 2.
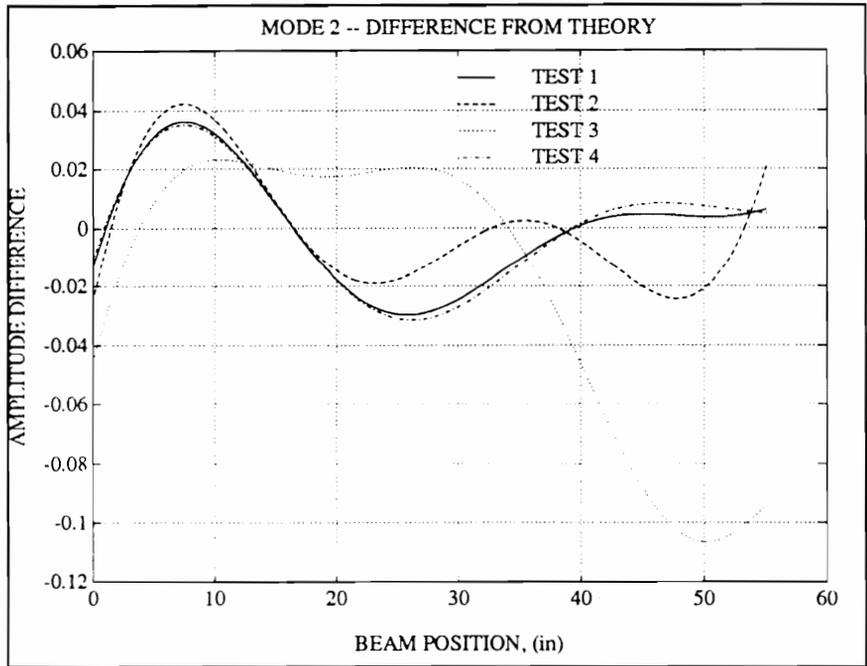
Figure 90 Difference between theoretical mode shape and mode shape estimates from tests 1 through 4 for mode 2.

314
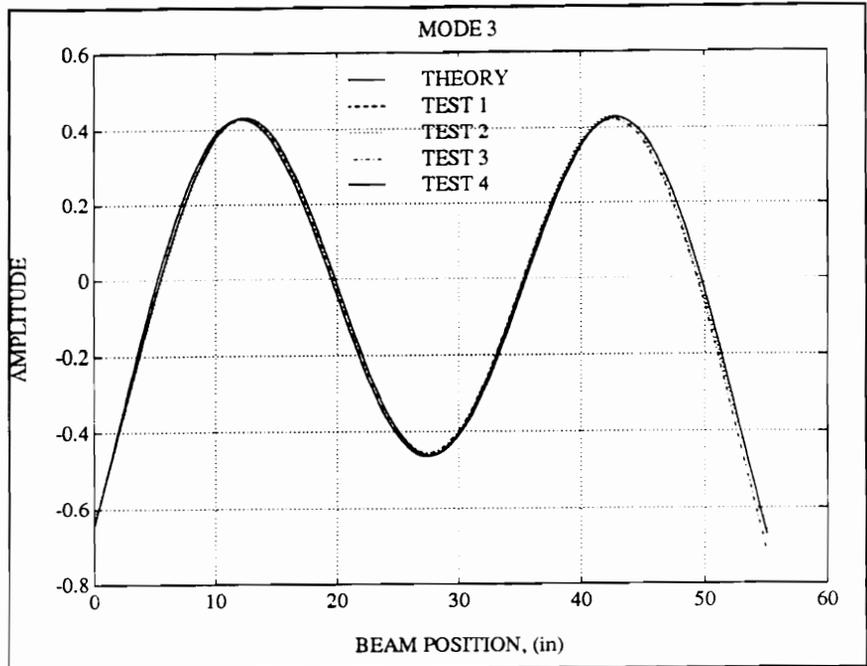
Figure 91 BCBA estimated mode shape from tests 1 through 4 and theory for mode 3.
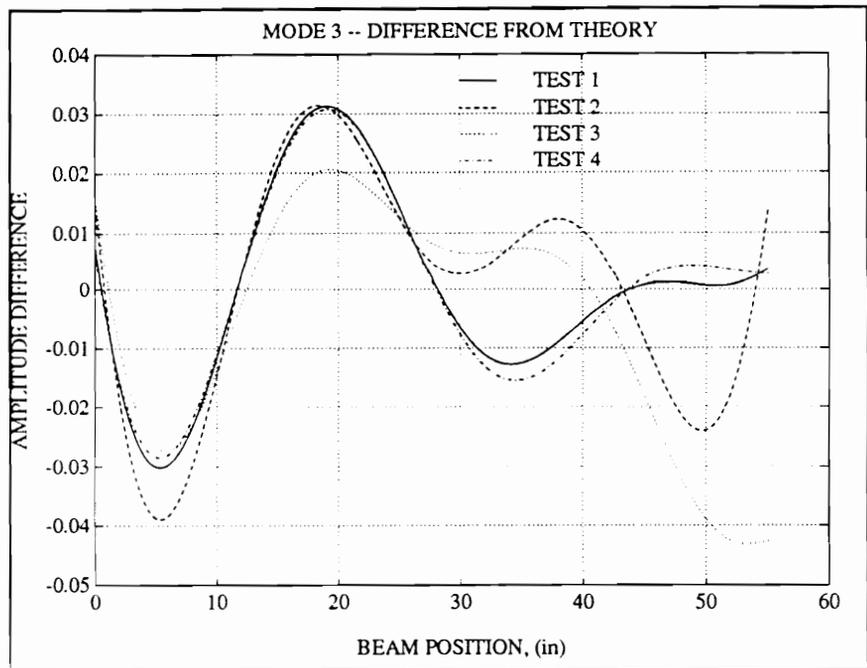
Figure 92 Difference between theoretical mode shape and mode shape estimates from tests 1 through 4 for mode 3.

315
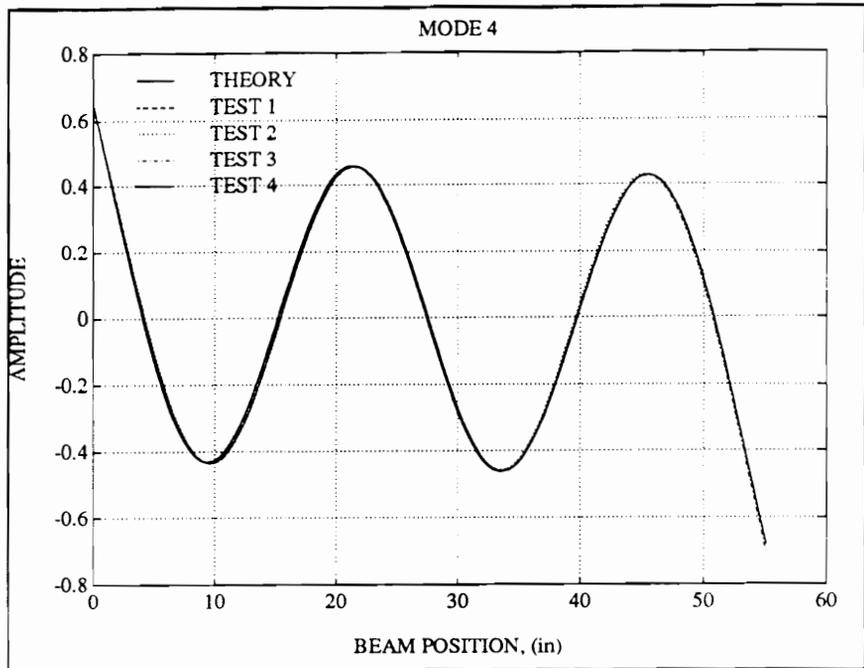
Figure 93 BCBA estimated mode shape from tests 1 through 4 and theory for mode 4.
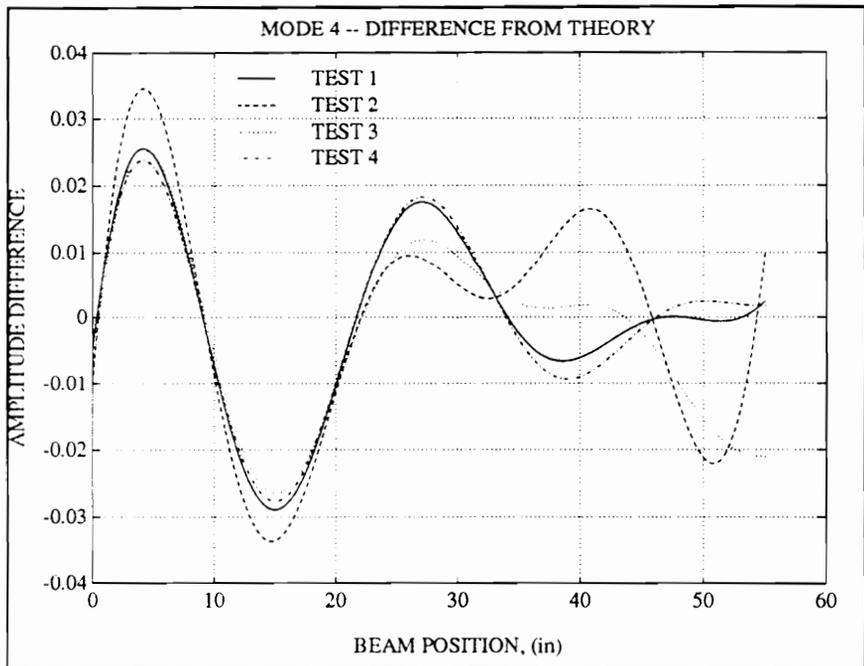
Figure 94 Difference between theoretical mode shape and mode shape estimates from tests 1 through 4 for mode 4.

316
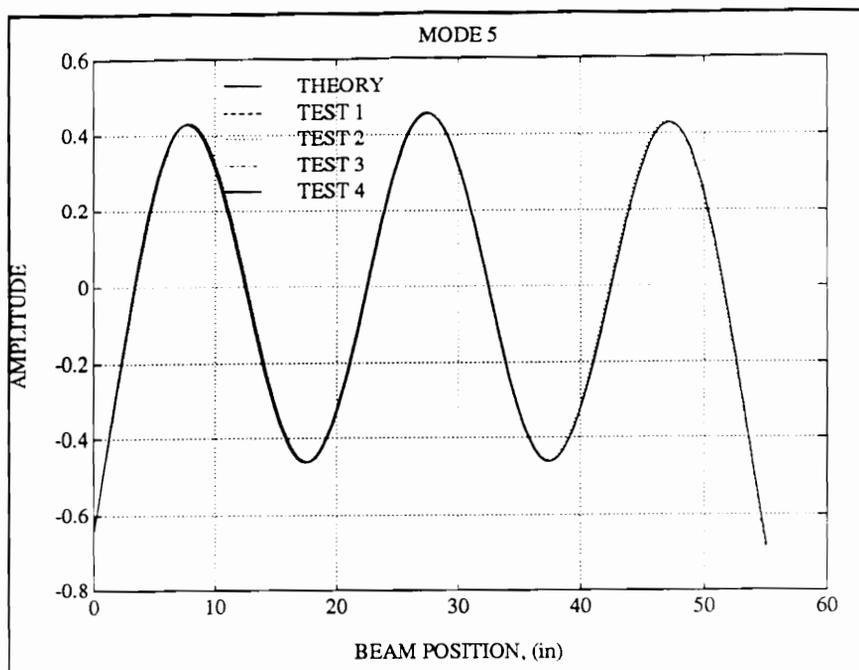
Figure 95 BCBA estimated mode shape from tests 1 through 4 and theory for mode 5.
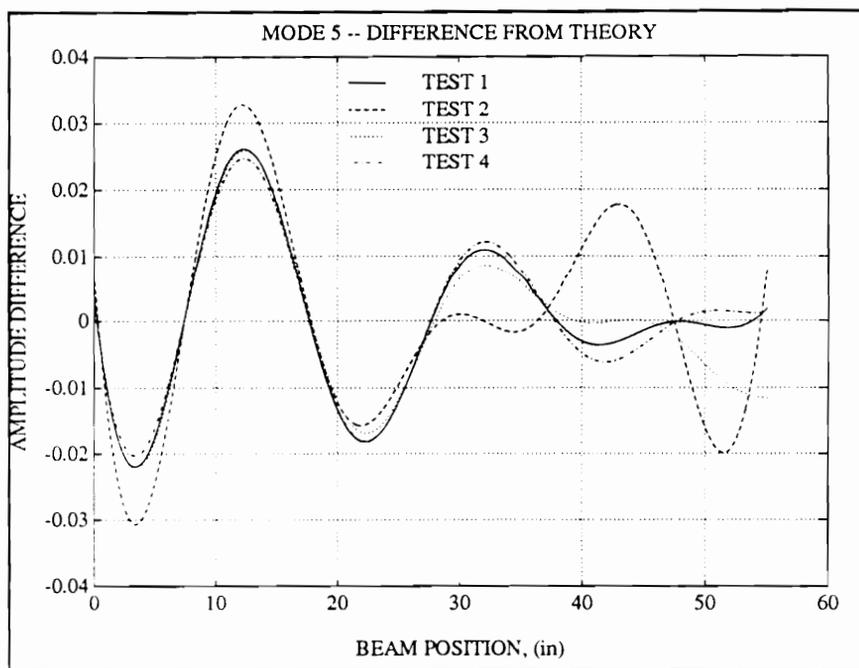
Figure 96 Difference between theoretical mode shape and mode shape estimates from tests 1 through 4 for mode 5.

317
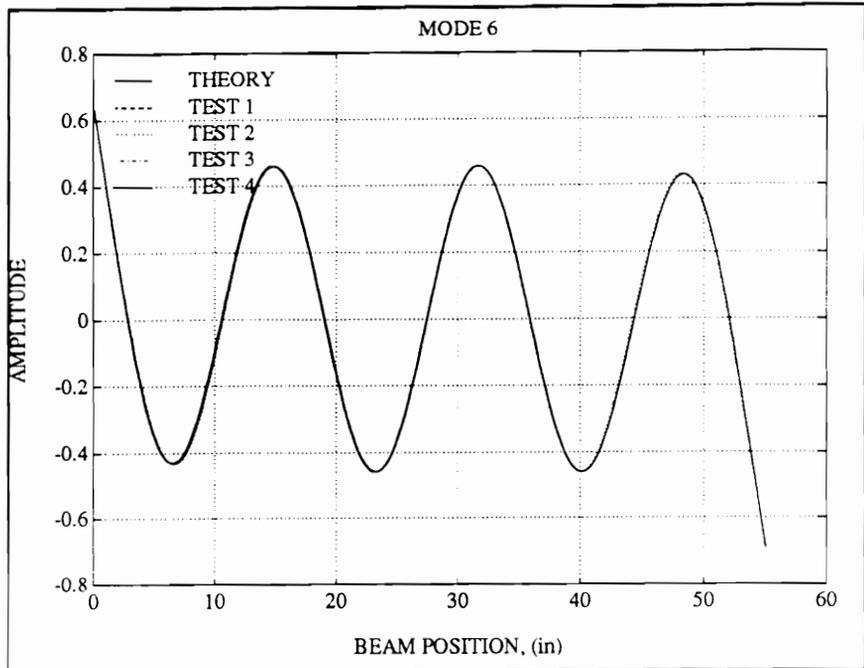
Figure 97 BCBA estimated mode shape from tests 1 through 4 and theory for mode 6.
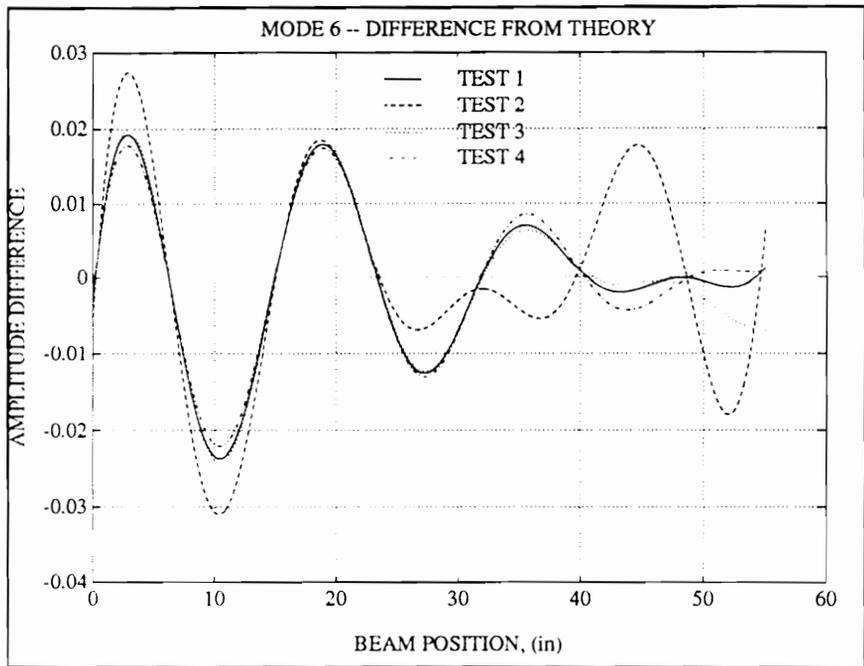
Figure 98 Difference between theoretical mode shape and mode shape estimates from tests 1 through 4 for mode 6.

318

In addition to the mode shapes corresponding to modes 1 through 6, additional rigid-body mode shapes were computed. All four tests included a mode that corresponded to rigid-body rotation of the beam. Test 4 also included a rigid body translation mode. An additional low mode was observed for Test 3. These modes should perhaps be termed quasi-rigid-body modes. The spatial frequencies are not identically zero, although they are very small (See Table XXV). There is some small visible deformation in the beam shape as well. However, with the exception of Test 3, the mode shapes closely approximated true rigid body modes for translation and rotation. These modes are important because they represent actual physical modes of vibration of the beam.

ORTHOGONALITY: In theory, the normal mode shapes are orthogonal. The orthogonality constraint applies to continuous mode shapes. The orthogonality can be stated as

$$\int_0^L \Phi_r(x)\Phi_s(x)dx = 0, \qquad r \neq s \tag{8.7}$$

If the mode shapes are length normalized, then the integral for $r=s$ is equal to the beam length, L.

For measured data, the mode shapes are known only at certain discrete frequencies. The orthogonality condition is not exact for discrete data. It can be expressed as

$$\sum_{k=0}^{N} \Phi_{r,k} \Phi_{s,k} \approx 0 \qquad r \neq s \qquad (8.8)$$

If $r=s$, then the summation is approximately equal to L for length normalized modes.

If the discrete length normalized mode shapes are given in matrix format such that $M = [\Phi_1 \ \Phi_2 \ \dots \ \Phi_n]$, then the product $M^T M$ should be approximately equal to LI, where I is the identity matrix. The orthogonality of the mode shapes for each test was checked in this manner. In all cases the orthogonality condition was approximately met. The deviations of the product matrix from the identity matrix were small, and of the same magnitude as those obtained from discretized theoretical mode shapes.

The orthogonality check results are tabulated in Table XXVI. This table presents the product $M^T M / L$ for each of the four tests. Since the matrix has been corrected for length, the result should be approximately equal to the identity matrix. The diagonal elements are

320

constrained to unity because the mode shapes were length normalized. The off-diagonal elements must be non-negative, and should be approximately zero. Inspection of Table XXVI shows that for all tests, the off-diagonal elements are two orders of magnitude smaller than the diagonal. This indicates a good approximation of the identity matrix.

RIGID-BODY MODES: All tests returned either one or two rigid-body modes. All four tests produced a rigid-body mode comprised principally of rigid-body rotation. Test 4 produced an additional mode corresponding to principally rigid-body translation. Test 3 produced a low-frequency mode that can not be classed as rigid. Although this mode shape can not be truly considered a rigid body mode, it is included here because of the corresponding low spatial frequency. Pure rigid-body motion was not observed in any case, however, with the exception of Test 3, the motion did approximate the rigid-body modes. In the case of the translational modes, some rotation is obviously present. Likewise, although not as noticeable, some translation is present in the rotational modes. In most cases, there is also some deflection of the beam, although this deflection is very small in comparison to either the vibrational modes or the rigid-body displacements. For frequencies of these modes, refer to Table XXV.

Figure 99 displays plots of the rotational modes for Tests 1, 2 and 4, along with the low-frequency mode from Test 3. The rotational modes estimated from Tests 1, 2 and 4 are

321

Table XXVI Orthogonality check for mode shapes obtained from Tests 1 through 4. Matrices are $\mathbf{M}^T\mathbf{M}/L$.

TEST 1

1.0000	0.0178	0.0123	0.0131	0.0183	0.0130
0.0178	1.0000	0.0178	0.0132	0.0134	0.0187
0.0123	0.0178	1.0000	0.0179	0.0138	0.0137
0.0131	0.0132	0.0179	1.0000	0.0180	0.0142
0.0183	0.0134	0.0138	0.0180	1.0000	0.0182
0.0130	0.0187	0.0137	0.0142	0.0182	1.0000

TEST 2

1.0000	0.0169	0.0113	0.0125	0.0175	0.0124
0.0169	1.0000	0.0173	0.0125	0.0130	0.0182
0.0113	0.0173	1.0000	0.0175	0.0133	0.0134
0.0125	0.0125	0.0175	1.0000	0.0178	0.0138
0.0175	0.0130	0.0133	0.0178	1.0000	0.0180
0.0124	0.0182	0.0134	0.0138	0.0180	1.0000

TEST 3

1.0000	0.0199	0.0148	0.0167	0.0202	0.0160
0.0199	1.0000	0.0209	0.0160	0.0165	0.0214
0.0148	0.0209	1.0000	0.0195	0.0152	0.0151
0.0167	0.0160	0.0195	1.0000	0.0189	0.0150
0.0202	0.0165	0.0152	0.0189	1.0000	0.0187
0.0160	0.0214	0.0151	0.0150	0.0187	1.0000

TEST 4

1.0000	0.0179	0.0124	0.0131	0.0184	0.0130
0.0179	1.0000	0.0179	0.0132	0.0135	0.0188
0.0124	0.0179	1.0000	0.0179	0.0138	0.0137
0.0131	0.0132	0.0179	1.0000	0.0181	0.0142
0.0184	0.0135	0.0138	0.0181	1.0000	0.0182
0.0130	0.0188	0.0137	0.0142	0.0182	1.0000

quite similar. The non-rigid-body nature of that from Tests 3 can be clearly seen.

The translational rigid-body modes are displayed in Fig. 100. The vertical axis scale was deliberately chosen identical to that of Fig. 99 for ease of comparison. These modes show little or no deflection. The slight slope for the two modes is opposed.
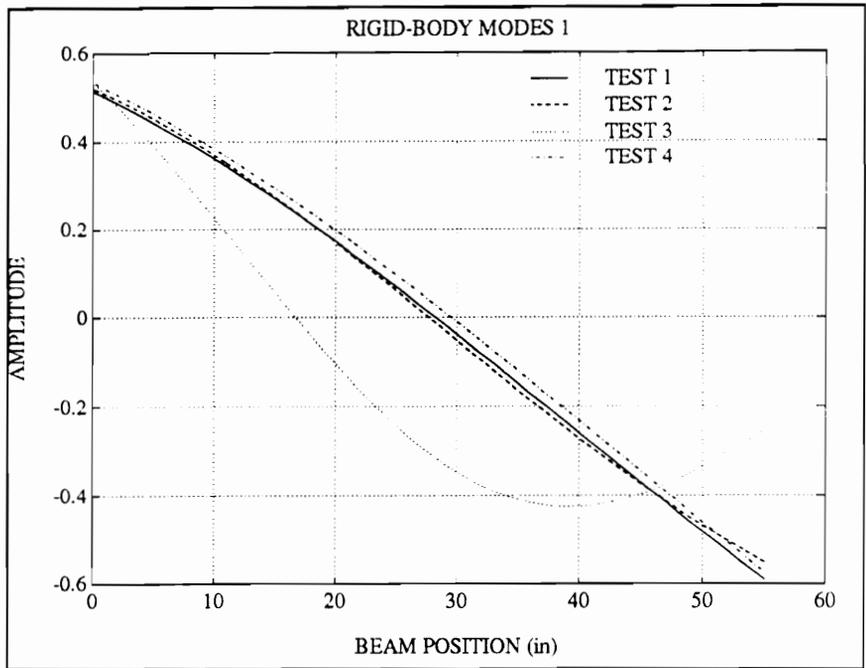
Figure 99 BCBA estimated rotational rigid body modes.
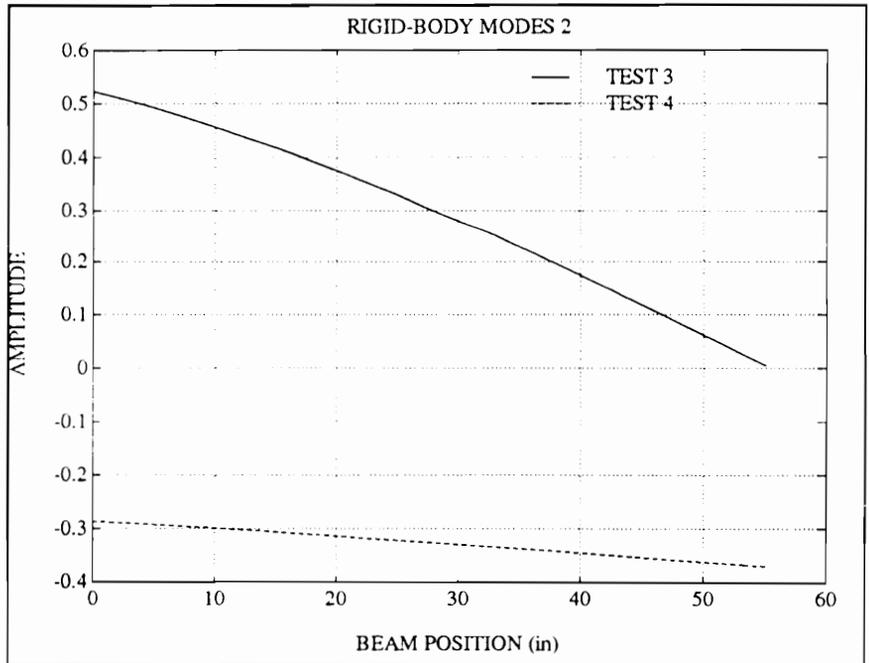
Figure 100 BCBA estimated translational rigid body modes.

324

MODAL WEIGHTING FACTORS: The modal weighting factors were computed for each of the nine data sets. The mode shapes from each of the four tests were used. This resulted in 36 sets of modal weighting factors. In general, good agreement with theory was obtained.

The estimated modal weighting factors from each data set were plotted along with theoretical values. Because of the similarity of many of these figures, only a representative sample are presented here. Figures 101, 102, and 103 depict the modal weighting factors from data sets 1, 5 and 6 respectively. Each figure plots theoretical values along with values obtained from Tests 1 through 4. The modal weighting factors have been normalized such that the peak value is unity. For theoretical values, a damping ratio of 0.01 was used.

From the figures it can be seen that the estimated modal weights from each test are close to each other. They are also close to the theoretical values, although some difference can be noted. This difference could be due to improper guess for the damping ratio.
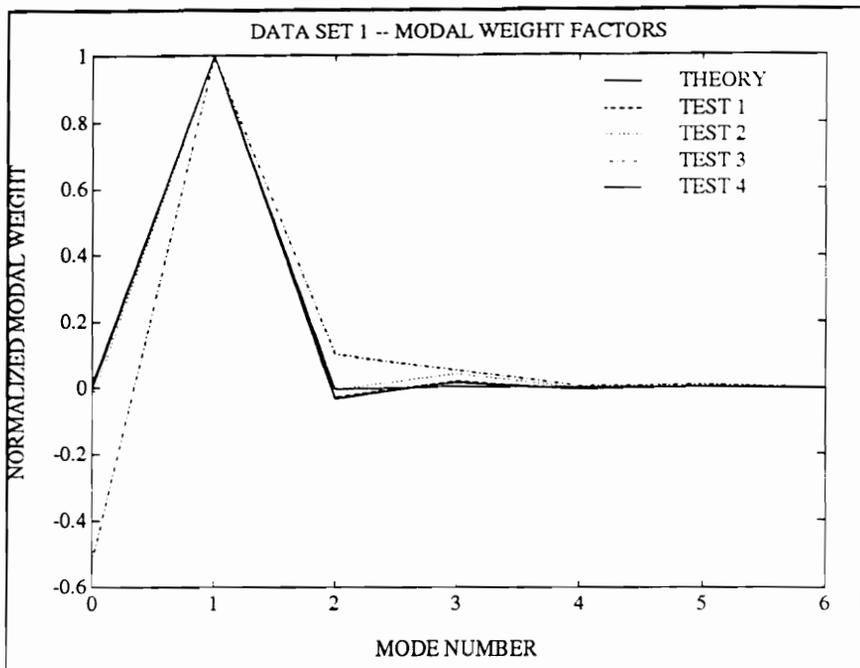
Figure 1 Modal weight factors from tests 1 through 4 and theory for data set 1.
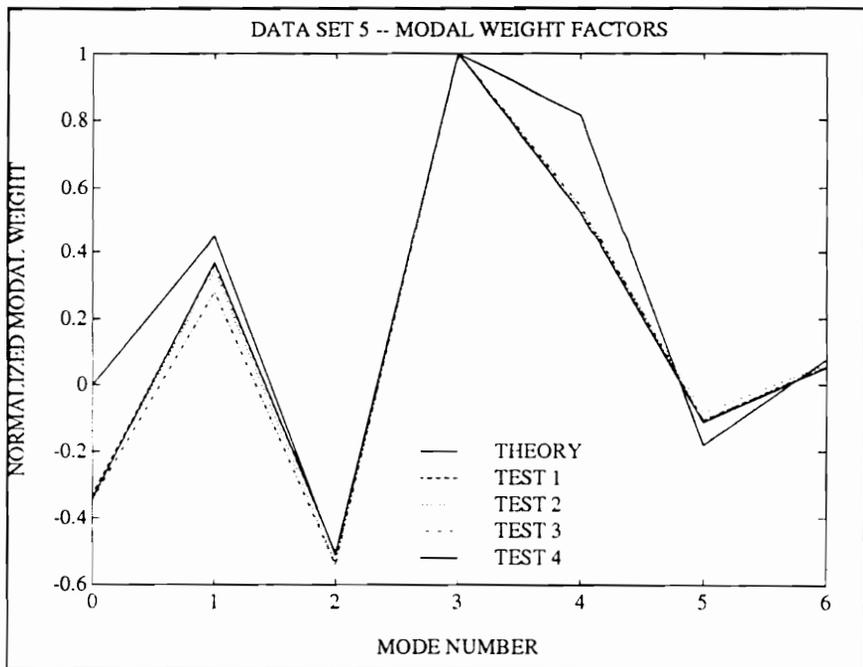
Figure 2 Modal weight factors from tests 1 through 4 and theory for data set 5.

326
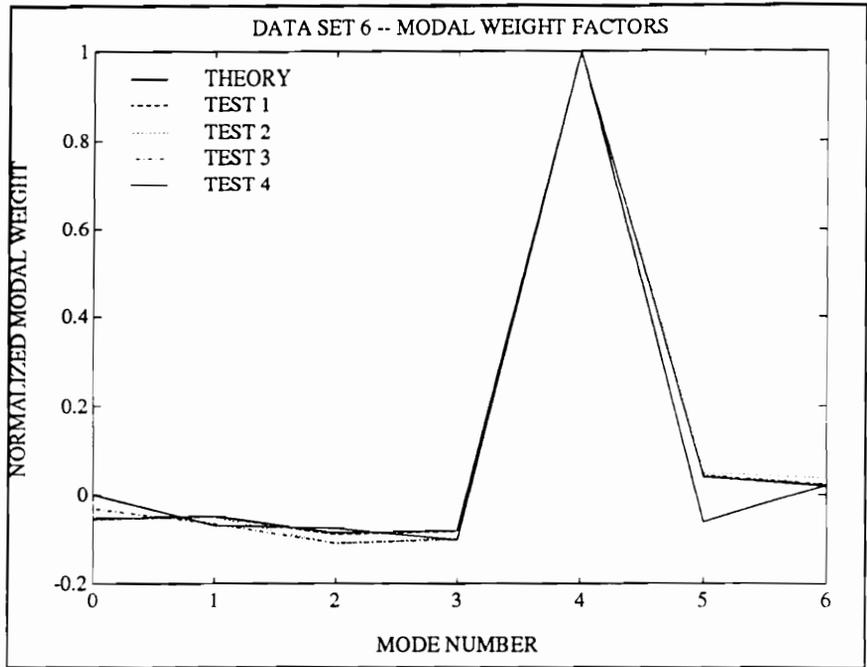
Figure 3 Modal weight factors from tests 1 through 4 and theory for data set 6.

OPERATING SHAPES: An important measure of the validity of the BCBA model is how well it fits the measured data. The fitted operating shape and residual were computed for each data set and each test using the procedure outlined in the previous section. These were plotted together along with the measured data. The correlation between measured and fitted data was very good in most cases. A select set of these plots is reproduced here to highlight the interesting features.

Figure 104 demonstrates the general ability of the BCBA method to model measured data. This figure presents the measured data from data set 6, along with the fitted model from Test 4. It is a typical case. The fitted model very closely matches the measured data. The residual is small, and shows little deterministic content. The propensity of the laser system to produce poorer data at points of highest curvature is apparent. In summary, the measured data is modeled well by the BCBA fit.

The quality of the measured data had a pronounced effect on the ability of the BCBA method to generate a well matched model. The poorest measured data obtained was that for data set 2. The poor quality of this data was also observed in the PSMA and LSSD experiments, in which this data set exhibited the largest sum of squared residuals. Nonetheless, the BCBA method generated an acceptable model of this data. The measured data and fitted operating shape, along with the residual, are plotted in Fig. 105. The BCBA model was obtained from Test 4. Inspection of this figure shows that a close fit

328

was obtained. The residual is small, although it does show some deterministic components, particularly near the ends of the beam. Figure 105 demonstrates that even poor quality measured data can be modeled reasonably well.

In contrast to Fig. 105, the data set and model presented in Fig. 106 presents the best measured data set. Data set 3 provided the cleanest data of all the measured data sets. The figure reveals almost no visible noise. The BCBA model, based on Test 4 mode shapes, is a near perfect fit of the measured data. The residual is very small, with no regions of large deviations. The region around $x=35$ inches shows the highest noise levels, and these remain small. Recall that this data set was not used in any of the tests. The excellent fit is even more meaningful in light of this fact. It is also worth noting that the models based on Tests 1 and 2 exhibited a small DC offset. The translational rigid-body modes present in Tests 3 and 4 corrected for this offset.

Several data sets exhibited a DC offset. This offset was most apparent when the residual was inspected. The magnitude of the offset ranged from zero to approximately ten percent. Data set 5 exhibited the worst case DC offset. Figure 107 presents the measured data from set 5 along with the fitted model based on Test 1. The offset is readily apparent, particularly on inspection of the residual. Otherwise, the fit is good. The residual shows only slight deterministic content, and the model matches the shape of the measured data. The lack of a translational rigid-body mode for Test 1 resulted in the

offset. This offset was removed by using BCBA models from Tests 3 or 4, which included the translational mode. Figure 108 shows the same data set along with a model based on Test 4 results. The improved quality of the fit is apparent.

In this experiment, only modes 1 through 6 were computed. Thus, for the data sets with excitation frequencies near the fifth or sixth mode, effects due to unmodeled modes were expected. Figure 109 reveals that this is indeed the case. This figure presents measured data from data set 9. The fitted model based on Test 1 is also plotted, along with the residual. The deterministic content of the residual is quite apparent. The shape of the residual corresponds to the mode shape for the seventh mode, which was not modeled. Otherwise, the model seems acceptable. The power of the BCBA method is its ability to compute as many modes as required. If accurate modeling of this data set was necessary, it would behoove the investigator to go back and recompute the seventh, and perhaps even higher mode shapes. The resulting model would be much improved. For the present case, this data was only presented to indicate the presence of unmodeled modal content. Careful inspection of the model and the residual should provide indications as to whether a poor model fit is due to unmodeled modes or to a poor parameter estimation. If doubt exists, it is a simple matter to compute additional modes and construct an extended model.
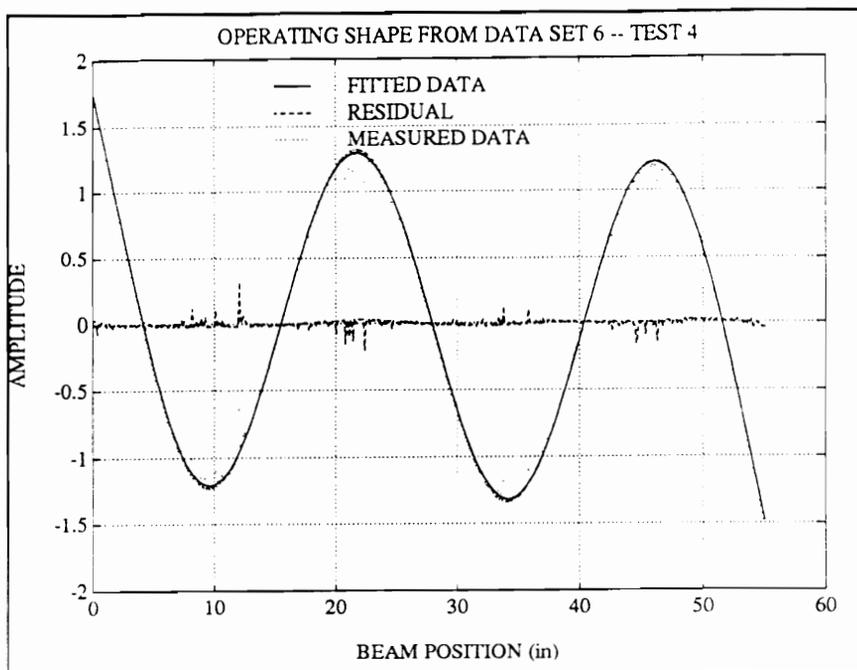
Figure 104 BCBA fitted operating shape, measured data, and residual from data set 6 and Test 4.
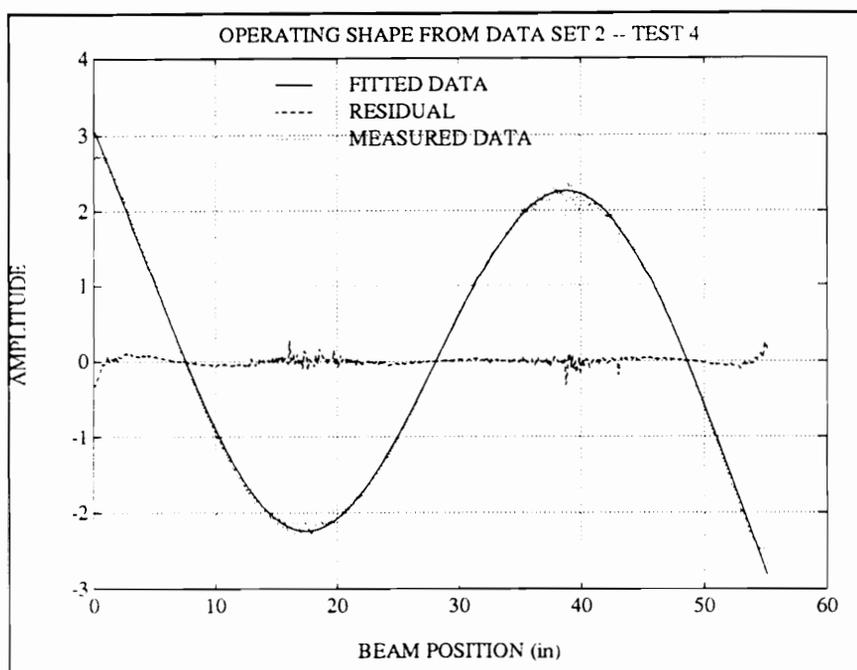
Figure 105 BCBA fitted operating shape, measured data, and residual from data set 2 and Test 4.

331
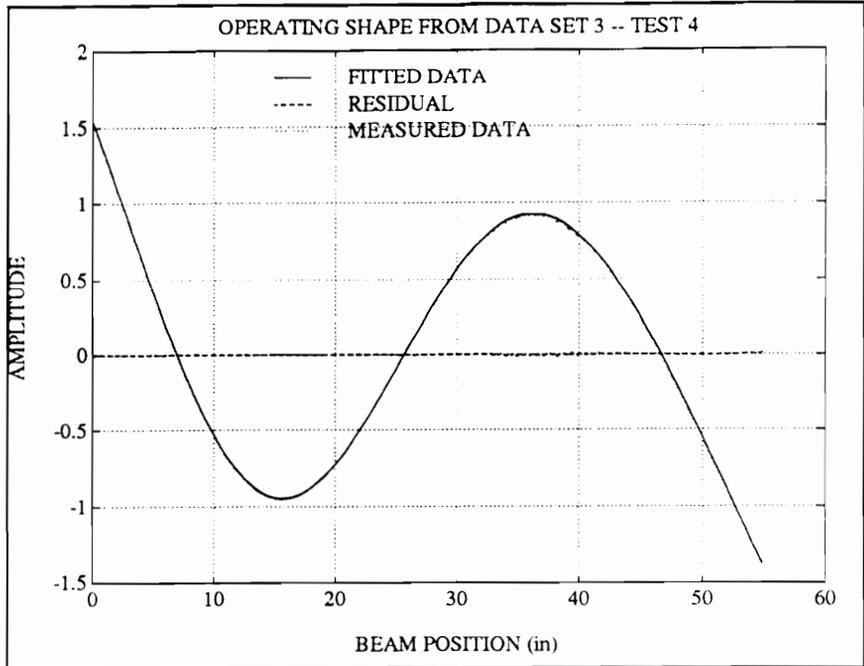
Figure 106 BCBA fitted operating shape, measured data, and residual from data set 3 and Test 4.
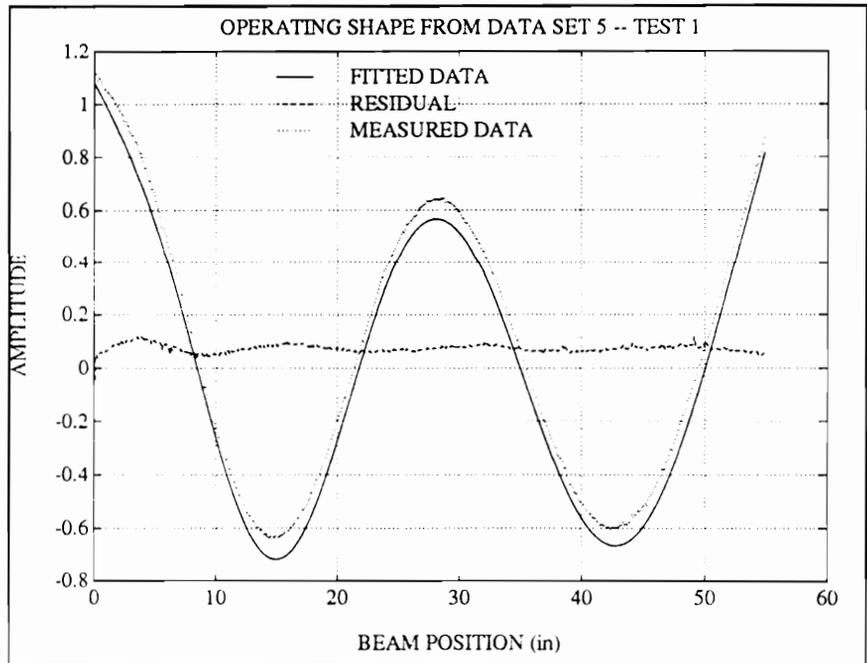
Figure 107 BCBA fitted operating shape, measured data, and residual from data set 5 and Test 1.

332
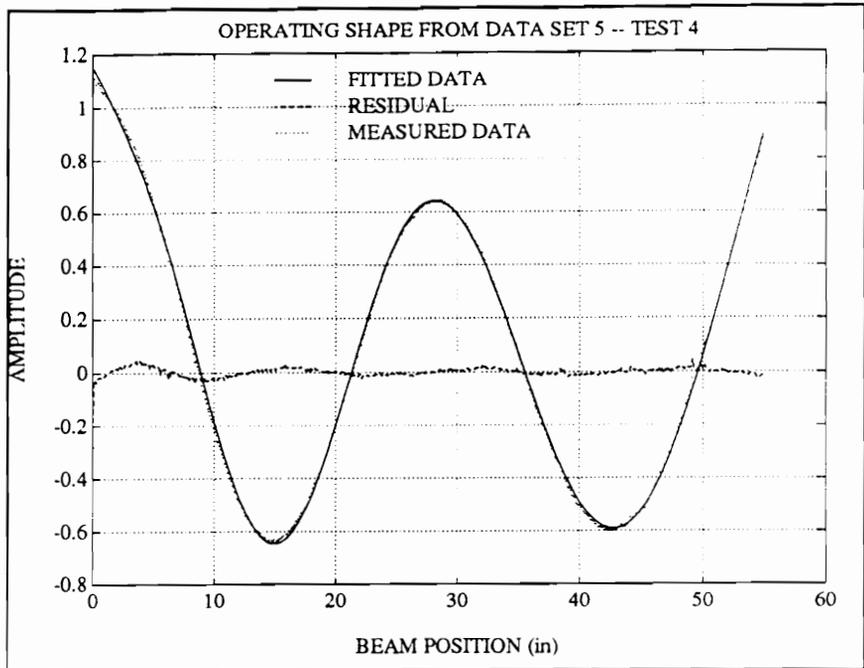
Figure 108 BCBA fitted operating shape, measured data, and residual from data set 5 and Test 4.
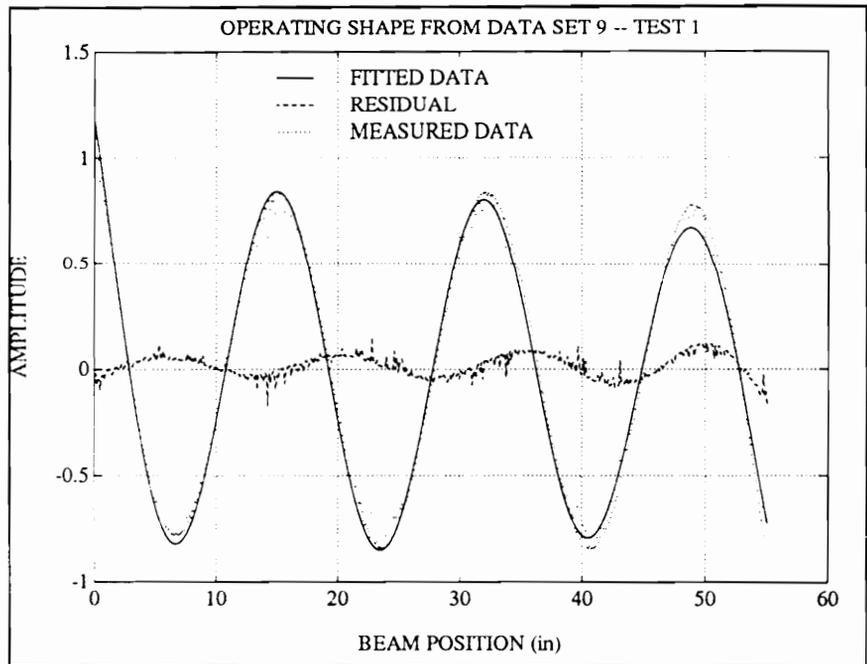
Figure 109 BCBA fitted operating shape, measured data, and residual from data set 9 and Test 1.

333

CONCLUSIONS AND RECOMMENDATIONS

The four tests of this experiment demonstrated the ability of the BCBA method to generate meaningful and accurate spatial modal models. Boundary conditions, spatial frequencies, mode shapes, and modal weighting factors have all been estimated accurately. The principal factor in constructing an accurate BCBA model is estimation of the deflection and spatial derivatives at the ends of the beam.

In summary, this experiment has demonstrated that the BCBA method can:

· Accurately generate spatial modal models.

· Accurately estimate out-of-band modes.

· Estimate rigid-body modes.

· Automatically impose theoretical constraints (such as orthogonality of mode shapes).

334

The method requires some refinement to be effective on a more general level. Several recommendations address some of these issues. It is recommended that further research be conducted in the following areas:

- Algorithms should be developed to obtain accurate derivatives at the boundaries of the beam regardless of the excitation frequency. (This will remove the restriction of resonance excitation.)

- The ability of the BCBA method to model rigid-body modes should be more fully investigated. For example, why did Tests 1 and 2 not produce a transnational rigid-body mode?

- The robustness of the BCBA method with respect to the beam material properties and derivative estimates should be investigated.

The BCBA method is a true spatial modal analysis technique. It is a powerful method which estimates general boundary conditions, spatial frequencies and normal mode shapes for uniform beams using only spatial data. It is a method with practical potential for modeling real world structures.

335

WIDE-BEAM EXPERIMENT

The objective of the algorithms presented in this dissertation is to fit spatial vibration data to classical beam theory. Euler-Bernoulli beam theory is one-dimensional, that is, only one spatial coordinate appears in the model. The underlying assumption is that all points on any transverse section of the beam vibrate uniformly. Timoshenko beam theory is similarly one-dimensional. For beams with a lateral dimension very small relative to the length dimension, one dimensional theories are satisfactory. However, as the lateral dimension of the beam increases, the vibration becomes increasingly two dimensional. An interesting problem involves application of one-dimensional beam theories to wide beams. This problem is investigated in the second experiment. The results show the feasibility of modeling a wide-beam using the LSSD algorithm.

OBJECTIVE

The objective of this experiment was to determine if one-dimensional beam analysis algorithms could generate meaningful models for beams with significant two-dimensional effects.

BACKGROUND

It is well recognized that beams do not vibrate in only one dimension. Euler-Bernoulli and Timoshenko beam theories provide good one-dimensional models where they are applicable. Euler-Bernoulli theory is applicable if both the width and depth of the beam are much smaller than the length. If the beam thickness is not small relative to the length, Timoshenko theory is appropriate. However, neither theory can fully represent a beam that is wide relative to the length. Full theoretical analysis of such beams requires three-dimensional elasticity theory, and is not amenable to analyses such as those presented in this dissertation. For discussions on three-dimensional elasticity solutions see, for example, Hutchinson (1981) or Stein (1989).

An alternate approach to the wide-beam problem is to treat the beam as a series of adjacent narrow beams. Thus, the beam is considered to be several narrow strips. Each strip, or longitudinal section, is modeled as a one-dimensional beam using classical beam theory. The lateral effects of vibration are revealed in the different modal parameters for the different models. This is the approach used for experiment two.

A prominent two-dimensional effect that is manifested in wide beams is anticlastic bending. One-dimensional theories assume that the surface of the beam remains planar in the lateral direction. A beam exhibiting anticlastic bending will have a curvature in this

337

direction. Furthermore, the curvature is opposite that in the length direction. This results in a shallow saddle shape.

Anticlastic effects are due to the interdependence of strains in three dimensions within an elastic body. Consider a beam subject to pure bending loads such that the curvature in the longitudinal direction is concave downward. Then the part of the beam that lies above the neutral axis will be in tension, and the part below the neutral axis will be in compression. The strain in the longitudinal direction is related to that in the lateral direction by Poisson's ratio. Thus, the compressive longitudinal strain below the neutral axis will cause the outer edges to 'bulge' outward. A good description of anticlastic bending can be found in Richard, et al (1993).

Very wide beams must be modeled as plates. Plates are inherently two-dimensional, and, of course, can not be accurately described using one-dimensional beam theories. The effects of plate and anticlastic behaviors can thus not be included in simple beam theories such as Euler-Bernoulli or Timoshenko. However, by modeling wide beams as a series of narrow beams, a composite model can be constructed that reflects two-dimensional effects.

The philosophy behind this experiment was not to derive a rigorous experimental model for wide beams. Rather, it was to investigate the possibility of using one-dimensional

338

theory to generate a smoothed, deterministic model of the beam. Since this task requires only that a smoothed model be generated, the minimum residual methods were employed. The resulting modal can not thus be termed a modal model in the strict sense.

IMPLEMENTATION

Spatial data was obtained for a wide beam. The setup was similar to that for the other experiments described in this chapter. The beam was suspended by an elastic support at one end so as to approximate free-free boundary conditions. The beam was excited by an electromagnetic shaker attached to the upper end of the beam. Harmonic excitation was used. The excitation frequencies corresponded to each of the first four natural frequencies of the beam. Table XXVI describes the beam parameters used in this experiment. Table XXVII presents the excitation frequencies.

Table XXVII Wide-Beam Parameters

BEAM DIMENSIONS		MATERIAL
Length	24.00 in	Aluminum
Width	6.00 in	
Thickness	0.75 in	

Table XXVIII Excitation frequencies for wide-beam experiment.

RESONANCE MODE	EXCITATION FREQUENCY (Hz)	THEORY NATURAL FREQUENCY (Hz)
1	271.2	265.8
2	745.8	732.6
3	1456.8	1436.2
4	2387.8	2374.1

The beam was scanned at 250 longitudinal locations and 5 transverse locations. Unlike the slender beam experiments, in which all transverse data sets were assumed equal and averaged, the 5 transverse columns of data were processed individually. The LSSD method was used for this analysis. The result was 5 models representing 5 longitudinal strips of the beam. These models were combined into a single 250x5 matrix from which a mesh plot of the modeled beam was constructed. The modeled data mesh was compared with a mesh of the original data to determine if the LSSD method had the capability of producing a smoothed model.

RESULTS

The results demonstrated the feasibility of using minimum residual beam modeling algorithms for smoothing two-dimensional data. The models generated with the LSSD method represented the operating shape of the wide beam. Estimated spatial frequencies varied from theory, a result of the bias inherent in the LSSD method.

The theoretical and estimated spatial frequencies of the beam are presented in Table XXVIII. Each transverse column of data produced a slightly different model (as was expected). The spatial frequencies corresponding to each transverse location are presented, along with the value obtained from Euler-Bernoulli theory. (Since Euler-Bernoulli theory is one-dimensional, the theoretical spatial frequency does not vary transversely.) The spatial frequency variation across the beam is readily apparent. All of the estimated spatial frequencies differ from theory by as much as 5%. This is a reflection of the LSSD bias error documented in previous chapters.

The smoothed models obtained from this experiment are more interesting than the spatial frequency estimates. These models, along with the measured data, are presented in Figs. 110 through 113. Figure 110 depicts a mesh plot of the first mode data. The top mesh is

341

Table XXIX Spatial frequencies versus lateral beam position for wide beam analysis. (Lateral position in inches).

LSSD ANALYSIS

POSITION	MODE 1	MODE 2	MODE 3	MODE 4
-2.7570	0.2031	0.3324	0.4666	0.5980
-1.2510	0.2042	0.3337	0.4654	0.5935
0.2550	0.2065	0.3361	0.4638	0.5986
1.7610	0.2053	0.3359	0.4630	0.5952
3.2680	0.2034	0.3340	0.4621	0.5979
THEORY $\Rightarrow$	0.1979	0.3285	0.4599	0.5914

measured data. Noise is apparent in this mesh. The bottom mesh shows the LSSD model. It is clear that the data has been smoothed in the model. However, little two-dimensional content is noted.

Figures 111, 112, and 113 show the measured and smoothed data for modes 2, 3 and 4 respectively. As with the first mode data, the LSSD method produced smoothed models of the measured data in all cases. As the mode number increases, the two-dimensional content also increases. The smoothed models accurately reflect these effects. Figure 113 is of particular interest. Of the four data sets, it exhibited the greatest noise content. This is visible as scatter in the measured data mesh. The fourth mode also included the most pronounced two-dimensional effects of the four data sets. The LSSD approach produced a very smoothed model that retained the two-dimensional effects.

342

MEASURED DATA

FITTED MODEL - LSSD METHOD
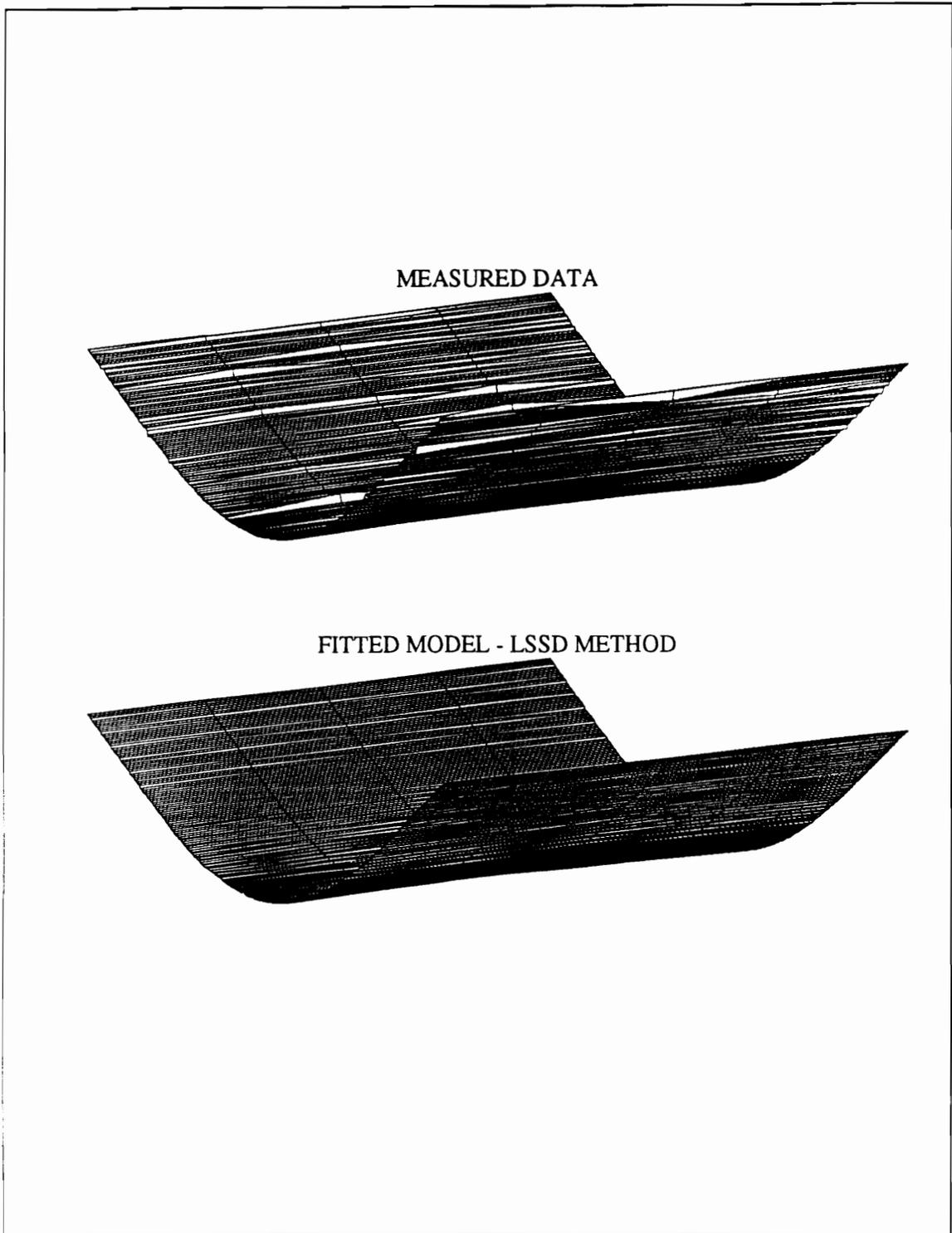
Figure 110 Measured data and fitted model for mode 1 -- wide
beam.

343

MEASURED DATA -- MODE 2
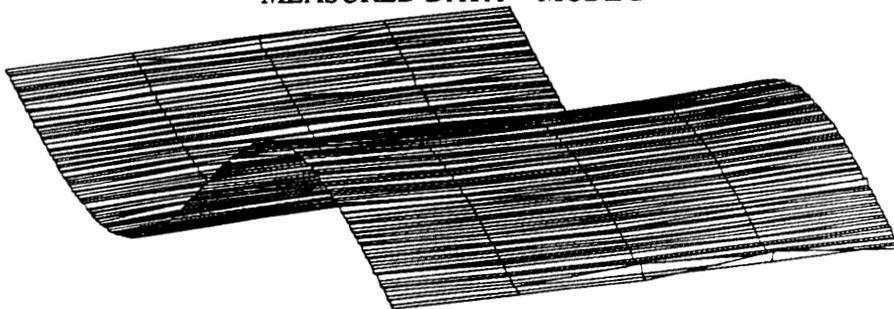
FITTED MODEL - LSSD METHOD
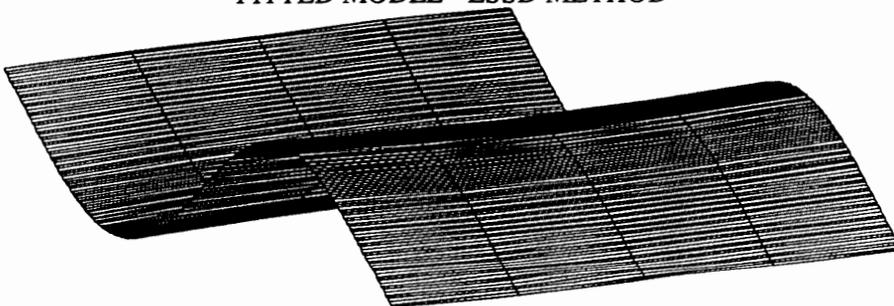
Figure 111 Measured data and fitted model for mode 2 -- wide beam.

344

MEASURED DATA -- MODE 3

FITTED MODEL - LSSD METHOD
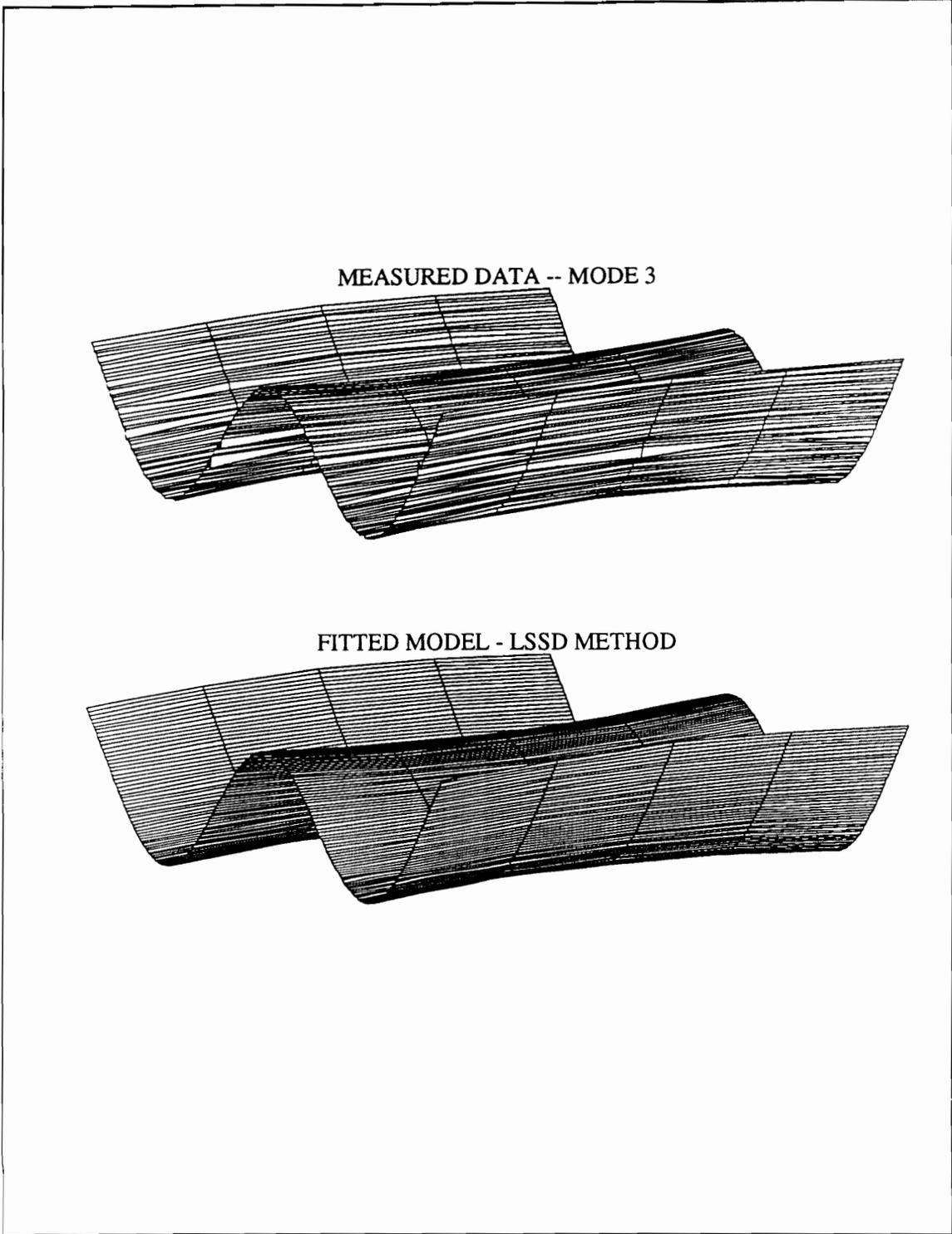
Figure 112 Measured data and fitted model for mode 3 -- wide beam.

345

MEASURED DATA -- MODE 4
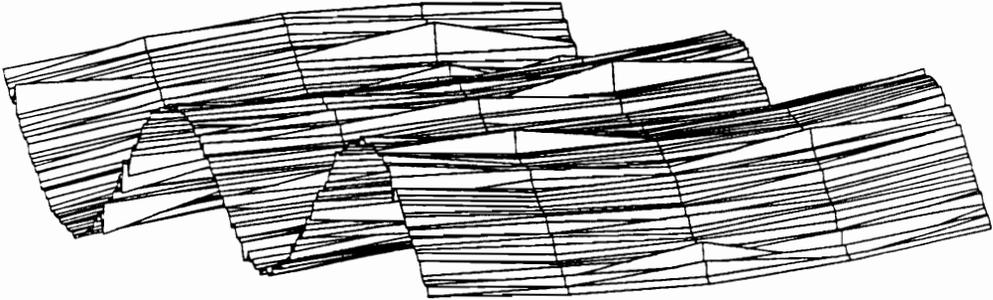
FITTED MODEL - LSSD METHOD
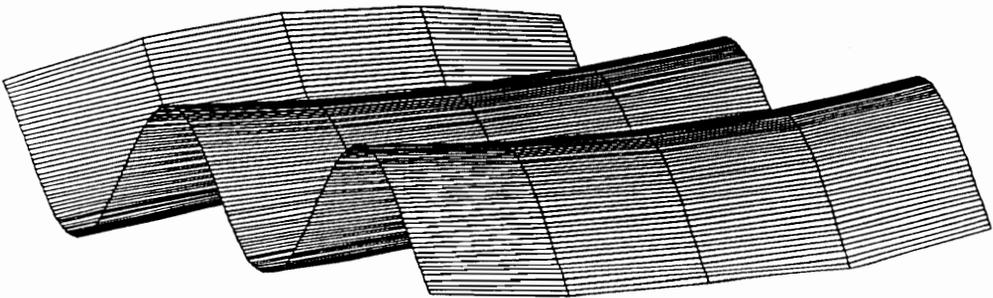
Figure 113 Measured data and fitted model for mode 4 -- wide beam.

346

CONCLUSIONS

The results of the wide-beam experiment indicate the minimum residual beam modeling algorithms can be used to effectively model beams with two-dimensional vibration. It is important to realize the limitations of this approach. The resulting models will not be modal models in the true sense. The approach should rather be considered a numerical approach to smoothing measured data. In this respect the LSSD method performs very well.

Classical beam theory does not address two-dimensional effects of beam vibration. Although the minimum residual methods presented in this dissertation are based on theory, they do not provide models that correspond well with theory. However, they can produce deterministic models that fit the measured data well. This is the sole task of data smoothing. Thus, for the application addressed in this experiment, the LSSD method was very successful. In summary, the wide-beam experiment demonstrated that:

· Minimum residual beam methods can effectively produce smoothed models of beam that contain two-dimensional vibration effects.

·

347

CHAPTER 9: CONCLUSIONS/RECOMMENDATIONS

The objective of the research presented in this dissertation was to develop a method for parametric spatial modal analysis of beams. The BCBA technique is such a method. It was shown that a meaningful modal decomposition for a beam could be obtained using this method. Spatial frequencies and mode shapes can be estimated accurately. Out of band modes can also be computed, and their effect quantified. The method is based strictly on spatial data. The critical step in the analysis is estimation of beam deflection and spatial derivatives at the ends of the beam. It was shown that in some cases, the LSSD method can be used to obtain such estimates.

Other methods were also investigated. Autoregressive models appeared to have much promise. However, difficulties were encountered in implementing these methods. One problem resulted from oversampling the data. This is a problem inherent in spatial beam analysis. A matrix delay factor provided a solution. This solution also provided a means to apply sinusoidal estimation methods to signals containing widely space sinusoids. This contribution is significant in many disciplines other than modal analysis.

Other problems were not so easily overcome. The autoregressive approach, like other minimum residual models, exhibits a bias error if the beam excitation frequency does not coincide with one of the natural frequencies of the beam. This error is due to the fact that

348

minimum residual models do not provide for modal decomposition. That is, modal parameters corresponding to the minimum residual do not correlate with the true modal parameters.

The Least Squares Spatial Domain method was also developed. This was another minimum residual approach. In this case, a multi-variate Newton's method was employed to perform a non-linear least squares fit of measured data to classical beam theory. Because it was also a minimum residual method, it was subject to some of the same restrictions as the autoregressive method. These methods are capable of producing smoothed models. However, they should not be considered true spatial modal analysis, since they do not reduce the measured data to vibrational modes. It was shown that these methods could be used to produce smoothed models of wide beams with two-dimensional content, however.

The principal conclusions drawn from this research can be summarized as:

· The BCBA method is an effective parametric spatial modal analysis approach.

· Minimum residual models can be used effectively to generate smoothed spatial data.

- Minimum residual methods exhibit a bias error unless excitation frequencies coincide with beam natural frequencies.

- The optimum sample rate for parametric sinusoidal estimation is 4 samples per period.

- Minimum residual methods can be used to obtain smoothed data for wide beams with significant two-dimensional components.

Most research generates as many questions as answers. A number of areas related to this research require additional study. Many of these have been noted in the text. The principal recommendations can be summarized as:

- New methods of estimating spatial derivatives at the beam boundaries should be developed. (This will permit more flexibility and accuracy with the BCBA method.)

- The BCBA method should be tested with beams having other than free-free boundary conditions.

- The BCBA theory should be expanded to enable analysis of structures of beams.

- Estimation of damping ratios using BCBA method should be investigated.

APPENDIX

A2.1 THE AUTOREGRESSIVE NATURE OF EXPONENTIAL FUNCTIONS

The family of exponential functions, including real, complex, and imaginary exponentials, has important applications in science and engineering. All of the trigonometric and hyperbolic functions belong to this family. Fourier analysis, a prevalent tool used by analysts in many fields, is based on fitting periodic functions with complex exponentials. Likewise, in the realm of time-domain signal processing, exponential functions are often used for fitting time series data. In particular, many sinusoidal estimation methods rely on fitting complex sinusoids to measured data. The roots of many of these methods can be traced back to 1795 when Gaspard Riche, Baron de Prony proposed a method for modeling the expansion of various gases using a linear combination of exponentials (Prony, 1795). (For a historical note see Kay and Marple, 1981.) Since then, his ideas have been developed into a method used for sinusoidal estimation. A more recent sinusoidal estimation method was developed by V.F. Pisarenko in 1973. Each of these methods, as well as a number of other time-domain spectral estimation methods rely on the autoregressive nature of exponential functions. This simply means that the value of a discrete exponential function, or linear combination of exponential functions, can be determined exactly from a finite number of previous values. Specifically, if the function at hand consists of a linear combination of m exponentials, the value the function at any

352

time can be exactly determined from the past m values of the function. Mathematically, this means that the discrete function

$$y_k = \sum_{i=1}^{m} A_i e^{w_i k} \qquad (1)$$

can be represented by the autoregressive equation

$$\sum_{i=0}^{m} a_i \, y_{k-i} = 0 \qquad (2)$$

where a_0 can be taken to be 1 without loss of generality. The autoregressive nature of exponential functions is easily seen in the equivalence of Eq. 1 and Eq. 2. This equivalence is crucial in many time-domain and spatial-domain analysis methods, which utilize an autoregressive model to fit trigonometric and exponential functions to measured data.

The following proof uses Z-transforms to demonstrate the equivalence of these equations. The proof proceeds by 1) taking the Z-transform of Eq. 1, 2) algebraically manipulating the resulting polynomial expression into the desired form, and 3) taking the inverse Z-transform to obtain Eq. 2. It assumes no restrictions on the exponential functions, i.e., the

353

coefficients A_i and the exponents w_i in Eq. 1 can be real, complex, or imaginary. If y_k is real, however, the coefficients and exponents must be either real or occur in complex conjugate pairs.

Proof:

Taking the Z-transform of Eq. 1 gives

$$Z[y_k] = Y(z) = \sum_{i=1}^{m} \frac{A_i z}{(z - e^{w_i})}$$

Finding the least common denominator gives the rational expression

$$Y(z) = \frac{\sum_{i=1}^{m} [A_i z \prod_{j=1, j \neq i}^{m} (z - e^{w_j})]}{\prod_{i=1}^{m} (z - e^{w_i})} \tag{4}$$

Expanding the products gives the polynomial representation

354

$$Y(z) = \frac{\sum\limits_{i=1}^{m} A_i z \sum\limits_{j=0}^{m-1} b_{j,i} \, z^{m-1-j}}{\sum\limits_{J=0}^{m} a_i \, z^{m-j}} \tag{5}$$

The polynomial coefficient a_j is the jth coefficient of the polynomial formed from expansion of the denominator of Eq. 4. Similarly, $b_{j,i}$ is the jth coefficient of the ith polynomial of the numerator. The ith polynomial is formed by expansion of all except the ith exponential term. Cross multiplying the denominator and subtracting the right hand side gives

$$Y(z) \sum\limits_{j=0}^{m} a_i \, z^{m-j} - \sum\limits_{i=1}^{m} A_i \sum\limits_{j=0}^{m-1} b_{j,i} \, z^{m-j} = 0 \tag{6}$$

Rearranging the summation terms gives

$$\sum\limits_{j=0}^{m} Y(z) a_j z^{m-j} - \sum\limits_{j=0}^{m-1} z^{m-j} \sum\limits_{i=1}^{m} A_i b_{j,i} = 0 \tag{7}$$

Noting that the ith coefficient of a polynomial is all possible combinations of its roots, taken i together, a relationship between a_j and $b_{j,i}$ can be found. This relationship is given by

355

$$a_j = b_{j,i} - b_{j-1,i}e^{w_i} \tag{8}$$

Substituting for $b_{j,i}$ in the inner summation of Eq. 7 gives

$$\sum_{i=1}^{m} A_i b_{j,i} = \sum_{i=1}^{m} A_i(a_j + b_{j-1,i}e^{w_i}) \tag{9}$$

$$= \sum_{i=1}^{m} A_i a_j + \sum_{i=1}^{m} A_i b_{j-1,i}e^{w_i} \tag{10}$$

Again substituting for $b_{j-1,i}$

$$= \sum_{i=1}^{m} A_i a_j + \sum_{i=1}^{m} A_i[a_{j-1} + b_{j-2,i}e^{w_i}]e^{w_i} \tag{11}$$

$$= \sum_{i=1}^{m} A_i a_j + \sum_{i=1}^{m} A_i a_{j-1}e^{w_i} + \sum_{i=1}^{m} A_i b_{j-2,i}e^{2w_i} \tag{12}$$

If this process is continued successively for all $b_{i,j}$, then we have

$$= \sum_{k=0}^{j} \sum_{i=1}^{m} A_i \rho_{j-k} e^{kw_i} \tag{13}$$

From Eq. 1, it is clear that

.

$$\sum_{k=0}^{j} \sum_{i=1}^{m} A_i \rho_{j-k} e^{kw_i} = \sum_{k=0}^{J} a_{j-k} y_k \tag{14}$$

Substituting this expression back into the inner sum of Eq. 7 gives

$$\sum_{j=0}^{m} a_j Y(z) z^{m-j} - \sum_{j=0}^{m-1} z^{m-j} \sum_{k=0}^{j} a_{j-k} y_k = 0 \tag{15}$$

By rearranging the sums Eq. 15 can be written as

$$\sum_{j=0}^{m} a_j Y(z) z^{m-j} - \sum_{j=0}^{m-1} a_j \sum_{k=0}^{m-j-1} y_k z^{m-j-k} = 0 \tag{16}$$

Again rearranging and factoring gives the final form

357

$$\sum_{j=0}^{m-1} a_j \left[Y(z)z^{m-j} - \sum_{k=0}^{m-j-1} y_k z^{m-j-k} \right] + a_m Y(z) = 0 \qquad (17)$$

Equation 17 can be easily inverse transformed by invoking two theorems of Z-transforms, namely

$$Z[y_{k+m}] = Y(z)z^m - \sum_{k=0}^{m-1} z^{m-k} y_k \qquad (18)$$

and

$$Z[ay_k] = aY(z) \qquad (19)$$

The inverse Z-transform of Eq. 17 is thus given by

$$\sum_{j=0}^{m-1} a_j y_{k+m-j} + a_m y_k = 0 \qquad (20)$$

Since this must hold for any value of k, then Eq. 20 is just as valid for y_{k-m} as for y_k. Shifting the time index by m and combining terms gives

$$\sum_{j=0}^{m} a_j y_{k-j} = 0 \qquad (21)$$

which is identical to Eq. 2. Thus it is proved that Eq. 1 and Eq. 2 are equivalent.

The equivalence of Eq. 1 and Eq. 2 is significant. Many real data sets can be modeled with linear combinations of exponentials. Since such a function exhibits autoregressive characteristics, exponential parameters can be conveniently estimated from measured data. The current research is involved in estimation of the vibrational parameters of a beam using spatial data. The shape of a vibrating beam can be modeled using exponential functions. In fact, classical Euler-Bernoulli beam theory explicitly describes beam mode shapes in terms of exponential functions. Thus an autoregressive approach can be used obtain parameter estimates of the dynamic characteristics of the beam.

A3.1 PC-MATLAB SCRIPT FILE LISTING FOR EXPERIMENT 1

```
% spp_2.m --> Computes frequency variance for SPP & noise
%
% Written by: Mark Archibald  10/15/92
%
% Required Variables:      None
%
% Required Functions:      gencircu --> Generates Delayed          %
                                        Circulent Matrix


nave = 50                        % Number of Averages
SNR  = [40 20 0];                % Signal-to-Noise Ratios
nnoise = length(SNR);
dt   = .001;                     % Sample Increment
t = (0:dt:199*dt)';              % Independent Variable
N = length(t);
f = (1:499)';                    % Frequency Vector
fD = f*dt;                       % SPSR Vector
F  = [];

rand('normal');

for k = 1:nnoise,                                % Loop For Each SNR
   for i=1:length(f);                            % Loop For Each Frequency
       v = sin(2*pi*f(i)*t);
       ms = (v'*v)/N;
       var = ms/(10^(SNR(k)/10));
       for j = 1:nave,                           % Loop For Averages
           r = sqrt(var)*rand(N,1);
           y = v+r;
           Y = gencircu(y,3,1);
           Y = [Y;Y(:,3:-1:1)];
           [u,s,vv] = svd(Y,0);
           poles = roots(vv(:,3));
           freq = sort(angle(poles))/(2*pi*dt);
           F = [F;freq(2)];
       end
```

360

```
        fvar(i,k) = std(F)^2;              % Compute Variance
        F = [];
    end
end

plot(fD,fvar);
title('FREQUENCY ERROR VS SAMPLE RATE');
xlabel('SIGNAL PERIOD / SAMPLE RATE RATIO');
ylabel('FREQUENCY VARIANCE');
```

A3.2 PC-MATLAB SCRIPT FILE LISTING FOR EXPERIMENT 2

```
% D_spp.m Computes Frequency variance for values of Delay Factor D
%
% Written by: Mark Archibald    10/15/92
%
% Required Variables:       None
%
% Required Functions:       gencircu --> Generates Delayed Circulent
%                                           Matrix

nave = 50;                   % Number of Averages
SNR  = [40 20 0];            % Signal-to-Noise Ratios
nnoise = length(SNR);
dt = 0.001;                  % Sample Interval
t = (0:dt:499*dt)';          % Independent Variable
N = length(t);
f = 2;                       % Signal Frequency
D = (1:125)';                % Delay Factor Vector
rand('normal');
v = sin(2*pi*f*t);           % Sinusoidal Signal
ms = (v'*v)/N;               % Mean Square Value of Signal

for k = 1:nnoise,                            % Loop for Each SNR
    disp(k);
    sd = sqrt(ms/(10^(SNR(k)/10))); % Std Deviation of Noise
    for j=1:nave,                            % Loop for Averaging
        r = sd*rand(N,1);                % Generate Noise
        y = v+r;
        for i=1:length(D),               % Loop for Delay Factors
            Y = gencircu(y,3,D(i));     % Compute Frequency
            Y = [Y;Y(3:-1:1)];
            [u,s,vv] = svd(Y,0);
            poles = roots(vv(:,3));
            freq  = sort(angle(poles))/(2*pi*dt*D(i));
            F(j,i) = freq(2);                % Frequency Estimate
        end
    end
    fvar(k,:) = std(F) .^2;              % Compute Variance
end
```

```
semilogy(D,fvar(1,:),'-',D,fvar(2,:),'--',D,fvar(3,:),':');
title('EFFECT OF DELAY FACTOR ON FREQUENCY ESTIMATION');
xlabel('DELAY FACTOR D');
ylabel('FREQUENCY VARIANCE');
hold on;
legend(.5,.95,'40 dB SNR','-');
legend(.5,.90,'20 dB SNR','--');
legend(.5,.85,' 0 dB SNR',':');
hold off;
```

A3.3 PC-MATLAB SCRIPT FILE LISTING FOR INCDOTLS ALGORIGHM

```
% Incremental Delay DOTLS Method (incdotls)
%
% Written By: Mark Archibald   11/16/92  v1.0
%
% Required Variables:      y --> Data Vector
%                          dt --> Sample Interval
%
% Produces averaged frequencies (favg) along with number of
% occurances of each frequency (si).
%
% NOTE: This program assumes that no sinusoidal frequencies are
% close to the Nyquist frequency. For measured data, use of
% anti-aliasing filters will ensure that this requirement is met.
%


D      = (1:30)';        % May Need To Change These Parameters
tol_fac = 80;            %

p = input('Input Model Order    : ');


c  = p+1;
ld = length(D);

[poles,DT]  = dotls(y,c,D(1),p,dt);   % Initial Freq. Estimate
poles       = poles.*finite(ones(p,1)./imag(poles));
[favg,damp] = pol2fre(poles,DT);

fsum    = [favg ones(p,1)];
fnewsum = fsum;

for d=2:ld,
    [poles,DT] = dotls(y,c,D(d),p,dt);    % New Frequency Estimates
    poles      = poles.*finite(ones(p,1)./imag(poles));
    [f,damp]   = pol2fre(poles,DT);

    tol  = 1/(tol_fac*DT);              % Check For Aliases
    fa   = alias(favg,DT);
    fnew = unalias(f,fa,tol,DT);
```

364

```
    for i=1:p,                          % Update fsum
        if fnew(i,1) == 0,
            break;
        elseif fnew(i,2) > 0,
            k = fnew(i,2);
            fnewsum(k,1) = fsum(k,1) + fnew(i,1);
            fnewsum(k,2) = fsum(k,2) + 1;
            favg(k)      = fnewsum(k,1)/fnewsum(k,2);
        else,
            fnewsum = [fnewsum;fnew(i,1) 1];
            favg    = [favg;fnew(i,1)];
        end
    end
    fsum = fnewsum;
end

[si,i] = sort(fnewsum(:,2));
favg   = favg(i);
k      = length(i);
si     = si(k:-1:1);
favg   = favg(k:-1:1);
disp([(1:k)' favg si]);




function [poles,DT] = dotls(y,c,D,p,dt);
%
% Delayed Oversize Total Least Squares  (DOTLS)
%
% Written by: Mark Archibald    11/11/92
%
% Input Arguments:           y  --> Data Vector
%                            c  --> Column Dimension
%                            D  --> Matrix Delay
%                            p  --> Model Order
%                            dt --> Sample Interval
%
% Output Arguments:          poles --> System Poles
%                            DT    --> Delayed Sample Interval
%
% Required Functions:        gencircu --> Generate Circulent Matrix
```

365

```
%                    solvea   --> Solve For AR Coefficents (OTLS)
%

DT = D*dt;
R  = gencircu(y,c,D);
[u,s,v] = svd(R,0);
A = solvea(v,p);
poles = roots(A);
```

```
function R = gencircu(y,c,D);
%
% Written by: Mark Archibald     04-29-92
%
% Variables Required: y --> Data Vector
%                     c --> Number of Columns
%                     D --> Delay Lag
%

N = max(size(y));

for i=1:c,
   R(:,i) = y( (c-i)*D+1 : N-(i-1)*D );
end

function  a = solvea(v,p);
%
% Derives AR Coefficients
% Written By: Mark Archibald  10/27/91
%
% Input Arguments:     v --> Right Singular Vector Matrix
%                      p --> Model Number
%
% Output Arguments:    a --> AR coefficients
%

c = length(v);

W = v(:,p+1:c);
C = W(p+2:c,1:c-p-1)\(-W(p+2:c,c-p));
C = [C;1];
a = W*C;
a = a(1:p+1);




function [freq,damp] = pol2fre(poles,dt);
%
% Computes Frequencies and Damping Ratios from Poles
%
% Written By: Mark Archibald    11/6/92
```

```
%
% Variable:        poles --> System Poles
%                  freq  --> Frequencies
%                  damp  --> Damping Ratios
%                  dt    --> Sample Interval
%

om   = angle(poles);
al   = -log(abs(poles));
damp = sqrt(al.^2 ./ (al.^2 + om.^2));
freq = (om ./ sqrt(1-damp.^2)) /(2*pi*dt);




function fa = alias(f,DT);
%
%    Compute aliased frequencies
%
%    Written By: Mark Archibald    11/10/92
%
%    Input Arguments:        f  --> True Frequencies
%                            DT --> Delay Sample Interval
%
%    Output Arguments:       fa --> Aliased Frequencies
%

p   = length(f);
fny = 1/(2*DT);
fa  = f;

fo = rem(f,fny);
n  = abs((f-fo)/fny);

for i=1:p,
   if abs(f(i)) > fny,
      if ((-1)^n(i)) < 0,
         fa(i) = sign(fo(i))*(fny-abs(fo(i)));
      else
         fa(i) = fo(i);
      end
   end
```

end

```
fa = [fa n];
```

.

```
function F = unalias(f,fa,tol,DT);
%
% Compares Old and New Frequencies and Removes Aliases
%
% Written By: Mark Archibald    11/10/92
%                               11/15/92 v2.0    (Matching Index)
%
% Input Arguments:         f   --> Frequency Vector
%                         fa  --> Pre-Aliasd Frequencies, Alias Index
%                 tol --> Comparison Tolerance
%                         DT  --> Delayed Sample Interval
%
% Output Arguments:        F   --> True Frequencies, Matching fa Index
%

p   = length(f);
fny = 1/(2*DT);
faw = [fa, (1:length(fa))'];
I   = zeros(p,1);

for i=1:p,
    [pw,dummy] = size(faw);
    d = abs(f(i)*ones(pw,1) - faw(:,1));
    [m,k] = min(d);
    if finite(m) == 0,
        F(i) = 0;
    elseif m < tol,
        n    = faw(k,2);
        F(i) = sign(f(i))*(fny*n + rem(n,2)*fny + (-1)^n*abs(f(i)) );
        I(i) = faw(k,3);
        faw  = [faw(1:k-1,:);faw(k+1:pw,:)];
    else
        F(i) = f(i);
    end
end
F=[F' I];
```

370

A5.1 PC-MATLAB SCRIPT FILES FOR PSMA

The PSMA code requires two parts. DOTLS utilizes the delayed oversize total least squares method to find the poles, and hence the spatial frequencies, of the beam. The second program, SOLVEC, solves for the modal coefficients.

DOTLS
```
% Delayed Oversize Total Least Squares Method (DOTLS)
%
% Written by: Mark Archibald    10-8-90       11/14/92
%
% Variables Required:     y  --> Data Vector
%                        dt --> Sample Interval
%


c = input('Input column dimension: ');
D = input('Input Matrix Delay (D): ');


R = gencircu(y,c,D);


DT = dt*D;


[u,s,v] = svd(R,0);


diag(s)
p = input('Input Model Order: ');


a = solvea(v,p);


poles = roots(a);


clear R;


lpole  = log(poles);


disp('poles              lpole');
disp([poles lpole]);
```

SOLVEC
```
% Solve for Beam Constants  (solvec)
```

```
%
% Written By:  Mark Archibald  10-8-90
%
% Required Variables:  x --> x-coord Vector
%                      b --> Discrete Beta value (Beta*DX)
%                      y --> Data vector
%                      DX --> Delayed Sample Interval
%

mat  = [];

j = sqrt(-1);
m = length(b);

B = [b.';-b.';j*b.';-j*b.']/DX;
B = B(:);

C = exp(x*B.');                    % Solve for Amplitudes
A    = C\y;

ynew = real(C*A);                  % Compute Residual
R    = y-ynew;
res  = (R'*R)
pause;

plot(x,R);
grid;
xlabel('BEAM POSITION, in.');
ylabel('RESIDUAL AMPLITUDE');
pause;

plot(x,y,'.',x,ynew,'-');
grid;
hold on;
legend(.1,.95,'MEASURED',':');
legend(.1,.90,'FITTED   ','-');
xlabel('BEAM POSITION, in.');
ylabel('VELOCITY AMPLITUDE');
hold off;
```

A5.2 PC-MATLAB SCRIPT FILE FOR LSSD

```
% LSSD -- Least Squares Spatial Domain Method
%
% Written By: Mark Archibald     12/15/92
%                                12/31/92  v1.1
%
% v1.1 --> Updated to reflect theory from Forsythe and Moler
%
%
% Required Variables:   b --> Initial Frequency Estimates
%                       y --> Data Vector
%                       x --> Independent Variable Vector
%

disp(' ');
disp('NEWTONS METHOD (BEAMS)');
disp(' ');


tol = 10e-13;


m    = length(b);
N    = length(y);
l    = 4*m;
dres = tol+1;
ores = y'*y;
j    = sqrt(-1);

if x(1) ~= 0,
   x = x - x(1)*ones(N,1);
   disp('Correcting X-Coordinate Origin');
   disp(' ');
end;

B    = [b.';-b.';j*b.';-j*b.'];
B    = B(:);
Ei   = exp(x*B.');
ab   = [Ei\y;b];
ynew = real(Ei*ab(1:4*m));
R    = y-ynew;
```

```
a   = zeros(4,m);
Pi = [];
Ti = [];
PE = [];

count = 0;

while dres > tol,
    a(:) = ab(1:4*m);
    ap   = diag([1;-1;j;-j])*a;
    at   = diag([1;1;-1;-1])*a;

    for i=1:m,                  %  Compute Derivative Functions
        k=4*(i-1)+1;
        ex = exp(x*B(k:k+3).');
        Pi(:,i) = ex*ap(:,i).*x;
        Ti(:,i) = ex*at(:,i).*(x.^2);
    end

    Pi = real(Pi);
    Ti = real(Ti);


    E  = Ei.'*Ei;                   % Sub-Matrix E

    P = Pi'*Pi - diag(Ti'*R);       % Sub-Matrix P

    Rx = ((R.*x)'*Ei).';            % Sub-Matrix PE
    pe = Pi.'*Ei;
    for i=1:m,
        k = 4*(i-1)+1;
        d = pe(1:m,k:k+3).';
        PE(:,i) = d(:);
        PE(k:k+3,i) = PE(k:k+3,i) + Rx(k:k+3).*[-1;1;-j;j];
    end

    J = [E PE; PE.' P];             % Jacobian Matrix

    F = [Ei.'*R;Pi.'*R];            % Evaluate Functions

    ab = ab + inv(J)*F;             % Update Parameters
```

374

```
b   = ab(4*m+1:5*m);
B = [b.';-b.';j*b.';-j*b.'];
B = B(:);
Ei = exp(x*B.');
ynew = real(Ei*ab(1:4*m));
R    = y-ynew;
res  = (R'*R);
dres = abs(res-ores);
ores = res;

count = count + 1;

disp(' ');
disp(count);
disp([res dres]);
disp(real(b'));
disp(cond(J));
end

disp(' ');
disp(' ');
count
bi  = real(b')
res
ab(1:4)


plot(x,y,'.',x,ynew,'-',x,R,'-');
title('MEASURED AND FITTED DATA');
xlabel('BEAM POSITION (IN)');
ylabel('AMPLITUDE');
grid;
```

A5.3 PC-MATLAB SCRIPT FILE FOR CONVERGENCE ANALYSIS

```
% res_ana --> Minimizing Function Analysis for LSSD Method
%
%           Plots Objective function versus spatial frequency
%
% Written By: Mark Archibald   12-29-92  v1.0
```

```
%                          3-2-93   v1.1
%
% v1.1 --> Correct Mistakes in Derivative and Objective Calculation
%
%  Required Variables:  y --> Data Vector
%                       x --> Independent Variable Vector
%                       b --> True Spatial Frequencies
%                       L --> Length of Beam
%                       M --> Normal Mode Shapes
%                       C --> Modal Coefficients
%                     mwf --> Modal Weighting Factor
%

disp('Minimizing Function Analysis for LSSD Method');

mode = ['MODE 1 ';'MODE 2 ';'MODE 3 ';'MODE 4 ';'MODE 5 ';'MODE 6 '];

i
% = input('Input Objective Mode: ');
j = sqrt(-1);
b = Bl/L;
m = length(b);

ibo = 0.8*b(i);
fbo = 1.2*b(i);
dbo = (fbo-ibo)/100;
bo  = (ibo:dbo:fbo)';          % Spatial Frequency Variations

S  = zeros(length(bo),1);
D  = zeros(length(bo),1);
Ss = zeros(length(bo),1);
Ds = zeros(length(bo),1);

DC = [C(:,1) -C(:,2) j*C(:,3) -j*C(:,4)];
y  = M*mwf;

Mi = M;

for k=1:length(bo),
   Bo = [bo(k) -bo(k) j*bo(k) -j*bo(k)];
   ex = exp(x*Bo);
```

376

```
    Cs  = ex\y;
    DCs = [Cs(1); -Cs(2); j*Cs(3); -j*Cs(4)];
    Pi  = x.*(ex*DCs) ;
    ys  = real(ex*Cs);

    R     = y-ys;                    % LS Coefficients
    Ss(k) = R.'*R;
    Ds(k) = -2*(R.'*Pi);

    Mi(:,i) = real(ex*C(i,:).') ;
    Pi      = x.*(ex*DC(i,:).')*mwf(i) ;

    ys    = Mi*mwf;                  % True Coefficients
    R     = y-ys;
    S(k) = R.'*R;
    D(k) = -2*(R.'*Pi);
end

plot(bo,S,'-',bo,D,':');
title([mode(i,:) 'OBJECTIVE FUNCTION']);
xlabel('SPATIAL FREQUENCY');
ylabel('SUM OF SQUARED RESIDUALS');
hold on;
legend(.1,.95,'RESIDUAL','-');
legend(.1,.90,'DERIVATIVE',':');
hold off;
```

A5.4 PC-MATLAB SCRIPT FILE FOR 2D CONVERGENCE ANALYSIS

```
% res2d_ana --> 2D Minimizing Function Analysis for LSSD Method
%
%      Generates Mesh of Objective function versus spatial frequencies
%
% Written By: Mark Archibald    3-4-93   v1.0
%
%
% Required Variables:  y --> Data Vector
%                      x --> Independent Variable Vector
%                      Bl --> True Spatial Frequencies
```

377

```
%               L --> Length of Beam
%               M --> Normal Mode Shapes
%               C --> Modal Coefficients
%             mwf --> Modal Weighting Factor
%

disp('2D Minimizing Function Analysis for LSSD Method');
disp(' ');

mode = ['MODE 1 ';'MODE 2 ';'MODE 3 ';'MODE 4 ';'MODE 5 ';'MODE 6 '];

index = input('Input Two Objective Modes [i,l]: ');
i = index(1);
l = index(2);
j = sqrt(-1);
b = Bl/L;
m = length(b);

iboi = 0.8*b(i);
fboi = 1.2*b(i);
dboi = (fboi-iboi)/25;
boi  = (iboi:dboi:fboi)';          % Spatial Frequency Variations
ibol = 0.8*b(l);
fbol = 1.2*b(l);
dbol = (fbol-ibol)/25;
bol  = (ibol:dbol:fbol)';          % Spatial Frequency Variations

S  = zeros(length(boi),length(bol));
Di = zeros(length(boi),length(bol));
Dl = zeros(length(boi),length(bol));
Da = zeros(length(boi),length(bol));

Ss  = zeros(length(boi),length(bol));
Dis = zeros(length(boi),length(bol));
Dls = zeros(length(boi),length(bol));
Das = zeros(length(boi),length(bol));

DC = [C(:,1) -C(:,2) j*C(:,3) -j*C(:,4)];
y  = M*mwf;

Mi = M;
```

```
for k=1:length(boi),
    for p=1:length(bol),
        Boi = [boi(k) -boi(k) j*boi(k) -j*boi(k)];
        exi = exp(x*Boi);
        Bol = [bol(p) -bol(p) j*bol(p) -j*bol(p)];
        exl = exp(x*Bol);

        Cs  = [exi exl]\y;
        DCsi = [Cs(1); -Cs(2); j*Cs(3); -j*Cs(4)];
        DCsl = [Cs(5); -Cs(6); j*Cs(7); -j*Cs(8)];
        Pi  = x.*(exi*DCsi) ;
        Pl  = x.*(exl*DCsl) ;
        ys  = real([exi exl]*Cs);

        R       = y-ys;               % LS Coefficients
        Ss(k,p) = R.'*R;
        Dis(k,p) = real(-2*(R.'*Pi));
        Dls(k,p) = real(-2*(R.'*Pl));

        Mi(:,i) = real(exi*C(i,:).') ;
        Mi(:,l) = real(exl*C(l,:).') ;
        Pi      = x.*(exi*DC(i,:).')*mwf(i) ;
        Pl      = x.*(exl*DC(l,:).')*mwf(l) ;


        ys      = Mi*mwf;             % True Coefficients
        R       = y-ys;
        S(k,p)  = R.'*R;
        Di(k,p) = -2*(R.'*Pi);
        Dl(k,p) = -2*(R.'*Pl);
    end
end

Da  = sqrt(Di.^2 + Dl.^2);
Das = sqrt(Dis.^2 + Dls.^2);

mesh(S);
title([mode(i,:) mode(l,:) 'OBJECTIVE FUNCTION']);

mesh(Da);
title([mode(i,:) mode(l,:) 'MAGNITUDE OF SLOPE']);
```

379

```
mesh(Ss);
title([mode(i,:) mode(l,:) 'OBJECTIVE FUNCTION -- LS COEFFICIENTS']);

mesh(Das);
title([mode(i,:) mode(l,:) 'MAGNITUDE OF SLOPE -- LS COEFFICIENTS']);
```

A5.5 PC-MATLAB SCRIPT FILE FOR EMPIRICAL CONVERGENCE ANALYSIS

```
% converg_ana --> LSSD Empirical Convergence Analysis
%
%  Written by: Mark Archibald          3/12/93
%
% Generates Synthesized beam operating shape using Beamsig
% Determines minimum and maximum inital frequency for convergence
%

disp(' ');
disp('LSSD Empirical Convergence Analysis');
disp(' ');

rand('normal');
SNR = [20;30;40];
Di = (0.9:-0.1:0.1);
Dj = (0.09:-0.01:0.01);
Li = (1.1:.1:1.9);
Lj = (0.01:0.01:0.09);
wi = [110;300;590;970;1450;2020];

low  = zeros(3,6);
high = zeros(3,6);

for mod = 1:6;
    w = wi(mod);
    [M,mwf,x,C,B] = beam(w);
    N = length(M);
    v = M*mwf;
    ms = (v'*v)/N;
    tb = B(mod);
```

```
for noise = 1:3,
    snr = SNR(noise);
    sd = sqrt(ms/(10^(snr/10)));
    y  = v + sd*rand(N,1);

    for i=1:9,              % Low Convergence Limit
        bi = Di(i)*tb;
        [ab,s] = lssd(bi,y,x);
        if s == -1, break, end;
    end
    I = Di(i)
    for j=1:9,
        F  = I + Dj(j);
        bi = F*tb;
        [ab,s] = lssd(bi,y,x);
        if s == -1, break, end;
    end
    low(noise,mod) = F*100;

    for i=1:9,              % High Convergence Limit
        bi = Li(i)*tb;
        [ab,s] = lssd(bi,y,x);
        if s == -1, break, end;
    end
    I = Li(i-1);
    for j=1:9,
        F  = I + Lj(j);
        bi = F*tb;
        [ab,s] = lssd(bi,y,x);
        if s == -1, break, end;
    end
    high(noise,mod) = F*100;
  end;
end;

disp('Columns are Modes 1:6, Rows are SNR 20:30:40 ');
disp(' ');
disp(low);
disp(high);
```

A6.1 PC-MATLAB SCRIPT FILES FOR BCBA

```
% BCBA  --> Boundary Condition Beam Analysis
%
% Written By:  Mark Archibald    4/19/93
%                               7/30/93 Corrected
%
% Program Tasks:
%    1. Load Data Files and Compute Derivatives
%    2. Compute Boundary Conditions, t j m c k
%    3. Solve Frequencies by DET(L) = 0
%    4. Solve for Coefficients & Normalize
%    5. Solve for Modal Weighting Factor
%
%


disp(' ');
disp('     BCBA ');
disp(' ');

%L = input('Input Beam Length: ');      % Input Beam Param.
%e = input('Input Beam EI/(rho A): ');
%e = sqrt(e);

L = 54.875;
e = sqrt(1.99e8);

% PART 1: Load Data & Compute Derivatives
disp(' ');
disp('Load Data & Compute Derivatives');
disp(' ');

vo = zeros(6,4);
vl = zeros(6,4);
w  = zeros(6,1);

%load \matlab\data\modelex;
%w(1) = 17*2*pi;             % Excitation Frequency
%b = .086;                   % Initial Frequency Guess
%y = mean(y')';
%lssd4;                      % Fit Model to Data
```

```
%C = ab(1:4);
%el = exp(L*B.');
%oe = ones(1,4);
%vo(1,:) = [ynew(1) oe*(C.*B) oe*(C.*B.^2) oe*(C.*B.^3)];
%vl(1,:) = [ynew(N) el*(C.*B) el*(C.*B.^2) el*(C.*B.^3)];


%load \matlab\data\mode2;
%w(2) = 47*2*pi;              % Excitation Frequency
%b = .1442;                   % Initial Frequency Guess
%y = mean(y')';
%lssd4;                       % Fit Model to Data
%C = ab(1:4);
%el = exp(L*B.');
%oe = ones(1,4);
%vo(2,:) = real([ynew(1) oe*(C.*B) oe*(C.*B.^2) oe*(C.*B.^3)]);
%vl(2,:) = real([ynew(N) el*(C.*B) el*(C.*B.^2) el*(C.*B.^3)]);


%load \matlab\data\mode3;
%w(3) = 93*2*pi;              % Excitation Frequency
%b = .1979                    % Initial Frequency Guess
%y(111,2) = 1.44;
%y = mean(y')';
%lssd4;                       % Fit Model to Data
%C = ab(1:4);
%el = exp(L*B.');
%oe = ones(1,4);
%vo(3,:) = [ynew(1) oe*(C.*B) oe*(C.*B.^2) oe*(C.*B.^3)];
%vl(3,:) = [ynew(N) el*(C.*B) el*(C.*B.^2) el*(C.*B.^3)];


pack;


load \matlab\data\mode4;
w(4) = 154*2*pi;             % Excitation Frequency
b = .2542;                   % Initial Frequency Guess
y = mean(y')';
lssd4;                       % Fit Model to Data
C = ab(1:4);
el = exp(L*B.');
oe = ones(1,4);
vo(4,:) = real([ynew(1) oe*(C.*B) oe*(C.*B.^2) oe*(C.*B.^3)]);
vl(4,:) = real([ynew(N) el*(C.*B) el*(C.*B.^2) el*(C.*B.^3)]);
```

383

```
load \matlab\data\mode5;
w(5) = 230.9*2*pi;          % Excitation Frequency
b = .3112;                  % Initial Frequency Guess
y = mean(y')';
lssd4;                      % Fit Model to Data
C = ab(1:4);
el = exp(L*B.');
oe = ones(1,4);
vo(5,:) = [ynew(1) oe*(C.*B) oe*(C.*B.^2) oe*(C.*B.^3)];
vl(5,:) = [ynew(N) el*(C.*B) el*(C.*B.^2) el*(C.*B.^3)];

load \matlab\data\mode6;
w(6) = 323.2*2*pi;          % Excitation Frequency
b = .3684;                  % Initial Frequency Guess
y = mean(y')';
lssd4;                      % Fit Model to Data
C = ab(1:4);
el = exp(L*B.');
oe = ones(1,4);
vo(6,:) = [ynew(1) oe*(C.*B) oe*(C.*B.^2) oe*(C.*B.^3)];
vl(6,:) = [ynew(N) el*(C.*B) el*(C.*B.^2) el*(C.*B.^3)];

vo = real(vo);
vl = real(vl);

clear Ti;
clear Ei;
clear Pi;
clear R;

pack;

% PART 2: Solve for Boundary Conditions
disp('Solve for Boundary Conditions');
disp(' ');

j = sqrt(-1);

% find Kt and J
mato = [vo(:,2) -vo(:,2).*(w.^2)];
veco = vo(:,3);
```

```matlab
matl = [-vl(:,2) vl(:,2).*(w.^2)];
vecl = vl(:,3);

tjo = nnls(mato,veco);
tjl = nnls(matl,vecl);

% find m and k
mato = [ vo(:,1).*(w.^2) -vo(:,1)];
matl = [-vl(:,1).*(w.^2)  vl(:,1)];
veco = vo(:,4);
vecl = vl(:,4);

mko = nnls(mato,real(veco));
mkl = nnls(matl,real(vecl));

% find c
co = nnls(-vo(:,1).*w,imag(veco));
cl = nnls( vl(:,1).*w,imag(vecl));

mcko = [mko(1); co; mko(2)];
mckl = [mkl(1); cl; mkl(2)];


% Save Result
t3tjmck = [tjo tjl;mcko mckl];

% PART 3: Solve DET(L) = 0
disp('Solve DET(L) = 0');
disp(' ');

A = [1 1 1 1;1 -1 j -j;1 1 1 1;1 -1 j -j];
B = [1 -1 -j j;1 1 -1 -1;1 -1 -j j;1 1 -1 -1];
D = zeros(4);
bi = (.01:.005:.4)';
n  = length(bi);
z  = zeros(n,1);
on = ones(2,4);
j  = sqrt(-1);

for i=1:n,
    b = bi(i);
```

```
        D(1,1) = (b^3)/([e*b^4  -j*e*b^2 -1]*mcko);
        D(2,2) = b/([1 -e*b^4]*tjo);
        D(3,3) = (b^3)/([-e*b^4 j*e*b^2 1]*mckl);
        D(4,4) = b/([-1 e*b^4]*tjl);
        ex = exp(L*[b -b j*b -j*b]);
        LAM = A.*[on;ex;ex] - D*(B.*[on;ex;ex]);
        z(i) = det(LAM);
end


plot(bi,real(z),bi,imag(z));
grid;



% For Real Modes Only:
bmode = [];

for i = 1:n-1,
    if sign(imag(z(i))) ~= sign(imag(z(i+1))),
        bl = bi(i);
        bh = bi(i+1);
        bmode = [bmode;findroot(bl,bh,e,mcko,mckl,tjo,tjl,L)];
    end;
end;



% Save Result
t3beta = bmode*L;

% PART 4: Solve for coefficients
disp('Solve for normal mode shapes');
disp(' ');

A = [1 1 1 1;1 -1 j -j;1 1 1 1;1 -1 j -j];
B = [1 -1 -j j;1 1 -1 -1;1 -1 -j j;1 1 -1 -1];
D = zeros(4);
on = ones(2,4);
j  = sqrt(-1);

n = length(bmode);

C = zeros(n,4);
```

```
C(:,1) = ones(n,1);

for i=1:n,
    b = bmode(i);
    D(1,1) = (b^3)/([e*b^4  -j*e*b^2 -1]*mcko);
    D(2,2) = b/([1 -e*b^4]*tjo);
    D(3,3) = (b^3)/([-e*b^4 j*e*b^2 1]*mckl);
    D(4,4) = b/([-1 e*b^4]*tjl);
    ex = exp(L*[b -b j*b -j*b]);
    LAM = A.*[on;ex;ex] - D*(B.*[on;ex;ex]);
    [u,s,v] = svd(LAM);
    vec = v(:,4);
    C(i,:) = vec.';
    phi(:,i) = real(exp(x*[b -b j*b -j*b])*vec);
    phi(:,i) = phi(:,i)*sqrt(L/(phi(:,i)'*phi(:,i)));

end

% Save Result
t3phi = phi;

plot(x,phi);



% PART 5: Solve for Modal Weighting Factors
disp('Solve for modal weighting factors');
disp(' ');

load \matlab\data\mode1ex;
y = mean(y')';
mwf1 = phi\y;

load \matlab\data\mode2;
y = mean(y')';
mwf2 = phi\y;

load \matlab\data\b50;
y = mean(y')';
mwf3 = phi\y;

load \matlab\data\b120;
```

```
y = mean(y')';
mwf5 = phi\y;

load \matlab\data\mode4;
y = mean(y')';
mwf6 = phi\y;

load \matlab\data\mode6;
y = mean(y')';
mwf9 = phi\y;
```

A7.1 PC-MATLAB SCRIPT FILE FOR BEAM SIMULATION PROGRAM (BEAMSIG)

BEAMSIG

```
% Generate Simulated Free-Free Beam Response to
%   Harmonic Forcing Function
%
%   Forcing Function:   P sin(wt)
%   Forcing Location:   a
%   Beam Parameters :   I,E,m
%   Spatial Freq.   :   B
%   Natural Freq.   :   wn
%   Normal Mode     :   M

%   Signal/Noise Rat:   SNR
%   Modal Weight Fac:   mwf

W = 3.0;          % in        width
H = 0.25;         % in        height
L = 54.;          % in       length
E = 27.7e6;        % psi       Modulus of Elasticity
m = 0.28;          % lb/in^3   Specific Weight


P = 1;
a = 0;

Bl = [4.730041; 7.853205;10.995608;14.137165;17.2787;20.4203];

m  = m*H*W*L/386.4;
I  = W*H^3/12;
wn = Bl .^2 * sqrt(E*I/(m*L^3));

N  = 450
dx = L/N;
x  = (0:dx:L-dx)';
mode = 'Six Modes'
```

```matlab
SNR = input('Input SNR (dB) : ');
w   = input('Input Forcing Frequency (rad/s): ');
C   = zeros(6,4);

j = sqrt(-1);

for i = 1:6,
    %   Generate Constants
    Q = (exp(Bl(i)) -.5*((1-j)*exp(j*Bl(i)) +(1+j)* ...
        exp(-j*Bl(i)) ))/(-(exp(-Bl(i)) -.5*( (1+j)*...
        exp(j*Bl(i)) + (1-j)*exp(-j*Bl(i)) )));
    C1 = 1;
    C2 = Q;
    C3 = ( (1+Q) + (Q-1)*j )/2;
    C4 = ( (1+Q) - (Q-1)*j )/2;

    %   Normalize Constants
    B = Bl(i)/L;
    H = 2*C2*L + 2*C3*C4*L + exp(2*Bl(i))/(2*B) + ...
        C2^2*exp(-2*Bl(i))/(-2*B);
    H = H + C3^2*exp(2*j*Bl(i))/(2*B*j) + ...
        C4^2*exp(-2*j*Bl(i))/(-2*B*j);
    H = H + 2*C3*exp(Bl(i)*(1+j))/(B*(1+j)) + ...
        2*C4*exp(Bl(i)*(1-j))/(B*(1-j));
    H = H + 2*C2*C3*exp(-Bl(i)*(1-j))/(-B*(1-j)) ;
    H = H + 2*C2*C4*exp(-Bl(i)*(1+j))/(-B*(1+j)) ...
        - 1/(2*B) - C2^2/(-2*B) ;
    H = H - C3^2/(2*B*j) - C4^2/(-2*B*j) - 2*C3/(B*(1+j)) - ...
        2*C4/(B*(1-j));
    H = H - 2*C2*C3/(-B*(1-j)) - 2*C2*C4/(-B*(1+j));

    C(i,1) = sqrt(L/H);
    C(i,2) = C(i,1)*C2;
    C(i,3) = C(i,1)*C3;
    C(i,4) = C(i,1)*C4;

    M(:,i) = C(i,1)*exp(B*x) + C(i,2)*exp(-B*x) + ...
        C(i,3)*exp(j*B*x) + C(i,4)*exp(-j*B*x);

    %       Compute Modal Weighting Factors
```

```
    a_index  = 1 + a*N/L;
    a_actual = x(a_index);

    mwf(i) = P*w*M(a_index,i) / (m*(wn(i)^2 - w^2));
end

% Generate Operating Shape
mwf = mwf';
y   = M*mwf;

if SNR ~= 99,
    ms = sum([y .* y])/N;
    var = ms/(10^(SNR/10));
    rand('normal');
    r = sqrt(var)*rand(N,1);
    y = y+r;
end

plot(x,y);
```

A7.2 PC-MATLAB SCRIPT FILE FOR PSMA ERROR ANALYSIS

```
% anapsma --> Analysis of PSMA Method
%
% Written by: Mark Archibald      3/12/93
%

disp(' ');
disp('PSMA Analysis Program -- ANAPSMA');
disp(' ')

mod = input('Input Mode Number: ');
SNR = input('Input SNR: ');

wi = [110;300;590;970;1450;2020];
w  = wi(mod);

[M,mwf,x,C,B] = beam(w);

N  = length(M);
dx = x(2)-x(1);
```

```
p  = 4;
tb = B(mod)*ones(4,1);
numavg = 3;
rand('normal');

v  = M*mwf;        %M(:,mod)*mwf(mod);
ms = (v'*v)/N;
sd = sqrt(ms/(10^(SNR/10)));

D  = [10 20 30 40];             %(1:3:10)';  %28)';
c  = (5:9)';      %14)';
ND = length(D);
Nc = length(c);
DC = zeros(ND,Nc);
TDC = zeros((Nc*DC),numavg);

for n = 1:numavg,
   for i=1:ND,
      for j=1:Nc,
         y = v + sd*rand(N,1);
         [poles,DX] = dotls(y,c(j),D(i),p,dx);
         bi = imag(log(poles))/DX;
         [dummy,indx] = min(abs(bi-tb));
         DC(i,j) = bi(indx);
      end;
   end;
   TDC(:,n) = DC(:);
end;

AVG = mean(TDC.');
STD = std(TDC.');

DC_avg = zeros(ND,Nc);
DC_std = zeros(ND,Nc);

DC_avg(:) = AVG;
DC_std(:) = STD;

mesh(DC_avg);
pause;
mesh(DC_std);
```

pause;

A7.3 PC-MATLAB SCRIPT FILE FOR LSSD ERROR ANALYSIS

```
% analssd --> Analysis of LSSD Algorithm
%
% Written by: Mark Archibald  3/10/93
%
% Estimates Mean and Standard Deviation of Parameter
%          Estimates From LSSD Method
%

clear;
numavg = 25;
AVGw = zeros(30,6);
STDw = zeros(24,6);
wni = [110;300;590;970;1450;2020];
for mod = 1:6,    %mod = input('Input Mode Number: ');
    SNR = [20;30;40];
    w  = wni(mod);
    [M,mwf,x,C,B] = beam(w);
    bi = B(mod)*1.05;
    v = M(:,mod)*mwf(mod);
    disp('One Constituent Mode');

%    v = M*mwf;              % Use for Multi-Mode Content
%    disp('Six Constituent Modes');

    N = length(v);
    ms = (v'*v)/N;
    rand('normal');

    AB = zeros(numavg,6);
    ab_avg = zeros(3,6);

    for i=1:3,
        snr = SNR(i);
        sd = sqrt(ms/(10^(snr/10)));
        for avg = 1:numavg;
            y = v + sd*rand(N,1);
```

393

```
            b = bi;
            [ab,count] = lssd(b,y,x);
            AB(avg,:) = [ab.' count];
        end;
        ab_avg(i,:) = mean(AB);
        ab_std(i,:) = std(AB);
    end;
    truparam = [C(mod,:) B(mod) mod; zeros(1,6)];
    AVGw((5*(mod-1)+1):(5*mod),:) = [ab_avg;truparam];
    STDw((4*(mod-1)+1):(4*mod),:) = [ab_std;zeros(1,6)];
end;

disp(AVGw);
disp(STDw);
```

A7.4 PC-MATLAB SCRIPT FILE FOR BCBA ERROR ANALYSIS

```
% stat_bcba --> Estimate mean and standard dev. of derivative estimates
%
% Written by: Mark Archibald
%

disp(' ');
disp('BCBA Statistical Analysis of Derivatives');
disp(' ');

rand('normal');

w = (.9:.01:1.1)';
w = w*585;
j = sqrt(-1);

nave = 50;
SNR  = 30;
L    = 54;
b    = .1842;

for i=1:length(w);
    [M,mwf,x,C,B] = beam(w(i));
```

```
    N = length(M);
    v = M*mwf;
    C = diag(mwf)*C;
    C = C.';
    C = C(:);
    B = [B.';-B.';j*B.';-j*B.'];
    B = B(:);
    el = exp(L*B.');
    oe = ones(1,length(B));
    vot(i,:) = real([v(1) oe*(C.*B) oe*(C.*B.^2) oe*(C.*B.^3)]);
    vlt(i,:) = real([v(N) el*(C.*B) el*(C.*B.^2) el*(C.*B.^3)]);
    ms = sum([v .* v])/N;
    sd = sqrt(ms/(10^(SNR/10)));
    for n = 1:nave,
        disp([i,n]);
        r = sd*rand(N,1);
        y = v+r;
        [ab,count,ynew] = lssd(b,y,x);
        b = real(ab(5))
        C = ab(1:4);
        B = [b;-b;j*b;-j*b];
        el = exp(L*B.');
        oe = ones(1,4);
        vo(n,:) = real([ynew(1) oe*(C.*B) oe*(C.*B.^2) oe*(C.*B.^3)]);
        vl(n,:) = real([ynew(N) el*(C.*B) el*(C.*B.^2) el*(C.*B.^3)]);
        if count == -1,
            n = n-1;
            b = b*1.1;
        end;
    end;
    meanVo(i,:) = mean(vo);
    stdVo(i,:)  = std(vo);
    meanVl(i,:) = mean(vl);
    stdVl(i,:)  = std(vl);
end;

plot(w,vot(:,1),'x',w,meanVo(:,1),'o',w,meanVo(:,1) + 2*stdVo(:,1),':');
```

REFERENCES

Archibald, C. M., and A. L. Wicks, *An Analysis of Sample Rate Considerations for Parametric Sinusoidal Estimation Methods*, Proc. 10th Int. Modal Ana. Conf., San Diego, Ca. 1992.

Archibald, C.M.,and Wicks, A.L., *An Alternative Time-Domain System Identification Algorithm*, Proc. 9th Int. Modal Ana. Conf., Florence, Italy, 1991.

Arruda, Jose Roberto, Sun, Fanping, and Mitchell, Larry D., *Spatial Domain Techniques For Modal Analysis Using A Laser Doppler Velocimeter*, Proc. 10th Int. Modal Ana. Conf., pp 656-664, San Diego, Ca. 1992.

Astrom, K.J., and Eykhoff, P., *System Identification -- A Survey*, Automatica, vol 7, pp 123-162, 1971.

Box, George E.P., and Jenkens, Gwilym M., Time Series Analysis Forecasting and Conrol, Holden-Day, 1976

Brown, D.L., Allemang, R.J., Zimmermann, R. and Mergeay, M. *Parameter Estimation Methods for Modal Analysis*, SAE Paper 790221, 1979.

Chang, T.C., and Craig, R.R., *Normal Modes of Uniform Beams*, J. Eng. Mech. Div., ASCE, vol 95, pp 1027-1031, August, 1969.

Cooley, J.W., and Tukey, J.W., *An Algorithm for the Machine Calculation of Fourier Series*, Math. Compu., vol 19, pp 297-301, 1965.

Cooper, J.E., and Wright, J.R., *Comparison of Some Time Domain System Identification Methods for Free Response Data*, Proc. 2nd Int. Symp. on Aeroelasticity and Struct. Dynamics, Aachen, W. Germany, 1985.

Cooper, J.E., *Comparison of Some Time-domain-system Identification Techniques Using Approximate Data Correlations*, Int. J. of Ana. and Exp. Modal Analysis, vol 4, pp 51-57, April 1989.

396

Cowper, G.R., *The Shear Coefficient in Timoshenko's Beam Theory*, J. of Applied Mech., ASME, vol 33, pp 335-340, June, 1966.

Cuenod, M., and Sage, A.P., *Comparison of Some Methods Used for Process Identification*, Automatica, vol 4, pp 235-269, 1968.

Ebner, Alan M., e al, *Steady Sae Vibration Of Damped Timoshenko Beams*, J. of the Struct. Div., Proc. of ASCE, pp 737-760, March, 1968.

Ewins, D.J., Modal Testing: Theory and Practice, Research Studies Press Ltd., Letchworth, England, 1986.

Fullekrug, U., *Structural-dynamics Identification in the Time Domain: Estimation of Modal Parameters Based on Forced Vibrations*, Int. J. of Ana. and Exp. Modal Analysis, vol 4, pp 58-67, April 1989.

Golub,Gene H., and Van Loan, Charles F., *An Analysis of the Total Least Squares Problem*, SIAM J. of Numer. Ana. vol 17, no 6, pp 883-893, Dec 1980.

Golub,Gene H., and Van Loan, Charles F., Matrix Computations, 2nd ed. John Hopkins Univ. Press, 1989.

Hildebrand, F.B., Inroduction to Numerical Analysis, McGraw-Hill, New York, 1956.

Huang, T.C., *The Effect of Rotatory Inertia and of Shear Deformation on the Frequency and Normal Mode Equations of Uniform Beams With Simple End Conditions*, J. of Applied Mech., ASME, vol 28, pp 579-584, December, 1961.

Hutchinson, J.R., and Zillmer S.D., *On the Transverse Vibration of Beams of Rectangular Cross-Section*, J. of Applied Mech., ASME, vol 53, pp 39-44, March 1986.

Hutchinson, J.R., *Transverse Vibrations of Beams, Exact Vrsus Approximate Solutions*, J. of Applied Mech., ASME, vol 48, pp 923-928, December, 1981.

Ibrahim, S.R., and Mikulcik, E.C., *A Method for the Direct Identification of Vibration Parameters from the Free Response*, Shock and Vibration Bulletin, vol 47, pp 183-198, 1977.

Kaneko, T., *On Timoshenko's Correction for Shear in Vibrating Beams*, Journal of Physics D, Applied Physics, vol 8, pp 1927-1936, 1975.

Kochersberger, K., Mitchell, L. D., and Wicks, A. L., *Structural Angular Velocity Extraction Using DFT-IDFT Techniques*, Proc. 9th Int. Modal Ana. Conf., pp 657-663, Florence, Italy, 1991.

Kay, Steven M., Modern Spectral Estimation: Theory and Application, Prentice-Hall, Englewood Cliffs, NJ, 1988.

Kay, S.M., and Marple, S.L., *Spectrum Analysis -- A Modern Perspective*, Proc. IEEE, vol 69, pp 1380-1419, Nov 1981.

Lawson, Charles L., and Hanson, Richard J., Solving Least Squares Problems, Prentice-Hall, Englewood Cliffs, NJ, 1974.

Liang, Z., and Inman, D.J., *Matrix Decomposition Methods in Experimental Modal Analysis*, Technical Brief, J. Vib. and Acous., vol 112, pp 410-413, 1990.

Marple, S.L., Jr., Digital Spectral Analysis, Prentice-Hall, Englewood Cliffs, N.J., 1987.

Meirovitch, Leonard, Elements of Vibration Analysis, McGraw-Hill, 1975.

Mindlin, R.D., and Deresiewicz, H. *Timoshenko Shear Coefficient for Flexural Vibration of Beams*, Proc. of 2nd U.S. National Congress of Applied Mechanics, ASME, New York, pp 175-178, 1954.

Pandit, Sudhakar M., and Mehta, Nakul P., *Data Dependent Systems Approach to Modal Parameter Identification*, Proc. 2nd Int. Modal Ana. Conf., Orlando FL, pp 35-43, 1984.

Pandit, Sudhakar M., et al., *Model Estimation of Lumped Parameter Systems Using Data Dependent System Models*, Proc. 4th Int. Modal Analysis Conf., Los Angles, CA, pp 414-421, 1986.

Patton, K.B., Analysis of Parametric Model Signal Processing Techniques For Signature Analysis, Masters Thesis, Virginia Polytechnic Institute and State University, Mechanical Engineering Dept., June 1988.

Pisarenko, V.F., *The Retrieval of Harmonics from a Covariance Function*, Geophys. J. R. Astr. Soc., vol 33, pp 347-366, 1973.

Press, William H., Flannery, Brian P., Teukolsky, Saul A., and Vetterling, William T., <u>Numerical Recipes In C: The Art of Scientific Computing</u>, Cambridge University Press, Cambridge, 1988.

Prony, G.R.B., *Essai experimental et analytique, etc.,* <u>J. Ec. Polytech.</u>, vol 1, Cashier 2, pp 24-76, 1795.

Rao, Singiresu, <u>Mechanical Vibrations</u>, Addison-Wesley, Reading, MA, 1986.

Richard, J., Lomenzo, R., and Wicks, A.L., *Obtaining Poisson's Ratio From the Dynamic Measurement of Anticlastic Bending in a Beam*, <u>Proc. 11th Int. Modal Ana. Conf.</u>, Orlando, Fl., pp 286-292, 1993.

Robinson, Enders A., *Historical Perspective of Spectrum Estimation*, <u>Proc. of IEEE</u>, vol 70, no 9, pp 885-906, September 1982.

Schmidt, R.O., <u>A Signal Subspace Approach to Multiple Emitter Location and Spectral Estimation</u> Ph.D. Dissertation, Stanford University, 1981.

Smith, Kevin E., *An Evaluation Of A Least Squares Time Domain Parameter Identification Method For Free Response Measurement,* <u>Proc. 2nd Int. Modal Ana. Conf.</u>, pp 610-615, 1984.

Smith, W.R., *Least-Squares Time-Domain Method for Simultaneous Identification of Vibration Parameters from Multiple Free-Response Records*, <u>AIAA Paper 81-0530</u>, 1981.

Stein, Manuel, *Vibration of Beams and Plate Strips With Three-Dimensional Flexibility*, <u>Journal of Applied Mechanics, ASME</u>, vol 56, pp 228-231, March 1989.

Stewart, G.W., <u>Introduction to Matrix Computations</u>, Academic Press, New York, 1973.

Timoshenko, S.P., *On the Correction for Shear of the Differential Equation for Transverse Vibration of Prismatic Bars*, <u>Philosophical Magazine</u>, Series 6, vol 41 pp 744-746, 1921.

Timoshenko, S.P., *On the Transverse Vibration of Bars of Uniform Cross Section*, <u>Philosophical Magazine</u>, vol 43 pp 125-131, 1922.

Timoshenko, Stephen P. and Gere, James M., <u>Mechanics of Materials</u>, 2ed. Brooks/Cole Engineering Division, Belmont, CA, 1984.

Udea, Tetsuhiko, and Iwasaki, Kazuo, *Vibration Analysis   in the Time Domain by the Real Eigenvalue Method*, <u>AIAA</u> <u>Paper</u> <u>87-0945</u>, 1987.

Warburton, G. B., <u>The</u> <u>Dynamical</u> <u>Behavior</u> <u>of</u> <u>Structures</u> 2nd <u>Ed</u>., Pergamon Press, London, 1976.

West, Robert L., Archibald, Charles M., and Wicks, Alfred L., *Spatial Modal Analysis Using Regressive and Autoregressive Techniques*, <u>Proc</u>. 11th <u>Int</u>. <u>Modal</u> <u>Ana</u>. <u>Conf</u>., Orlando, FL, 1993

Wilkerson, <u>The</u> <u>State</u> <u>of</u> <u>the</u> <u>Art</u> <u>in</u> <u>Numerical</u> <u>Analysis</u>, ed. D. Jacobs, Academic Press, London, 1977.

Yang, Y., *A Time Domain Identification Technique: The Oversize Eigenmatrix Method*, <u>J</u>. <u>Vib</u>. <u>Acous</u>. <u>Stress</u> <u>and</u> <u>Reliability</u> <u>in</u> <u>Design</u>, vol 107, pp 53-59, 1985.

Yule, G.U., *On a Method of Investigation Periodicities in Disturbed Series, With Special Reference to Wolfer's Sunspot Numbers*, <u>Phil</u>. <u>Trans</u>. <u>Roy</u>. <u>Soc</u>. <u>London</u>, A, vol 226, pp 267-298, 1927.

VITA

Charles Mark Archibald was born in Birmingham, Alabama, the son of a Methodist minister. After a tour of duty with the U. S. Navy, he returned to Alabama to complete his education. As an undergraduate, he studied mechanical engineering at the University of Alabama and the University of Alabama in Huntsville, where he graduated with honors in 1988. In 1990, he obtained his master's degree in mechanical engineering from Virginia Tech. After completion of his Ph.D. degree, Mark hopes stay in academics teaching and conducting research.